ANDROGEN METABOLISM IN ADIPOSE TISSUE AND LIVER AND THE IMPACT OF FEMALE ANDROGEN EXCESS

by

AMARAH VIOLA ANTHONY, BSc, MSc

A thesis submitted to the University of Birmingham for the degree of
DOCTOR OF PHILOSOPHY

Institute of Metabolism and Systems Research
College of Medical and Dental Sciences
University of Birmingham
August 2023

Abstract

Androgens are key regulators of metabolic and reproductive health in women. Imbalances in androgen metabolism can lead to conditions of female hyperandrogenism, such as polycystic ovary syndrome (PCOS). PCOS is associated with an extensive list of comorbidities including adipose dysregulation and metabolic associated steatotic liver disease (MASLD). Activation of C_{19} androgens via intracrine pathways within metabolically active tissues, such as adipose and liver, are important determinants of local androgen action. Both classic and 11-oxygenated androgens contribute to female hyperandrogenism, yet despite the importance of 11-oxygenated in female androgen excess, the tissue-specific pathways of these androgens are not fully understood. Adipose tissue is a key tissue involved in the activation classic and 11-oxygenated androgen precursors, via the enzyme Aldo Keto Reductase family 1 member 3 (AKR1C3), and therefore plays a central role in the systemic metabolic health of women with hyperandrogenism. The liver is also a major site of systemic androgen metabolism and known to express androgen-activating enzymes. Even though liver and adipose are important metabolic tissues and androgen target tissues, there is a need to delineate the local/intracrine pathways of androgen metabolism to be able to better understand the tissue specific links between androgen excess and metabolic complications. Here, I demonstrate the importance of AKR1C3 regulation on androgen metabolism in adipose tissue. I also describe the liver as a site of androgen deactivation which rapidly inactivates androgens via A-ring reduction of both classic and 11-oxygenated androgens.

Multi-steroid profiling of *ex vivo* female adipose tissue incubation models revealed AKR1C3 as the key enzyme of androgen activation in adipose, activating both classic and 11-oxygenated androgen precursors androstenedione and 11-ketoandrostenedione to their respective active metabolites. Activation of 11-oxygenated androgens by AKR1C3 was seven-fold greater than activation of classic androgens. Selective inhibition of AKR1C3 significantly reduced the generation of active androgens, with a greater effect on 11-oxygenated androgens. AKR1C3 inhibition could therefore prove to be a successful therapeutic target to treat female hyperandrogenism.

Ex vivo human liver tissue incubations, together with normothermic machine liver perfusion, identified the liver as a site of androgen inactivation for both classic and 11-oxygenated androgens, predominantly leading to the formation of inactive end stage A-ring reduced metabolites. 11β-hydroxysteroid dehydrogenase type 1 (HSD11B1) played a key role for the regulation of the levels of 11-oxygenated androgens, by converting active 11-keto androgens and their 11-keto precursors to their inactive, 11β-hydroxy counterparts. The liver therefore does not contribute to intracrine androgen activation, and these results provide a strong foundation upon which a deeper understanding of the involvement of androgen metabolism in the comorbidities of female hyperandrogenism, such as MASLD, can be built.

Acknowledgements

Firstly, I would like to express immense gratitude to my wonderful supervisors Prof Wiebke Arlt, Dr Lina Schiffer and Dr Angela Taylor. Thank you for your continued support, mentorship and encouragement. I could not have asked for a better team of supervisors. I have been extremely lucky to have you.

I would also like to thank my co-supervisor Prof Simon Afford and his team at the Institute of Immunology and Immunotherapy, particularly George Clarke, Angus Hann and Jingwen Mao, who have been instrumental in the success of my work with normothermic machine liver perfusion and made the experience a very positive one.

I would like to thank my family for supporting me during this journey. To my parents, words cannot begin to express the love and gratitude I have for you. There have been times when I have lost sight of my goals, but you have been there to put me back on track every time. Thank you for being my anchors during difficult times and biggest supporters during good ones. I hope to continue to make you proud. To my godparents, June, Glenn and Leon, whom I love dearly. Thank you for your words of wisdom, encouragement and for always being in my corner.

I would also like to thank everyone in the Arlt lab group and members of the Institute of Metabolism and Systems Research I have had the pleasure of working with. Special thanks to Alessandro Prete, who has given me invaluable advice, and Fozia Shaheen, who has been a joy to work alongside.

Finally, and most importantly, I would like to thank God, who has been my guiding force and strength throughout this journey.

Table of Contents

LIST OF FIGURES

CHAPTER 1

CHAPTER 2

CHAPTER 3

CHAPTER 4

CHAPTER 5

LIST OF TABLES

CHAPTER 1

CHAPTER 2

CHAPTER 3

CHAPTER 4

CHAPTER 5

ABBREVIATIONS

- 11βOHAn: 11β-hydrodyandrosterone
- 11βOHEt: 11β-hydroxyetiocholanolone
- 11βOHT: 11β–hydroxytestosterone
- 11K-3α-adiol: 11-keto-3α-androstandadiol
- 11KA4: 11-ketoandrostenedione
- 11KAn: 11-ketoandrosterone
- 11KDHT: 11-ketodihydrotestosterone
- 11KEt: 11-ketoetiocholanolone
- 11KEtG: 11-ketoetiocholanolone glucuronide
- 11KT: 11-ketotestosterone
- 11βOHA4: 11-βhydroxyandrostenedione
- 3α-adiol: 3α-androstanediol
- 5α-DHT: 5α-dihydrotestosterone
- 5α-dione: 5α-androstanedione
- A4: androstenedione
- AKR1C2: Aldo Keto Reductase family 1 member 2
- AKR1C3: Aldo Keto Reductase family 1 member 3
- AKR1D1: Aldo Keto Reductase family 1 member 1
- AKR1D1: aldo keto reductase family 1 member 1
- AMH: Anti-Mullerian hormone
- An: Androsterone
- AR: human androgen receptor

- ASRM: American Society for Reproductive Medicine
- BAY1: BAY1128668
- BAY2: BAY2299242
- BMI: body mass index
- CYP11B1: cytochrome P450 11β-hydroxylase
- CYP19A1: cytochrome P450 aromatase
- DHEA: dehydroepiandrosterone
- DHEAS: dehydroepiandrosterone sulfate
- DMEM: Dulbecco's Modified Eagle Medium
- DMSO: dimethyl sulfoxide
- DNL: *de no* lipogenesis
- E1: Estrone
- E2: 17β-Estradiol
- E2S: 17β-Estradiol sulfate
- EDTA: Ethylene Diamine Tetra Acetic Acid
- ELISA: enzyme-linked immunosorbent assay
- Et: etiocholanolone
- EtG: etiocholanolone glucuronide
- FFAs: free fatty acids
- FSH: follicle stimulating hormone
- GC-MS: gas chromatography-mass spectrometry
- GLUT-4: glucose transporter 4
- GnRH: gonadotropin releasing hormone
- HA: hyperandrogenism
- HCC: hepatocellular carcinoma
- HDHs: high density lipoproteins
- HE: hepatic encephalopathy
- HMDS: hexamethyldisilazane
- HPO: hypothalamic–pituitary–ovarian
- HSD11B1: 11β-hydroxysteroid dehydrogenase type 1
- HSD11B2: 11β-hydroxysteroid dehydrogenase type 2
- HSD3B1: 3β-hydroxysteroid dehydrogenase
- IR: Insulin resistance
- LDLs: low-density lipoproteins
- LH: luteinising hormone
- LLOQ: lower limit of quantification
- MAS: MASLD activity score
- MASH: metabolic dysfunction-associated steatohepatitis
- MASLD: metabolic associated steatotic liver disease
- MEM: minimal essential medium
- MeOH: methanol
- MRM: Multiple reaction monitoring
- NAFLD: non-alcoholic fatty liver disease
- NASH: non-alcoholic steatohepatitis
- NIH: National Institute of Child Health and Human Development

- NMLP: normothermic machine liver perfusion
- OD: oligoovulation
- PBMCs: peripheral blood mononuclear cells
- PBS: phosphate buffered saline
- PCOM: polycystic ovarian morphology
- PCOS: polycystic ovary syndrome
- SAF: steatosis, activity and fibrosis
- SCS: static cold storage
- SGBS: Simpson-Golabi-Behmel Syndrome
- SHBG: sex hormone binding globulin
- SPE: solid phase extraction
- SRD5A2: 3-Oxo-5α-steroid 4-dehydrogenase (5α-reductase) type *2*
- SRD5A1: 3-Oxo-5α-steroid 4-dehydrogenase(5α-reductase) type 1
- T: testosterone
- TLC: thin layer chromatography
- TRIzol: RNA isolation lysis reagent
- UHPLC-MS/MS: ultra-high performance liquid chromatography mass spectrometry
- ULOQ: upper limit of quantification

CHAPTER 1

GENERAL INTRODUCTION

1.1. Androgen biosynthesis and metabolism

1.1.1. Overview of steroidogenesis

The purpose of this thesis was to investigate androgen metabolism in adipose and liver in relation to hyperandrogenism, with a particular focus on the consequences of female androgen excess. In women, steroid biosynthesis occurs in the adrenal glands, the placenta, and the ovaries, as described below.

1.1.1.1. Adrenal steroidogenesis

Steroids are a class of intricate lipophilic molecules, that regulate multiple biological processes in the body throughout the life span [1]. They consist of four fused rings (three 6 membered rings and one 5 membered ring), each of which may contain different functional groups [2]. All steroids originate from cholesterol **(Figure 1.1).** Cholesterol can be derived from various sources including low-density lipoproteins (LDLs) and high density lipoproteins (HDLs) [3], utilization of carbon atoms from acetic acid in the endoplasmic reticulum [4-6], hydrolysis of cholesterol esters stored in lipid droplets into free cholesterol by ester hydrolases [7, 8], selective cellular uptake and free cholesterol in the plasma membrane [9, 10]. This process occurs in the adrenal cortex, gonads and the placenta [11]. The adrenal glands are triangular shaped organs that sit on top of the kidneys, weigh approximately 5 grams and by adulthood are one thirteenth the size of the kidneys (50 mm in height, 30 mm in breadth and 10 mm thickness) [12]. Each gland is composed of two sections; the outer cortex and inner

medulla [12]. The adrenal cortex is ‘yellow-ish’ in colour and is the larger section of the two. In contrast, the medulla has a more ‘reddish-brown’ hue and accounts for only 15% of the gland [12]. The inner medulla plays a vital role in the body’s ‘fight or flight’ response, releasing catecholamines such as norepinephrine (noradrenaline) and epinephrine (adrenaline) [12]. The adrenal cortex, on the other hand, is responsible for the secretion of vital hormones that regulate the immune system, metabolism and salt and water balance [12]. It is made up of three distinct zones each of which have specific roles in steroidogenesis (**Figure 1.1**) [12]. The fitting mnemonic “salt, sugar, sex’’ is often used to describe the function of each zone, details of which are outlined below [3, 9, 12, 13]:

Zone 1: The *Zona Glomerulosa* (outermost zone)

The zona glomerulosa synthesises mineralocorticoids, the most important being aldosterone. Aldosterone is involved in the renin-angiotensin-aldosterone system, responsible for electrolyte balance and regulation of blood pressure [9, 12].

Zone 2: The *Zona Fasciculata* (middle layer)

The zona fasciculata predominantly releases glucocorticoids. Of these, cortisol is arguably the most prominent. Cortisol is involved in the regulation of blood sugar via gluconeogenesis, controls the immune system, modulates fat metabolism and is a vital hormone involved in the stress response, often referred to as the body’s ‘stress hormone’. Cortisol secretion is controlled by the adrenocorticotropic hormone regulation, released from the pituitary gland [9, 12, 13].

Zone 3: The *Zona Reticularis* (inner zone)

The final zone of the adrenal cortex, the zona reticularis, produces C_{19} steroids - namely, dehydroepiandrosterone (DHEA), androstenedione (A4), which are converted to active androgens, such as testosterone (T), 5α-dihydrotestosterone (5α-DHT) in peripheral tissue [9, 12, 13]. While 11-oxygenated androgens originate from classic androgens produced in the zona reticularis, it has been proposed that hydroxylation of A4 and T to produce 11-βhydroxyandrostenedione (11βOHA4) and 11-βhydroxytestosterone (11βOHT) mainly occurs in the zona fasciculata, but at the border between the zona reticularis and zona fasciculata [14, 15]. However, as the adrenal does not produce large amounts of T, conversion to 11βOHT is minimal [16]. 11βOHA4 and 11βOHT are then converted to active 11-oxygenated metabolite 11-ketotestosterone (11KT) in peripheral target tissue [9, 12, 13]. Androgens play a central role in development of secondary sexual characteristics [9, 12, 13]. Androgen production begins in childhood, between 4 and 7 years of age [17, 18]. Androgen secretion in children is minimal but increases with age, concurrent with the growth of the Zona Reticularis [18]. In teenagers and adult females, the adrenal gland is the main source of androgens and their precursors. It should be noted that adrenal biosynthesis of androgens is not the major contributor to circulating androgens in adult males, where the testes make the major contribution [9].

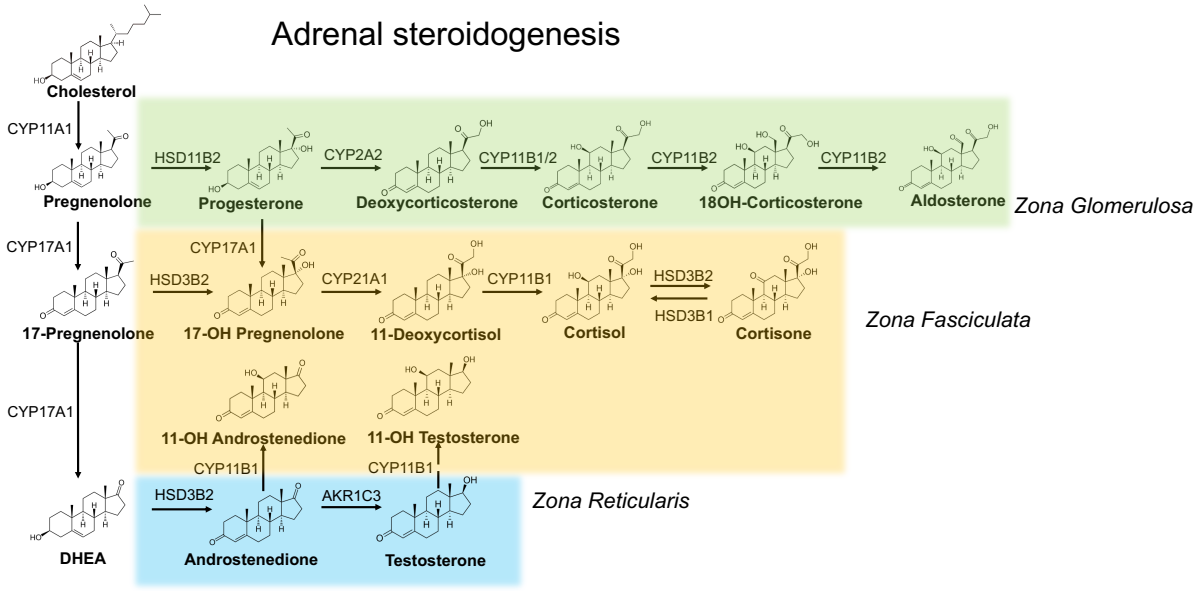

Figure 1.1 Steroidogenesis in the adrenal glands. Steroid pathways are colour coordinated according to the zone they predominantly take place. Zona glomerulosa (green), zona fasciculata (orange), zona reticularis (blue). Dashed lines represent minimal conversion of substrate.

1.1.1.2. Gonadal steroidogenesis: the ovaries

The gonads are also a site of *de novo* steroidogenesis but are not activated until puberty. Post puberty, steroidogenesis is stimulated by the development of the hypothalamic-pituitary-gonadal axis [9]. The ovaries are female gonads, consisting of germ cells (oocytes) and somatic cells (theca cells, granulosa cells and stromal cells) [19]. Theca cells are stimulated by luteinising hormone (LH) to produce the androgen precursors DHEA and A4 from cholesterol (**Figure 1.2**). A4 can be converted to 5α-androstanedione (5α-dione) and active androgen T, respectively by the enzyme Aldo Keto Reductase family 1 member 3 (AKR1C3) [20]. A4 can be released into circulation, although the majority enters granulosa cells and is converted to T by AKR1C3 and Estrone (E1) by cytochrome P450 aromatase (CYP19A1). Granulosa cells are stimulated to express CYP19A1 by follicle stimulating hormone

(FSH) [21]. T, for the most part, is released into circulation but can diffuse into granulosa cells, where it is converted by 17β-Estradiol (E2) and 17β-Estradiol sulfate (E2S) [20, 22]. Low amounts of 5α-DHT can also be produced in granulosa cells by conversion of T via 5α-reductases [22].

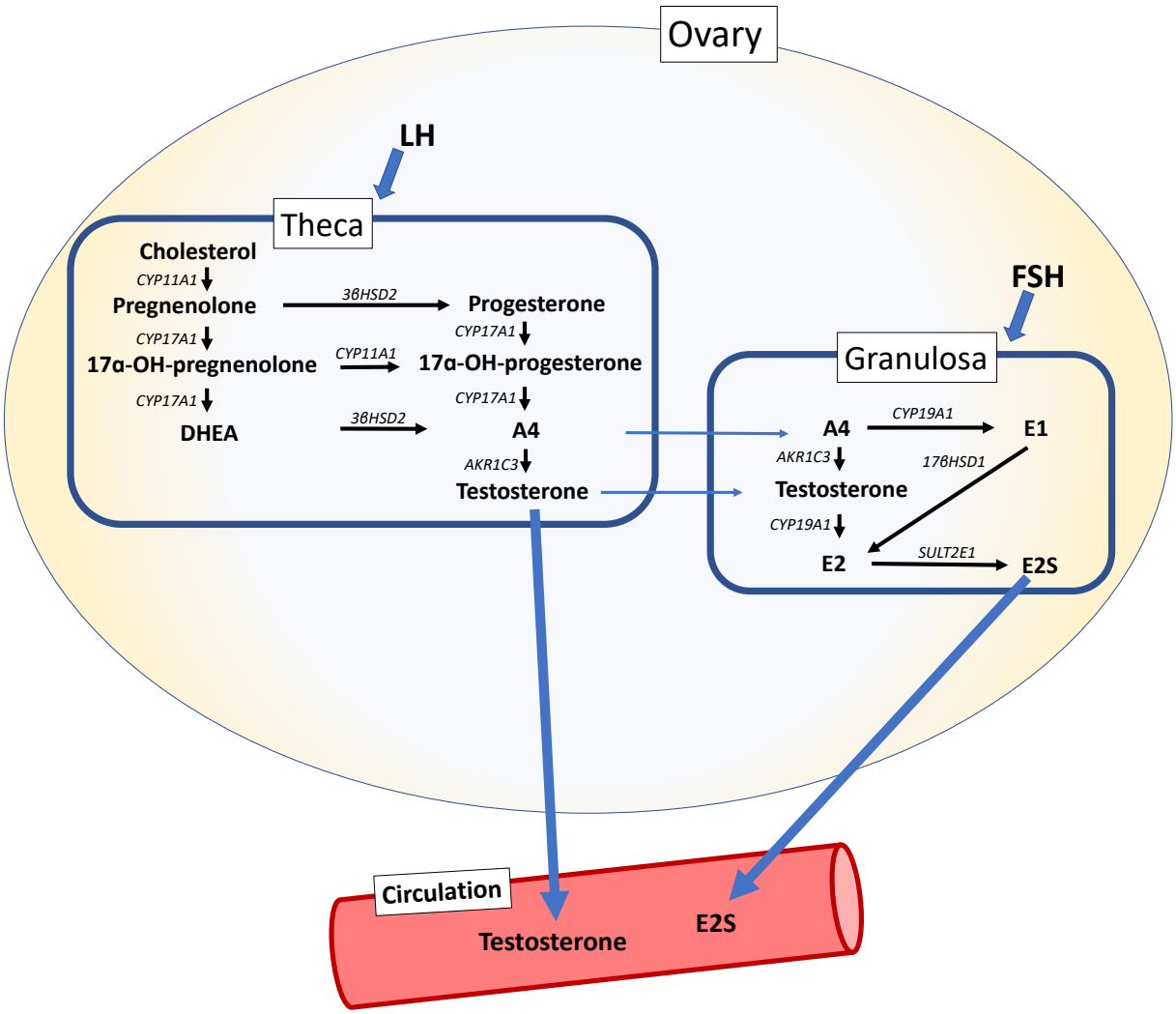

Figure 1.2 Steroidogenesis in the ovary. In theca cells, stimulated by LH, cholesterol is converted through a series of enzymatically-catalysed reactions resulting in production of androgens A4 and T. Androgens synthesised by theca cells are transported to granulosa cells where the undergo aromatisation to oestrogens.

1.1.2. Androgen biosynthesis

As introduced above, androgen precursors are produced in the adrenal gland and are subject to downstream activation across multiple tissues that do not biosynthesise androgens *de novo* [9]. The level of activation and the steroid pathway followed is heavily dependent on the expression of steroidogenic enzymes in said target tissue [9]. Androgen activation is therefore cell specific. This process of peripheral controlled activation is termed 'intracrinology' [9].

1.1.2.1. Classic androgen biosynthesis

In the classic androgen pathway, originating from cholesterol, DHEA is the initial androgen precursor (**Figure 1.1 and Figure 1.3**). Interestingly, the zona reticularis abundantly expresses sulfotransferase (SULT2A1), which converts DHEA to dehydroepiandrosterone sulfate (DHEAS) [9]. Resultantly, DHEAS is the primary steroid released from the adrenal gland and the most abundant steroid in circulation [9]. Remaining DHEA can be released into circulation, be converted to A4 in the adrenal gland via 2 beta-hydroxysteroid dehydrogenase (HSD3B2) or to A4 in peripheral tissue via 3 beta-hydroxysteroid dehydrogenase (HSD3B1) [9]. A4 also undergoes minimal conversion to T in the adrenal gland [23]. In peripheral tissue, the enzyme AKR1C3 plays a central role in androgen activation and is responsible for the conversion of inactive A4 to T, renowned for its androgenic activity and notoriety in conditions of hyperandrogenism [9]. 5α-reduction of T via 3-Oxo-5α-steroid 4-dehydrogenase type 1 (SRD5A1) or type 2 (SRD5A2) leads to generation of 5α-DHT, the most potent androgen [9]. A4 can also serve as a substrate to 5α-reductase to form 5α-dione, which can subsequently be converted to 5α -DHT, bypassing conversion to

T. This is known as the alternate 5α-androstanedione pathway [9]. It is important to note that SRD5A1 has a higher affinity for A4 over T, so in peripheral tissue where SRD5A1 is abundant, the alternate 5α-androstanedione pathway dominates [9]. Inactivation of classic androgens takes place via aldo keto reductase family 1 member 1 (AKR1D1), which yields the inactive metabolite etiocholanolone (Et) [9, 24]. Both 5α-DHT and 5α-dione can be converted to inactive metabolites androsterone (An) and 3α-androstanediol (3α-adiol), respectively, via Aldo Keto Reductase family member 1 member 2 (AKR1C2) [9].

1.1.2.2. 11-oxygenated androgen biosynthesis

Although previously disregarded as physiologically insignificant, in the last ten years the importance of 11-oxygenated androgens has been given due attention with the discovery of their metabolism to active androgens [16, 25]. Generation of 11-oxygenated androgens begins with conversion of cholesterol to DHEA and A4, in the adrenal gland (**Figure 1.3**). At this point, the adrenal specific enzyme cytochrome P450 11β-hydroxylase (CYP11B1) hydroxylates A4 to form the major adrenal 11-oxygenated precursor 11β-hydroxyandrostenedione (11βOHA4). This reaction can also take place for T, forming 11β-hydroxytestosterone (11βOHT), but to a much lesser degree in the adrenal gland due to minimal substrate (T) production [25, 26]. A recent study showed that 11βOHA4 is the most abundant unconjugated steroid in adrenal-vein serum samples [15]. 11βOHA4 and 11βOHT are converted to 11-ketoandrostenedione (11KA4) and 11KT, respectively, via 11β-hydroxysteroid dehydrogenase type 2 (HSD11B2) [25, 26]. Although 11KA4 and 11KT can be synthesised in the adrenal gland, which has low levels of HSD11B2, the majority of

11βOHA4 and 11βOHT is released into circulation. 11βOHA4 is converted to 11KA4 primarily in the kidney, which has high HSD11B2 levels, and re-enters circulation. Subsequently, 11KA4 can re-enter peripheral tissue, such as adipose, where it is converted to 11KT [25, 26]. AKR1C3 plays a key role in peripheral androgen activation once more and converts inactive precursor 11KA4 to active 11KT, an androgen with equal potency and efficacy to T [9, 27]. Although 11βOHT is a substrate for 11βHSD2 and can be converted to 11KT, the majority of 11KT is generated by peripheral conversion of 11βOHA4 to 11KA4, followed by 11KT [16]. 11KT is further converted to 11-ketodihydrotestosterone (11KDHT) via SRD5A2, the most potent 11-oxygenated androgen [9, 25, 26]. Although conversion of T to DHT is efficiently catalysed by SRD5A1, 11KT is a poor substrate for SRD5A1 and conversion to 11KDHT is only efficiency catalysed by SRD5A2 [24]. From here, the metabolism of the 11-oxygenated androgens mirrors that of the classic androgen metabolic pathway, involving the same metabolising enzymes (**Figure 1.3**) [26]. 11βOHA4 and 11βOHT are substrates for SRD5A1/2 yielding 11βOH-5α-dione and 11OH-5α-DHT, respectively [28]. 11KA4 and 11KT are substrates for AKR1D1, and can yield 11-ketoetiocholanolone (11KEt), an inactive androgen metabolite [24, 26]. Notably, all 11-keto androgens, except 11-keto-3α-androstandediol (11K-3α-adiol), can be converted to their 11-hydroxylated products via 11β-hydroxysteroid dehydrogenase type 1 (HSD11B1), meaning HSD11B1 regulates circulating active androgen levels [16, 26]. In comparison to classic androgens, 11-oxygenated androgens are the predominant circulating androgens in women with disorders of androgen excess, such as polycystic ovary syndrome (PCOS) [29, 30]. Michael O'Reily and team showed that serum concentrations of 11KA4, 11KT, 11βOHA4 and 11βOHT were significantly higher in a cohort of 114 women with PCOS

compared to 49 healthy control subjects [29]. The total contribution of 11-oxygenated androgens to the circulating pool was significantly higher in PCOS subjects (53%) compared to body mass index (BMI) matched controls (44%). A link between BMI and 11-oxygenated androgens in women with PCOS was also identified. Serum levels of 11βOHA4, 11KA4, and 11βOHT were significantly increased in obese women with PCOS, compared to non-obese women with PCOS [29]. Interestingly, Nanba and team, who investigated serum androgen levels in 100 premenopausal and 100 post-menopausal women reported 11-oxygenated androgens, unlike classic androgens, do not decline with age [29, 31]. Notably, Nanba *et al* showed that 11βOHA4, 11βOHT and 11KT concentrations were higher in postmenopausal women compared to premenopausal women [31]. Given that 11βOHA4 is a major adrenal product, and its peripheral downstream metabolism produces more active androgens than classic androgen precursors, 11-oxygenated androgens have extreme quantitative importance [28].

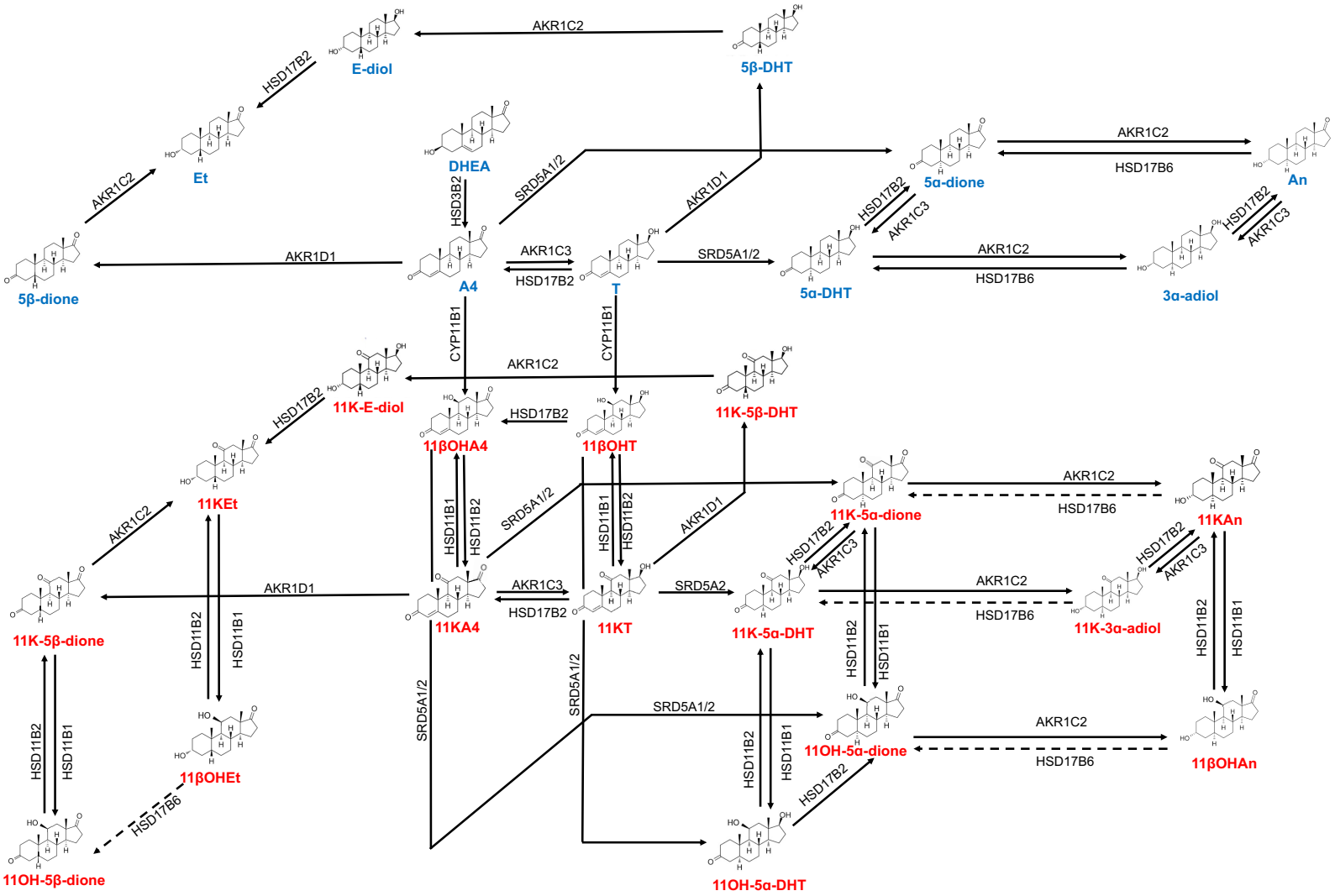

Figure 1.3 Metabolism pathway of C19 androgens. Classic androgens are highlighted in blue, 11-oxygenated androgens are highlighted in red. Dashed lines represent speculative enzymatic conversion.

Androgens exert their effects by binding to recognition sites on the androgen receptor, leading to its activation [32]. The androgen receptor is structurally similar to other steroid receptors, consisting of the three main functional domains; the DNA binding domain, the N-terminal transcriptional domain and the ligand binding domain [32, 33]. Androgens bind to the androgen receptor, causing a conformational change, namely dissociation of chaperone proteins and binding to androgen receptor nuclear localisation signals (which import the receptor to the nucleus) [32, 34]. The formed androgen/androgen receptor complex undergoes translocation to the nucleus, dimerises and binds to androgen response elements (AREs), within classical target genes, to modulate gene transcription [32, 35].

1.1.3. Peripheral activation of classic and 11-oxygenated androgen activation in adipose and liver tissue

1.1.3.1. Androgen metabolism in adipose and liver

AKR1C3 and SRD5A1/2 are crucial enzymes in the generation of active androgens in peripheral tissue, specifically adipose and liver. As described above, AKR1C3 converts inactive precursors A4 and 11KA4 to their active products T and 11KT, which can be further converted to the most potent androgens 5α-DHT and 11K-5α-DHT, respectively [9, 25]. AKR1C3 is highly expressed in adipose tissue, alongside expression of SRD5A1 (**Figure 1.4**) [36, 37]. SRD5A1 has higher affinity for A4 over T and it is therefore of note, DHT production in adipose tissue, even though minimal, is formed by 5α-reduction of A4. This preference has been shown in preadipocyte cultures [38]. When treated with 30 nmol/L of either A4 or T for 24 hours, DHT was detected and

found to significantly increase in A4 treated cultures only. T was found to be converted back to A4 over DHT [38]. While the downstream metabolism of classic androgens in adipose tissue has been extensively characterised, the metabolism of 11-oxygenated androgens, is yet to be explored. As described above, there is a distinct correlation between increased BMI and increased circulating 11-oxygenated androgens levels, particularly in women with conditions of hyperandrogenism such as PCOS, highlighting the importance of adipose tissue for 11-oxygenated androgen activation. Due to 11-oxygenated androgens being a relatively new discovery, the exact mechanistic pathways in adipose tissue models have not been reported. Adipose is complex and there are multiple cells, and continuous interconversion involved in androgen metabolism [25, 30].

The liver is known to express AKR1C3, SRD5A1 and SRD5A2 (**Figure 1.4**) [9]. However, 5β reductase AKR1D1 is also abundantly expressed in liver tissue when compared to other peripheral tissues [9]. Investigations of mRNA levels of AKR1C3 and AKR1D1 in 22 donors using real time quantitative PCR, showed comparable expression between the two enzymes (0.52×10^6 copy/μg and 0.5×10^6 copy/μg, respectively) [39]. The liver therefore has the potential for significant activation and deactivation of both classic and 11-oxygenated androgens. However, androgen metabolism in liver has not been extensively investigated and remains a matter of conjecture. Appropriate models to investigate liver androgen metabolism, especially for the new class of 11-oxygenated androgens, would provide much needed clarity.

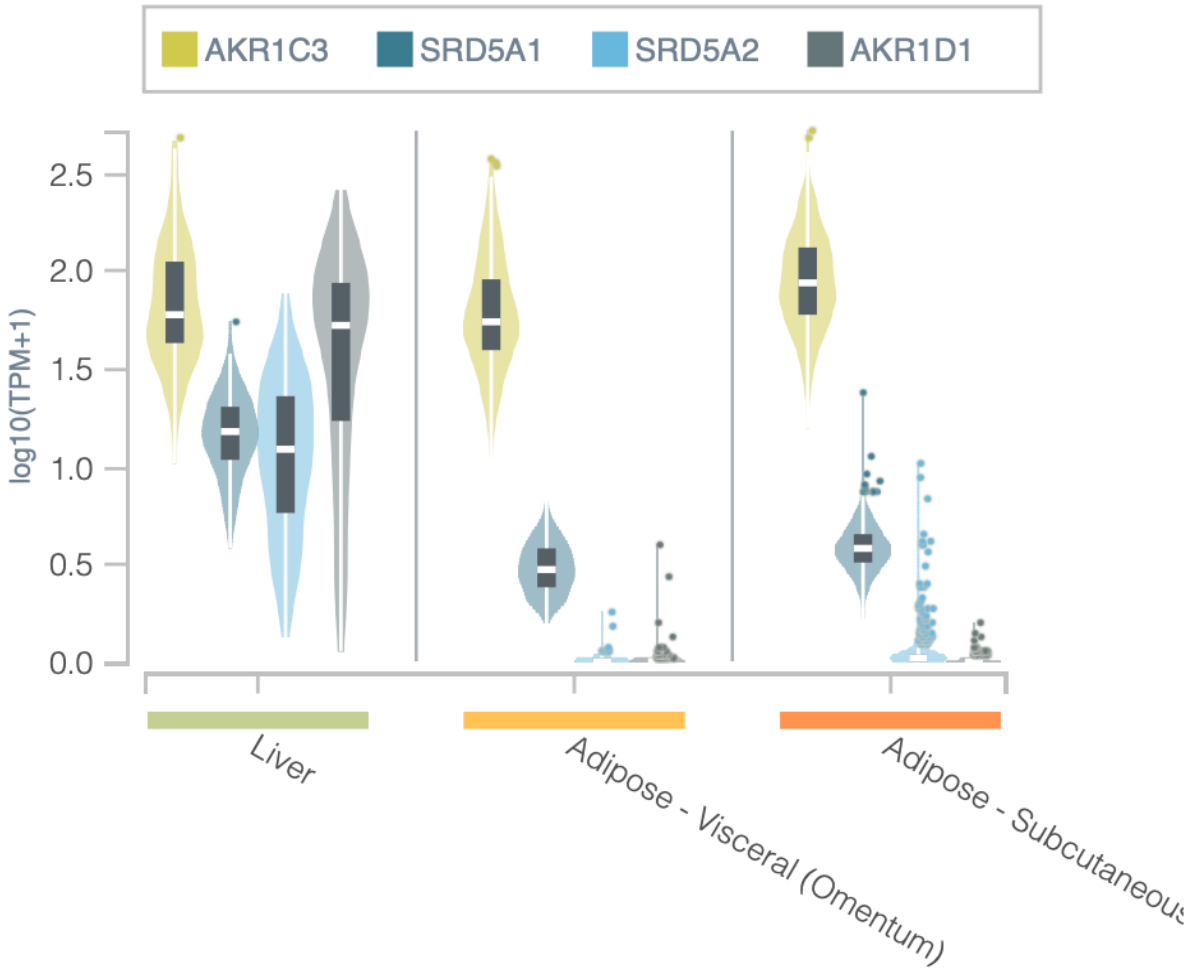

Figure 1.4 GTEx expression for AKR1C3, SRD5A1, SRD5A2 and AKR1D1 in liver and adipose. Accessed 17.05.23. Combined male and female. Data Source: GTEx Analysis Release V8 dbGaP Accession phs000424.v8.p2. Sample size: liver; n= 226, Omental adipose tissue; n=541, Subcutaneous adipose tissue; n=663.

1.1.3.2. Androgen metabolism and excretion

Steroids are lipophilic, meaning they prefer fatty environments and are not soluble in water [9]. Classic androgens predominately circulate the body bound to plasma proteins sex hormone binding globulin (SHBG) and albumin [40, 41]. Only a small fraction of classic androgens are non-protein bound or in their 'free' form [40, 41]. Currently there is no data on 11-oxygenated androgens and if they circulate bound to SHBG. As steroids are lipophilic, they must undergo hepatic phase 1 and phase 2

metabolism to increase their solubility and allow urinary or biliary excretion (**Figure 1.5**) [9, 20]. Initially, steroids undergo reactions to add or remove functional groups, by way of reduction or hydroxylation (phase 1), which primarily serve as target sites for glucuronide or sulfate conjugation (phase 2) [9, 20]. Traditionally, phase 1 and phase 2 metabolism occur sequentially, however this may not always be the case. Recent studies have shown oxidation/ reduction enzymes can act on already conjugated steroids [9].

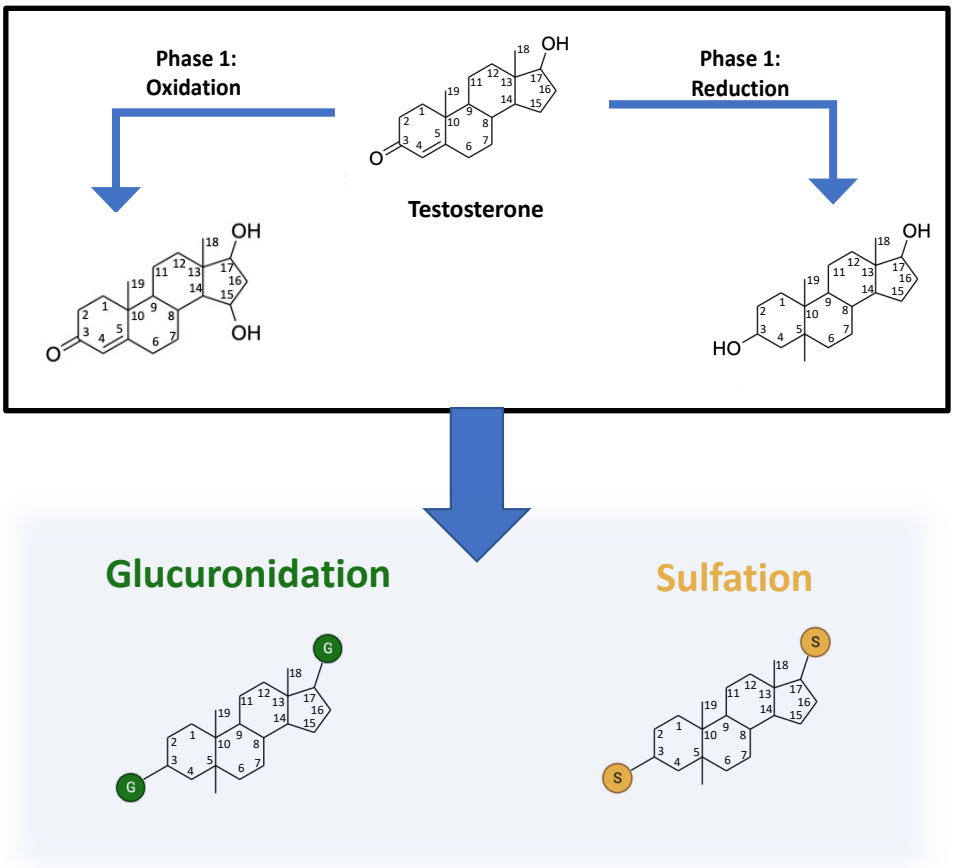

Figure 1.5 Example phase 1 and phase 2 reactions for testosterone. Phase 1 metabolism is a combination of 5α/β reduction of the D4 double bond and 3-keto group to 3α/β-hydroxy group, in addition to α/β oxidations at positions 1, 2, 6, 7, 11, 15, 16 and 18 on the steroid structure. Phase 2 reactions comprise of conjugation of 3 or 17 hydroxy groups.

1.1.4. Ultra-high performance liquid chromatography-tandem mass spectrometry as a tool for multi-androgen profiling

This thesis is centred on understanding androgen metabolism in adipose and liver tissue, particularly in females. Ultra-high performance liquid chromatography mass spectrometry (UHPLC-MS/MS) was employed for the separation and quantification of steroid metabolite production in experimental samples. Historically, immunoassays such as radioimmunoassay and enzyme-linked immunosorbent assay (ELISA), have been the routine technique for steroid measurement [42]. These assays were often chosen for their commercial availability, easy sample preparation and minimal costs [42]. However, immunoassays are based on antibody recognition and due to the structural similarity of steroids, are vulnerable to cross reactivity, which can result in reduced method specificity [42]. In recent years, UHPLC-MS/MS has increasingly been used [42, 43]. Unlike, immunoassays, UHPLC-MS/MS is much less susceptible to cross reactivity as steroid identification is achieved by chromatographic separation and identification of fragmentation patterns, although steroids with similar structures may fragment similarly [44]. Due to the mechanism by which UHPLC-MS/MS performs, it can accommodate measurement of multiple steroids at the same time, has higher specificity and is fast becoming the ‘gold standard’ method for the measurement of steroid hormones for the diagnosis of endocrine disorders, especially disorders of androgen excess [42, 43, 45, 46].

1.1.4.1. Basic principles of ultra-high performance liquid chromatography

UHPLC-MS/MS is a combination of analyte separation by ultra-high performance liquid chromatography (UHPLC) and detection by tandem mass spectrometry (MS/MS) (**Figure 1.6**) [47]. UHPLC is performed using either normal phase or reverse phase separation, with reverse phase being most commonly used. Reverse phase chromatography incorporates a non-polar stationary phase and polar mobile phase (usually methanol/water) [47, 48]. Reverse phase chromatography is used when the analytes of interest are insoluble in polar solvents, such as lipophilic steroids [48]. The stationary phase consists of silica packed metal column, with adsorbed hydrophobic alkyl chains ($-CH_2-CH_2-CH_2-CH_3$), which can range in length from C4 to C18 [49]. For the separation of small molecules such as steroids, the use of a C18 column is recommended [49]. During reverse phase UHPLC, samples are loaded onto the column and chromatographic separation of steroid analytes is achieved by taking advantage of the varied interactions of each steroid with the alkyl chains, a factor dependent on their different polarities [47]. The interaction between the steroid and non-polar solid phase can only be overcome by altering the polarity of the mobile phase. Steroids will therefore remain on the column until this interaction is severed. Steroids with greater polarity will interact with the polar mobile phase over the non-polar stationary phase with greater ease, and are therefore the first to elute off the column [47, 50]. The gradual increase in mobile phase polarity consequentially results in the sequential elution of each steroid off the column [47, 50]. The exact time of analyte elution is known as the retention time. Chromatography therefore facilitates separation of analytes within a mixture. This is especially important when analytes have the same m/z values, which cannot be distinguished by the mass spectrometer.

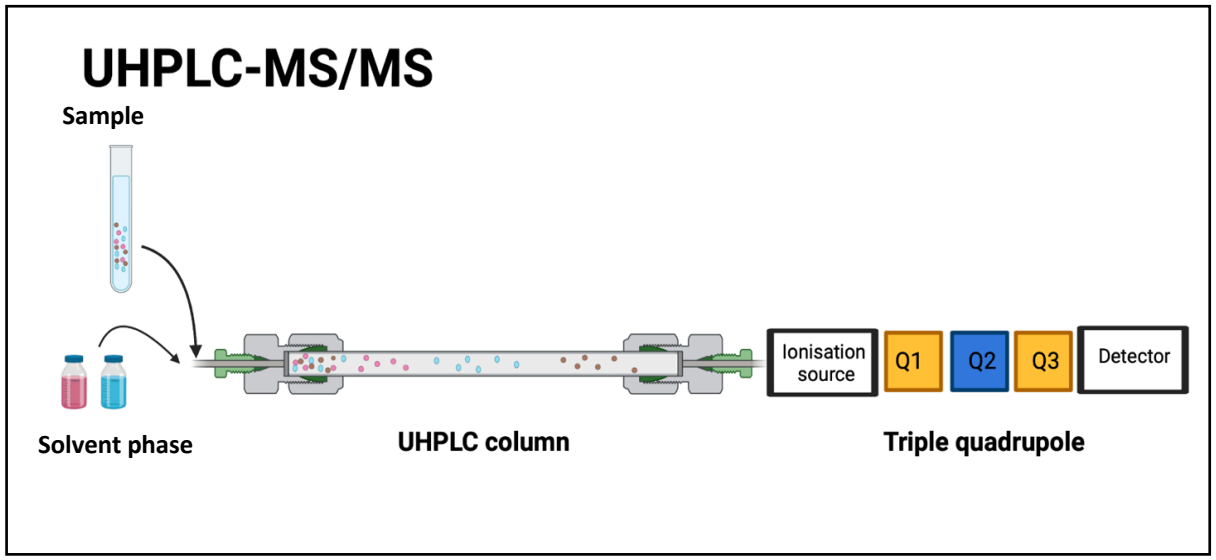

Figure 1.6 Schematic diagram of UHPLC-MS/MS. Abbreviations: Q1; quadrupole 1, Q2; quadrupole 2 (collision cell), Q3; quadrupole 3.

After UHPLC separation, each analyte can be identified and quantified using MS/MS (**Figure 1.6**). The tandem mass spectrometer is made up of three quadrupoles [44]. Before entering the first quadrupole, analytes must be ionised [44, 47, 50, 51]. Electrospray ionisation (ESI) the most common ionisation source for steroid measurement [52]. During ESI, dissolved steroids are subject to a high energy electrical charge, which produces ions that are transferred to the gaseous phase [52]. Analytes with different mass will have a different mass to charge *m/z* ratios [44, 47, 50, 51]. The ionised analytes, known as “parent ions”, enter the first quadrupole where they are subject to an electrical field that allows only user-selected ions, based on their *m/z* ratios, to pass onto the collision cell [44]. The collision cell contains a neutral gas, such as argon, that collides with the ‘’parent ions’’ and acts as a “molecular smasher” and causes fragmentation by collision induced dissociation (CID). Selected ions formed from CID, known as “daughter ions” enter the third quadrupole [44, 53]. The daughter ions are subject to an electrical field, which permits only desired ions

(selected by the user) to pass onto the detector [44, 50]. For quantitation two stable mass transitions for each analyte, a quantifier and qualifier are required [44, 50]. Analyte identification is then achieved by comparison of retention time and mass transitions, known as multiple reaction monitoring (MRM), to reference compounds. The final output is a chromatogram, which shows the response of each steroid as a peak aligned to their retention times. The area under the curve is used to calculate exact concentrations using a calibration series of samples with known concentrations. Expected analyte concentrations should lie within the linear range of the calibration series (**Chapter 2 & 3**).

Internal standards are added in a fixed amount to all samples, including calibration standards to ensure accurate quantification. They compensate for variation introduced during extraction, ionisation and some matrix effects [54]. Internal standards are isotopically labelled analogues of the steroid of interest. For example, a commonly used internal standard for testosterone is testosterone-d_3, containing three deuterium's in place of hydrogens [55]. Labels such as ^{13}C, ^{2}H or ^{15}N, are often used as they have very similar physiochemical properties to their unlabelled analogues, but different mass transitions. An additional benefit to the use of these labels is that chromatography remains the same, making them ideal internal reference compounds [54]. Analyte concentrations are calculated based on the ratio of area under the curve (response) of analytes relative to area under the curve (response) of the internal standard. As the same amount of internal standard is added to each sample and calibrator, it should theoretically remain constant across all extractions.

1.2. Androgen excess, polycystic ovary syndrome and adipose

1.2.1. Polycystic ovary syndrome

Polycystic ovary syndrome (PCOS) is an endocrine disorder, affecting women of reproductive age, worldwide [56]. Contrary to what its name might suggest, the syndrome is a complex disease that is characterised by an intertwining network of biochemical and morphological factors, namely androgen excess, enlarged and dysfunctional ovaries and insulin resistance [56, 57]. Androgen excess is a key biochemical driver of PCOS and the majority of patients with the condition exhibit hyperandrogenism (**Figure 1.7**) [58].

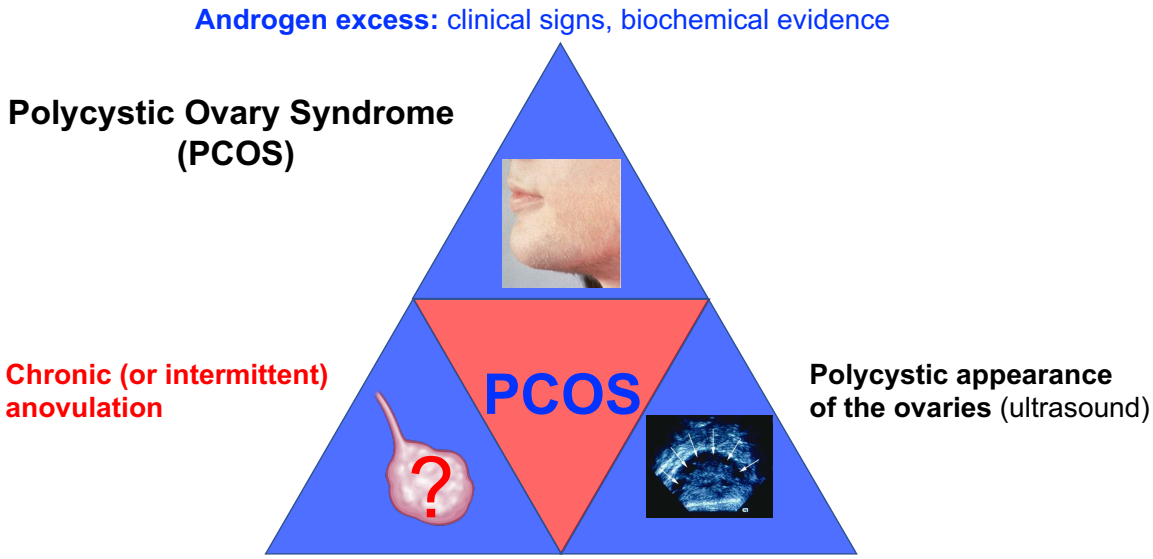

Figure 1.7 Graphical representation of the three defining features in PCOS. Androgen excess, polycystic ovaries on ultrasound and menstrual cycle irregularities. Reprinted with kind permission from Wiebke Arlt.

PCOS was first described by Stein and Leventhal in 1935 and is the most common endocrine disorder affecting approximately 3 - 20% women of reproductive age, worldwide [59-61]. However, due to the heterogenous nature of PCOS and therefore

inconsistent clinical presentations, up to 75% of women remain undiagnosed [60]. Morphological presentation of PCOS is defined as the appearance of enlarged ovaries with fluid filled follicles, between 2 and 9 mm, on one or both ovaries [61]. Hyperandrogenism contributes to prominent features of PCOS such as impaired follicular development, ovarian cysts, anovulation and irregular menstrual cycle [57]. PCOS is not just a reproductive disorder and is also associated with a host of co morbidities such as hirsutism, obesity, insulin resistance, type 2 diabetes, cardiovascular disease and metabolic associated steatotic liver disease (MASLD) [62, 63] (**Figure 1.8**).

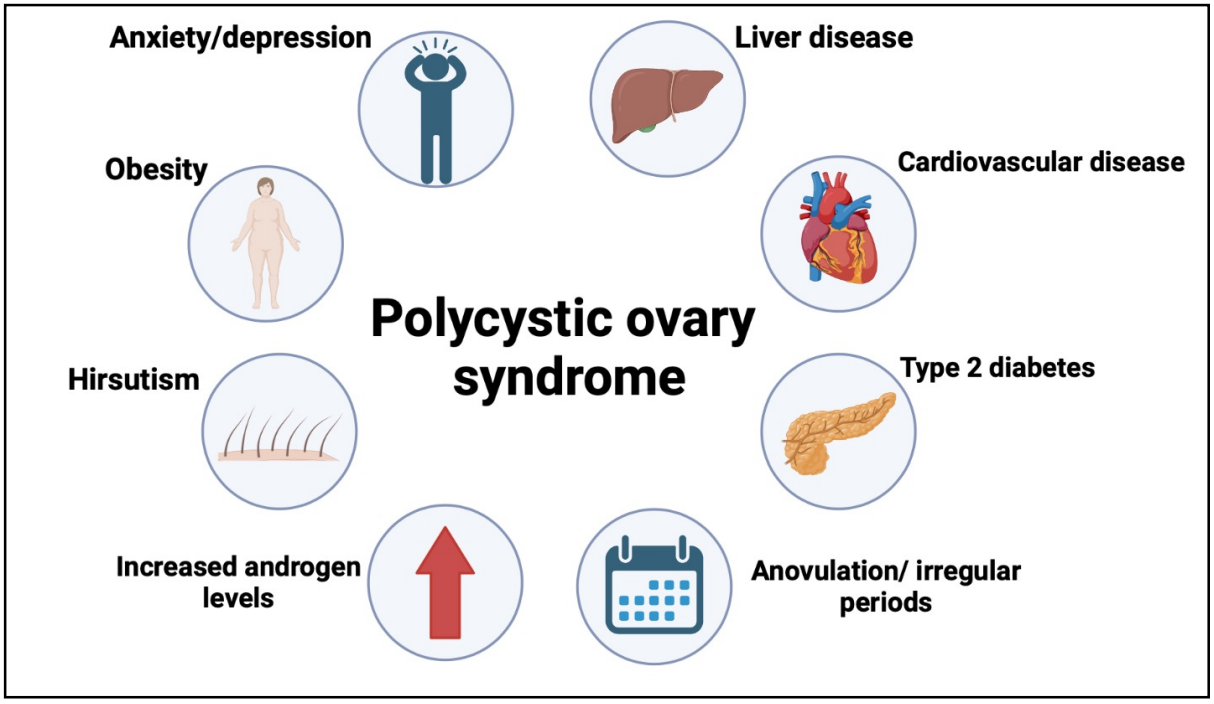

Figure 1.8 Symptoms and comorbidities of PCOS.

Currently, there is no known cure for PCOS and treatments therefore focus on suppression of symptoms [64]. Women are often grouped into two subcategories which treatment options are based on; those seeking fertility and those who are not

[64]. For women seeking fertility, therapies such as Clomiphene citrate (anti-oestrogen) and Letrozole (aromatase inhibitor) are considered first line treatments to induce ovulation and reduce risk of multiple follicle development [65]. For women who are not seeking fertility, treatment is often focussed on reducing circulating androgen levels. In such cases, the combined oral contraceptive is often recommended by gynaecologists [64]. The oral contraceptive pill is also often offered alongside anti-androgens [66]. However, these therapies do not address the underlying causes of PCOS, and most importantly, do not reverse them. Anti-androgens bind to the androgen receptor (AR) to block androgen binding but do not reduce circulating androgen levels [67]. Thus, anti-androgens and oral contraceptives do not reduce the levels of circulating androgens, a consideration that should not be ignored [36]. A treatment specifically designed to treat the cause of PCOS, by reducing circulating levels of androgens (from ovarian and peripheral androgen production), ergo addressing the vast clinical manifestations of PCOS that are induced by androgen excess such as obesity, anovulation, ovarian follicular development and insulin resistance is undeniably needed. Interventions to address androgen production are therefore extremely promising.

1.2.1.1. Diagnostic criteria

Although reports of PCOS can be traced back to the 5th century BC [68], gynaecologists Irving Ereller and Michael Levantal are considered to be the first clinicians to describe the syndrome, in 1935 [68]. They reported seven cases of women who exhibited menstrual disorders, hirsutism, infertility and enlarged ovaries [69, 70]. Despite this description, there was no formal diagnostic criteria for PCOS until 1990

[71]. The National Institute of Child Health and Human Development (NIH) sponsored a meeting between experts in medical and reproductive endocrinology, who voted on what diagnostic criteria should include [71]. The final verdict chosen, now known as the NIH criteria, was clinical and/or biochemical evidence of hyperandrogenism (HA), and ovulatory dysfunction, i.e., oligoovulation and/or anovulation (OD) [71, 72] **(Table 1.1**). Polycystic ovarian morphology (PCOM) was only deemed 'suggestive' of PCOS as, at the time, it was accepted that 20-30% of women with regular menstruation patterns and no evidence of hyperandrogenism, may also show PCOM [71, 72]. In 2003, the European Society for Human Reproduction and Embryology and the American Society for Reproductive Medicine (ASRM) introduced the Rotterdam criteria, which included PCOM as one of the main features [71] (**Table 1.1**). According to the Rotterdam criteria, women must present with at least two of three main features to receive a diagnosis [72, 73]. The aim of the Rotterdam criteria was to be more inclusive and the addition of PCOM increased the potential PCOS phenotypes from one to four (**Table 1.1**) [71]. Just three years later in 2006, the AE-PCOS criteria was developed by the Androgen Excess Society, who concluded that PCOS is fundamentally a disorder of androgen excess, and a clear diagnosis cannot be established without evidence of biochemical or clinical presentation of hyperandrogenism. The task force therefore decided that HA, in addition to OD and exclusion of other endocrine related disorders should be the diagnosis criteria [74, 75] (**Table 1.1**). In 2012, the NIH revised their original definition of PCOS and recommended the use of the Rotterdam criteria, providing phenotype assignment is specified at the time of diagnosis (**Table 1.1**) [71]. Depending on the diagnostic criteria used, the incidence of PCOS is subject to variation. According to the 2012 NIH criteria,

PCOS affects approximately 5-8% of women [71], although with the introduction of the Rotterdam criteria prevalence of PCOS this increased to 2-21% [76]. Based on AE-PCOS criteria, prevalence slightly reduces to 2-17% [76]. Nevertheless, PCOS is a significant problem amongst the female community.

Table 1.1 Diagnostic criteria for PCOS. Abbreviations: HA; hyperandrogenism, OD; ovulatory dysfunction, PCOM; polycystic ovarian morphology.

	National Institute of Health (1990)	Rotterdam (2003)	Androgen Excess PCOS society (2006)	National Institute of Health (2012)
HA	✓	✓	✓	✓
OD	✓	✓	✓	✓
PCOM	-	✓	-	✓
Number of criteria required	Both criteria required	Two of three required	Both criteria required, plus exclusion of other endocrine related disorders	Two of three criteria required, plus identification of phenotype at diagnosis

1.2.1.2. Measurement of hyperandrogenism

Biochemical HA is usually established by measurement of steroid biomarkers in serum or 24-hour urine (collection of urine over 24 hours) [77]. Due to the cost of steroid measurement in urine by gas chromatography-mass spectrometry (GC-MS), serum measurement of T by immunoassay or UHPLC-MS/MS is the most common method for HA identification [77]. The use of T as a marker for biochemical HA, however, is not ideal. T predominantly circulates bound to SHBG, and only the unbound fractions enter target tissue [77]. As a result, and due to intracrine activation/ inactivation, serum testosterone levels may not accurately reflect tissue levels. Investigations by Mick O' Reilly and team, who measured classic androgens in serum and adipose tissue of ten PCOS subjects, showed T and 5α-DHT, were significantly higher in adipose tissue in

PCOS subjects and BMI matched controls [36]. The question of which steroid should be measured to diagnose hyperandrogenism is still a matter of uncertainty between clinicians [78]. Arguments for the measurement of A4 in place of, or alongside measurement of T have been proposed, but A4 is still inconsistently measured due to uncertainty of its diagnostic value [77, 78]. There are studies, albeit limited, that suggest as many as 10% of PCOS patients are misclassified as normoandrogenic if A4 is not measured [77]. Measurement of DHEA and even DHEAS have also been proposed [78]. Therefore, understanding androgen metabolism and activation in target tissue, such as adipose and liver, is essential to establish new biomarkers of androgen excess, which may be classic androgen precursors, or 11-oygenated androgens.

1.2.1.3 Aetiology

Although PCOS is a condition that affects a large proportion of the female community, its aetiology is still not completely understood [79]. It is, however, well known that PCOS is an amalgamation of causative factors, with hyperandrogenism being the central link (**Figure 1.9**) [80].

In healthy women, LH, in synergy with FSH, is responsible for ovarian follicle growth and ovulation [81]. LH stimulates theca cells to produce androgens that are converted to oestrogen by the enzyme CYP19A1 [22, 82]. In women with PCOS, hyperandrogenism leads to the over production of LH, by disruption of the negative feedback loop responsible for LH secretion [80]. Elevated LH levels cause dysregulation of the hypothalamic–pituitary–ovarian (HPO) axis, which leads to an overabundance of gonadotropin releasing hormone (GnRH) [80]. GnRH is a hormone

that promotes the production of LH and FSH, but when in excess, stimulates the production of LH over FSH [80]. As a consequence of increased LH production, initiated by androgen excess, theca cells are subject to hyperplasia. This causes follicular arrest, resulting in the build-up of fluid filled follicles on the periphery of the ovary with characteristic pearl-like appearance [80]. Increased theca cell and follicular expression further serve to contribute to excess androgen production, repeating the above cycle [80]. Hyperandrogenism may also cause symptoms of PCOS via over production of Anti-Mullerian hormone (AMH) [80]. AMH is a hormone known to inhibit ovulation and development of ovarian follicles, causing follicular arrest [80]. Women with PCOS have been found to have 2-3-fold higher Increased AMH, a direct result of hyperandrogenism [80, 83]. Additionally, androgens have been shown to drive the early stages of follicle development yet are inhibitory to the later stages of follicle maturation, resulting in many early stage follicles and lack of ovulation in PCOS [84].

Insulin resistance, closely linked with hyperandrogenism, is not only a symptom of PCOS but also a major driver [80, 85, 86]. Although it is difficult to discern a causal relationship between hyperandrogenism and insulin resistance, due to each disorder exacerbating the other, it is thought that insulin resistance in PCOS can be induced by hyperandrogenism via reduction in the expression of glucose transporter 4 (GLUT-4), a key glucose transporter [80, 87]. Moreover, as the pancreas also express the AR [88], it has been reported that excess androgen levels in women with PCOS has a direct effect β cell function, leading to insulin resistance via β cell dysfunction (insulin hypersecretion) [89]. Androgen excess may also increase the abundance of skeletal muscle fibres which have minimal insulin sensitivity [80]. Insulin resistance stimulates

ovarian theca cells to produce androgens and also contributes to the overproduction of androgens in peripheral tissue such as adipose tissue, resulting in a cycle of androgen induced insulin resistance which further promotes hyperandrogenism, which in turn further induces insulin resistance [29, 90, 91]. A recent study identified a link between adipose tissue, androgen excess and insulin resistance [36] (**1.2.2**).

Due to the multi-faceted nature of PCOS, as demonstrated by the intertwined network of biochemical and neuroendocrine contributing factors, it is difficult to pinpoint causative factors of hyperandrogenism. Excess androgen biosynthesis by the ovaries and peripheral activation of androgen precursors are key contributors, although influencing factors may also be environmental, diet induced and/or genetic [80]. PCOS has been associated with familial clustering, and is therefore thought to have a significant genetic component [92]. AKR1C3, which is responsible for the conversion of inactive androgen precursors to active androgens (**1.1**), is thought to play a central genetic role. Polymorphisms of this enzyme have been associated with PCOS susceptibility and development [92]. Furthermore, polymorphisms in the gene encoding for sex hormone binding globulin (SHBG) have also been associated with hyperandrogenism [92, 93]. Mutations in *SHBG* gene lead to low circulating SHBG levels and therefore increase levels of circulating unbound, biologically active androgens [92].

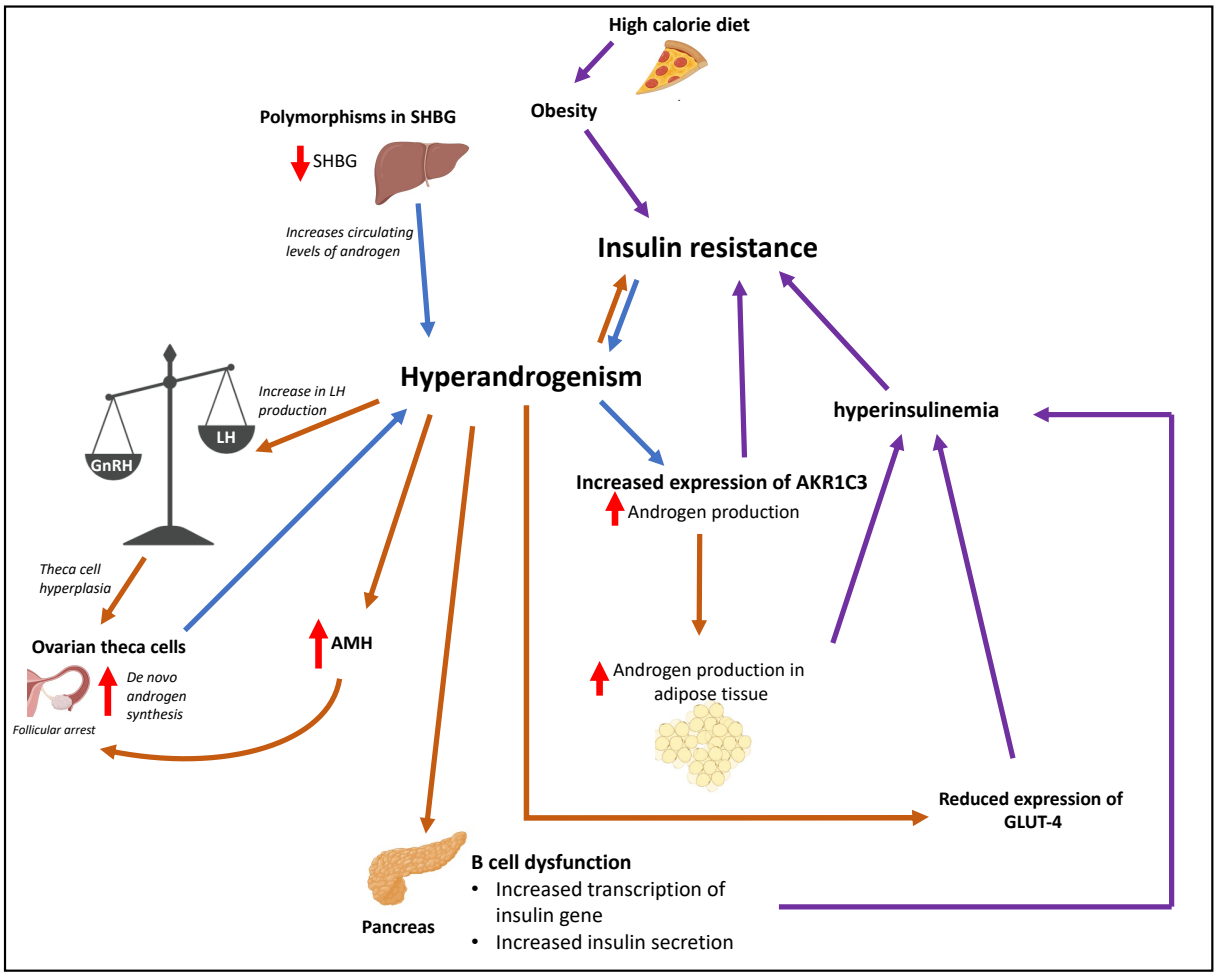

Figure 1.9 Hyperandrogenism induced factors contributing to PCOS.

1.1.1.4 Adverse reproductive and metabolic health outcomes in PCOS

PCOS has substantial adverse reproductive and metabolic health outcomes [57]. Due to its very nature, it is a major cause of infertility among women of reproductive age, but also manifests itself in a spectrum of co morbidities [94]. Based on the Rotterdam/2012 NIH criteria, PCOS can be subdivided into four phenotypes A - D, (**Table 1.1**) [61, 76, 94]. The type of phenotype a woman has, largely dictate the clinical manifestations she may experience, as described below [94, 95].

Phenotype A: known as ‘classic’ or ‘frank’ PCOS and is arguably the most symptomatically aggressive, when comparing associated risks. It is often termed ‘complete’ PCOS, due to the fact that it encompasses the three main features of PCOS (hyperandrogenism, PCOM, and ovulatory dysfunction) [76]. Women who have phenotype A, show the higher rate of menstrual irregularities, such as anovulation or oligo ovulation [76]. Women with this phenotype also show higher incidence of hirsutism (approximately 60-70%) [76]. Hirsutism is described as excessive hair growth in a male like pattern and is a direct result of hyperandrogenism [94]. Insulin resistance is also a risk factor that is increased with phenotype A PCOS [94, 95], affecting 35 to 85% of sufferers, independent of body mass index (BMI) and fat distribution [96]. Certain prospective population studies have shown women with phenotype A have an undesirable lipid profile, greater risk of atherogenic dyslipidaemia and obesity [96]. There is also increasing indication that women with phenotype A are more likely to suffer from MASLD, as a direct result of hyperandrogenism, compared to healthy controls [76, 94, 95].

Phenotype B: named ‘classic non-polycystic ovary PCOS [61], owing to the fact that women with this phenotype do not shown PCOM, only hyperandrogenism and ovulatory dysfunction [61, 96]. Adverse clinical health outcomes for phenotype B are similar to phenotype A, but less severe [76, 96]. Also symptoms may manifest themselves to a lesser degree of severity than phenotype A, women with phenotype B have distinct menstrual dysfunction, associated with increased risk insulin resistance, obesity, have greater BMIs and show significant increase in risk for MASLD [76, 95].

Phenotype C: often referred to as 'non-classic ovulatory PCOS' [95]. Women in this cohort exhibit hyperandrogenism and PCOM but have regular menstrual patterns [61, 76, 94, 95]. Interestingly, although this phenotype is also characterised by hyperandrogenism, serum androgen levels are more moderate and hirsutism, atherogenic lipids, obesity and insulin resistance are exhibited to a much lesser extent than for phenotypes A and B [95]. Prevalence of metabolic syndrome is still, however, greater than phenotype D [95].

Phenotype D: this phenotype is aptly termed 'non-hyperandrogenic PCOS' as women with this phenotype do not have elevated serum androgen levels but do display PCOM and ovulatory dysfunction [95]. They have mild insulin resistance, reduced risk of metabolic syndrome, lower LH and increased SHBG levels, compared to phenotypes A, B and C [76, 94, 95].

The prevalence of each phenotype differs between studies conducted in multiple regions of the world [95], however the general consensus is that phenotype A dominates, present in over 60% of cases [95, 96]. Remaining phenotypes B, C and D have similar prevalence, although phenotype D is the least frequent of the three [95-97].

1.2.2. Androgen excess, insulin resistance and dyslipidaemia

Insulin is a hormone released by the β-cells in the islets of Langerhans of the pancreas [98]. Insulin is secreted, primarily, in response to dietary glucose ingestion. A process named glucose-induced stimulation (**Figure 1.10**) [98]. Post secretion from β cells,

insulin circulates through the body via the bloods stream and binds to insulin receptors on target tissue, specifically skeletal muscle, liver tissue and adipose tissue and elicits a tissue specific response [98-100]. Insulin signal transduction pathways differ, depending on the type of tissue being stimulated. For example, in liver tissue, insulin promotes uptake of glucose and conversion to glycogen, whereas in adipose tissue, insulin stimulates glucose uptake, supresses lipogenesis and release of free fatty acids (FFAs) into circulation [99, 101]. Insulin resistance (IR) is described as defected biological response to insulin secretion in target tissues [102]. Naturally, it is often synonymous with hyperinsulinemia, due to the lack of glucose uptake in serum resulting in beta cells releasing more insulin as a compensatory response [102]. In women with PCOS, hypertrophy and hyperplasia of adipocytes, suppression of lipolysis and increase in *de novo* lipogenesis (DNL) in adipose tissue is related to insulin resistance [90, 103]. In states of insulin resistance adipocyte diameter can be up to 25% larger in women with PCOS, compared to non-insulin resistant women who do not have PCOS [103].

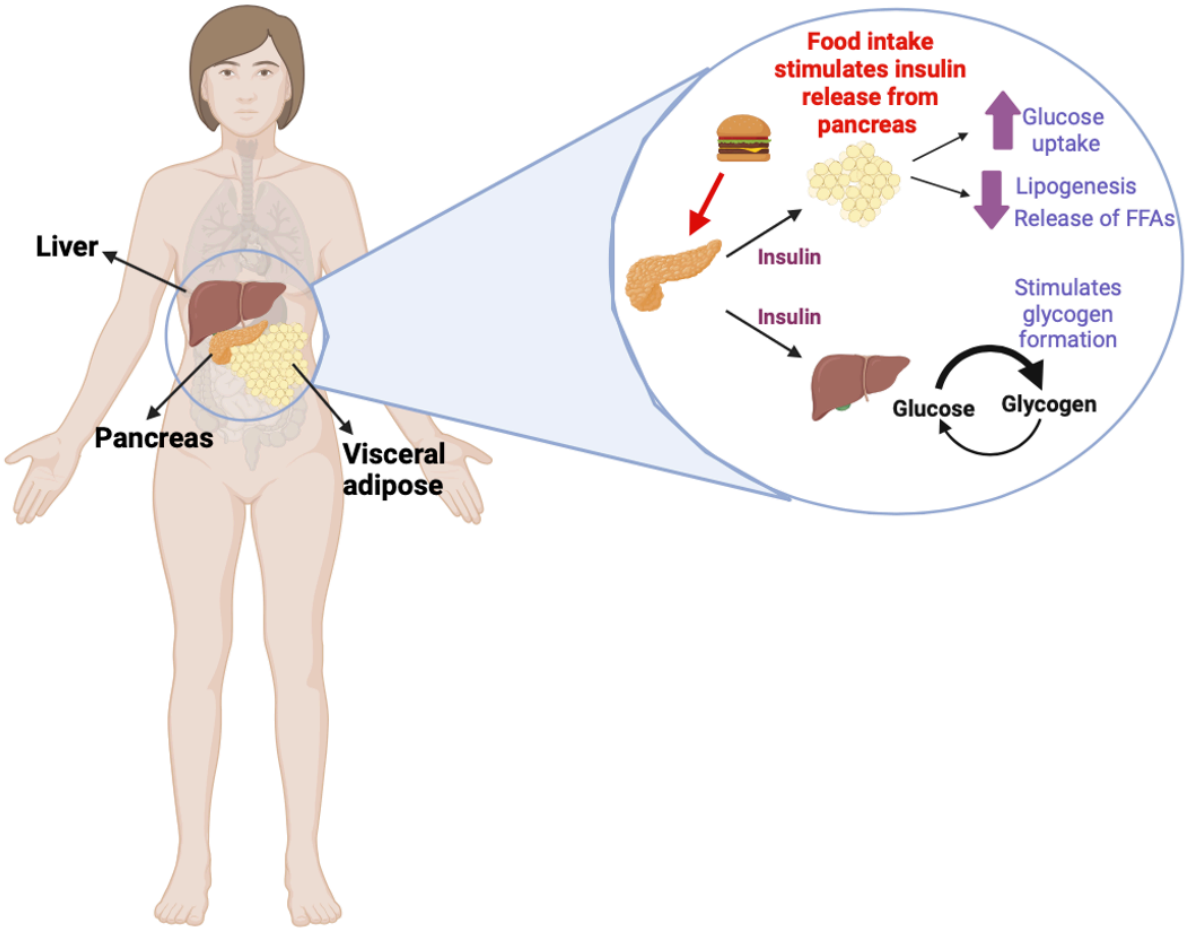

Figure 1.10 Insulin action in adipose and liver.

Previously, adipose tissue was merely viewed as a site for lipid storage [103]. We now know that adipose tissue can in fact be considered a complex metabolically active endocrine organ, due to its significant contribution to and regulation of endocrine processes [90, 103]. Comprised of multiple cell types, adipose tissue is responsible for numerous processes from regulation of glucose metabolism to secretion of signalling molecules that regulate metabolism, immune function and energy expenditure [103]. In PCOS, hyperandrogenism is heavily linked with adipocyte IR [36, 104]. Androgen excess in adipose tissue is especially associated with abdominal fat accumulation in

women with PCOS [104]. The enzyme AKR1C3 is key to understanding androgen excess in general, but specifically in adipose tissue. It is responsible for the conversion of inactive classic and 11-oxygenated androgen precursors, A4 and 11KA4, to their active androgen counterparts T and 11KT (**1.1**). AKR1C3 is widely expressed in adipose tissue and therefore a major contributor to androgen generation, driving IR [104]. Mick O'Reilly and team showed acute androgen exposure led to suppression of lipolysis *in vivo* and increased *in vitro* DNL [36]. They measured markers of lipid metabolism in women with PCOS and controls, post treatment with androgen precursor DHEA and found glycerol was reduced in PCOS patients compared to controls, coherent with reduced lipid mobilization [36]. They also confirmed androgen influence on adipocyte lipogenesis, using *in vitro* cell models and found treatment with testosterone and 5α-DHT, after 24 hours, increased the messenger RNA levels of acetyl-CoA-carboxylase, which is the rate limiting step in lipogenesis [36]. *In vitro* DNL increase was also observed during exposure to testosterone and 5α-DHT in the absence of insulin, confirming the androgen excess leads to lipogenesis independent of insulin resistance [36]. *In vivo* correlations between circulating testosterone and insulin levels, also supported the impact of androgens on IR. AKR1C3 expression is regulated by insulin [36, 104]. *In vitro* studies have conclusively shown a direct causal relationship between insulin and AKR1C3 expression. Simpson-Golabi-Behmel Syndrome (SGBS) cells (adipose tissue cell line model) and primary female subcutaneous adipocytes showed significant increase in AKR1C3 mRNA expression when exposed to elevated insulin levels [36]. Thus, in adipose tissue, there is a clear cycle occurring whereby overproduction of androgens by AKR1C3 is followed by lipid accumulation via decreased lipolysis and increased DNL. This causes systemic insulin

resistance and hyperinsulinemia, which leads to an increase in AKR1C3 expression, ergo further contributing to androgen excess [36]. The cycle continues in this manner (**Figure 1.11**) [36]. It is also important to note that the imbalances in lipolysis and DNL, leading to fat accumulation in adipose tissue, can lead to a fatty acid overspill and excess fatty acids forcibly stored in other tissue, particularly liver tissue (**1.3**) [36].

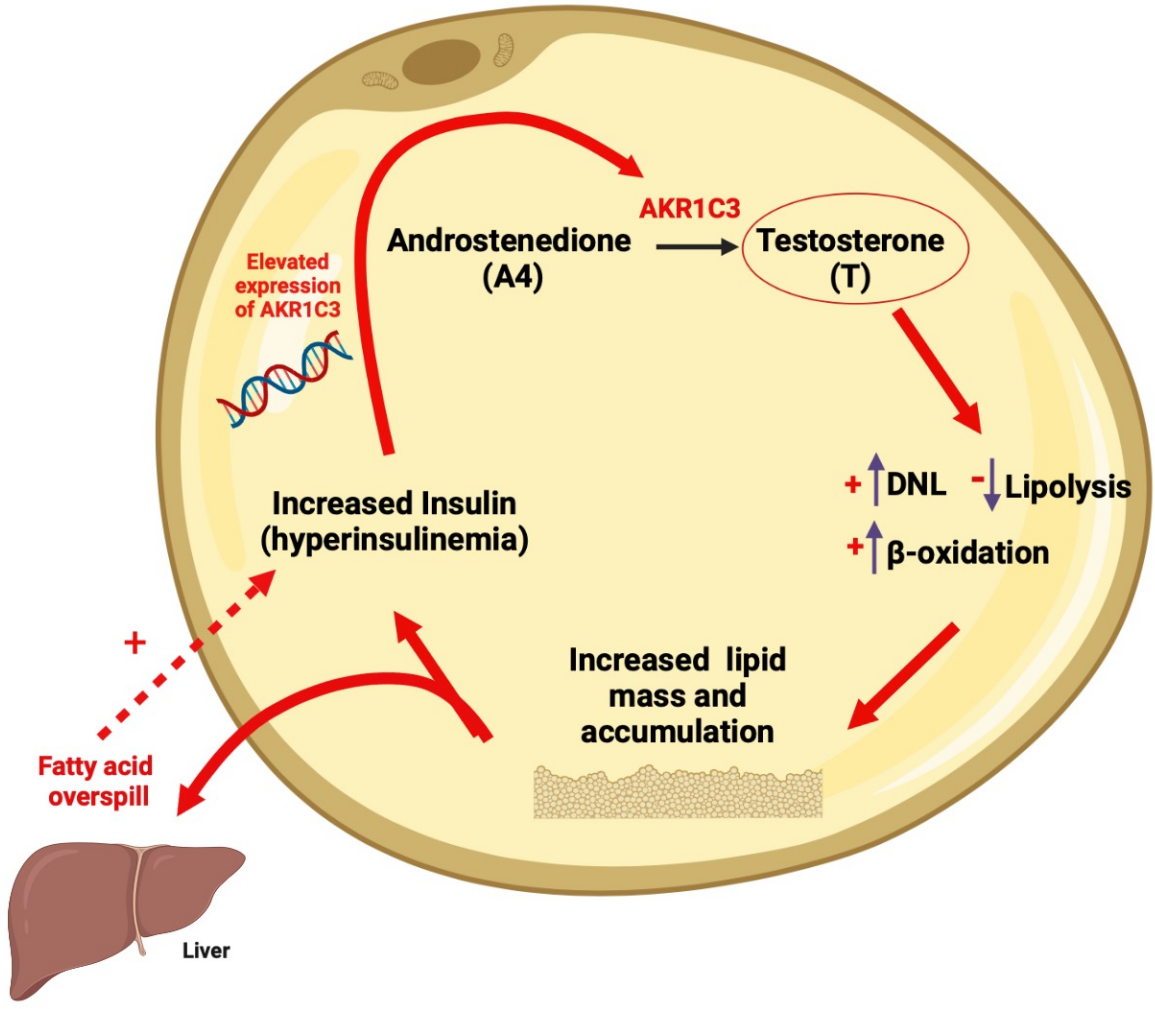

Figure 1.11 Schematic representation of the mechanistic relationship between androgen excess, insulin resistance and lipotoxicity in adipose tissue.

1.3. Androgen excess, metabolic dysfunction and metabolic associated steatotic liver disease

1.3.1. Metabolic associated steatotic liver disease and polycystic ovary syndrome

In recent years, there has been increasing evidence to suggest a direct link between PCOS and development of metabolic associated steatotic liver disease (MASLD), formally known as non-alcoholic fatty liver disease (NAFLD), until June 2023 [105, 106]. This link is thought to be a direct result of hyperandrogenism [105]. Research has shown that women diagnosed with PCOS are four times more likely to develop MASLD than women who do not suffer from the condition [106]. A retrospective longitudinal study compared incidences of MASLD in 63,120 women with PCOS and 121,064 age, BMI and location matched non-PCOS controls over a period of 16 years. Incidence rates of MASLD per 10, 000 person years in the PCOS cohort were 9.4, compared to 3.9 in the control patient cohort [105]. Serum testosterone and SHBG, was also assessed for 71,061 and 49,625, respectively. Significantly, women with increased testosterone levels (above 3 nmol/L, compared to reference 1 nmol/L) had a 2.4-fold increased hazard risk for MASLD (**Figure 1.12**) [105]. Since SHBG is a protein that binds to hormones, rendering them inactive, women with reduced levels of SHBG (below 30 nmol/L, compared to reference 60 nmol/L), had an almost 5-fold increase in risk for MASLD (**Figure 1.12**). Importantly, this increased risk for MASLD in PCOS patients was BMI independent, meaning obesity is not a defining factor in risk for MASLD in women with PCOS, but rather hyperandrogenism is the chief underlying contributor.

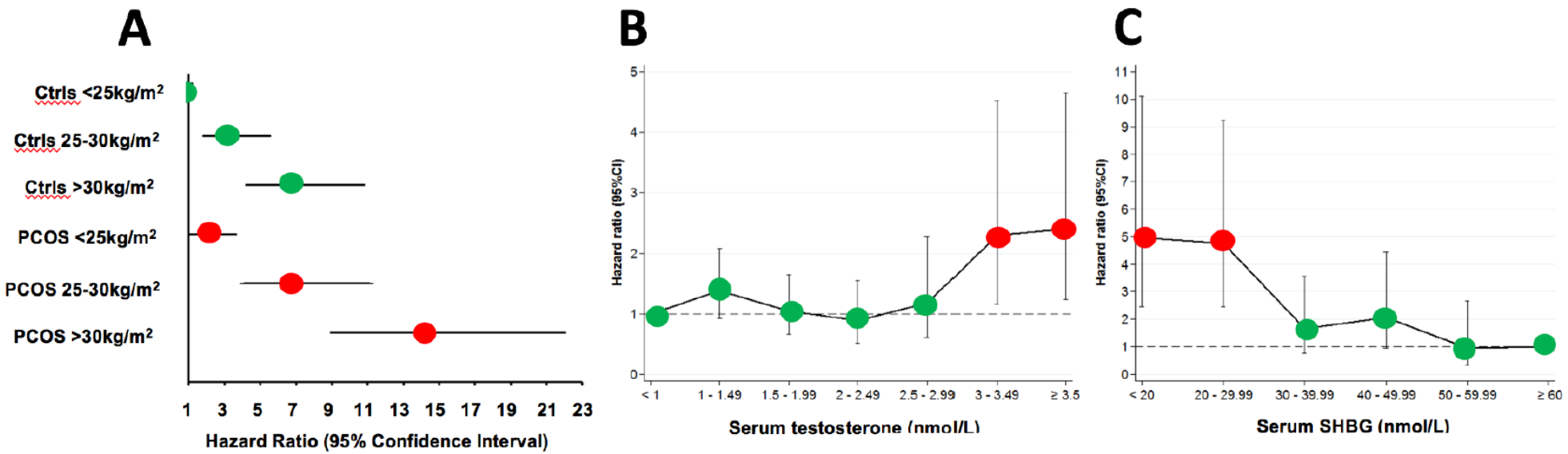

Figure 1.12 (A) Impact of BMI and polycystic ovary syndrome on the hazard for metabolic associated steatotic liver disease (B) Hazard of metabolic associated steatotic liver disease according to serum testosterone (C) Hazard of metabolic associated steatotic liver disease according to serum sex hormone binding globulin. (Adapted from [99]).

MASLD is also associated with risk for insulin resistance and due to the close link between MASLD, IR, diabetes, androgen excess and obesity, MASLD is often considered to be the hepatic manifestation of PCOS [36, 107, 108]. The links between MASLD and PCOS are so distinct, that MASLD is considered as a secondary disease of metabolic dysfunction, in conditions of hyperandrogenism such as PCOS [109]. So much so, that the previous name of NAFLD (used until just a few weeks ago) had been a matter of debate for many years, with many hepatologists believing this name was exclusionary and did not reflect the complex nature of the condition [86, 110, 111]. The name MASLD, developed by the American Association for the study of Liver Disease, has therefore now replaced NAFLD. MASLD is believed to reflect metabolic influences of the disease spectrum appropriately.

1.3.2. Metabolic associated steatotic liver disease

MASLD is an umbrella term that encompasses a series of progressive diseases, defined by excessive build-up of fat in the liver with the exclusion of other influences such as excessive alcohol intake, drug treatments or infection [107, 112]. It is the most common cause of liver disease in the western world, affecting approximately 25% of people in Europe, and 35% of people in the USA [107, 113]. Due to the continued rise in incidences of MASLD, and potentially fatal prognosis if later stages are reached, many hepatologists believe it will become of the most significant health issue of our time and the leading cause of liver transplantation in just 10-20 years [108].

MASLD is a spectrum of 4 major diseases, which are further separated into two sub groups; non-progressive and progressive [114] (**Figure 1.13**). Non-progressive

MASLD, known as liver steatosis, is characterised as excessive accumulation (>5%) of fat deposit in hepatocytes with the absence of inflammation or fibrosis, and often asymptomatic [112, 114]. It is the most benign disease on the spectrum and reversible if detected early [114]. The majority of patients with MASLD will present with steatosis, without further progression to later stages [114]. Progressive MASLD consists of metabolic dysfunction-associated steatohepatitis (MASH) formally known as non-alcoholic steatohepatisis (NASH), cirrhosis and hepatocellular carcinoma (HCC). Approximately 10-20% of those diagnosed with steatosis will progress onto MASH [115]. MASH is defined as inflammation of the liver, with sustained scarring and ballooning (cell enlargement) due to moderate fibrosis [116]. In 10-15% of patients diagnosed with MASH will progress to cirrhosis [117]. Cirrhosis is a result of prolonged inflammation and scarring, irreversible and can lead to blood flow blockages [114]. HCC is the final stage of MASLD and the most severe. It occurs in approximately 85% of patients diagnosed with cirrhosis and is characterised by the presence of cancerous tumours constituting more that 90% of the liver [118].

The early stages of MASLD are commonly associated with extra -hepatic co morbidities such as insulin resistance, type 2 diabetes mellitus, chronic kidney disease, obesity and cardiovascular disease [119]. Treatments for MASLD are therefore dependent on the stage of disease and accompanying co morbidities [120]. Pharmacological intervention is often reserved for patients who present with extreme fibrosis (later stages of MASH), although patients who present with early stages of MASLD (steatosis and early onset MASH), may be given treatments such as Pioglitazone, Vitamin E and the like to treat symptoms [120]. However, patients with

the least severe forms of MASLD are often encouraged to manage their symptoms with diet and lifestyle changes [120]. Due to the severe liver deterioration post cirrhosis and HCC, they typically can only be treated with liver transplantation [120].

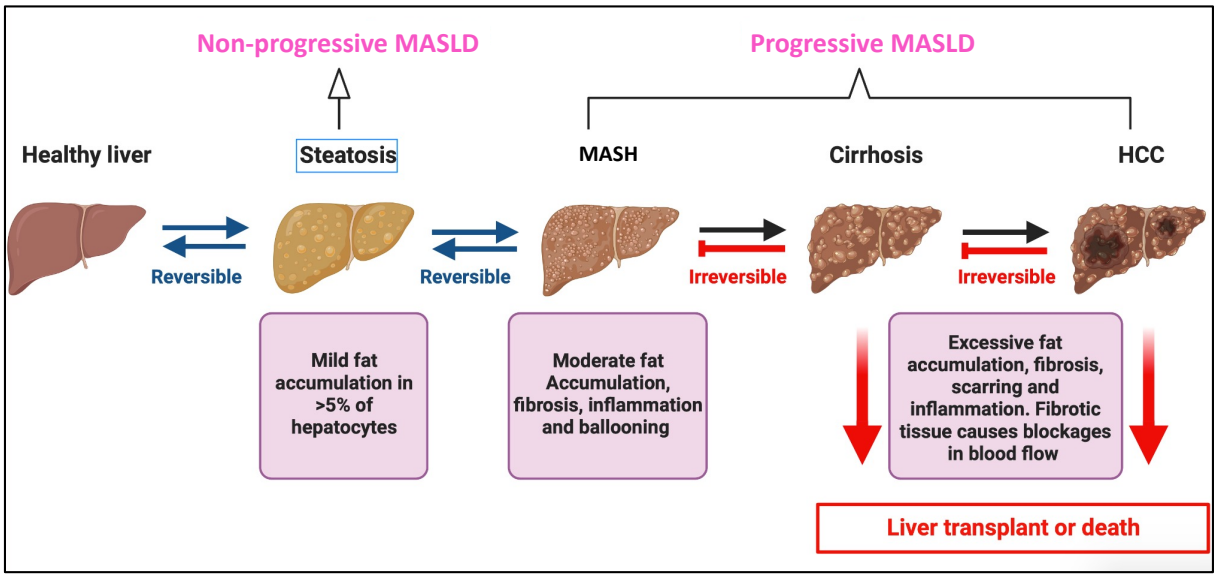

Figure 1.13 Stages of metabolic associated steatotic liver disease (MASLD).

1.3.2.1. Diagnostic criteria

Histologically, MASLD and alcohol induced liver disease are indistinguishable. Therefore, a diagnosis of MASLD can only be made in the absence of secondary causes such as excessive alcohol consumption, use of medications that lead to hepatic disease or hereditary disorders [107, 121]. Patient consumption of alcohol must be less than 20 g per day for women and less than 30 g per day for men [108, 115].

Liver biopsy is the gold standard method for detection and diagnosis of liver fat accumulation and damage [122]. Less invasive diagnostic methods include the use of ultrasound and magnetic resonance elastography [122]. Once a diagnosis has been made, histology is used to grade the extent of disease. Two grading systems are

currently used: the MASLD activity score (MAS) and the steatosis, activity and fibrosis (SAF) score [122]. The NAS is an assessment of three characteristics: steatosis, ballooning and inflammation [122]. According to severity, each characteristic receives a score between zero and eight. The final sum is then used to make a diagnosis [122]. A diagnosis of MASH cannot be made using the NAS alone, and it is recommended it is used to diagnose in conjunction with SAF. The SAF score is similar NAS but more extensive, as it is based on four characteristics: steatosis, ballooning, lobular inflammation and fibrosis. Each factor receives a score between zero and two, which is summed and used to classify disease stage [122].

1.3.2.2. Aetiology

In 1998, the 'two-hit hypothesis' for MASLD onset was proposed [123, 124]. This model described the initial onset excess lipid accumulation of fat in the liver (steatosis) as the 'first-hit', induced by metabolic syndrome, especially androgen induced IR [123, 124]. The fact that MASLD is first induced by metabolic syndrome, further fuels the hypothesis that MASLD is the hepatic manifestation of PCOS, in the same manner that obesity and dyslipidaemia can be seen as the adipose manifestation of PCOS. The progression of MASLD from steatosis to the more sinister stages is thought to require a 'second hit'. The 'second hit' involves a range of factors including oxidative stress, mitochondrial dysfunction, genetic factors and microbiome factors (**Figure 1.14**) [123-125]. In recent years, the 'two-hit' hypothesis has been replaced by the 'multiple hit' hypothesis, which was designed to give a more comprehensive, representation of the complex intertwining processes involved in MASLD. Although even in this model, the

key feature for initial MASLD development continues to be insulin resistance and hyperandrogenism [124].

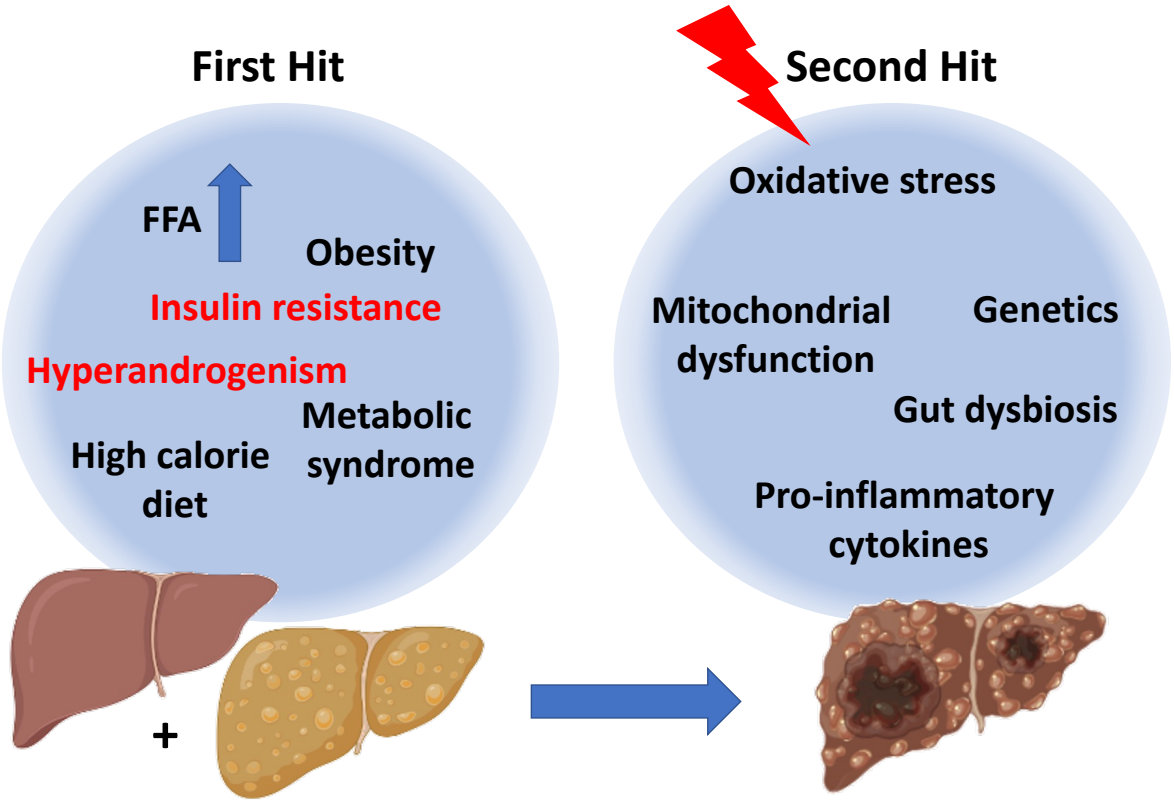

Figure 1.14 Two-hit hypothesis for MASLD onset.

1.3.2.3. Clinical presentation and adverse health outcomes

MASLD patients are often asymptomatic, meaning they can go undetected until disease progression reaches liver cirrhosis [109]. For the few patients that do show symptoms, complaints may be fatigue, enlargement of the liver, acanthosis nigricans, malaise or lipomatosis [108, 122]. As a result of minimal symptoms, MASLD is often only discovered during abdominal ultrasound during routine health check-ups or visits for other medical concerns [109]. Patients with MASLD do show an increased risk of

developing metabolic syndrome and therefore symptoms associated with conditions such as heart disease, overt diabetes, insulin resistance and obesity [109]. When later stages of MASLD are reached, such as cirrhosis a, symptoms and clinical manifestations become more apparent. Patients suffering from cirrhosis may experience ascites, pruritus, hepatic encephalopathy (HE), in addition to general pain, loss of appetite, depression, fatigue and anxiety [126]. Ascites (fluid accumulation between the abdominal lining and abdominal organs) is the most common symptom of cirrhosis and when in the early stages, can lead to a 50% chance of one year mortality [126]. When more aggressive, this increases to 75% chance of one year mortality [126]. HE is also a common clinical manifestation of cirrhosis, which is defined as a spectrum of neurological and psychological abnormalities [126, 127]. Patients with HE can expect sleep-wake cycle disturbances, disorientation, mood changes, problems concentrating and confusion [126, 127]. Patients with end stage HCC may present with a variety of symptoms and manifestations, including ascites and HE but also jaundice, abdominal masses, weight loss and most commonly, abdominal pain [118].

1.3.3. Androgen excess, insulin resistance and dyslipidaemia in liver disease

As with PCOS, the pathophysiology of IR concerning MASLD is not straightforward, and there are many influencing factors that seem to contribute to a vicious cycle involving insulin resistance, *de novo* lipogenesis in adipose and liver tissue, hyperandrogenism and excess dietary fatty acid intake, wherein disruption in the finely tuned system causes imbalances [128-130].

1.3.3.1. Hyperandrogenism and insulin resistance in liver

Hyperandrogenism and IR are principal risk factors in MASLD and often present together [131, 132]. Studies have shown that hyperandrogenism alone can lead to MASLD, presumably through aggravation of insulin resistance [131]. It is well known that chronic androgen excess in women can lead to insulin resistance and hepatic fat accumulation [133]. Links between IR Hyperandrogenism are also evidenced by studies that show lower levels of SHBG, accompanied by high levels of key androgen testosterone, increase risk for MASLD [105].

Importantly, this link between androgen excess and insulin resistance is only found in women, specifically women with PCOS [133]. A recent study found 12-week exposure to DHT led PCOS-like mice to develop androgen induced hepatic steatosis, increased lipid deposition and inflammation, as well as obesity and insulin resistance [131]. *In vitro* and *in vivo* studies conducted by Andrisse *et al.* have shown deletion of liver specific ARs, prevented DHT induced insulin resistance and restored insulin sensitivity in liver specific AR knockout mice [134]. Since androgen excess and IR are key for both MASLD and PCOS, there is a clear relationship between the two disorders. However, the mechanisms by which MASLD and PCOS are tied remain unclear [131]. Local androgen activation in target tissue is a key contributor to circulating androgens levels, as shown by Mick O'Reilly in adipose tissue [36]. However, the local activation of androgens in the liver has not been investigated, which, considering the contribution of hyperandrogenism to MASLD onset, can no longer be overlooked. It is therefore vital to comprehensively understand androgen metabolism in liver, which may lead to the elucidation of the direct involvement of such tissue in androgen excess, and

subsequent identification of more appropriate biomarkers to establish androgen excess, particularly in disorders of female androgen excess, and importantly, to identify suitable targets for the reduction of local androgen activation.

1.3.3.2. Hyperandrogenism, insulin resistance, adipose tissue and hepatic dyslipidaemia

Hyperandrogenism may play a role in MASLD indirectly through adipose tissue [36]. In healthy individuals, FFAs are predominantly generated in adipose tissue [128, 135]. FFAs released into the blood stream from adipose tissue are up taken by liver and undergo ß-oxidation, to be fluxed out as low-density lipoprotein, incorporated into complex lipids or stored locally in hepatocytes as intracellular lipid droplets [128, 135]. During androgen induced insulin resistance, lipid generation in adipose is increased as a result of upregulated DNL and reduced lipolysis [36]. Clearance by ß-oxidation or lipid incorporation cannot compensate for the overwhelming influx of FFAs, resulting in accumulation of FFAs in hepatocytes by hepatic storage [36, 120, 130, 135]. Excess hepatic storage of FFAs, and subsequent steatosis onset, further aggravates hepatic insulin resistance which also further aggravates hepatic DNL, causing the cycle to continue [120, 128]. Recent studies, using stable isotopic labelling, have shown that in individuals with MASLD on a calorie deficit diet, 60% of triacylglycerols were synthesised from circulating FFAs. This suggests that excess fatty acid accumulation in the liver is most likely sourced from adipose tissue [129]. Adipose tissue can be considered an endocrine organ, that also secretes a group of hormones known as cytokines [136]. Of these cytokines, adipokines, such as adiponectin are of special interest when it comes to adipose tissue, insulin resistance and MASLD. Adiponectin

is responsible for the regulation of fatty acid oxidation and inhibition of lipid accumulation in the liver. Moreover, it regulates insulin sensitivity in liver tissue. Studies have shown that patients with MASLD, show reduced serum adiponectin levels, which is associated with androgen induced insulin resistance [36, 136].

1.4. Normothermic machine liver perfusion

1.4.1. Principles of Normothermic machine liver perfusion

This thesis established normothermic machine liver perfusion (NMLP) as a tool to study androgen metabolism. NMLP is an *ex situ* tool that is mainly used to assess liver viability prior to transplantation and as an alternative preservation method to static cold storage (SCS), which can cause severe ischaemia-reperfusion injury in livers with steatosis [137, 138]. As introduced in **1.3.2**, patients with irreversible end stage liver disease are treated with liver transplantation [138]. However, whilst the number of patients waiting to receive a donor continues to rise, the number of livers deemed suitable for transplantation remains alarmingly low [138]. This has created a large need for viable livers, worsened by the fact that many donor livers are discarded for reasons such as being too old or too fatty [139]. NMLP aims to reduce severity of reperfusion injury and therefore expand the donor pool [138, 140]. The principle of NMLP is to mimic the physiological environment of the liver *in vivo* [139]. [138]. During NMLP, the liver is maintained and physiological temperatures (37 ºC) and the hepatic artery, portal vein and bile duct are cannulated (**Figure 1.15**) [141]. The liver is perfused with perfusion fluid, which usually consists of either packed red blood cells or a bovine haemoglobin oxygen carrier, supplemented with nutrients (such as glucose and insulin) and additional agents to prevent occurrences of thrombosis, cellular oedema

and free radical injury [139]. Two centrifugal oxygenator pumps provide oxygen to perfusate and circulate perfusate through the circuit. NMLP therefore facilitates the continuation of liver metabolic functions, and assessment of liver health in real time [141]. Assessment parameters include lactate consumption, oxygen consumption, bile production and blood flow resistance [141]. NMLP also has other applications for the study of liver physiology. One such application includes the evaluation of 'defatting cocktails' to reverse liver steatosis [142]. Using NMLP, Boteon and team treated five fatty livers, discarded for transplantation, with a cocktail of drugs and compared tissue triglyceride levels to five non-treated controls. They showed that, in comparison to the control group, the 'drug cocktail treated group, tissue triglyceride levels reduced by 38%, expression of marker for oxidative injury were down regulated, liver shown enhanced urea production, lower vascular resistance and higher production of bile [142]. Another application of NMLP is metabolic profiling. Bral and team looked at the metabolism of transaminases (graft injury markers), added to the perfusate circuit, over a period of 48 hours [143].

NMLP is emerging as an encouraging investigative tool for the assessment of liver physiology. It not only provides a promising technique the addition of exogenous compounds to the liver, but also maintains liver metabolic functioning. For this reason, this thesis established NMLP as a tool to study androgen metabolism, by the addition of classic and 11-oxygenated precursors A4 and 11KA4 to the perfusion circuit. Initial investigations using NMLP identified substantial endogenous androgen generation, and for this reason [$^{13}C_3$]-labelled A4 and 11KA4 precursors were used.

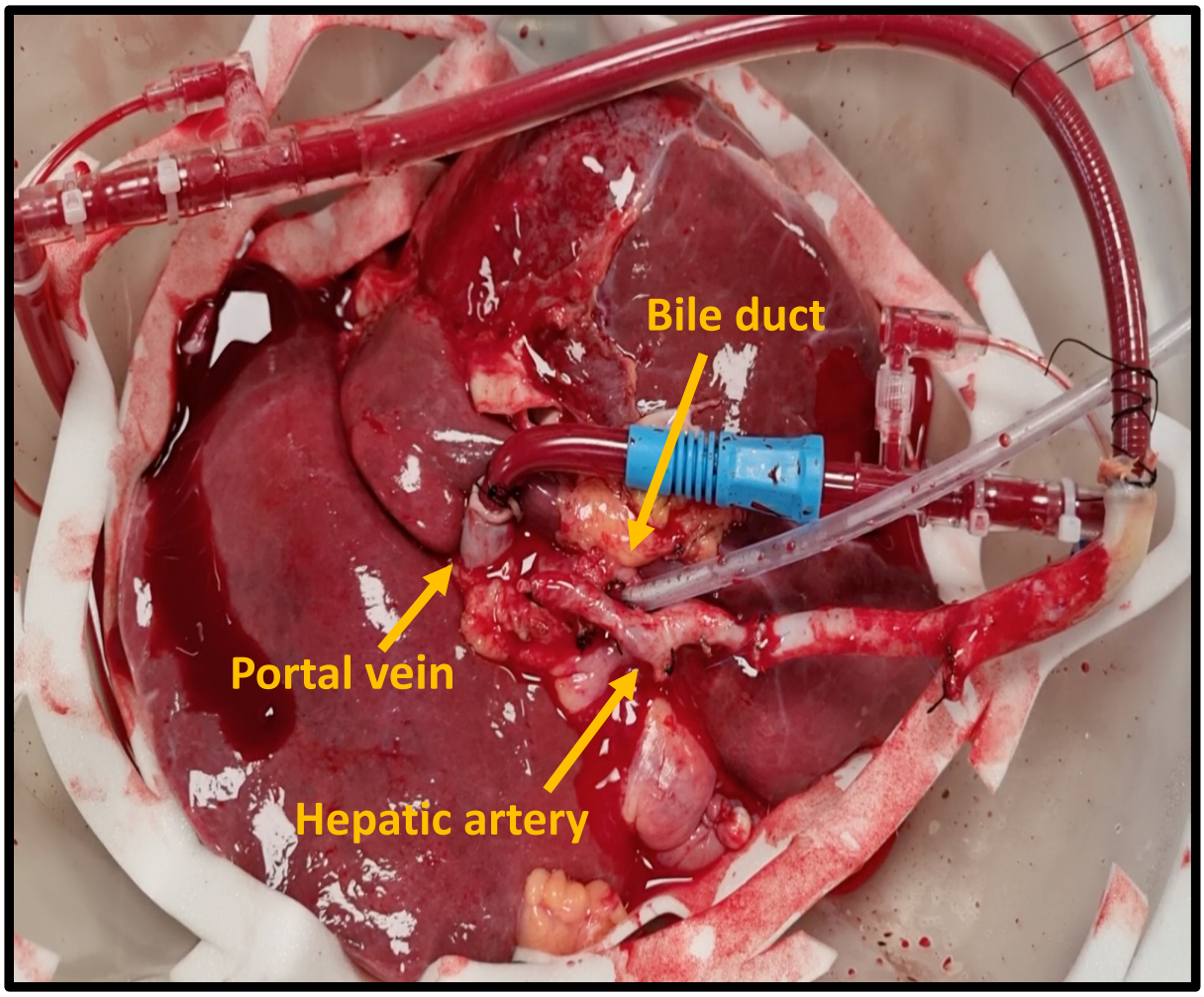

Figure 1.15 Liver during normothermic machine liver perfusion (NMLP).

1.5. Conclusions and research aims

1.5.1. Conclusions

In conclusion, adipose and liver are key sites of androgen action, linking androgen excess and systemic metabolic health. Adipose tissue is a key mediator of classic and 11-oxygenated androgen activation via the steroidogenic enzyme AKR1C3. In conditions of hyperandrogenism, such as PCOS, androgen generation in adipose is a major driver, leading to adverse effects on lipid handling such as obesity, dyslipidaemia and insulin resistance. The role of AKR1C3 in classic androgen activation in adipose tissue is well established, but its contribution to 11-oxygenated androgen remains to

be established. The contribution of 11-oxygenated androgens to the androgen pool is significant. Studies measuring serum androgens levels have shown, unlike classic androgens, 11-oxygenated androgens do not decline with age in women and are the predominant circulating androgens in women with PCOS [144, 145]. Additionally, the active 11-oxygenated androgens 11KT and 11K-5α-DHT, are just as potent as classic androgens T and DHT. Given that 11OHA4 is a major 11-oxygenated androgen released from the adrenal gland and is converted to more active metabolites than classic precursors in peripheral tissue, an in-depth analysis of the local activation and inactivation of these androgens will provide a strong framework for the mechanisms by which female androgen excess impacts on adipose tissue. Furthermore, as AKR1C3 plays such a central role in adipose androgen activation, inhibition of this enzyme may prove to be a promising therapeutic for the significant reduction in both classic androgen and 11-oxygenated peripheral activation. The development of MASLD in women as a consequence of androgen excess has been well established. However, the metabolic profile of classic and 11-oxygeneated androgens in the liver has not yet been explicitly explored. The importance of local androgen activation has been highlighted, and thus, an in-depth analysis of the local activation and inactivation of these androgens will provide a strong framework for the mechanisms by which female androgen excess impacts on fat accumulation in the liver. Elucidation of androgen metabolism in the liver will also serve to uncover the possible synergistic relationship between adipose and liver as metabolic target tissues.

The separation and measurement of androgens is often conducted using LC-MS/MS. However, the characterisation of androgens from multiple pathways is an analytical

challenge, that has not previously been addressed. To comprehensively investigate multiplex androgen metabolism in the liver, a new LC-MS/MS method developed for androgen analysis only, is required.

1.5.2. Research aims

Taking the above into account, this thesis aimed to answer the following questions:

1) Is it feasible to develop an accurate and efficient UHPLC-MS/MS method for multi-androgen profiling?

An assay for multi-androgen profiling for a panel of seventeen classic and 11-oxygenated androgens was developed. This method was developed by characterising chromatographic separation, retention times, characterising ionisation and MRMs. The assay underwent method validation to confirm accuracy and precision. MRMs were also adapted to accommodate for the quantification of [$^{13}C_3$]-labelled metabolites.

2) What is the activity of AKR1C3 in female adipose tissue, and what is the impact of AKR1C3 inhibition on classic and 11-oxygenated androgen levels?

Sub aim 1:

To investigate androgen metabolism, women undergoing elective gynaecological surgery were recruited to donate omental and subcutaneous adipose tissue. The project employed primary human adipose tissue incubations as an *ex vivo* tool and liquid chromatography tandem mass spectrometry to profile the metabolism of classic and 11-oxygenated precursors in adipose tissue.

Sub aim 2:

AKR1C3 is the crucial enzyme for the activation of both classic and 11-oxygenated androgens and hence potential drug target for the reduction of androgen excess and associated metabolic complications in PCOS. This project established the effect AKR1C3 inhibition on androgen metabolism in a Human Embryonic Kidney 293 (HEK293) cell line model with over expression of AKR1C3, and in adipose *ex vivo* incubations. Two AKR1C3 inhibitors were provided through collaboration with the pharmaceutical company BAYER.

3) What is the metabolic profile of classic and 11-oxygenated androgens in the liver?

To answer this question, the project employed primary liver tissue incubations. Primary tissue, as well as normothermic machine perfusion of whole livers was used to assess the metabolic activity of the liver in real time. Normothermic machine liver perfusion is an *ex vivo* tool primarily used to assess liver viability for transplantation and was established in this project as a novel model to study steroid metabolism. Livers were perfused with precursor steroids including classic and 11-oxygenated androgen precursors and their metabolism was profiled by LC-MS/MS.

CHAPTER 2

GENERAL METHODS

2.1 Steroid measurement by ultra-high performance liquid chromatography-tandem mass spectroscopy (UHPLC-MS/MS)

2.1.1 Preparation of external and internal standards

All androgens were acquired as powders from Makaira Limited (London, UK), Sigma-Aldrich (Gillingham, UK) and/or Steraloids (Newport, USA), (**Table 2.1**). Stock solutions of each androgen were prepared at 1 mg/mL in UHPLC methanol (Biosolve, Dieuze, France). These stock solutions were combined and diluted to make 0.1 mg/mL (stock 2) and 0.01 mg/mL (stock 3) solutions in 50 % (vol/vol) UHPLC grade methanol/ UHPLC grade water (Biosolve, Dieuze, France). Calibrators for each analyte, ranging from 0 to 100 ng/mL, were prepared using stock 2 and stock 3 in a matrix that matched the matrix of the sample. For this thesis, the sample matrix was either cell culture media, hemopure or serum (for serum samples, the matrix for calibrators was substituted with 0.1% bovine serum albumin in phosphate buffer saline). Internal standards used for each androgen were acquired as powders (**Table 2.1**) and prepared in deuterated methanol and 1 mg/mL. A combined internal standard mixture (1 μg/mL) of each internal standard was prepared in 50 % (vol/vol) UHPLC grade water/ UHPLC grade methanol. In cases where a stable isotope labelled analyte was not available, the internal standard with the closest retention time, ionisation and extraction characteristics to the analyte of interest was used for quantification.

Deuterated isotope labelled steroids used were DHEA-d6, A4-d7, T-d3, 5α-DHT-d3, An-d4, Et-d5, 3α-adiol-d3, 11KA4-d10, 11βOHA4-d7, 11KEt-d10 and 11KT-d3.

Table 2.1 Suppliers of standards, [^{13}C]-labelled standards and deuterium labelled internal standards.

Androgen Trivial name	Chemical nomenclature	Androgen abbreviation	Supplier of androgen and catalogue #	Internal standard selected for quantification	Supplier of internal standard and catalogue #
Dehydroepiandrosterone	5-androstene-3β-ol-17-one	DHEA	Sigma-Aldrich D4000	DHEA-d6	Sigma-Aldrich 709549
Androstenedione	4-androstene-3,17-dione	A4	Sigma-Aldrich 46033	A4-d7	CDN Toronto Research Chemicals D5305
[$^{13}C_3$]-Androstenedione	4-androstene-3,17-dione-1,2,3-[$^{13}C_3$]	[$^{13}C_3$]-A4	Qmx IS9044/10	A4-d7	CDN Toronto Research Chemicals D5305
Testosterone	4-androstene-17β-ol-3-one	T	Sigma-Aldrich T6147	Test-d3	Sigma-Aldrich T2655
5α-dihydrotestosterone	5α-androstane-17β-ol-3-one	5α-DHT	Sigma-Aldrich A8380	5α-DHT-d3	Cerilliant D077
5α-androstanedione	5α-androstane-3,17-dione	5α-dione	Steraloids A1630	5α-DHT-d3	Cerilliant D077
Androsterone	5α-androstane-3α-ol-17-one	An	Steraloids A2420	An-d4	IsoSciences 14235
Etiocholanonlone	5β-3α-hydroxy-androstan-17-one	Et	Makaira Limited	Et-d5	IsoSciences 14319
Androstanediol	5α-androstane-3α,17β-diol	3α-adiol	Sigma-Aldrich D4000	3α-Adiol-d3	Sigma-Aldrich 908258
11β-hydroxyandrostenedione	4-androstene-11β-ol-3,17-dione	11βOHA4	Sigma-Aldrich A3009	11OHA4-d7	Cambridge Isotope Labs DLM-9697
11β-hydroxytestosterone	4-androstene-11β,17β-diol-3-one	11βOHT	Steraloids A5760	11OHA4-d7	Cambridge Isotope Labs DLM-9697
11β-hydroxyandrosterone	11β-hydroxyandrost-4-ene-3,17-dione	11βOHAn	Steraloids A1330	11KEt-d5	CDN Isotopes D-5626
11β-hydroxy-5α-androstanedione	5α-androstane-11β-ol-3,17-dione	11βOH5α-dione	Steraloids A2660	11KEt-d5	CDN Isotopes D-5626
11β-hydroxyetiocholanolone	(5β)-3α-hydroxy-androstan-11β-ol-17-one	11βOHEt	Steraloids A3120	11KEt-d5	CDN Isotopes D-5626

[$^{13}C_3$]-11-ketoandrostenedione	4-androstene-3,11,17-trione-1,2,3-$^{13}C_3$	[$^{13}C_3$]-11KA4	Toronto Research Chemicals A305602	11KA4-d10	Toronto Research Chemicals A305604
11-ketoandrostenedione	4-androstene-3,11,17-trione	11KA4	Sigma-Aldrich 284998	11KA4-d10	Toronto Research Chemicals A305604
11-ketotestosterone	4-androstene-17β-ol-3,11-dione	11KT	Steraloids A6720	11KT-d3	IsoSciences 16144
11-ketoetiocholanolone	(5β)-3α-hydroxy-androstan-11,17-dione	11KEt	Steraloids A3460	11KEt-d5	CDN Isotopes D-5626
11-ketoandrosterone	5α-androstane-3α-ol-11,17-dione	11KAn	Steraloids A2280	11KEt-d5	CDN Isotopes D-5626
11-keto-5α-dihydrotestosterone	5α-androstane-17β-ol-3,11-dione	11K-5α -DHT	Steraloids A2375	11OHA4-d7	Cambridge Isotope Labs DLM-9697
11-keto-5α-androstanedione	5α-androstane-3,11,17-trione	11K-5α-dione	Steraloids A2900	11KEt-d5	CDN Isotopes D-5626

2.1.2 Sample preparation

Solid phase extraction (SPE)

As steroids can be conjugated to either glucuronides or sulphates in circulation [9] (**Chapter 1**), steroid conjugates within collected samples were enzymatically hydrolysed by sulfatase Helix Pomatia, in order to measure the combined concentrations of conjugated and unconjugated steroids.

For solid phase extraction, the sample volume was 500 µL. Samples and calibrators were transferred to a 96-well plate (Porvair, Hampshire, UK) and treated with 20 uL of internal standard mixture, containing all internal standards (**Table 2.1**). Samples were treated with 500 µL of helix pomatia mixture (2.2 mg/mL sulfatase and 3.3 mg/mL Sodium L-ascorbate) in sodium acetate buffer (0.2 M, pH 5) and incubated for three hours at 60°C. This enzymatically deconjugated the steroids from their glucuronide and sulphate esters. Steroids were extracted using a C_{18} solid phase extraction column (100 mg, 16.9 % carbon, 53 µm particle diameter, 68 Å pore diameter, Biotage, Uppsala, Sweden). The column was activated with 1 mL of UHPLC grade methanol and washed with 1 mL of UHPLC grade water, after which 800 uL of sample and buffer mix was loaded onto the column. The loaded column was washed with an additional 1 mL of UHPLC grade water and finally androgens were eluted in 800 uL UHPLC grade methanol, into a 96 well plate (Porvair, 2 mL, no glass inserts). The eluate was then evaporated at 60 °C under a stream of nitrogen. The dried extracts were stored at -20 °C for UHPLC-MS/MS analysis at a later date or reconstituted in 200 µL 50 % (vol/vol) UHPLC grade water and UHPLC grade methanol for immediate UHPLC-MS/MS analysis.

Liquid-Liquid extraction

Androgens were extracted from 200 µL of sample, which was added to hexamethyldisilazane (HMDS) treated thin layer chromatography (TLC) tubes. Samples were treated with 10 uL of internal standard mixture and vortexed at 800 rpm for 5 minutes. Steroids were extracted using 1 mL of methyl tert-butly ether (MTBE). Post addition of MTBE, samples were vortexed for 10 minutes at 1500 rpm and incubated for 30 minutes at 24°C for separation of lower aqueous phase and upper organic MTBE phase. The steroid/organic MTBE fraction was transferred to a 96-well plate (Porvair, 2 mL, no glass inserts) and solvent was evaporated at 60 °C under a stream of nitrogen. Following solvent evaporation, the dried extracts were stored at -20 °C for UHPLC-MS/MS analysis at a later date or reconstituted in 200 µL 50 % (vol/vol) UHPLC grade water and UHPLC grade methanol for immediate UHPLC-MS/MS analysis.

2.1.3 Chromatographic separation

This thesis employed two UHPLC methods. Method (1) was developed and optimised as part of this project for the ex vivo liver model sample analysis (**Chapter 3**), and method (2) was a previously validated UHPLC method designed for serum multi-steroid analysis [55].

Method 1:

Chromatographic separation of androgens and internal standards was achieved by a H-class Waters Acquity ultra high performance liquid chromatography system with a 50 µL loop (UHPLC; Waters Ltd, Wilmslow, UK) using a Phenomenex Luna Omega column, polar C_{18}, 50 x 2.1 mm, 100 Å, 1.6 µm (Phenomenex, Macclesfield, UK) at 60

°C. Volume of reconstituted sample was 10 µL. Mobile phase A was comprised of UHPLC grade water containing 0.1 % formic acid (vol/vol) and mobile phase B comprised of UHPLC grade methanol (Biosolve). Mobile phase B percentage was increased from 45 % to 70 % over 4 minutes, with a flow rate of 0.6 mL/min, proceeded by a wash step with 95 % mobile phase B until 4.2 minutes and equilibration at starting gradients from 4.5 minutes until the injection of the next sample. Ammonium fluoride was infused post-column at a concentration of 6 mmol/L 50 % (vol/vol) UHPLC water/ UHPLC methanol and at a flow rate of 5 µL/min. Total run time was 5 minutes. The auto sampler was maintained at 10 °C.

Method 2 [55]:

Chromatographic separation of androgens and internal standards was achieved using the system described above, with changes to the chromatographic gradient. Mobile phase A was comprised of UHPLC grade water containing 0.1 % formic acid (vol/vol) and mobile phase B comprised of UHPLC grade methanol (Biosolve). Mobile phase B percentage was increased from 45 % to 75 % over 5 minutes, with a flow rate of 0.6 mL/min, proceeded by a wash step with 95 % mobile phase B until 5.2 minutes and equilibration at starting gradients from 5.5 minutes until the injection of the next sample. Ammonium fluoride was infused post-column at a concentration of 6 mmol/L 50 % (vol/vol) UHPLC water/ UHPLC methanol and at a flow rate of 5 µL/min. Total run time was 6 minutes. The auto sampler was maintained at 10 °C.

2.1.4 Tandem mass spectrometry

The UHPLC elute was directed into a XEVO TQ-XS mass spectrometer (Waters Ltd) where steroids were ionised using electrospray ionisation in positive ion mode, with a capillary voltage of 4.0 kV, source temperature of 150 °C and a desolvation temperature of 600 °C. Gas flow and cone gas was sustained at 1200 L/h and 150 L/h, respectively. Multiple reaction monitoring (MRM) was used for analyte detection. For each steroid a molecular ion was designated and 2 mass transitions (**Table 2.2**). Quantifier mass transitions were used to quantify each analyte, and qualifier mass transitions were used to confirm correct identification of analyte. Selection of quantifier transitions were chosen according to the transitions that showed highest peak area. Target Lynx software was used for androgen quantification. The peak area of the analyte relative to the peak area of internal standard (peak area of analyte/peak area of internal standard) was plotted against the nominal concentrations of each calibrator. A linear least square regression curve was used to quantify analyte concentrations.

Table 2.2 Quantifier and qualifier mass transitions, cone voltages and collision energies of each analyte and internal standard.

Steroid	Quantifier transition	Cone voltage (kV)	Collision energy (eV)	Qualifier transition	Cone voltage (kV)	Collision energy (eV)
A4	287.1 > 96.9	42	18	287.1 > 108.9	42	22
T	289.1 > 96.9	26	20	289.1 > 108.9	26	24
5α-DHT	291.1 > 255.0	38	16	291.1 > 159.0	38	22
5α-dione	289.1 > 271.0	28	16	289.1 > 96.9	28	16
An	291.1 > 273.2	12	8	291.1 > 255.2	12	16
Et	291.1 > 255.0	16	12	291.1 > 273.1	16	8
3α-adiol	275.0 > 257.1	38	10	275.0 > 148.8	38	10
11βOHA4	303.1 > 285.2	34	14	303.1 > 267.1	34	16
11βOHT	305.2 > 269.2	16	14	305.2 > 121.1	16	20
11βOHAn	307.1 > 271.1	2	10	307.1 > 289.2	2	8
11βOH5α-dione	305.1 > 269.0	32	14	305.1 > 96.9	32	28
11βOHEt	307.0 > 270.8	2	10	307.0 > 253.2	2	8
11KA4	301.1> 120.6	24	22	301.1 > 90.5	24	46
11KT	303.1 > 120.6	48	26	303.1 > 90.5	48	50
11KEt	287.0 > 229.2	36	16	287.0 > 269.0	36	16
11KAn	305.1 > 287.2	26	10	305.1 > 269.1	26	12
11K5α-DHT	305.0 > 104.9	28	32	305.0 > 287.0	28	14
11K5α-dione	303.0 > 285.1	38	14	303.0 > 108.9	38	20
[$^{13}C_3$]-A4	290.1 > 99.9	20	20	290.1 > 111.9	20	20
[$^{13}C_3$]-T	292.1 > 99.9	48	22	292.1 > 111.9	48	24
[$^{13}C_3$]- 5α-DHT	294.1 > 258.1	42	14	294.1 > 161.9	42	22
[$^{13}C_3$]-5α-dione	292.1 > 274.0	34	16	292.1 > 99.9	34	26
[$^{13}C_3$]-An	294.1 > 276.2	12	8	294.1 > 258.2	12	16
[$^{13}C_3$]-Et	294.1 > 258.0	12	12	294.1 > 276.1	12	6
[$^{13}C_3$]-3α-adiol	278.1 > 260.1	28	10	278.1 > 95.8	28	28
[$^{13}C_3$]-11βOHA4	308.1 > 288.2	34	14	308.1 > 270.1	34	16

[$^{13}C_3$]-11βOHT	308.2 > 272.2	16	14	308.2 > 124.1	16	20
[$^{13}C_3$]-11βOHAn	310.1 > 292.2	2	10	310.1 > 274.1	2	8
[$^{13}C_3$]-11βOH5α-dione	308.1 > 272.1	32	14	303.1 > 99.9	32	28
[$^{13}C_3$]-11βOHEt	310.0 > 273.8	2	10	310.2 > 256.2	2	8
[$^{13}C_3$]-11KA4	304.1 > 123.6	24	22	304.1 > 93.5	24	46
[$^{13}C_3$]-11KT	306.1 > 123.6	48	26	306.1 > 93.5	48	50
[$^{13}C_3$]-11KEt	290.0 > 232.2	36	16	290.0 > 272.0	36	16
[$^{13}C_3$]-11KAn	308.1 > 290.2	26	10	308.1 > 272.1	26	12
[$^{13}C_3$]-11K5α-DHT	308.0 > 107.9	28	32	308.0 > 290.0	28	14
[$^{13}C_3$]-11K5α-dione	306.0 > 288.1	38	14	306.0 > 111.9	38	20
Internal standard	**Quantifier transition**	**Cone voltage (kV)**	**Collision energy (eV)**	**Qualifier transition**	**Cone voltage (kV)**	**Collision energy (eV)**
11KT-d3	306.2 > 262.1	20	22	306.2 > 124.1	20	22
11KEt-d5	292.0 > 274.1	4	18	292.0 > 292.1	16	10
A4-d7	294.1 > 108.9	42	22	294.1 > 96. 9	42	18
Test-d3	292.1 > 108.9	26	24	296.1 > 96.9	26	22
DHEA-d6	295.1 > 259.0	28	12	295.1 > 219.0	28	14
DHT-d3	294.1 > 258.1	22	16	294.1 > 159.1	22	22
Et-d5	296.1 > 260.0	12	12	296.1 > 220.0	16	12
Adiol-d3	278.0 > 151.8	38	10	278.0 > 80.0	38	10
An-d4	295.1 > 277.2	24	12	295.1 > 259.7	24	12

2.2 Androgen metabolism in Human embryonic cell line 293 (HEK293) cells overexpressing steroid-metabolizing enzymes

2.2.5 Human embryonic kidney 293 (HEK293) culture

HEK293 cells were cultured in minimal essential medium (MEM) (Sigma Aldrich, Cambridge, UK), supplemented with 2 mM L-glutamine, 100 Units/mL Penicillin, 100 ug/mL streptomyocin and 2.5 mg/dL fetal bovine serum (Sigma Aldrich, Cambridge, UK) at 37 °C, 5% CO_2. Cells were grown in T-75 flasks (Fisher Scientific, Loughborough, UK) and the medium was routinely changed every 2-3 days. Cells were grown to 80-90% confluency prior to cell passage, as assessed by a light optical microscope, 10X magnification. The supplemented media was removed, and cells were washed with 5 mL sterile phosphate buffered saline (PBS), before incubation with 3 mL sterile 0.25 % (w/v) Trypsin- Ethylene Diamine Tetra Acetic Acid (EDTA) (Fisher Scientific, Loughborough, UK) and incubated at 37°C for 2 minutes to allow the cell monolayer to detach from the flask. Cell detachment was confirmed by light optical microscope. Cells displayed a rounded morphology and free-floating in cell culture medium. Trypsin-EDTA was deactivated by addition of 6 mL growth medium to the flask. Cells were pelleted by centrifugation at 25°C (3 minutes, 1200 RPM). The supernatant was discarded, and the cell pellet resuspended in 4-10 mL of growth media, depending on cell confluency and desired split ratio (between 1:4 and 1:10). 1 ml of the cell suspension was then seeded in T-75 flasks and incubated once more at 37 °C and 5% CO_2. Cells were cultured up to a maximum of 20 passages.

2.2.2 DNA Transfection of HEK293 cells

Transfections were conducted in T-75 flasks and 12-well plates. The plasmid construct pcDNA3_AKR1C3 was a gift from Prof. J. Adamski (Helmholtz Zentrum München, Germany). The plasmid construct pCMVXL4_AKR1D1 was a gift from Jeremy Tomlinson, (University of Oxford, UK). The plasmid construct pcDNA3.1_AKR1C2 was purchased from GenScript (New Jersey, USA). The plasmid pCMV7_SRD5A2, pCMV7_SRD5A1 were gifts from Prof. D.W. Russell (UT Southwestern Medical Centre, Dallas, USA). The plasmid constructs pcDNA3.2_H6PDH and pcDNA3_11BHSD1 were gifts from Prof. K. Chapman (University of Edinburgh, UK). The total amount of plasmid DNA used for T-75 flasks was 23 ug and 1 ug/well for 12 well plates. For co-transfection, plasmid DNAs was added in a 1:1 ratio.

T-75 flask: Growth medium was removed from flask and cells were washed with PBS, as described above, before fresh medium was added to the flask. Transfection mixture was made up in a 1:3 ratio of DNA to Fugene HD Transfection reagent (Promega, madison, USA). Desired volume of DNA (calculated according to concentration of DNA plasmid in ng/µL) was added to a separate tube. 69 µL of transfection reagent was also added to the tube. Total volume was made up to 1173 µL using phenol red free MEM medium supplemented with 100 units/mL penicillin, 100ug/mL streptomyocin and 2 mM L-glutamate. The DNA mixture was incubated for 5 – 10 minutes at 24 °C. The DNA mixture was added dropwise to the T-75 flask, using a p1000 micropipette. Cells were then left to incubate at 37 °C and 5% CO_2 for 24 hours, prior to use in experiments.

12-well plate (each well): HEK293 cells were plated at a cell density of 0.5 X 10^6 cells/well in 1 mL of growth medium and left to incubate 37 °C and 5% CO_2 for 24 hours. Post incubation, growth medium was removed from the wells and replaced with fresh growth medium. The transfection DNA mixture was made up in a 1:3 ratio of DNA to Fugene HD Transfection reagent. 1 ug plasmid DNA and 3 µL transfection reagent was added to a separate tube. The total volume was made up to 50 µL using phenol red free MEM medium, supplemented with 100 units/mL penicillin, 100ug/mL streptomyocin and 2 mM L-glutamate. The transfection mixture was then incubated for 5 – 10 minutes at 24 °C. The mixture was then added dropwise to the well, using a p1000 micropipette. Cells were then left to incubate at 37 °C and 5% CO_2 for 24 hours, prior to use in experiments.

2.2.3 AKR1C3 activity assay in transiently transfected HEK293 cells

HEK293 cells were transfected with 23 µg of the plasmid pcDNA3_AKR1C3 in a T-75 flask, as described above. After 24 hours of incubation, cells were assessed for viability by trypan blue exclusion test and live cells were counted. Cells were plated (0.5 X 10^5 live cells/well) in 48-well plates and incubated for an additional 24 hours (37 °C and 5% CO_2). Growth medium was replaced with 250 µL of phenol red free MEM, containing 100 nmol/L of either A4 or 11KA4, from 1 mg/mL stock solutions in methanol, with or without the AKR1C3 inhibitors BAY1128668 (BAY1), consisting of a steroidal core structure or BAY2299242 (BAY2), consisting of a non-steroidal 'next generation' core structure, in dimethyl sulfoxide (DMSO). Final concentrations of DMSO and methanol (MeOH) were kept constant at 0.1% and 0.003%, respectively, in all assay treatments. Additional cell-free incubations of all treatments and vehicle-

treated cells (DMSO and/or MeOH in medium) were prepared as controls. 200 µL of medium was collected at specific time points after the start of the incubation and stored in HMDS treated glass test tubes at 4 °C until liquid-liquid extraction for androgen analysis by UHPLC-MS/MS. The results were normalised to the amount of total protein in the respective well. Each biological replicate was performed as four technical replicates for each treatment. IC_{50} values for inhibitors were calculated by Prism 9 non-linear regression curve fit algorithm.

2.2.4 Total protein quantification from cultured cells

Total protein was quantified for each well at the end of the AKR1C3 activity assay for normalisation of the activity data. Cell lysis was achieved by addition 25 µL of passive lysis buffer (0.2 % (vol/vol) Trition X-100, 10 % glycerol, 3 % TPE, 0.008 % EDTA in distilled water) to each well. After 1 freeze/thaw cycle, the protein concentration in the lysates was determined using DC Protein Assay (Bio-Rad, Hertfordshire, UK). The assay was performed in a 96-well microtiter plate, according to the manufacturer's instructions. Briefly, five standard dilutions between 0 to 1.25 mg/mL of bovine serum albumin (BSA) in lysis buffer, were prepared. 10µL of cell lysate and bovine standards were added to a 96 well plate before 200 µL of dye reagent was added to each well. The plate was incubated at 24 °C for 5 minutes and absorbance was measured at 750 nm. The absorbance for standards was plotted against their known concentrations to create a linear regression curve. The slope intercept of the regression curve was then used to calculate the total protein concentration in each cell.

2.2.5 Generation of [^{13}C] labelled androgen standards using HEK293 cells

Due to reduced commercial availability and cost of [^{13}C]-labelled metabolites, we could not acquire all labelled downstream metabolites that were required as standards for the LC-MS/MS assay. To overcome this issue, HEK293 cells were used to generate each [^{13}C]-metabolite by a series of sequential transfections. pcDNA3_AKR1C3, pc CMVXL4 _AKR1D1, pcDNA3.1_AKR1C2, pCMV7_SRD5A2 pCMV7_SRD5A1, pcDNA3.2_H6PDH and pcCR3_11βHSD1 transfection, were staggered sequentially by 24 hours, to generate each [^{13}C]-labelled classic and 11-oxygenated metabolite (**Figure 2.1 and Figure 2.2**). Initially, cells were plated and transfected with required plasmid DNA in 12 well plates, as described above in section **2.2.2**. Growth media was removed, and cells were treated with 1 mL phenol red free MEM medium, containing 5 µmol/L [$^{13}C_3$]-A4 or [$^{13}C_3$]-11KA4. Each biological replicate was performed as three technical replicates. Following 24-hour incubation, conditioned media was collected and carried over to cells transfected with the appropriate enzyme for generation of subsequent downstream metabolite. This process was followed to generate all metabolites, as outlined in **Figure 2.1 and 2.2**. Aliquots (200 µL) were collected at each stage for UHPLC-MS/MS analysis.

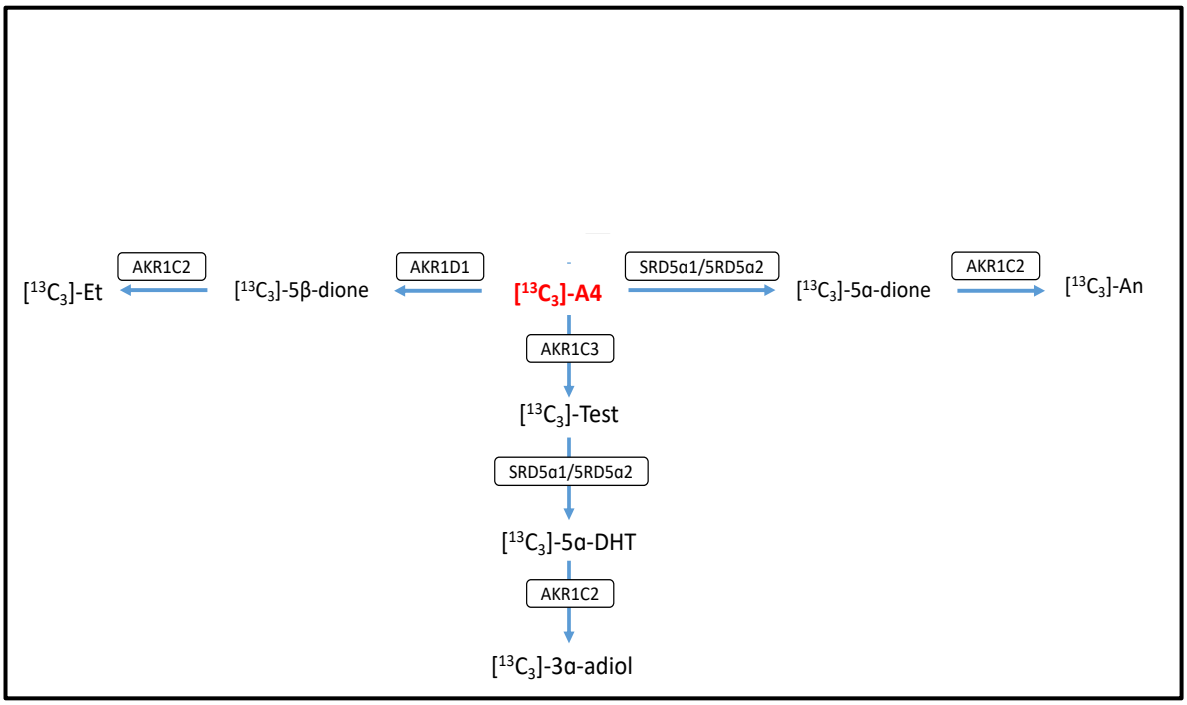

Figure 2.1 Generation of classic [$^{13}C_3$]-labelled androgen metabolites from [$^{13}C_3$-A4].

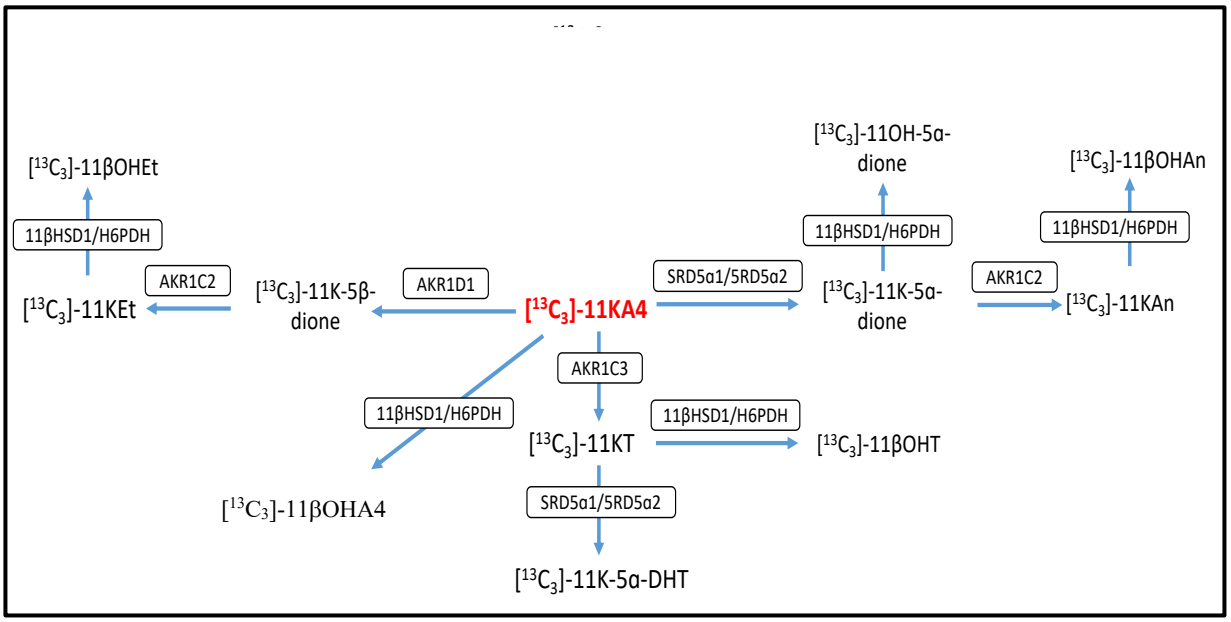

Figure 2.2 Generation of 11-oxygenated [$^{13}C_3$]-labelled androgen metabolites from [$^{13}C_3$-11KA4].

2.3 Androgen metabolism in an *ex vivo* adipose model

Freshly resected female human subcutaneous and omental adipose tissue was collected suspended in Dulbecco's Modified Eagle Medium/Ham's F-12 nutrient mixture (DMEM/ Ham's F-12) supplemented with 100 units/mL penicillin, 100 µg/mL streptomycin, 33µM Biotin and 17µM Panthotenic acid and transferred to the lab at room temperature. Tissue was washed in PBS and 100-200 mg tissue pieces were diced into four smaller equal pieces. Tissue was then suspended in DMEM/ Ham's F-12, supplemented with 100 units/mL penicillin, 100 µg/mL streptomycin, 33µM Biotin and 17µM Panthotenic acid, containing 100 nmol/L of either A4 or 11KA4 with or without the AKR1C3 inhibitor BAY2. Androgen stocks were provided as 1 mg/mL stocks in MeOH and diluted as required in medium. Final concentrations of DMSO and MeOH were kept constant at 0.1% and 0.003%, respectively, in all assay treatments. Additional cell-free incubations of all treatments and vehicle-treated cells (DMSO, MeOH and/or BAY2 in medium) were prepared as controls.

Treated tissue was incubated in a HI-200 hybridisation incubator at 37 °C and rotated at 20 rpm for 24 hours. 1 mL of medium was collected after 24 hours. Medium samples were centrifuged for 10 minutes (4000 rpm, 4°C), transferred to a sterile Costar 1.7 mL low binding snap cap minicentrifuge tubes and stored at -80 °C for liquid-liquid extraction.

2.4 Androgen metabolism in an ex vivo liver model

Whole liver was preserved in Wisconsin fluid, in ice, for transportation to the laboratory. The liver was then cut into slices and transferred Dulbecco's Modified Eagle Medium (DMEM) at 4º C prior to processing. Tissue was subsequently washed in PBS and 300-

400 mg of tissue was diced into four smaller equal cubes. Diced tissue was then suspended in Williams E medium, supplemented with 100 units/mL penicillin, 100 µg/mL streptomyocin, 2 mM L-glutamate and containing 100 nmol/L of either DHEA, A4, T, 11OHA4, 11OHT, 11KA4 or 11KT. Additional cell-free incubations of all treatments and vehicle-treated cells (MeOH in medium) were prepared as controls. Treated tissue was incubated in a HI-200 hybridisation incubator at 37 °C and rotated at 20 rpm for 48 hours. Androgen stocks were provided as 1 mg/mL stocks in MeOH and diluted as required, in medium. 1 mL of medium was collected at different timepoints over the 48-hour period. Medium samples were centrifuged for 10 minutes (4000 rpm, 4 °C), transferred to a sterile Costar 1.7 mL low binding snap cap minicentrifuge tubes and stored at -80 °C for solid phase extraction.

2.5 Androgen metabolism in a normothermic machine liver perfusion model

2.5.1 Device preparation procedure

NMLP procedures were carried as previously described [146]. The device of choice was a Liver Assist (Groningen, the Netherlands), which has a semi-closed circuit, using two rotary pumps, to provide simultaneous perfusion of the hepatic artery and portal vein [146] (**Figure 2.3**). Liver was transported to the lab on ice, in Wisconsin fluid, at hypothermic temperatures. Livers was subsequently washed in ice water and cleaned of any unwanted tissue. The hepatic artery, portal vein and bile duct openings were cannulated with 20 Fr Medos cannulae and flushed with 2 L of 10% dextrose solution at 37°C. The Organ Assist device was primed with approximately 2 L of perfusion fluid. The contents of which are outlined in **Table 2.3**. The liver was then situated inside the device reservoir and cannulae were connected to the perfusion circuit. Perfusion

temperatures and pressures were set manually. Arterial pressure was maintained between 50-60 mmHg, while portal vein pressure was maintained between 8-10 mmHg. Flow rates and resistances were monitored in real-time, using the device display, every 30-60 minutes throughout the duration of the perfusion. Target flow rate was 0.25 mL/min/g liver tissue for hepatic artery and 0.75 mL/min/g liver tissue for the portal vein. Target flow rates were achieved by adjustment of perfusion pressures, as required. Perfusion temperature was maintained at 37°C. Oxygen supply was maintained at >10 kPa in the arterial circuit. Liver viability was assessed by blood-gas analysis (Cobas b 221, Roche Diagnostics, Indianapolis, USA) of arterial and venous perfusion fluid. Assessed parameters were pO_2 and pCO_2, pH, O_2 saturation, haemoglobin, chloride, calcium, sodium, haematocrit, bicarbonate, glucose and lactate levels. Pre-perfusion weight of the liver was recorded.

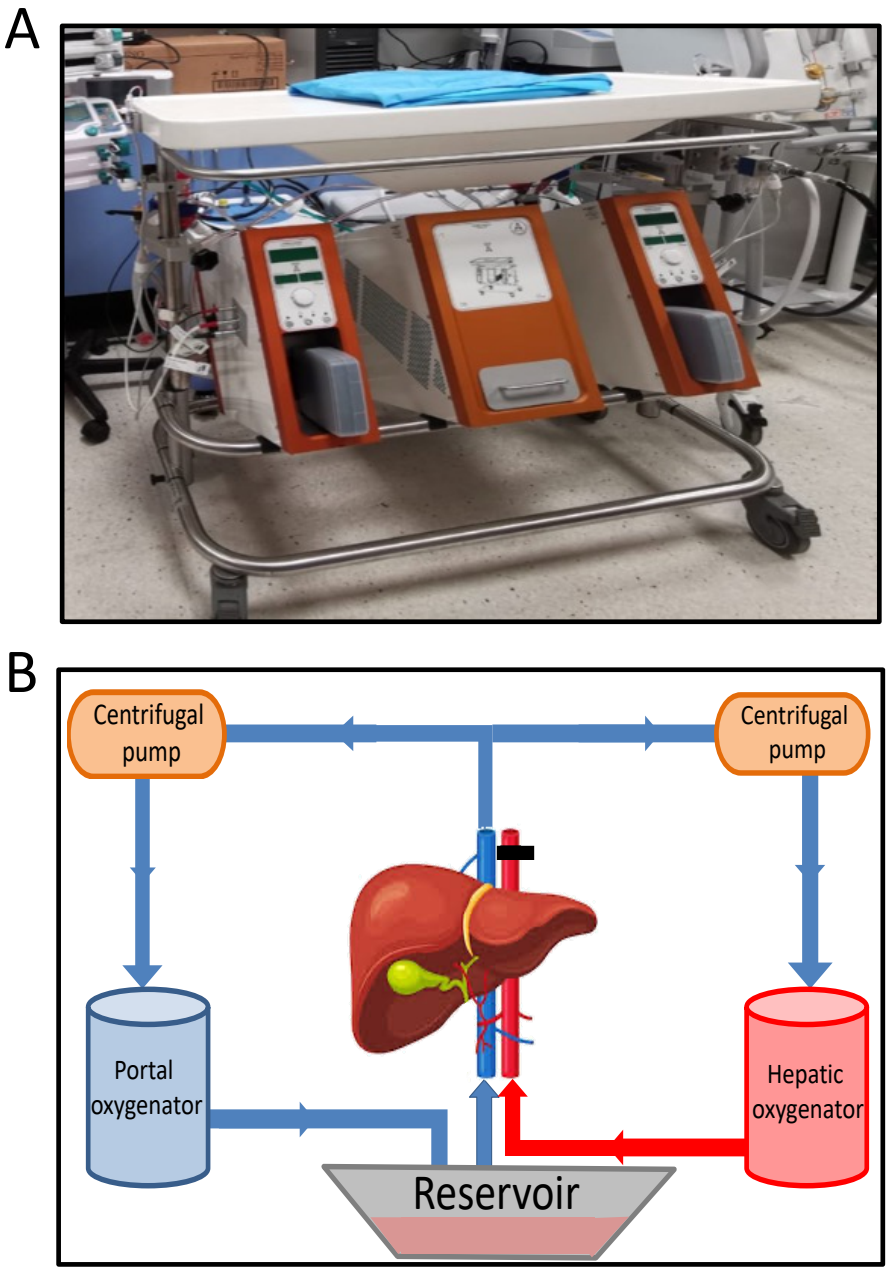

Figure 2.3. (A) Liver Assist NMLP device (B) Schematic representation of the perfusion circuit.

Table 2.3 Perfusion fluid constituents, amounts and suppliers.

Constituent	**Volume (mL)**	**Supplier**
Bovine oxygen carrier, hemopure or *Group O Packed red blood cells*	750	Hemoglobin Oxygen Therapeutics LLC, Cambridge, MA *NHS Blood and Transplant, Birmingham, UK*
5% w/v human albumin solution	1000	Iburex 5, CSL Behring GmbH, Germany
Sodium bicarbonate 8.4%	30	B. Braun Medical Limited, UK
10% calcium gluconate	10	B. Braun Medical Limited, UK
Constituent	**Mass (mg)**	**Supplier**
Gentamicin	60	Cidomycin, Sanofi, UK
Epoprostenol	0.008/hour	Flolan, GlaxoSmithKline, UK
10% v/v Aminoplasmal	50	B.Braun Medical Limited, UK
Phytomenadione	0.1	Konakion, Roche Products Ltd, UK
Vancomycin	500	Wockhardt, UK
Constituent	**Volume (I.U/mL)**	**Supplier**
Heparin	10,000	Wockhardt, UK

2.5.2 Androgen precursor metabolism assay using NMLP

NMLP is a promising tool for metabolism studies under near-physiological conditions, because the liver remains metabolically active during the perfusion [139, 141]. This thesis employed NMLP to characterise the downstream metabolic conversion of the androgen precursors A4 and 11KA4. Due to endogenous /residual androgen detection in perfusate samples, [$^{13}C_3$]-labelled precursors were used during investigations.

The Liver Assist device and liver were prepped as described above. The liver was perfused in the absence of exogenous androgens, until liver viability was confirmed to be within the required criteria (lactate clearance < 2mmol/L in 2 hours, evidence of bile production, in combination with two or more of the following: homogenous perfusion, vascular flow >150 mL/min for hepatic artery and > 500mL/min for portal vein). Confirmation of viability took between 2-3 hours. After confirmation of liver viability, 200 nmol/L of [$^{13}C_3$]-A4 from either a 100 µg/mL stock in acetonitrile or 1 mg/mL stock in MeOH or [$^{13}C_3$]-11KA4 from a 1 mg/mL stock in MeOH was added to the perfusate reservoir or hepatic artery cannula. Acetonitrile/ MeOH concentration was kept at approximately 0.05% and 0.006%, respectively. Perfusate samples (4 mL), taken from the hepatic artery oxygenator, were collected every 30 minutes for 4 hours and then every 2 hours until the end of the perfusion. Samples were immediately snap frozen and stored at -80 ºC for solid phase extraction, at a later date. Liver biopsies were taken before the start (T0) and periodically throughout until the end of the perfusion. 8 mm punch biopsies were collected from left and right lobes, and immediately snap frozen in liquid nitrogen and stored at -80 ºC for future analysis.

2.6 Real time quantitative PCR

2.6.1 RNA isolation from human liver tissue

Tissue collected for RNA analysis was immediately snap frozen in liquid nitrogen and stored at -80 ºC. After 1 freeze/thaw cycle RNA from human liver tissue was prepared using the RNeasy Plus Mini Kit (Qiagen, Manchester, UK). 30 mg of tissue was homogenised (Gen 125 homogeniser, Fisher Scientific, UK) in 1 mL total RNA isolation lysis reagent (TRIzol). Immediately prior to use, MaXtract High Density tubes were prepared for use and centrifuged at 12, 000 x g for 30 seconds. TRIzol Homogenate was added directly to the prepared tube. Chloroform was added to the tube (0.2 mL), which was mixed thoroughly for 15 seconds to ensure complete fusion of organic and aqueous phases. Tubes were then incubated at 24 °C for 2-3 minutes. The tube was then centrifuged at 12, 000 x g for 5 minutes at 4 °C for phase separation. The upper aqueous phase was transferred to gDNA eliminator spin column, placed in a collection tube. Spin column was centrifuged at 8000 x g for 30 seconds and 600 µL of 70 % ethanol was added to the supernatant, which was subsequently loaded onto a RNAeasy mini spin column. Remaining purification steps were conducted according to the manufacturer's instructions. RNA concentration was measured using a nanodrop spectrophotometer (ND-1000, LabTech, Sussex, UK) using the absorbance of the sample at 260 nm.

2.6.2 Generation of cDNA and semi-quantitative PCR

cDNA was produced by reverse transcription of 960 ng RNA using Applied BiosystemsTM TaqManTM Reverse Transcription Reagents, following the manufacturer's protocol, with random hexamers. Quantitative PCR was conducted on

QuantStudio-5 (Fisher Scientific, Loughborough, UK) 384 well system using TaqManTM Gene Expression Assays (FAM-labelled) and the SensiFASTTM Probe Hi-ROX kit (Bioline). Dilutions of pooled cDNA were prepared for each target. The relative cDNA content was plotted against Ct value for each target and primer efficiency (E) was calculated as $10^{[-1/slope]}$. ΔCt was calculated as Ct ([Target]-Geometric mean (Ct [18S], Ct [GAPDH]). Gene expression in arbitrary units (A.U.) was calculated as 1000*(E^-ΔCt). Genes and Taqman assay identifiers are outlined in **Table 2.3** below.

Table 2.4 Taqman Gene Expression Assay Identifier codes for qPCR analysis.

Gene	***Taqman assay Identifier***
11β-Hydroxysteroid dehydrogenase type 1 (HSD11B1)	*Hs001547870*
11β-Hydroxysteroid dehydrogenase type 2 (HSD11B2)	*Hs00388669*
Aldo Keto reductase 1D1 (AKR1D1)	*Hs00818881*
Aldo Keto reductase 1C3 (AKR1C3)	*Hs00366267*
Glyceraldehyde 3-phosphate dehydrogenase (GAPDH)	*Hs99999905*
18S rRNA housekeeping gene (18S)	*Hs03003631*

CHAPTER 3

DEVELOPMENT AND OPTIMISATION OF A UHPLC-MS/MS METHOD FOR MULTI-ANDROGEN PROFILING

3.1. Introduction

Steroid analysis is an important clinical tool used to diagnose a range of endocrine disorders [147-149]. Traditionally, measurement of individual steroids, by techniques such as immunoassay, have been used to characterise endocrine dysregulation. However, in recent years the benefits of multi-steroid profiling have become apparent [55]. In comparison to immunoassays, ultra-high performance liquid chromatography-tandem mass spectrometry (UHPLC-MS/MS) provides greater specificity, has similar sensitivity, faster analysis times and the ability to measure multiple steroids in a single assay [50, 150, 151]. UHPLC-MS/MS permits multi-steroid analysis by separation of analytes within a mixture according to their polarity and subsequent identification and quantification according to fragmentation patterns. Briefly, analytes interact with the stationary phase (solid matrix) and these interactions are overcome by decreasing the polarity of the mobile phase (typically a mixture of aqueous and organic solvents) over time allowing for the sequential elution of analytes off the column. Post elution, analytes are ionised, fragmented, and detected according to their mass to charge ratio (*m/z*). Analyte identification is then achieved by comparison of retention time and mass transitions to reference compounds (**Chapter 1**). Although immunoassays are generally still the method of choice for steroid analysis in clinical chemistry laboratories [152], UHPLC-MS/MS is an emerging technique, rapidly gaining prestige [153].

UHPLC-MS/MS is routinely used for measurement of individual analytes or small panels of androgen metabolites, particularly in the diagnosis of female hyperandrogenism [147-149]. However, despite their quantitative importance, 11-oxygenated androgens are not measured in clinic. Current UHPLC-MS/MS methods used for androgen quantification have been designed for multi-steroid profiling and include an array of additional steroids outside of the androgen functional class [9, 30, 154]. A UHPLC-MS/MS assay focussed on androgen precursors, active androgens and downstream metabolites would provide novel insights into androgen metabolism. A UHPLC-MS/MS assay can be optimised for high recovery and sensitivity for investigation of androgens, their precursors and 11-oxygenated androgens in hyperandrogenic conditions. In this chapter the development of an UHPLC-MS/MS method to monitor the complex androgen metabolome is described. This was utilised to investigate androgen metabolism in the human liver (**Chapter 1, Aim 1**).

Chapter 5 describes how NMLP was used to study androgen metabolism in human liver tissue. The conversion of downstream androgen metabolites was investigated, using stable isotopes to avoid interference from endogenous steroid generation, [$^{13}C_3$]-A4 and [$^{13}C_3$]-11KA4. This assay was used to monitor androgen conversion during NMLP in acellular blood carrier, hemopure. Although our assay was designed for androgen analysis in hemopure, it could also provide valuable insight on androgen metabolic pathways, without interference from endogenous steroids, in a variety of laboratory and clinical experiments.

Complete validation of new UHPLC-MS/MS methods is a key to ensure reliable and reproducible results. Validation parameters must be investigated for each analyte and include lower and upper limits of quantification, selectivity, sensitivity, carry over, accuracy, intra- and inter- assay imprecision, recovery and matrix effects [50, 155].

Here, I describe the development and optimisation an UHPLC-MS/MS assay the separation and quantification of seventeen classic and 11-oxygenated androgens (**Table 3.1**). This method was adjusted for the separation and quantification of sixteen [^{13}C]-labelled classic and 11-oxygenated androgens. Method validation was conducted using previously published and clinically recognised protocols [55, 155]. Applicability of these methods was further established by their successful application to investigate androgen metabolism in *ex vivo* human liver tissue models.

Table 3.1 Trivial name, abbreviation and functional class of each androgen precursor, active androgen and androgen metabolite included in the UHPLC-MS/MS assays.

Androgen trivial name	Androgen abbreviation	Functional class
Dehydroepiandrosterone	DHEA	Classic androgen precursor
Androstenedione	A4	Classic androgen precursor
Testosterone	T	Classic androgen
5α-dihydrotestosterone	5α-DHT	Classic androgen
5α-androstanedione	5α-dione	Classic androgen metabolite/precursor

Androsterone	An	Classic androgen metabolite
Etiocholanonlone	Et	Classic androgen metabolite
Androstanediol	3α-adiol	Classic androgen metabolite
11β-hydroxyandrostenedione	11βOHA4	11-oygenated androgen precursor
11β-hydroxytestosterone	11βOHT	11-oxygenated androgen
11β-hydroxyandrosterone	11βOHAn	11-oxygenated androgen metabolite
11β-hydroxy-5α-androstanedione	11βOH5α-Dione	11-oxygenated androgen metabolite
11β-hydroxyetiocholanolone	11βOHEt	11-oxygenated androgen metabolite
11-ketoandrostenedione	11KA4	11-oygenated androgen precursor
11-ketotestosterone	11KT	11-oygenated androgen
11-ketoetiocholanolone	11KEt	11-oxygenated androgen metabolite
11-ketoandrosterone	11KAn	11-oxygenated androgen metabolite

3.2. Materials and methods

3.1.1. Preparation of external and internal standards

Steroid stocks were prepared as described in 2.1. Calibrators for each analyte, ranging from 0 to 100 ng/mL, were prepared using stock 2 (1 μg/mL) and stock 3 (0.1 μg/mL) in matrix matched to the sample (i.e., cell culture media or acellular blood substitute hemopure) (**Table 3.2**).

Table 3.2 Calibrant concentrations for androgen quantification (5 mL per calibrant). Stock 2 is made up in 50% (vol/vol) UHPLC methanol and UHPLC water, containing all analytes at 1000 ng/mL. Stock 3 is made up in 50% (vol/vol) UHPLC methanol and UHPLC water, containing all analytes at 100 ng/mL.

Calibrant number	Added volume of serum steroid stock 3 (μL)	Added volume of dilutant matrix (μL)	Final concentration (ng/mL)
C0	0	5000	0
C1	10	4990	0.2
C2	25	4975	0.5
C3	50	4950	1
C4	125	4875	2.5
C5	150	4850	3
Calibrant number	**Added volume of serum steroid stock 2 (μL)**	**Added volume of dilutant matrix (μL)**	**Final concentration (ng/mL)**
C6	25	4975	5
C7	50	4950	10

C8	250	4750	50
C9	400	4600	80
C10	500	4500	100

3.1.2. Preparation of samples

3.1.2.1. Solid phase extraction

Androgens were extracted by solid phase extraction using the same method as described in detail in **Chapter 2; 2.2.2**. For method validation only, 500 uL of sample matrix and calibrators were treated with 500 µL sodium acetate buffer (0.2 M, pH 5), without sulfatase from *Helix pomatia* enzyme hydrolysis reagent, and then incubated for 1 hour at 60 °C, to simulate enzymatic hydrolysis.

3.1.2.2. Liquid-liquid extraction

[^{13}C]-labelled androgens generated *in vitro* (**Chapter 2; 2.2.5**) were extracted by liquid-liquid extraction, as described in **Chapter 2; 2.2.2.** Extracted samples were treated with 10 uL of internal standard mixture, incorporating DHEA-d6, A4-d7, An-d4, Et-d5, 11KA4-d10 and 11OHA4-d7 deuterium labelled internal standards only.

3.1.3. Tandem mass spectrometry

Optimised characteristics for the mass spectrometer were electrospray ionisation in positive ion mode, with a capillary voltage of 4.0 kV, source temperature of 150 °C and a desolvation temperature of 600 °C. Gas flow and cone gas was sustained at 1200 L/h and 150 L/h, respectively. For each steroid a molecular ion was designated and 2

stable mass transitions, a quantifier and qualifier determined. Target Lynx software was used for androgen quantification (**Chapter 2**).

3.1.3.1. Selection and optimisation of mass transitions for multi androgen profiling UHPLC-MS/MS

Identification and optimisation of quantifier and qualifier mass transitions, cone energies and collision energies, was performed by direct infusion of 0.2 mg/mL of each analyte, in 50 % (vol/vol) UHPLC water/ UHPLC methanol into the mass spectrometer (20 μL/min). Infusion of 6 mmol/L NH_4F and UHPLC flow rate of 0.3 mL/min was applied to simulate elution conditions of each analyte. Molecular ions and/or base peaks ions were identified manually, and optimised MS/MS transitions (**Table 3.3**) were determined using IntelliStart software program.

3.1.3.2. Selection and optimisation of mass transitions for [$^{13}C_3$]-labelled multi androgen UHPLC-MS/MS

Mass transition optimisation could not be performed by direct infusion of each [^{13}C]-analyte into the mass spectrometer, due to their limited commercial availability. Therefore, HEK293 cells overexpressing steroid metabolising enzymes to generate analytical amounts of each [^{13}C]-metabolite were used. Mass transitions for each [^{13}C]-labelled steroid were predicted, based on the analysis of the commercially available standard of non-labelled steroid equivalent, taking into account the position of the [^{13}C] labels. The predicted mass transitions were confirmed by injection of the respective [^{13}C]-labelled analytes prepared using HEK293 cells through the column. Transitions that gave the largest, reproducible peak area were selected for quantification.

3.1.4. Confirmation of steroid extraction efficiency for normothermic machine liver perfusion perfusate

Prior to extraction and LC-MS/MS analysis of hemopure perfusate, it was important to confirm that the standard hydrolysis protocol using sulfatase from *helix pomatia* was sufficient at deconjugating sulfatases and glucuronides in the hemopure perfusate matrix. Etiocholanolone glucuronide (EtG) and 11-ketoetiocholanolone glucuronide (11KEtG) were used as a reference for the hydrolysis efficiency of sulfatase *helix pomatia* on classic and 11-oxygenated androgens and metabolites.

To determine hydrolysis efficiency in hemopure, samples were spiked with 100 nmol/L of EtG or 11KEtG and split into two batches. Steroid conjugates in the first batch were hydrolysed by addition of sulfatase *helix pomitia* mixture and extracted by solid phase extraction (**Chapter 2**; **2.1.2**). Steroid conjugates in the second batch were treated with sodium acetate buffer, in place of sulfatase, and extracted by solid phase extraction. The experiment was performed with technical triplicates. Percentage hydrolysis efficiency was calculated using the below formula.

$$\%\, Hydrolysis = \; 100 - \left(\left(\frac{concentration\ (acetate\ buffer)}{concentration\ (sulfatase)} \right) \times 100 \right)$$

3.1.5. Validation of analytical performance

Validation parameters were to identify standard of the assay when applied to androgen metabolism during ex vivo analysis. Therefore, validation procedures were conducted

using the two matrices used during *ex vivo* androgen metabolism analysis and NMLP, Williams E cell culture media and hemopure, respectively (**Chapter 5**).

3.1.5.1. Limits of quantification

The lower limit of quantification (LLOQ) was defined as the lowest concentration whereby 10 technical replicates of spiked samples could be accurately measured with an intra-assay imprecision that deviates from the nominal concentration by ≤ 20 % and accuracy between – 20 % and + 20 %.

The upper limit of quantification (ULOQ) was defined as the highest concentration whereby 10 technical replicates of spiked samples could be accurately measured with an intra-assay imprecision that deviates from the nominal concentration by ≤ 20 % and an accuracy between – 20 % and + 20 %.

1.2.1.1 Accuracy

To determine accuracy, ten individually prepared samples were spiked with a mixture of all analytes at three different concentrations (7.5, 25 and 75 ng/mL). and run in the same batch. Bias between the measured and nominal concentrations calculated as a percentage of between – 15 % and + 15 % was considered ideal, and between – 20% and + 20 % acceptable.

3.1.5.2. intra-assay (within run) precision

To determine intra-assay imprecision, samples were spiked with a mixture of analytes at three different concentrations (7.5, 25, 40 and 75 ng/mL). The same spiked sample was extracted 10 times by solid phase extraction and run in the same batch. Variance between measured concentration, calculated as percentage relative standard deviation (CV), of ≤ 15 % was deemed ideal, with ≤ 20 % acceptable.

3.1.5.3. Inter-assay (between run) imprecision

To determine inter-assay imprecision, matrix samples were spiked with all analytes at 40 ng/mL. Analytes were extracted by solid phase extraction ten times in two independent batches, run on different days. Variance between measured concentrations, calculated as percentage relative standard deviation (CV), of ≤ 15 % was deemed ideal, with ≤ 20 % acceptable.

1.2.1.1 Linearity

Linearity of the calibration series used within this assay was confirmed by the independent preparation and solid phase extraction of three calibration series. The peak area of the analyte relative to the internal standard peak area was plotted against the nominal concentration of each calibrator to produce a linear least regression square curve. To be acceptable, the mean value for each calibrator concentration must not deviate more than ± 20 % from the nominal concentration, and the correlation coefficient (R^2) for each calibration curve must be ≥ 0.99.

3.1.5.4. Matrix effects and recovery

Sample matrix was spiked with a mixture containing all analytes, at three concentrations (7.5, 25 and 75 ng/mL) prior to solid phase extraction (pre extract) and after solid phase extraction (post extract). 20 µL of an internal standard mixture was added to pre and post extracts, for normalisation of observed concentrations. The experiment was performed with technical triplicates. The below formulas were used to determine percentage matrix effects and recovery for each analyte. Mean matrix effects values between – 15 % and + 15 % were considered optimal, and values between – 20% and + 20 % were acceptable. Mean recovery between 80 % and 120 % was considered acceptable.

$$\%\, Matrix\ effect = \left(\frac{concenration\ (post\ extract) - nominal\ concentration}{nominal\ concentration}\right) \times\ 100$$

$$\%\, Recovery = \left(\frac{concentration\ (pre\ extract)}{concentration\ (post\ extract)}\right) \times\ 100$$

3.1.5.5. Percentage carry-over

Percentage carry-over was determined by injection of a 100 ng/mL sample (highest calibrant concentration) followed immediately with a blank sample (50 % (vol/vol) UHPLC water/ UHPLC methanol). The peak area of the analyte detected in the blank sample, relative to the peak area of each analyte detected in the 100 ng/mL sample was used to calculate percentage carry-over. A carry over of ≤ 0.2 % was considered acceptable.

3.2. Results

3.2.1. Quantification by tandem mass spectrometry

Mass transitions for each analyte were optimised based on the molecular ion peak and mass transitions that generated stable, high sensitivity ions. Quantifier and qualifier mass transitions, cone voltages, collision energies and retention times for each analyte and internal standard are shown in **Table 3.3** below. Modified MRMs for [^{13}C]-analytes were chosen based on the molecular ion peak and mass transitions that generated stable, high sensitivity ions. The incorporation of three [^{13}C] labels to each analyte on positions 1,2 and 3 of the steroid structure, increased the m/z values of all analytes by 3 mass units. Therefore, when quantifying [$^{13}C_3$]-labelled analytes, internal standards containing 3 deuterium labelled hydrogen atoms (T-d3, 5α-DHT-d3, and Adiol-d3) were not incorporated. Quantifier and qualifier mass transitions cone voltages, collision energies, retention times and modified internal standards for each [$^{13}C_3$]-labelled analyte are outlined in **Table 3.4** below.

Table 3.3 Quantifier and qualifier mass transitions, retention times, cone voltages and collision energies of target analytes and internal standards.

Steroid	Molecular species	Retention time (min) (approx.)	Quantifier transition	Cone voltage (kV)	Collision energy (eV)	Qualifier transition	Cone voltage (kV)	Collision energy (eV)
DHEA	$[M\text{-}H_2O+H]^+$	2.4	271.1 > 253.0	28	12	271.1 > 213.0	28	14
A4	$[M+H]^+$	2.1	287.1 > 96.9	42	18	287.1 > 108.9	42	22
T	$[M+H]^+$	2.4	289.1 > 96.9	26	20	289.1 > 108.9	26	24
5α-DHT	$[M+H]^+$	2.9	291.1 > 255.0	38	16	291.1 > 159.0	38	22
5α-dione	$[M+H]^+$	2.7	289.1 > 271.0	28	16	289.1 > 96.9	28	16
An	$[M+H]^+$	3.4	291.1 > 273.2	12	8	291.1 > 255.2	12	16
Et	$[M+H]^+$	3.2	291.1 > 255.0	16	12	291.1 > 273.1	16	8
3α-adiol	$[M\text{-}H_2O+H]^+$	3.3	275.0 > 257.1	38	10	275.0 > 148.8	38	10
11βOHA4	$[M+H]^+$	1.4	303.1 > 285.2	34	14	303.1 > 267.1	34	16
11βOHT	$[M+H]^+$	1.5	305.2 > 269.2	16	14	305.2 > 121.1	16	20
11βOHAn	$[M+H]^+$	1.9	307.1 > 271.1	2	10	307.1 > 289.2	2	8
11βOH5α-dione	$[M+H]^+$	1.7	305.1 > 269.0	32	14	305.1 > 96.9	32	28
11βOHEt	$[M+H]^+$	1.8	307.0 > 270.8	2	10	307.0 > 253.2	2	8

11KA4	$[M+H]^+$	1.1	301.1> 120.6	24	22	301.1 > 90.5	24	46
11KT	$[M+H]^+$	1.3	303.1 > 120.6	48	26	303.1 > 90.5	48	50
11KEt	$[M+H]^+$	1.8	287.0 > 229.2	36	16	287.0 > 269.0	36	16
11KAn	$[M+H]^+$	1.9	305.1 > 287.2	26	10	305.1 > 269.1	26	12
11K-5α-DHT	$[M+H]^+$	1.5	305.0 > 104.9	28	32	305.0 > 287.0	28	14
11K-5α-dione	$[M+H]^+$	1.3	303.0 > 285.1	38	14	303.0 > 108.9	38	20
Internal standard	**Molecular species**	**Retention time (min) (approx.)**	**Quantifier transition**	**Cone voltage (kV)**	**Collision energy (eV)**	**Qualifier transition**	**Cone voltage (kV)**	**Collision energy (eV)**
11KA4-d10	$[M+H]^+$	1.1	311.0 > 264.5	46	16	311.0 > 120.5	44	22
11βOHA4-d7	$[M+H]^+$	1.4	310.1 > 292.1	30	14	310.1 > 146.6	30	17
11KT-d3	$[M+H]^+$	1.2	306.2 > 262.1	20	22	306.2 > 124.1	20	22
11KEt-d5	$[M+H]^+$	2.3	292.0 > 274.1	4	18	292.0 > 292.1	16	10
A4-d7	$[M+H]^+$	2.1	294.1 > 108.9	42	22	294.1 > 96. 9	42	18
Test-d3	$[M+H]^+$	2.3	292.1 > 108.9	26	24	296.1 > 96.9	26	22
DHEA-d6	$[M+H]^+$	2.4	295.1 > 259.0	28	12	295.1 > 219.0	28	14
DHT-d3	$[M+H]^+$	2.9	294.1 > 258.1	22	16	294.1 > 159.1	22	22
Et-d5	$[M+H]^+$	3.2	296.1 > 260.0	12	12	296.1 > 220.0	16	12

Adiol-d3	$[M-H_2O+H]^+$	3.2	278.0 > 151.8	38	10	278.0 > 80.0	38	10
An-d4	$[M+H]^+$	3.4	295.1 > 277.2	24	12	295.1 > 259.7	24	12

Table 3.4 Quantifier and qualifier mass transitions, retention times, cone voltages, collision energies and internal standard for each [$^{13}C_3$]-analyte.

Steroid	Molecular species	Retention time (min) (approx.)	Quantifier transition	Cone voltage (kV)	Collision energy (eV)	Qualifier transition	Cone voltage (kV)	Collision energy (eV)	Internal standard
[$^{13}C_3$]-A4	$[M+H]^+$	2.1	290.1 > 99.9	20	20	290.1 > 111.9	20	20	A4-d7
[$^{13}C_3$]-T	$[M+H]^+$	2.4	292.1 > 99.9	48	22	292.1 > 111.9	48	24	A4-d7
[$^{13}C_3$]- 5α-DHT	$[M+H]^+$	2.9	294.1 > 258.1	42	14	294.1 > 161.9	42	22	Et-d5
[$^{13}C_3$]-5α-dione	$[M+H]^+$	2.8	292.1 > 274.0	34	16	292.1 > 99.9	34	26	A4-d7
[$^{13}C_3$]-An	$[M+H]^+$	3.5	294.1 > 276.2	12	8	294.1 > 258.2	12	16	An-d4
[$^{13}C_3$]-Et	$[M+H]^+$	3.3	294.1 > 258.0	12	12	294.1 > 276.1	12	6	Et-d5
[$^{13}C_3$]-3α-adiol	$[M-H2O+H]^+$	3.4	278.1 > 260.1	28	10	278.1 > 95.8	28	28	An-d4
[$^{13}C_3$]-11βOHA4	$[M+H]^+$	1.3	306.1 > 288.2	34	14	306.1 > 270.1	34	16	11OHA4-d7
[$^{13}C_3$]-11βOHT	$[M+H]^+$	1.5	308.2 > 272.2	16	14	308.2 > 124.1	16	20	11OHA4-d7
[$^{13}C_3$]-11βOHAn	$[M+H]^+$	1.9	310.1 > 292.2	2	10	310.1 > 274.1	2	8	11KEt-d5
[$^{13}C_3$]-11βOH-5α-dione	$[M+H]^+$	1.6	308.1 > 272.1	32	14	303.1 > 99.9	32	28	11KEt-d5
[$^{13}C_3$]-11βOHEt	$[M+H]^+$	1.8	310.0 > 273.8	2	10	310.2 > 256.2	2	8	11KEt-d5

[$^{13}C_3$]-11KA4	$[M+H]^+$	1.0	304.1 > 123.6	24	22	304.1 > 93.5	24	46	11KA4-d10
[$^{13}C_3$]-11KT	$[M+H]^+$	1.2	306.1 > 123.6	48	26	306.1 > 93.5	48	50	11KA4-d10
[$^{13}C_3$]-11KEt	$[M+H]^+$	1.7	290.0 > 232.2	36	16	290.0 > 272.0	36	16	11KEt-d5
[$^{13}C_3$]-11KAn	$[M+H]^+$	1.8	308.1 > 290.2	26	10	308.1 > 272.1	26	12	11KEt-d5
[$^{13}C_3$]-11K-5α-DHT	$[M+H]^+$	1.5	308.0 > 107.9	28	32	308.0 > 290.0	28	14	11KEt-d5
[$^{13}C_3$]-11K-5α-dione	$[M+H]^+$	1.3	306.0 > 288.1	38	14	306.0 > 111.9	38	20	11KEt-d5

3.2.2. Chromatographic separation

This method was optimised to separate seventeen androgens, with a focus on separation of analytes with the same m/z values that cannot be separated by tandem mass spectrometry (**Figure 3.1**)**.** As described in **Chapter 2**, analytes in this method were separated over a period of 4 minutes using a linear gradient of 45 % to 70 % UHPLC methanol. Four pairs of analytes coeluted (11βOHA4 (m/z 303) and 11K-5α-dione (m/z 303); 11βOHT (m/z 305) and 11K-5α-DHT (m/z 305); 11βOHAn (m/z 307) and 11KAn (m/z 305); 11βOHEt (m/z 307) and 11KEt (m/z 287). Coelution of 11OHAn and 11KAn and of 11βOHEt and 11KEt, was not problematic as they have different molecular ions, mass transitions and we were able to demonstrate minimal interference (**Table 3.3**). However, interference between 11βOHA4 and 11K-5α-dione and could not be avoided as mass transitions were identical. Interference between 11βOHT and 11K-5α-DHT could also not be avoided, despite different selected transitions. To confirm this, each analyte was injected separately, and peaks were detected when the mass transitions of the non-injected analyte were monitored. Accurate quantitation of these is only possible through further method optimisation. As 11K-5α-dione has been shown to readily convert to 11KAn in *in vitro* models, and significant generation of 11K-5α-DHT is not expected where ADKR1D1 is highly expressed, neither metabolite would be expected to be present or interfere with measurement of 11βOHA4 and 11βOHT [24]. 11K-5α-dione and 11K-5α-DHT were therefore removed from the assay. No peaks were detected in the blank sample of (matrix only).

[^{13}C]-labelled analytes were separated using the same linear gradient as described above. The method separated sixteen [^{13}C]-labelled analytes, with the same m/z values, included in the assay (**Figure 3.2**). Coelution between [$^{13}C_3$]-11βOHA4 (m/z 306) and [$^{13}C_3$]-11K-5α-dione (m/z 306) and also [$^{13}C_3$]-11βOHT (m/z 308) and [$^{13}C_3$]-11K-5α-DHT (m/z 308) was identified. Interference between [$^{13}C_3$]-11βOHA4 and [$^{13}C_3$]-11K-5α-dione and could not be avoided as quantifier mass transitions were identical. Although there is a difference in mass transitions for [$^{13}C_3$]-11βOHT and [$^{13}C_3$]-11K-5α-DHT, interference could not be avoided. To confirm this, each analyte was injected separately, and peaks for the non-injected analyte were detected in both cases. For the same reasons as described above, [$^{13}C_3$]-11K-5α-dione and [$^{13}C_3$]-11K-5α-DHT were removed from the assay. No peaks were detected in the blank sample (matrix only). A small shift in retention times for [^{13}C]-labelled analytes was observed, in comparison to their unlabelled equivalents. Interestingly, five classic analytes showed ~ 0.1 minute increase in retention times, whereas for eight 11-keto and 11-hydroxylated analytes, there was an ~ 0.1minute decrease in retention time

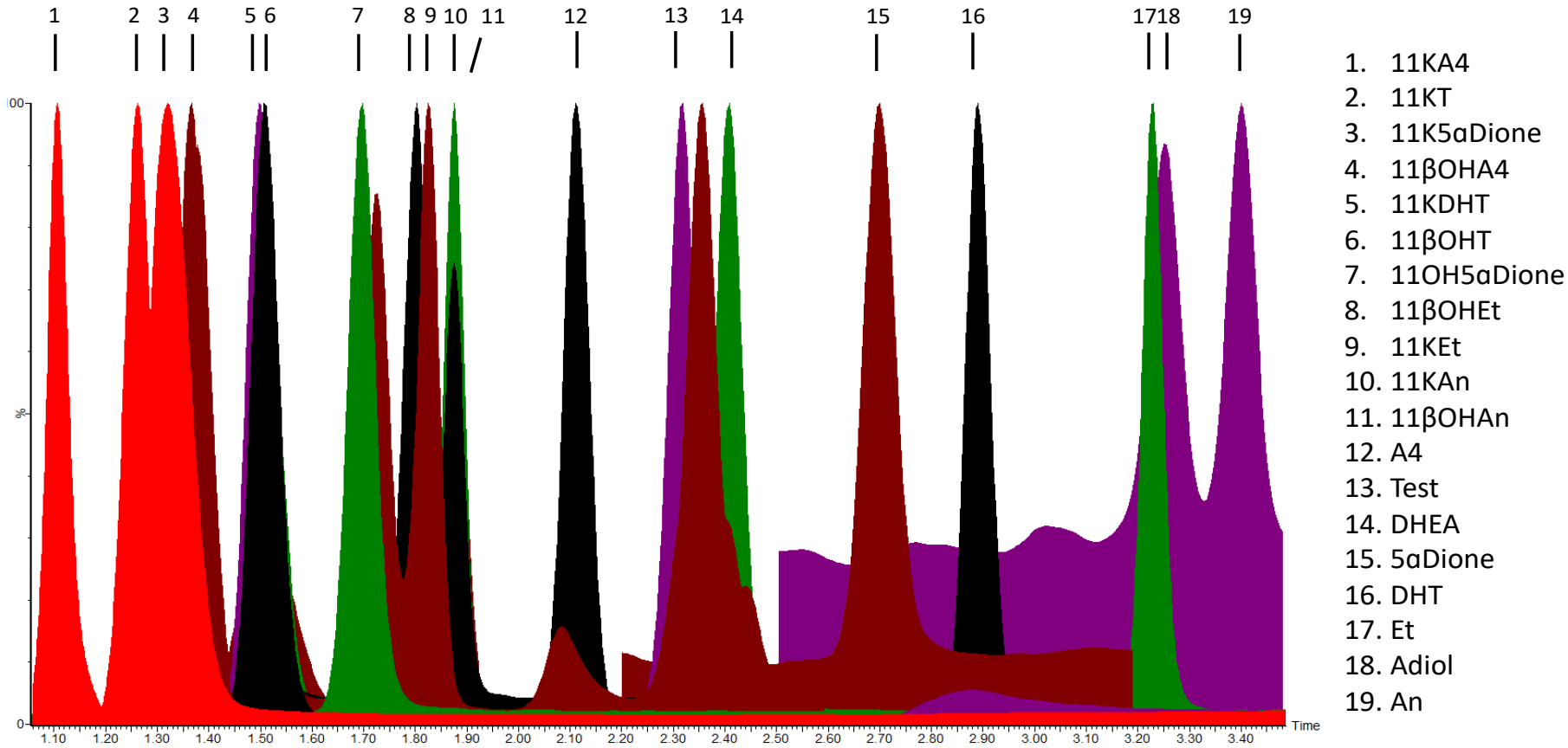

Figure 3.1 Chromatogram demonstrating separation of classic and 11 oxygenated steroids using ultra-high performance liquid chromatography mass spectrometry.

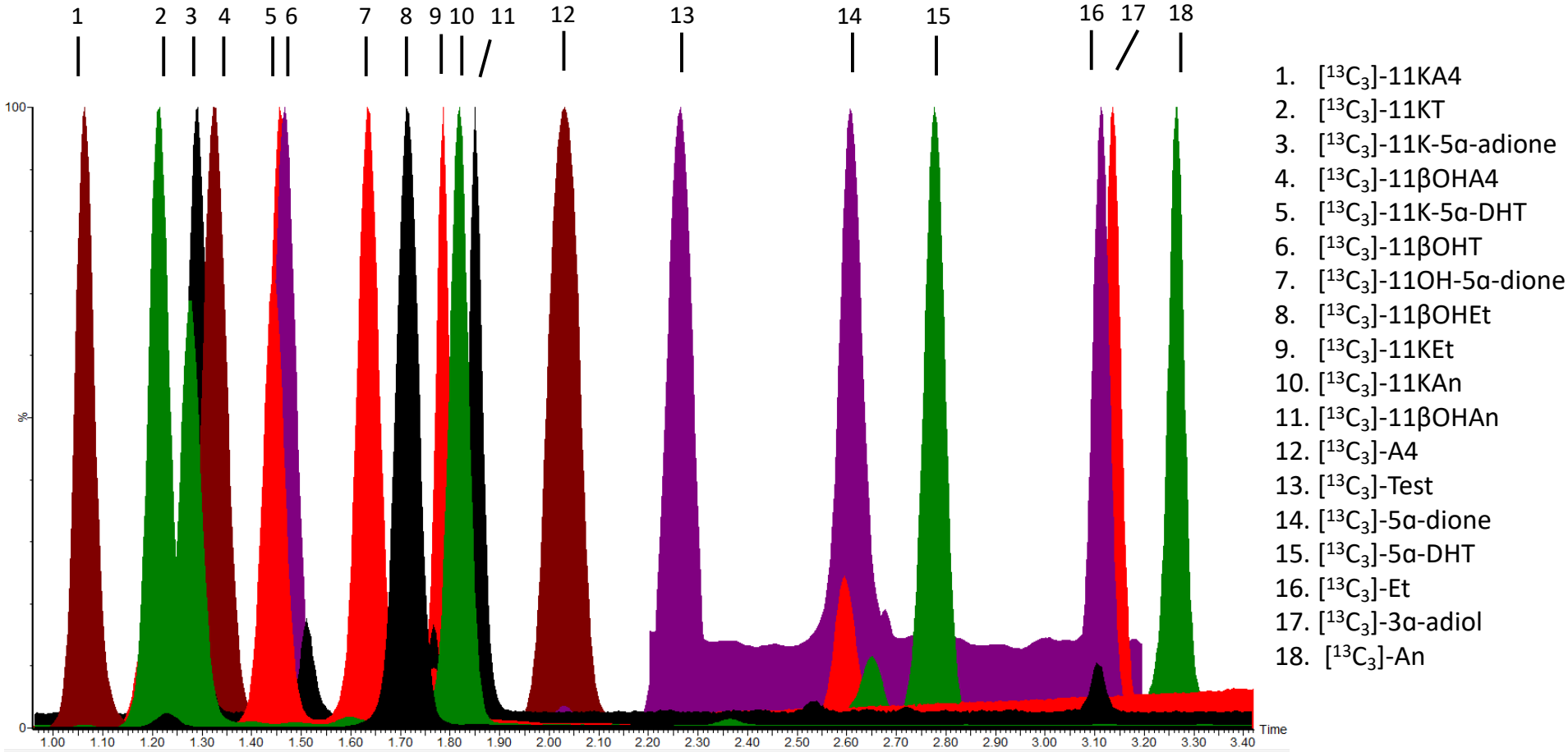

Figure 3.2 Chromatogram demonstrating separation of [^{13}C]-labelled androgens using ultra-high performance liquid chromatography mass spectrometry.

3.2.3. Confirmation of steroid extraction efficiency for NMLP perfusate

Prior to extraction and UHPLC-MS/MS analysis of perfusate used during NMLP (**Chapter 5**), it was important to confirm that the standard hydrolysis protocol using sulfatase from *helix pomatia,* followed by SPE (**Chapter 2**), was sufficient at deconjugating glucuronides in the hemopure perfusate matrix, which was used as a blood substitute during NMLP exogenous androgen metabolism investigations. The hydrolysis efficiency of sulfatase from *helix pomatia* was approximated using EtG and 11KEtG as indicators of hydrolysis efficiency for classic and 11-oxygenated metabolites, respectively. Investigations revealed that the ability of sulfatase to remove the glucuronide conjugate from EtioG and 11KetioG was 96 % ± 0.09 % and 90 % ± 1.14 %, respectively (**Figure 3.3**).

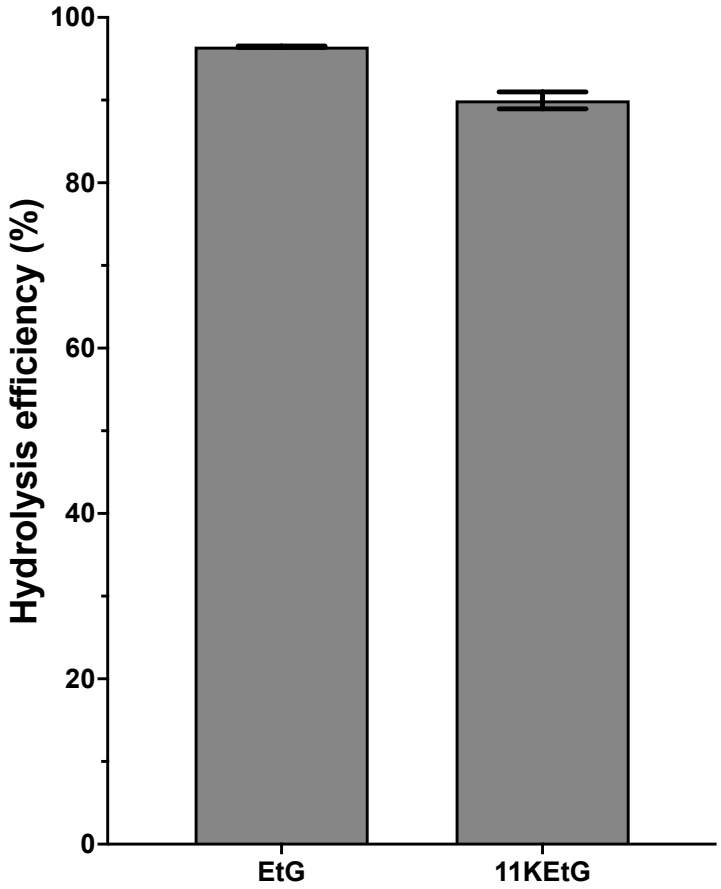

Figure 3.3 Hydrolysis efficiency of sulfatase from helix pomatia to remove glucuronide conjugates from Etiocholanolone glucuronide (EtiG) and 11-ketoetiocholanolone glucuronide (11KEtG) in NMLP blood substitute perfusate, hemopure. Results are representative of three technical replicates and are expressed as the mean ± standard deviation.

3.2.4. Validation of analytical performance

This UHPLC-MS/MS androgen method was specifically designed for application to Williams E medium and hemopure, due to these being the incubation media of choice during *ex vivo* liver tissue incubations and NMLP perfusion fluid, respectively (**Chapter 5**). Due to limited commercial availability of [^{13}C]-labelled analytes, validation procedures were conducted for application to hemopure using non-labelled steroids. The reason ^{13}C labelled isotopes are such excellent internal standards is their identical behaviour (ionisation, recovery etc) to the non-labelled steroids. This property allowed

us to extrapolate our validation data, assuming the [^{13}C]-labelled compounds act as their non-labelled analogues. Therefore, we expect the results from our non-labelled validation represent the limits for ^{13}C labelled steroids.

The developed UHPLC-MS/MS method was applied to investigate androgen metabolism in human liver, a major site of phase II conjugation (**Chapter 1**) [9]. All samples were therefore initially hydrolysed by sulfatase helix pomatia for 3 hours prior to SPE to deconjugate them from their sulphate and glucuronide esters (**Chapter 2**). To avoid unnecessary wastage of sulfatase enzyme during method development and validation procedures, hydrolysis was simulated by incubating samples with sodium acetate buffer (pH 5) for 1 hour, followed by SPE. I confirmed modifying sample preparation did not cause any changes in ionisation or observed analyte concentration, by extracting a calibration series containing all analytes in two batches. The first batch was incubated with sulfatase hydrolysis mixture for 3 hours and the second batch was incubated with sodium acetate buffer for 1 hour. **Figure 3.4** shows the responses detected for each analyte were consistent between extraction methods.

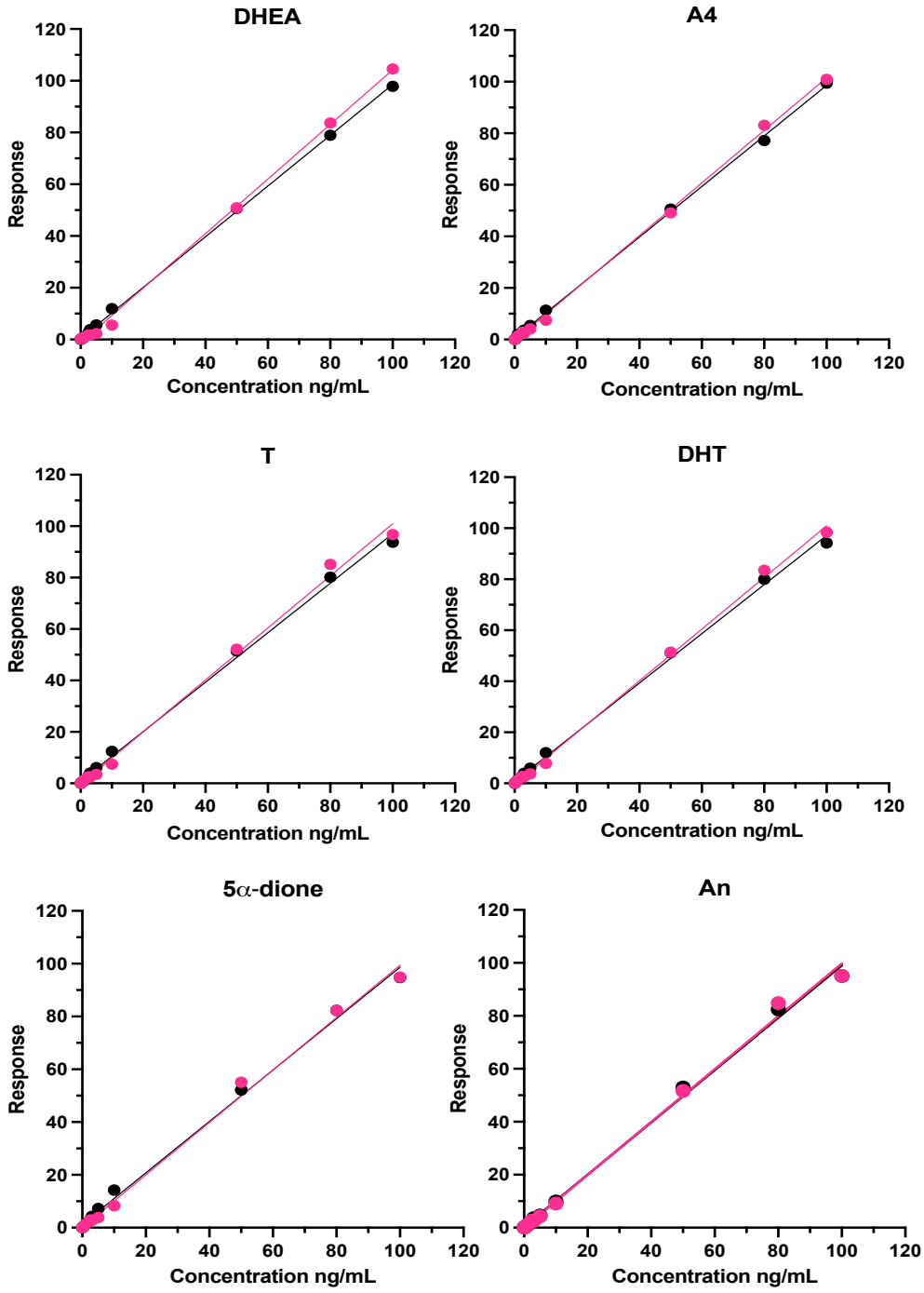

Figure 3.4 UHPLC-MS/MS calibration curves showing the relative area of each analyte to internal standard (response) plotted against calibrant concentration for analytes post 3 hour hydrolysis by sulfatase helix pomatia and 1 hour incubation with sodium acetate buffer. Pink data points show analyte concentration post incubation with sulfatase helix pomatia hydrolysis mixture. Black data points show analyte concentration post incubation with sodium acetate buffer.

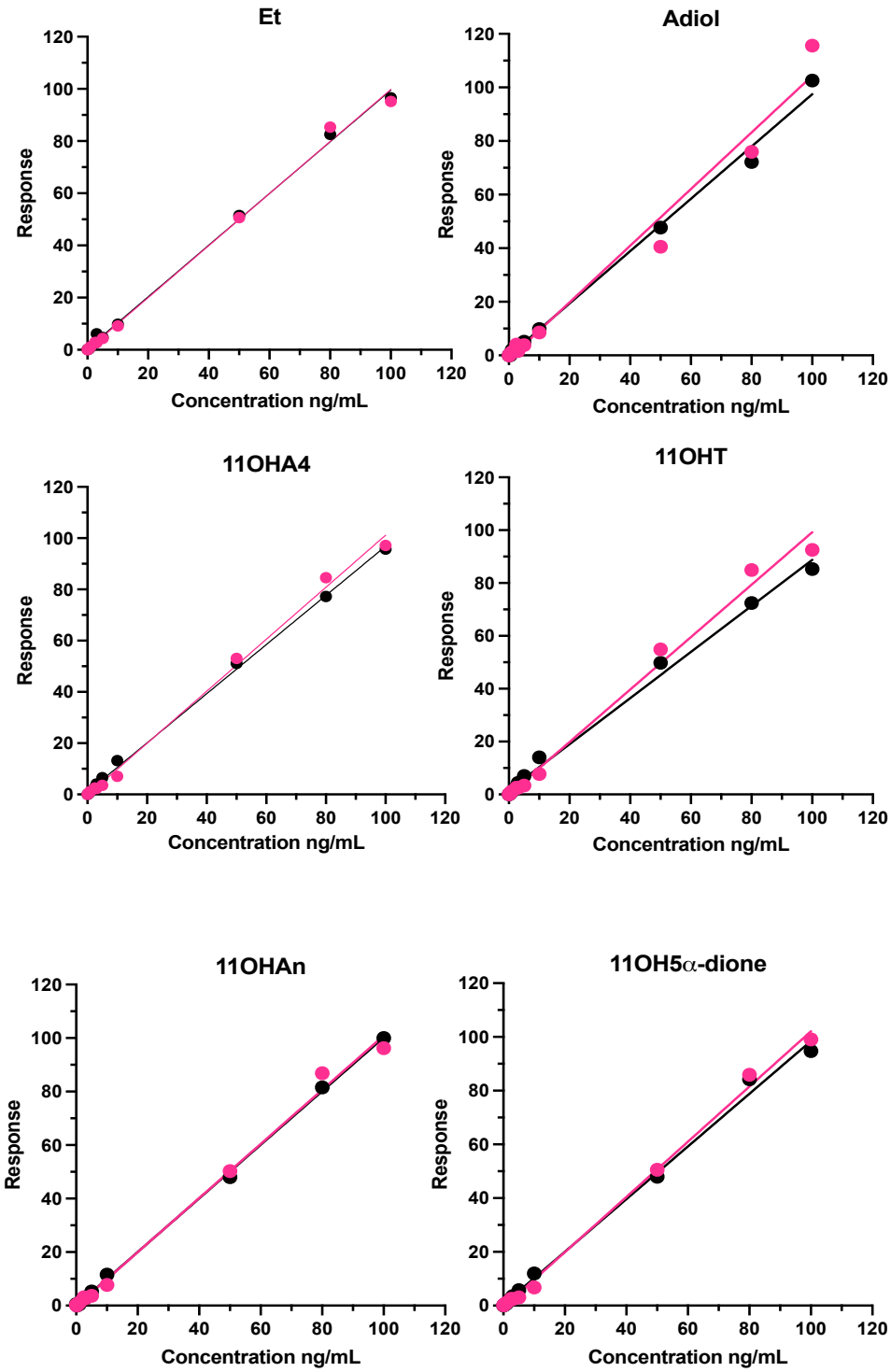

Figure 3.4 UHPLC-MS/MS calibration curves showing the relative area of each analyte to internal standard (response) plotted against calibrant concentration for analytes post 3 hour hydrolysis by sulfatase helix pomatia and 1 hour incubation with sodium acetate buffer. Pink data points show analyte concentration post incubation with sulfatase helix pomatia hydrolysis mixture. Black data points show analyte concentration post incubation with sodium acetate buffer.

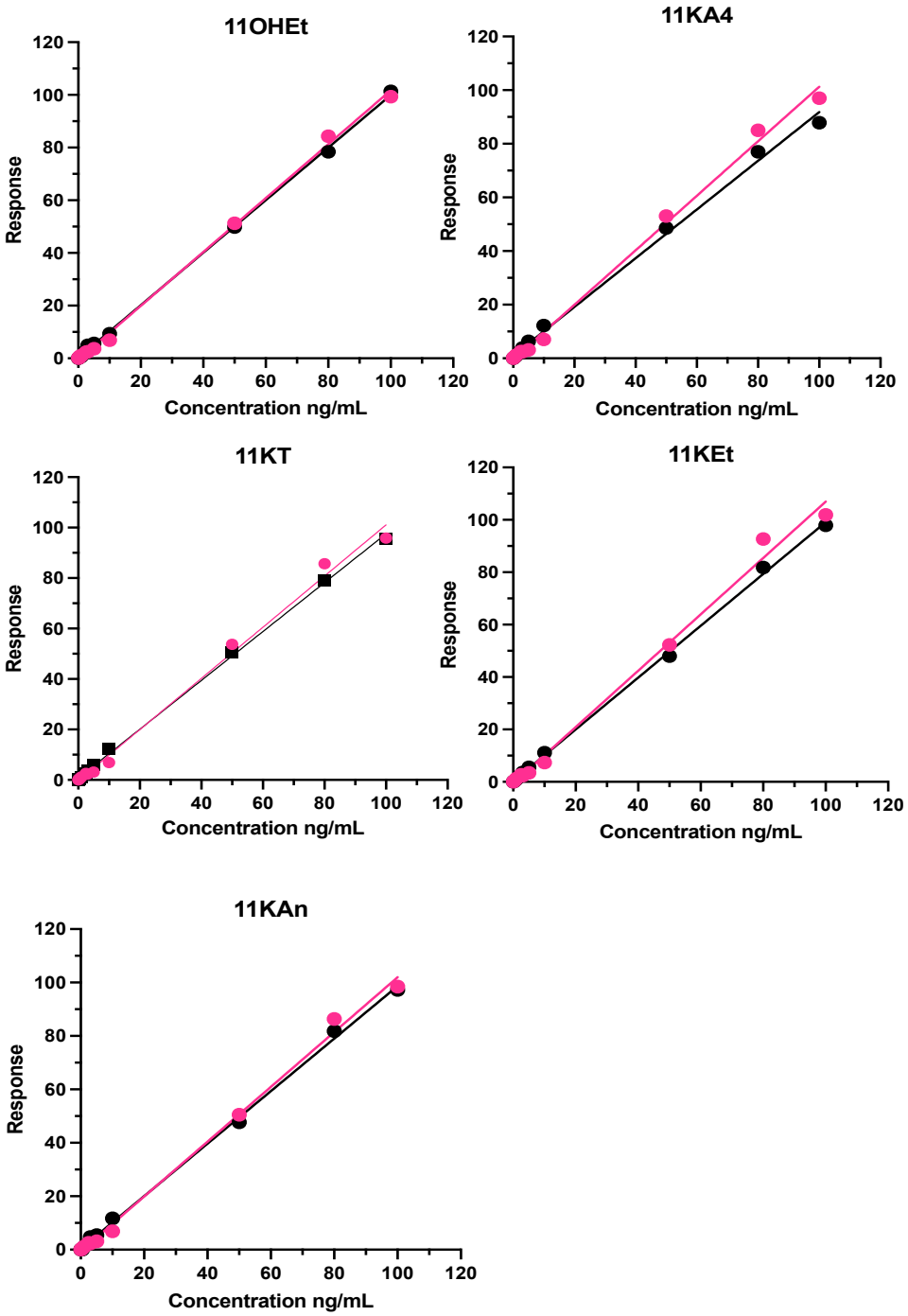

Figure 3.4 UHPLC-MS/MS calibration curves showing the relative area of each analyte to internal standard (response) plotted against calibrant concentration for analytes post 3 hour hydrolysis by sulfatase helix pomatia and 1 hour incubation with sodium acetate buffer. Pink data points show analyte concentration post incubation with sulfatase helix pomatia hydrolysis mixture. Black data points show analyte concentration post incubation with sodium acetate buffer.

3.2.4.1. Matrix effects, recovery and carryover

Matrix effects in Williams E, calculated at three concentrations (7.5, 25, and 75 ng/mL), were within the acceptable range (-20% to + 20%) for all analytes, ranging between –19.1% to 20% (**Table 3.5**), with values in the ideal range at all three concentrations for 6 steroids. Negative values can indicate ion suppression and positive values can indicate ion enhancement [156]. Matrix effects for A4 and T could not be accurately determined at 75 ng/mL, as this concentration is above the ULOQ for both (**Table 3.7**). Recoveries were calculated at the same three concentrations and ranged between 82.3% and 119.2%, which was within the acceptable criteria. Carry over was ≤ 0.2% for each analyte (**Table 3.5**). Mean matrix effects within hemopure at three concentration levels (7.5, 25, and 75 ng/mL) showed significant variation, ranging between -62.4% and 50.2% (**Table 3.6**). Percentage recoveries were acceptable for 11-keto analytes, at all concentrations, ranging from 88 % to 116%. However, recoveries for 11-hydroxylated and classic analytes (excluding DHEA, An, Et and 11βOHEt at 7.5 ng/mL, 3α-adiol at 25 ng/ mL and DHEA at 75 ng/ mL) were notably low, ranging between 16.9 % to 68.8 % (**Table 3.6**). Carry-over was <0.2 % for all analytes at 100 ng/mL.

Table 3.5 Matrix effects, recovery and carry over for all analytes within Williams E cell culture media. Matrix effects and recovery were assessed at 7.5 ng/ mL, 25 ng/mL and 75 ng/mL Carry-0ver was assessed at 100 ng/mL.

Analyte	Matrix effects (%) (n = 3)			Recovery (%) (n = 3)			Carry over (%)
	7.5 ng/mL	25 ng/mL	75 ng/mL	7.5 ng/mL	25 ng/mL	75 ng/mL	100 ng/mL
DHEA	16.5	16.8	5.6	102.0	97.1	101.0	3.3E-04
A4	17.6	-1.1	n/a	97.9	99.6	n/a	4.4E-04
T	18.9	-1.1	n/a	115.0	91.2	n/a	1.2E-04
5α-DHT	19.4	19.6	18.8	108.0	97.7	95.1	6.7E-04
5α-dione	20.0	9.6	2.4	119.2	97.6	82.3	1.2E-04
An	18.9	-5.3	-4.4	107.1	99.3	100.2	8.6E-05
Et	16.1	5.7	3.5	115.6	106.1	105.3	6.9E-04
3α-adiol	12.1	-2.6	-8.3	96.8	91.0	116.2	6.6E-03
11βOHA4	13.3	7.0	8.1	104.5	98.3	112.7	3.0E-05
11βOHT	20.0	17.6	8.6	114.6	106.5	114.3	1.3E-04

11βOHAn	5.12	1.9	8.7	104.1	96.8	93.4	8.4E-03
11βOH5α-dione	14.2	12.6	10.3	102.2	93.5	91.8	9.0E-05
11βOHEt	10.1	1.3	17.3	102.9	97.3	95.5	7.4E-05
11KA4	8.3	-10.2	-2.6	101.8	107.2	89.4	2.5E-05
11KT	-19.1	-11.1	-16.3	105.5	105.2	100.7	3.0E-05
11KEt	9.2	11.6	-15.7	88.7	103.0	106.1	3.3E-04
11KAn	18.2	-12.2	-14.3	96.4	103.2	91.4	3.5E-05

Table 3.6 Matrix effects, recovery and carry-over for all steroids within hemopure (acellular oxygen carrier). Matrix effects and recovery were assessed at 7.5 ng/ mL, 25 ng/mL and 75 ng/ mL. Carry-over was assessed at 100 ng/mL

Analyte	**Matrix effects (%) (n = 3)**			**Recovery (%) (n = 3)**			**Carry-over (%)**
	7.5 ng/mL	**25 ng/ mL**	**75 ng/mL**	**7.5 ng/mL**	**25 ng/mL**	**75 ng/mL**	**100 ng/mL**
DHEA	-10.1	-10.4	-42	16.9	59.3	86.0	2.1E-03

A4	4.7	45.0	-49.7	22.3	99.6	49.5	1.1E-04
T	28.1	-6.0	n/a	42.9	49.4	59.0	1.6E-04
5α-DHT	3.0	0.1	n/a	56.2	57.8	62.5	2.1E-02
5α-dione	23.9	38.7	11.0	39.5	45.4	57.7	1.4E-04
An	27.3	-9.6	-48.9	43.0	50.6	54.3	6.5E-04
Et	36.6	35.0	45.0	101.8	100.4	100.8	3.9E-03
3α-adiol	-27.8	0.3	-0.8	90.2	114.0	100.0	1.2E-02
11βOHA4	19.6	7.8	2.4	32.36	56.6	55.7	9.0E-05
11βOHT	18.0	1.0	-4.0	40.5	63.1	61.3	9.5E-05
11βOHAn	-62.4	-0.1	-8.4	41.5	68.8	66.9	6.5E-04
11βOH5α-dione	16.3	17.3	19.4	43.4	51.9	59.9	1.2E-03
11βOHEt	50.2	6.9	27.4	85.9	65.4	61.1	4.9E-02
11KA4	19.4	33.4	32.7	95.0	116.0	100.3	2.0E-05
11KT	-1.1	16.7	20.5	96.6	115.0	99.8	9.0E-05

11Ket	32.9	-52.1	-60.8	88.0	116.2	99.7	6.5E-04
11KAn	-8.1	31.1	36.3	100.8	111.8	99.0	1.2E-03

3.2.4.2. Limits of quantification, accuracy and precision

As matrix effects and analyte recovery did not meet the outlined validation criteria, it can only be classified semi-quantitative. Taking these findings into account, LLOQ/ ULLOQ, accuracy and imprecision was not investigated when applied to hemopure.

LLOQ within Williams E ranged between 0.5 ng/mL (~1.7 nmol/L) and 2.5 ng/mL (~8.3 nmol/L), for most androgens, except 3α-adiol, which had a lower limit of 7.5 ng/mL (~25 nmol/L) due to its low sensitivity. ULOQ ranged between 75 ng/mL (~ 250 nmol/L) and 100 ng/mL (~333 nmol/L) for most androgens with the exceptions of A4 and T, which had ULOQs of 50 ng/mL (~167 nmol/L) and 40 ng/mL (~ 33 nmol/L), respectively (**Table 3.7**). Accuracy at three concentration levels (7.5, 25, and 75 ng/mL) was between -15.8 to 19.6% and intra-assay imprecision was between 2.9% and 19.2% (**Table 3.7**)**.** 12 out of 17 steroids were within ideal ranges for accuracy at all concentrations (-15% to +15%). Only 5 were not within ideal ranges at all concentrations but were within the acceptable range (-20% to +20%). For intra-assay imprecision, 15 out of 17 steroids were within the acceptable range at all concentration and only 2 were just outside the ideal range but comfortably within the acceptable range. Values for A4 and T at 75 ng/mL were excluded due to this concentration being above their ULOQs.

Table 3.7 Limits of quantification, accuracy (bias) and intra-assay (within-run) imprecision of Williams E samples spiked with 7.5 ng/mL, 25 ng/mL and 75 ng/mL of all analytes.

Analyte	LLOQ ng/mL (nmol/L)	ULOQ ng/mL (nmol/L)	Accuracy, bias (%) (n=3)		
			7.5 ng/mL	25 ng/mL	75 ng/mL
DHEA	2.5 (8.7)	80 (277.8)	11.1	10.2	2.0
A4	1 (3.5)	50 (174.8)	9.2	-5.2	n/a
T	1 (3.5)	40 (138.9)	9.3	-12.2	n/a
5α-DHT	1 (3.5)	100 (344.8)	12.7	9.8	5.0
5α-dione	2.5 (8.7)	80 (277.8)	10.1	6.9	6.4
An	2.5 (8.6)	100 (344.8)	7.4	1.5	-2.0
Et	1 (3.5)	100 (344.8)	5.7	2.2	3.5
3α-adiol	7.5 (25.7)	75 (256.8)	5.5	10.4	7.3
11βOHA4	0.5 (1.7)	100.0 (331.1)	12.2	13.2	-10.7
11βOHT	0.5 (1.6)	100.0 (328.9)	19.5	16.7	-12.3

11βOHAn	1 (3.5)	100 (344.8)	-15.6	-0.1	4.3
11βOH5α-Dione	0.5 (1.7)	100.0 (331.1)	-6.9	-4.6	4.0
11βOHEt	0.5 (1.6)	80.0 (261.4)	-15.8	-7.0	6.1
11KA4	2.5 (8)	100 (322.6)	15.0	8.8	1.1
11KT	1 (3.3)	100 (331.1)	10.1	6.6	3.2
11Ket	2.5 (8.2)	100.0 (328.9)	19.6	13.9	14.5
11KAn	0.5 (1.6)	100.0 (328.9)	15.3	8.6	9.9

Inter-assay (between run) imprecision assessed at 40 ng/mL was within the ideal range and values were between 2.7 % to 15 % (**Table 3.8**). Intra-assay imprecision at this concentration was also within ideal limits, ranging between 1.8 % and 9.1 %. Linearity was determined by assessment of three independent calibration curves. Curves were linear in-between LLOQ and ULOQ, and each individual calibrant did not exceed ± 20 % from nominal concentrations and had R^2 values ≥ 0.99 for all analytes.

Table 3.8 Inter-assay (between run) and intra-assay (within run) imprecision of Williams E media samples spiked with 7.5, 25, 40 and 75 ng/mL of all analytes.

	Inter-assay imprecision, CV (%)	**Intra-assay imprecision, CV (%)**			
Analyte	**40 ng/mL**	**7.5 ng/mL**	**25 ng/mL**	**40 ng/mL**	**75 ng/mL**
DHEA	4.7	9.1	5.7	1.8	4.4
A4	10.5	9.4	7.3	5.7	n/a
T	9.8	8.4	8.0	3.5	n/a
5α-DHT	3.4	8.0	6.5	4.1	2.9
5α-dione	12.2	11.5	6.0	9.1	3.6
An	6.0	10.5	7.9	3.0	3.6
Et	6.0	6.7	5.9	4.0	3.4
3α-adiol	13.9	14.0	9.6	6.3	19.2
11βOHA4	4.8	5.4	6.3	4.3	3.7
11βOHT	4.9	6.4	6.2	4.0	4.0

11βOHAn	6.0	6.7	7.1	7.5	4.5
11βOH5α-dione	2.7	10.3	7.5	3.1	5.0
11βOHEt	6.1	16.4	4.7	8.0	3.6
11KA4	9.7	9.2	7.2	2.9	9.1
11KT	5.3	9.5	13.4	2.1	2.9
11Ket	15	7.9	11.6	6.8	4.9
11KAn	11.9	9.0	10.8	3.1	8.0

3.3. Discussion

3.3.1. UHPC-MS/MS can be successfully tailored for multi-androgen profiling

This chapter describes the development, optimisation and validation of quantitative multi-androgen steroid profiles using liquid chromatography tandem mass spectrometry. The assay is a high-throughput, efficient analytical tool for the evaluation of both classic and 11-oxygenated androgen precursors and metabolites during *ex vivo* human liver androgen metabolism investigations. The liver is a known site of extreme metabolic activity and coupled by the fact that androgen metabolism is complex, involving constant interconversion between metabolites (**Figure 1.4, Chapter 1**), a UHPLC-MS/MS assay capable of comprehensively profiling of both classic and 11-oxygenated androgens was required. When considering androgen metabolism, particularly in the context of female hyperandrogenism such as PCOS, the inclusion of 11-oxygenated metabolites is vital [29, 157]. 11-oxygenated androgens are the

predominant androgens in PCOS and do not decline with age in both healthy women and women with PCOS [15, 29, 31]. They are key contributors to the circulating androgen pool and must not be overlooked. Importantly, due to their origin (peripheral conversion of 11βOHA4), 11-oxygenated androgens also provide an understanding of differential adrenal and peripheral androgen generation in women [158]. As 11-oxygenated androgens were previously thought insignificant in regard to female hyperandrogenism, they are not currently measured in clinic, meaning the development of a single UHPLC-MS/MS assay for the measurement of classic and 11-oxygenated androgens has not been a point of focus, and thus not previously reported. The assay described here, includes an extensive panel of seventeen classic and 11-oxygenated androgen precursors, active androgens and downstream metabolites. Previously reported UHPLC-MS/MS assays have included between three to ten androgens, mainly focusing on active androgens and their immediate precursors, or solely classic androgens [149, 159, 160].

Androgen metabolism investigations using the NMLP model required incorporation [$^{13}C_3$]-A4 and [$^{13}C_3$]-11KA4 precursors. Therefore, I adapted the UHPLC-MS/MS method to investigate androgen metabolism using exogenous [^{13}C]-labelled androgens by modifications to MRMs. The use of transiently transfected HEK293 cells, overexpressing steroidogenic enzymes (**Chapter 2**), enabled the synthesis of labelled androgens, confirmation of MRMs and mass transition optimisation. This method therefore provides the ability to carve out a comprehensive picture of differential metabolic pathways of classic and 11-oxygenated androgens, in the absence of interference from endogenous steroids. To the best of my knowledge, a UHPLC-

MS/MS method capable of simultaneously profiling an extensive panel of sixteen [$^{13}C_3$]-labelled classic and 11-oxygenated androgen precursors and metabolites, has not been reported. The incorporation of [$^{13}C_3$]-labelled metabolites within this UHPLC-MS/MS method, is therefore novel.

3.3.2. UHPLC-MS/MS assay met clinical method validation standards when applied to cell culture media

As described above, this method was designed to profile androgen metabolism in two *ex vivo* human liver models. In the first liver model, tissue was suspended in Williams E cell culture medium, containing exogenous androgens. The second model was NMLP, which incorporated acellular blood carrier hemopure as a blood substitute (**Chapter 5**). The method was therefore validated for application Williams E cell culture media and hemopure, with only Williams E media fulfilling to required validation criteria. All androgens can be quantified in Williams E media with acceptable matrix effects, accuracy (% bias), intra-assay imprecision and inter-assay imprecision (% CV), carry-over and recovery. These results demonstrate the reliability, robustness and accuracy when using Williams E media. During validation procedures of this multi-androgen profiling method, co-elution between two pairs of analytes (11K-5α-dione and 11βOHA4; 11βOHT and 11K-5α-DHT) was identified. Despite alterations to solvent gradients, run time and choice of chromatography column, separation of these analytes could not be achieved without compromising the separation of the other analytes included in the method. It has been shown that 5α reduction of 11KT to 11K-5α-DHT is not feasible via SRD5A1, and when SRD5A2 is co expressed with AKR1D1, the 5β reduction of 11KT to 11KEt dominates [24]. Co-expression of SRD5A1 and

AKR1D1 in Hep G2 liver cells, showed the 5β reduction of 11KT to 11Ket was primary [24]. For this reason, and due to the expression of AKR1D1 in liver tissue (**Chapter 1, Figure 1.4; Chapter 5, Figure 5.1**), significant generation of 11K-5α-DHT, that would interfere with 11βOHT measurement, would not be expected. 11K-5α-DHT was therefore removed from the assay. It has also been shown that 11K-5α-dione readily converts to 11KAn [24]. The presence 11K-5α-dione, in quantifiable amounts or amounts that would interfere with 11βOHA4 measurement, would not be expected. 11K-5α-dione was therefore also removed from the assay. Even with the exclusion of these analytes, the assay remains a useful tool for multi-androgen profiling, within the context of this project and wider applications.

3.3.3. Multi-androgen profiling by UHPLC-MS/MS has important clinical applications for the diagnosis of hyperandrogenism

This UHPLC-MS/MS method was developed for specific application to profiling androgen metabolism in ex vivo human models, but also has wider translational applications. Currently, for the diagnosis of conditions of hyperandrogenism in women, such as PCOS, single steroid measurements of serum testosterone, are primarily taken [77]. However, it has now become clear that measurement of testosterone alone is inadequate. Testosterone largely circulates bound to the protein SHBG, only dissociating to enter target tissue [77]. It has therefore been proposed that additional steroids, such as androgen precursors DHEA and A4, are more representative of androgen excess, which would reduce the number of women that go undetected and are misclassified as normoandrogenic [77]. Furthermore, the discovery 11-oxygenated androgens highlighted the need for clinical measurement of these androgens

alongside classic androgens. When investigating androgen metabolism, particularly where hyperandrogenism is concerned, the inclusion of 11-oxygenated androgens is vital as they are key contributors to the circulating androgen pool [29, 157]. The evidence for that 11KA4 and 11KT should also be routinely measured to ascertain hyperandrogenism is undeniable, but investigations have also highlighted the need for measurement of further downstream metabolites, such as 11βOHAn, which is already accepted as a urinary marker for the crucial 11-oxygenated precursor, 11βOHA4 [24, 29-31, 158]. The UHPLC-MS/MS method I developed as part of this thesis, provides a means by which these androgens can be profiled simultaneously and accurately. The method has been fully validated for application to Williams E cell culture media but with appropriate alterations to sample preparation and matrix effect investigations, can be applied to other matrices including saliva, serum, tissues. It could therefore be used a clinical tool to enhance androgen profiling for the diagnosis of conditions of hyperandrogenism. With an 'all-inclusive' approach to multi-androgen profiling and a run time of just 5 minutes, this assay meets routine clinical LC-MS/MS analysis standards and can be considered a 'ready-to-go' clinical analytical androgen profiling tool. Additionally, the method could be appropriately applied to other *in vitro* cell culture medias and used to characterise androgen metabolism in a variety of laboratory experimental conditions.

3.3.4. Limitations

Despite the power of UHPLC-MS/MS as an analytical tool, it is still vulnerable to matrix effects [161]. This assay is no exception. When applied to hemopure, significant matrix effects were observed (**Table 3.6**). This was the case for all analytes across the three

concentration levels investigated. Taking these findings into account, LLOQ/ ULLOQ for analytes were not investigated when applied to hemopure as these parameters are dependent on ionisation efficiency, which was clearly compromised. As a result, using this matrix the method can only be classed as semi quantitative, where androgens can be positively detected, but with quantification subject to larger variation than Williams E. Although the reason behind matrix effects are not completely understood [162], it is thought that the co-elution of substances can compete with analytes to gain charge, reducing analyte ability to transfer to the gas phase [161-163], or conversely to provide charge to enhance signal. These substances include salts, peptides, buffers, ion pairing reagents phospholipids and amino acids [161-163]. Hemopure is of bovine origin, composed of glutaraldehyde-polymerized bovine haemoglobin in Ringers lactate (consisting of sodium chloride, potassium, sodium lactate [164]) and during NMLP is mixed with 5% albumin (diluted in 0.9% sodium chloride saline). Any one of these constituents could have caused or contributed to the inferences observed. Although complete elimination of matrix effects is difficult, there are ways to reduce them, and they can be somewhat normalised through use of appropriate internal standards. This method incorporates deuterium labelled internal standard analogues for each analyte, and where an exact analogue was unavailable, internal standards were chosen specifically for these analytes based on their retention times, ionizability and extraction efficiencies. Thus, without further optimisation, when applied to hemopure as the sample matrix, this assay can still be used to provide an informative picture, allowing investigation into androgen metabolic pathways. For the explorative purpose of this thesis, the aim was to characterise the nature and patterns of the pathways of androgen metabolism, a qualitative method is sufficient. A semi-

quantitative method is therefore more than sufficient. Williams E would be the preferred matrix for a quantitative method but cannot be used during NMLP, as it is not an oxygen carrier and cannot provide hepatocytes with required oxygen/ nutrients. Hemopure is also chosen for use during NMLP over donated human blood, as it is analyte free and therefore does not contribute to the residual endogenous steroid pool. Limiting the level of endogenous steroids present in the model serves to reduce enzyme competition and therefore improve detection of downstream [$^{13}C_3$]-labelled metabolites. There has to be a compromise between the methodological optimal and the mass spectrometry optimal.

Limitations include inability to fully validate the [^{13}C]-labelled method using [^{13}C]-labelled analytes and adjustments to sample preparation for the purposes of validation (exclusion of sulfatase *helix pomitia* hydrolysis mixture). It was not possible to produce enough [^{13}C]-labelled metabolites using transiently transfected HEK293 cells, in the necessary quantities for validation. The choice to use [^{13}C]-labelled isotopes, opposed to other isotopic labels, for NMLP was based on the fact that the physiochemical properties, and therefore behaviour (ionisation, recovery etc), of [^{13}C]-labelled isotopes are identical to the non-labelled steroids [54, 165]. This property allowed for the extrapolation of validation data, assuming the [^{13}C]-labelled compounds act similar to their unlabelled analogues. Therefore, the results from validation for performance of non-labelled androgen analytes can be presumed to represent the limits for [^{13}C]-labelled analytes. This principle was also applied when using unlabelled androgens in the calibration series for quantification of [^{13}C]-labelled metabolites. Of course, independent method validation of each labelled analyte would be ideal, but this was

beyond the scope of this thesis due to lack of commercial availability. Adjustments to sample preparation for the purposes of validation (exclusion of sulfatase *helix pomitia* hydrolysis mixture), may also be seen as a limitation.

3.3.5. Conclusions

In conclusion, this chapter describes the development of a high-throughput UHPLC-MS/MS method capable of quantifying both classic and 11-oxygenated androgens in one assay. The method was developed for the measurement of seventeen classic and 11-oxygenated androgens. The method met clinical validation criteria when applied to Williams E cell culture media and can be used semi-quantitatively when using hemopure. Mass transitions were modified to accommodate for the measurement of sixteen [$^{13}C_3$]-labelled classic and 11-oxygenated androgens. This provided a toolbox of methods, with well-defined validation data for each. These methods can thus be applied to the investigation of androgen metabolism in *ex vivo* human liver.

CHAPTER 4

ALDO KETO REDUCTASE FAMILY 1 MEMBER 3 (AKR1C3) ACTIVITY IN FEMALE ADIPOSE TISSUE AND IMPACT OF AKR1C3 INHIBITOR TREATMENT

4.1. Introduction

Once disregarded as a relatively inert site of triglyceride storage only, adipose tissue has now been established as a metabolically active endocrine organ in its own right [166]. As discussed in **Chapter 1**, local androgen activation in adipose tissue plays a central role in the development of symptoms characterising PCOS, leading to abnormal body fat deposit, lipolysis dysregulation and insulin resistance [36, 103, 167, 168]. Additionally, women prescribed the oral contraceptive pill, with the intention to reduce ovarian androgen generation, can still experience hyperandrogenism [169]. The enzyme AKR1C3, which is responsible for the activation of inactive androgen precursors to active products, is highly expressed in adipose tissue (both subcutaneous and omental) (**Chapter 1; Figure 1.4**). Adipose tissue is therefore a key regulator in the level and bioactivity of sex steroids, and thus a major contributor to excess androgen levels observed in women with PCOS [167]. The metabolism of classic androgens in adipose tissue is well established, whereby A4 is readily activated to T via AKR1C3, and T can be further converted to 5α-reduced metabolite 5α-DHT

[37, 170, 171]. 11-oxygenated androgens have been discovered relatively recently, and their metabolism within adipose tissue has not been profiled. Since 11-oxygenated androgens are the predominant androgens in PCOS and measured circulating androgen levels may not represent local androgen activation [29, 36, 37, 77], an understanding of the local activation of these androgens within adipose tissue, a key metabolically active androgen regulator, is vital. Additionally, a recent cross-sectional study showed active 11-oxygenated androgens increase with increases in BMI, indicating a potential role of adipose tissue in the activation of 11-oxygenated androgens [30].

The mechanisms by which adipose upregulates androgen generation are complex, consisting of multiple influences and contributors (**Chapter 1**). O'Reilly et al. described a vicious cycle occurring in adipose tissue where excess androgen generation leads to lipid accumulation via decreased lipolysis and increased DNL, which causes systemic insulin resistance and increased AKR1C3 expression, further contributing to androgen excess [36]. In order to address the excess androgen generation in adipose, this cycle must be broken. As the enzyme AKR1C3 plays such a central role in this cycle, it could serve as a therapeutic target in order to break the cycle. This chapter therefore explores the potential of AKR1C3 as a drug target for the reduction of androgen excess and associated metabolic complications in PCOS. We were provided two AKR1C3 inhibitors, BAY1 (MW; 462.6) and BAY2 (MW; 365.4), through collaboration with the pharmaceutical company Bayer HealthCare Pharmaceuticals LLC (Berlin, Germany).

Here, an ex vivo model of both omental and subcutaneous female adipose tissue was used to determine local androgen generation, particularly focusing on AKR1C3 activity, and the impact of an AKR1C3 inhibitor on androgen activation. Importantly, for the first time this study investigated 11-oxygenated androgen metabolism, in addition to classic androgens (**Chapter 1; Aim 2**).

4.2. Materials and methods

4.2.1. AKR1C3 activity assay using HEK293 cells

HEK293 cells were cultured and transiently transfected with pcDNA3_AKR1C3, as described in **Chapter 2; 2.2**. To identify a suitable sample collection time for inhibitor dose response tests, cells overexpressing AKR1C3 were then treated with 100 nmol/L of either A4 or 11KA4 in MEM medium, from 1 mg/mL stocks in methanol, for 24 hours. Medium samples were taken periodically over the 24-hour incubation time and androgens extracted by liquid-liquid extraction before being quantified using UHPLC-MS/MS (**Chapter 2; 2.1; Chromatographic method 1**). The results were normalised to the amount of total protein in the respective well.

4.2.2. AKR1C3 Inhibitor dose response assay using HEK293 cells

HEK293 cells were cultured and transiently transfected with pcDNA3_AKR1C3, as described in **Chapter 2; 2.2.** HEK293 overexpressing AKR1C3 were then treated with 100 nmol/L of either A4 or 11KA4 in the presence and absence of seven BAY1 and BAY2 inhibitor concentrations. Medium samples were collected after 4 hours, androgens were extracted by liquid-liquid extraction and quantified by UHPLC-MS/MS (**Chapter 2; 2.1; Chromatographic method 1**). The results were normalised to the

amount of total protein in the respective well. Each biological replicate was performed as four technical replicates for each treatment. IC_{50} values for inhibitors were calculated by Prism non-linear regression curve fit algorithm.

4.2.3. Androgen metabolism in an *ex vivo* adipose tissue model

4.2.3.1. Subject selection

Participants were recruited from Birmingham Women's hospital, Birmingham, UK. Women aged 36 to 60 years undergoing selective gynaecological surgery were recruited. Inclusion and exclusion criteria are outlined in **Table 4.1** below. Participant age, BMI, ethnicity and medical history is outlined in **Table 4.2** below. Biopsy samples were collected by the performing surgeon at the beginning of the surgical procedure. Twenty-three women were included in the study, three of which reported a formal diagnosis of PCOS. Experiments with adipose tissue were approved by the West Midlands – Black Country Research Ethics Committee (IIH:WT, REC 14/WM/0011, IRAS 142942; and 11OXO, REC 19/WM/0183 IRAS 221491).

Table 4.1 Study inclusion criteria for analysis of female androgen metabolism using *ex vivo* adipose tissue incubations. Abbreviations: BMI; body mass index.

Inclusion Criteria	Exclusion Criteria
Pre/post-menopausal women aged between 36 to 60 years	Women on hormone replacement therapies, including hormonal contraception or metformin
BMI between 20 to 36 kg/m^2	

Candidate for selective gynaecological surgery (hysterectomy, myomectomy or removal of ovarian cysts)	

Table 4.2 Self-reported participant age, BMI, ethnicity, menstrual cycle and PCOS status. Abbreviations: BMI; body mass index, PCOS; polycystic ovary syndrome. Participants were given a study questionnaire in order to self-report medical history. Regular periods were defined as a period approximately every 28 days.

Participant	Age (years)	BMI (kg/m^2)	Self-reported ethnicity	Regular Periods (yes/no)	Report of PCOS Diagnosis (yes/no)
1	52	32	British (mixed parentage)	No	No
2	74	36	White	No	No
3	41	21	British	Yes	No
4	41	38	African-Caribbean	No	Yes
5	49	28	not stated	Yes	Yes
6	54	36	White British	No	No
7	47	24	White British	Yes	No
8	55	27	African	No	No
9	51	25	White/ Afro Caribbean	No	No
10	54	26	Asian	No	No
11	47	32	White British	Yes	Yes
12	60	26	White	No	No
13	48	26	White British	Yes	No
14	52	36	Black	No	No
15	63	23	White	No	No
16	42	25	Indian British	Yes	No
17	46	24	British Indian	Yes	No
18	44	20	White	Yes	No

19	45	27	Indian	Yes	No
20	51	27	Black Caribbean	Yes	No
21	48	31	British Pakistani	No	No
22	48	35	British Pakistani	Yes	No
23	36	20	British Pakistani	Yes	No
Minimum age/ BMI	36	20	n/a	n/a	n/a
Maximum age/ BMI	60	38	n/a	n/a	n/a

4.2.3.2. Experimental procedure

The procedure was conducted as outlined in detail in **Chapter 2, section 2.3**. Briefly, freshly resected female human subcutaneous and omental adipose tissue (100-200 mg) was washed in PBS and diced into four smaller equal pieces. Tissue was suspended in DMEM/ Ham's F-12 supplemented with 100 units/mL penicillin, 100 µg/mL streptomyocin, 33µM Biotin and 17µM Panthotenic acid containing 100 nmol/L of either A4 or 11KA4 with or without the AKR1C3 inhibitor BAY2. As introduced in **Chapter 2**, the difference between steroidal inhibitors BAY1 and BAY2 is their structure, with BAY1 being steroidal and BAY2 being non-steroidal. These investigations incorporated BAY2, as a non-steroidal structure was the preferred choice due to its reduced toxicity and *in vivo* side effects and effects in ongoing trials. Additional cell-free incubations of all treatments and vehicle-treated cells were prepared as controls. Treated tissue was incubated at 37 °C and rotated at 20 rpm for 24 hours. 1 mL of medium was collected after 24 hours. Medium samples were centrifuged for 10 minutes (4000 rpm, 4°C), transferred to a sterile Costar 1.7 mL low binding snap cap minicentrifuge tubes and stored at -80 °C for liquid-liquid extraction. A blood sample from each patient was also taken, centrifuged for 10 minutes (200 g, 4°C) and serum was stored at -80°C until analysis by UHPLC-MS/MS.

4.2.4. Androgen extraction and quantification by UHPLC-MS/MS

Androgens were extracted from cell culture media and serum by liquid-liquid extraction and quantified using a previously validated UHPLC-MS/MS assay [55], as detailed in **Chapter 2; Section 2.1**. Briefly, androgens and internal standard separation was achieved by a H-class Waters Acquity ultra high-performance liquid chromatography

system with a 50 µL loop using a Phenomenex Luna Omega column at 60 °C. Volume of reconstituted same was 10 µL. Mobile phase A was comprised of UHPLC grade water containing 0.1 % formic acid (vol/vol) and mobile phase B comprised of UHPLC grade methanol. Mobile phase B percentage was increased from 45 % to 75 % over 5 minutes. The tandem mass spectrometry parameters used to quantify androgens investigated in this chapter are outlined in **Table 4.3** below.

Table 4.3 Quantifier and qualifier mass transitions, retention times, cone voltages, collision energies and internal standard for target analyte. Stable isotope labelled version of 11βOHT was unavailable, therefore and 11βOHA4-d7 was used.

Steroid	Retention time approx. (min)	Mass transition (m/z) Quantifier *Qualifier*	Cone voltage (kV)	Collision energy (eV)	Internal standard
A4	2.0	287.2 > 109.1 *287.2 > 97.1*	26 26	22 22	A4-d7
T	2.3	289.2 > 97.1 *289.2 > 109.1*	40 40	20 24	T-d3
11KA4	1.0	301.1 > 121.1 *301.1 > 257.1*	44 44	22 22	11KA4-d10
11KT	1.2	303.1 > 121.0 *303.1 > 259.1*	20 20	22 22	11KT-d3
11βOHA4	1.3	303.1 > 285.1 *303.1 > 267.1*	30 30	14 16	11βOHA4-d7
11βOHT	1.5	305.2 > 269.2 *305.2 > 121.1*	16 16	14 20	11βOHA4-d7

4.3. Results

4.3.1. AKR1C3 activity in transiently transfected HEK293 cells

In order to evaluate concentration dependent inhibition of AKR1C3 by inhibitors BAY1 and BAY2, HEK293 cells overexpressing AKR1C3 were treated with classic androgen precursor A4 and 11-oygenated precursor 11KA4. Cells were initially treated with

A4/11KA4 in the absence of inhibitors, to identify a suitable timepoint for sample collection during dose response investigations. Analysis of time course experiments identified 24 hours as the incubation time leading to maximum product formation (**Figure 4.1**). After 24 hours, conversion of 11KA4 to 11KT was approximately 3 times more than conversion of A4 to T, indicating preferential activation of 11KA4 by AKR1C3. From this initial analysis, 4 hours was identified as a suitable timepoint for sample collection during BAY1/2 inhibitor dose response investigations, as it was within the linear range for both 11KA4 and A4 conversion.

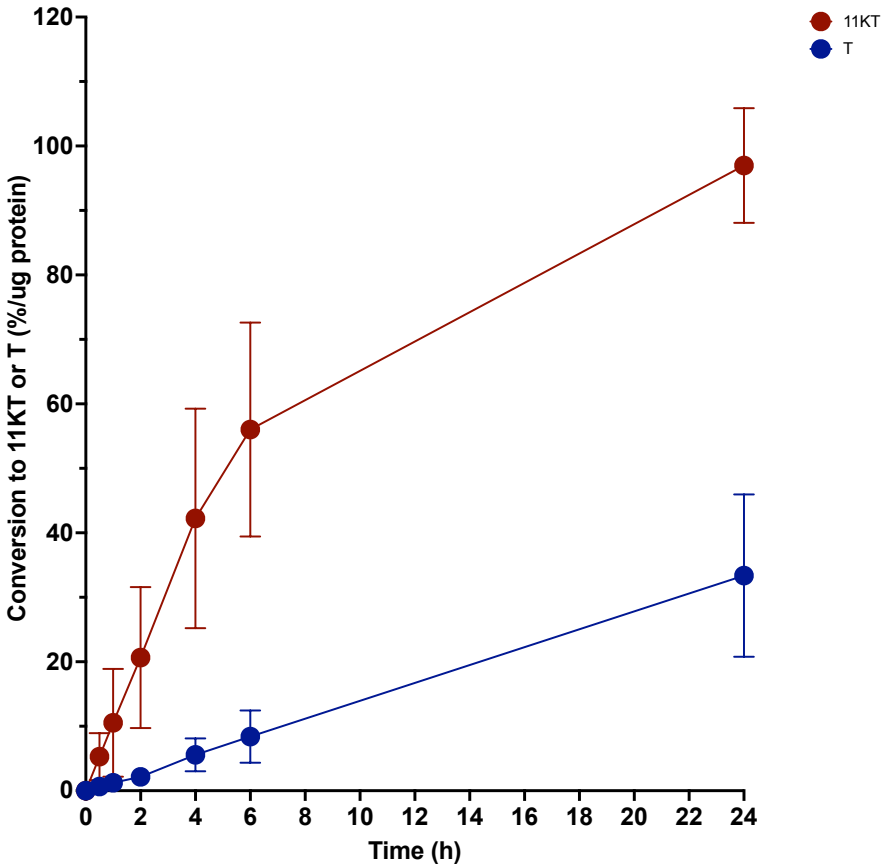

Figure 4.1 Conversion of 100 nmol/L A4 to T (blue) and 100 nmol/L 11KA4 to 11KT (red) over time in HEK293 cells transiently overexpressing AKR1C3. Cells were treated with 100 nmol/L of either A4 or 11KA4, and their respective products, T and 11KT, were quantified using UHPLC-MS/MS. Each data point is representative of four biological replicates (n=4). Mean ± SD (GraphPad Prism version 9.5) is indicated. Each biological replicate is representative of the mean of three technical replicates. Data are shown as percent relative to concentration of A4 or 11KA4 added. Product formation was quantified by UHPLC-MS/MS and normalised to the total protein content.

4.3.2. AKR1C3 inhibitors show IC50 values in the low nanomolar range in HEK293 cells overexpressing AKR1C3

Inhibitor dose response experiments in transfected HEK 293 cells confirmed the ability of BAY1 (steroidal structure) and BAY2 (non-steroidal structure) to inhibit AKR1C3 activity (**Figure 4.2**). As expected, increasing the concentration of inhibitor caused a progressive decrease in the concentration of T and 11KT detected. Both inhibitors lead to almost 100% inhibition at 300 nmol/L. Analysis of inhibitor potency identified BAY1 to have an IC_{50} value of 8 nmol/L (95 % confidence interval 5-14 nmol/L), yet BAY2 had a higher IC_{50} of 15 nmol/L (95 % confidence interval 12-19 nmol/L), when inhibiting T generation. The preference for activation of 11-oxygenated precursor 11KA4 by AKR1C3 was reflected in the concentration required for maximum inhibition. For conversion of 11KA4 to 11KT, maximum inhibition by BAY1 and BAY2 (95% and 94 %, respectively) was not observed until 1000 nmol/L for BAY1 and BAY2, the highest concentration investigated. However, by analysis of IC_{50} values, BAY1 was again identified to have a lower IC_{50} value, than BAY2, of 12 nmol/L (95 % confidence interval 6 – 25 nmol/L) compared to 19 nmol/L (95 % confidence interval 12 – 34 nmol/L), for BAY2. From these initial investigations, 300 nmol/L was chosen as the inhibitor concentration to be progressed forward for use in *ex vivo* incubations. This was deemed the most suitable concentration as, for both testosterone and 11KT production, 300 nmol/L was the lowest concentration tested resulting in near maximum inhibition.

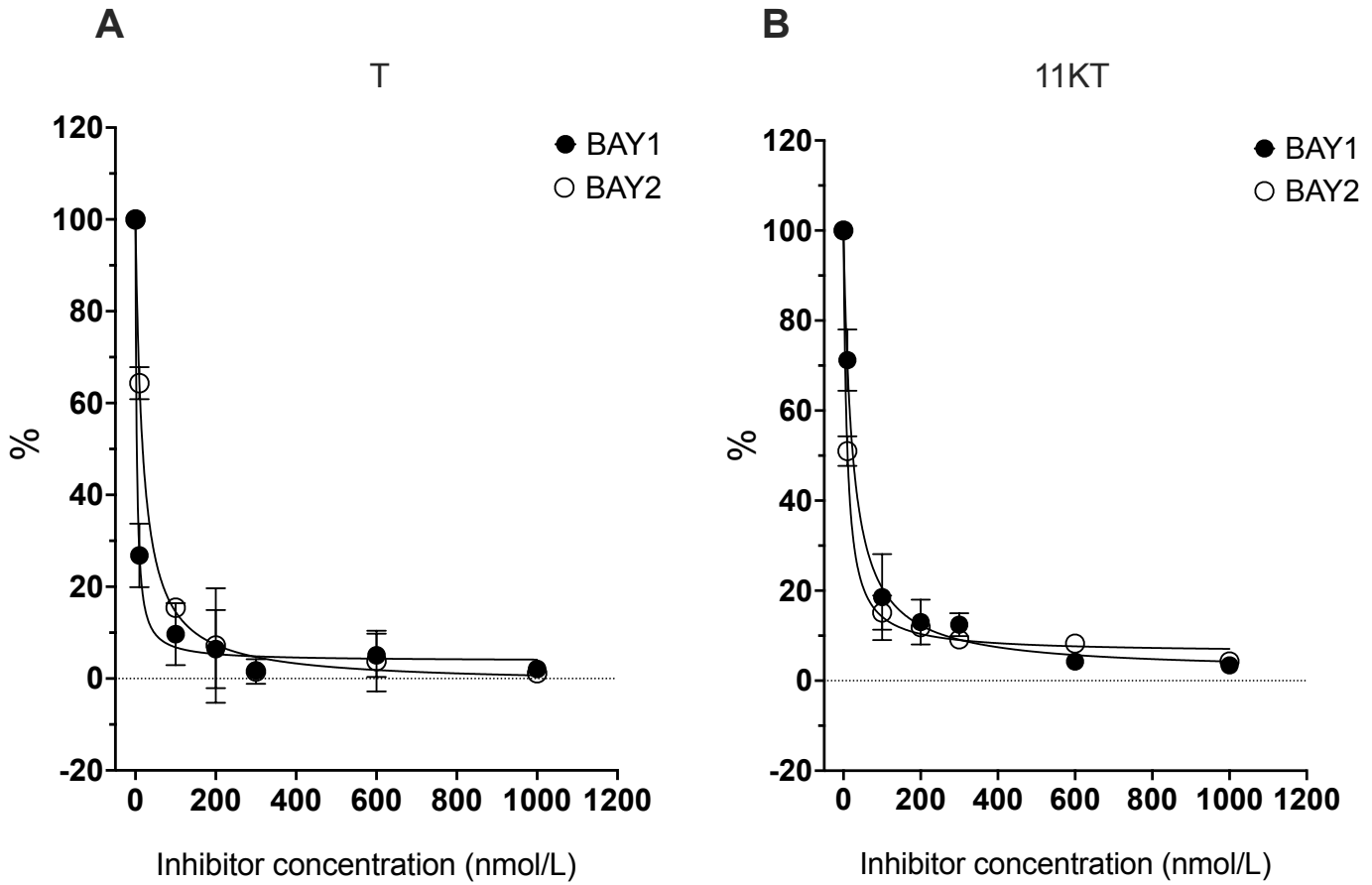

Figure 4.2 Conversion of (A) A4 to T and (B) 11KA4 to T by AKR1C3 in HEK 293 cells overexpressing AKR1C3, in the presence of increasing concentrations of inhibitors BAY1 (purple) and BAY2 (green). Cells were treated with 100 nmol/L of substrate, in the presence of 10, 100, 200, 300, 600 and 100 nmol/L BAY1 or BAY2 AKR1C3 inhibitors for 24 hours. Each data point is representative of three independent biological replicates experiments (n=3). Mean ± SD (Prism version 9.5.0) is indicated. Each biological replicate is representative of the mean of three technical replicates. Non-linear fit regression curve was conducted using GraphPad Prism version 9.5. Data are shown as percent relative to concentration of T or 11KT formed in the absence of inhibitor. Product formation was quantified by UHPLC-MS/MS and normalised to the total protein content.

4.3.3. AKR1C3 preferentially activates 11-oxygenated androgens in female adipose tissue

Initial time course investigations using subcutaneous and omental adipose tissue (**Figure 4.3)**, revealed 24 h to be appropriate incubation time for substantial AKR1C3 activity (generation of active androgens T, 11KT, 11βOHT), allowing for robust product quantification.

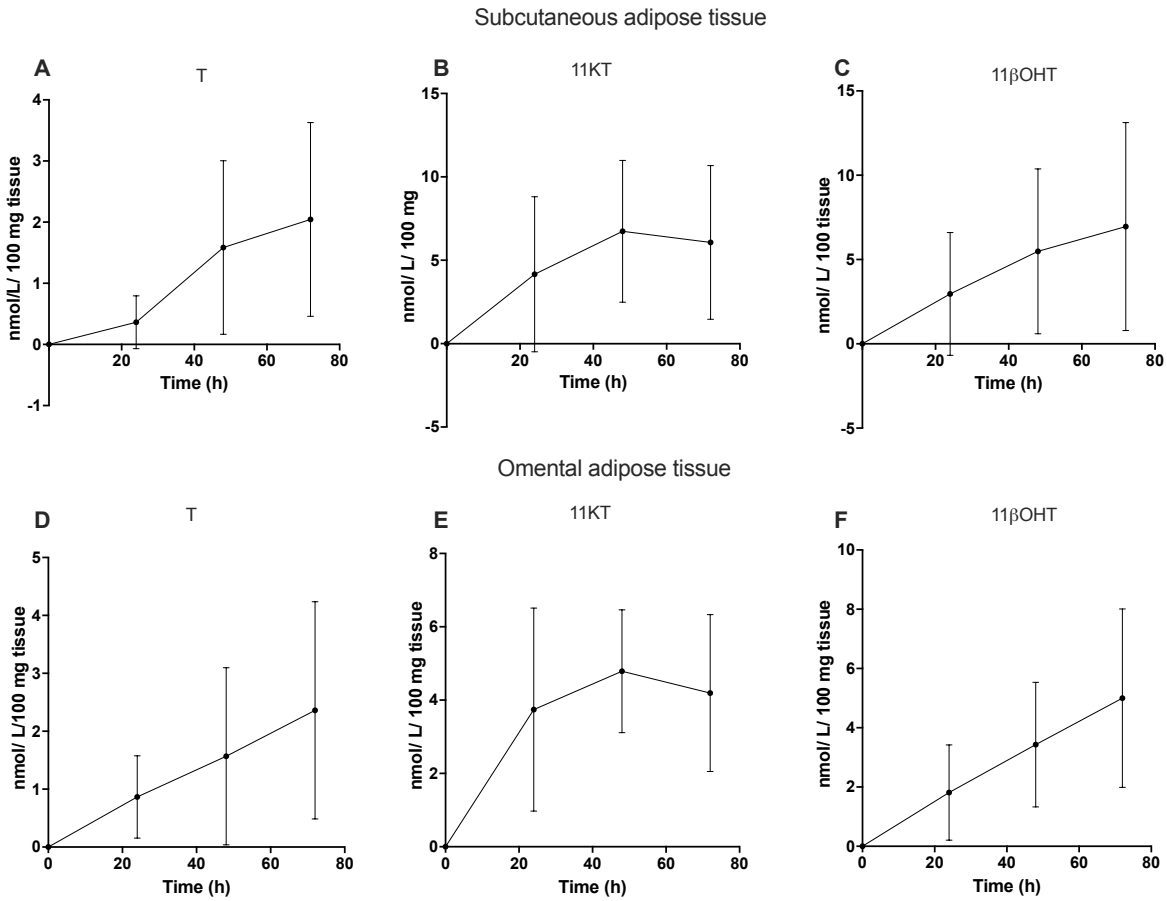

Figure 4.3 Time dependent conversion of classic androgen precursor A4 to T and 11-oxygenated precursor 11KA4 to 11KT and 11βOHT in subcutaneous (A,B and C) and omental (D,E and F) female adipose tissue. Adipose tissue was treated with 100 nmol/L of either A4 or 11KA4 and incubated for 72 hours. Medium samples were taken at 24, 48 and 72 h. Data point points are representative of four biological replicates (n=4) and shown as mean ± standard deviation (performed using GraphPad Prism version 9.5).

To determine the potential for AKR1C3 inhibition as a suitable therapeutic for female hyperandrogenism, particularly in cases of PCOS, it was important to confirm AKR1C3 activity in adipose tissue, in the absence of inhibitor (**Figure 4.4**). Incubations with A4 in both subcutaneous and omental adipose tissue showed significant AKR1C3 activity, yielding respective 17β-hydroxy product, T. While A4 was detected in all incubations with A4, due to incomplete conversion, detection was minimal. Conversion to further downstream metabolites from T was not detected. Incubations with 11KA4 also yielded 17β-hydroxy product 11KT in subcutaneous and omental adipose tissue. 11KT was further converted, to a lesser extent, to its 11β-hydroxy metabolite 11βOHT, via HSD11B1. The dominant metabolite, generated in incubations with 11KA4 was 11KT. 11βOHA4 was also detected, although to a much lesser degree than 11KT and 11βOHA4. Generation of active 11-oxygenated products (11KT+ 11βOHT) was approximately ten times greater than generation of active classic metabolite T, clearly indicating a generation of 11-oxygenated products is favoured in both subcutaneous and omental tissue adipose (**Figure 4.4**). Observed generation of T and 11KT did not significantly differ between subcutaneous and omental tissue. Interestingly however, the mean detection of 11βOHT was reduced in omental tissue, although this difference was determined insignificant ($P = 0.9$).

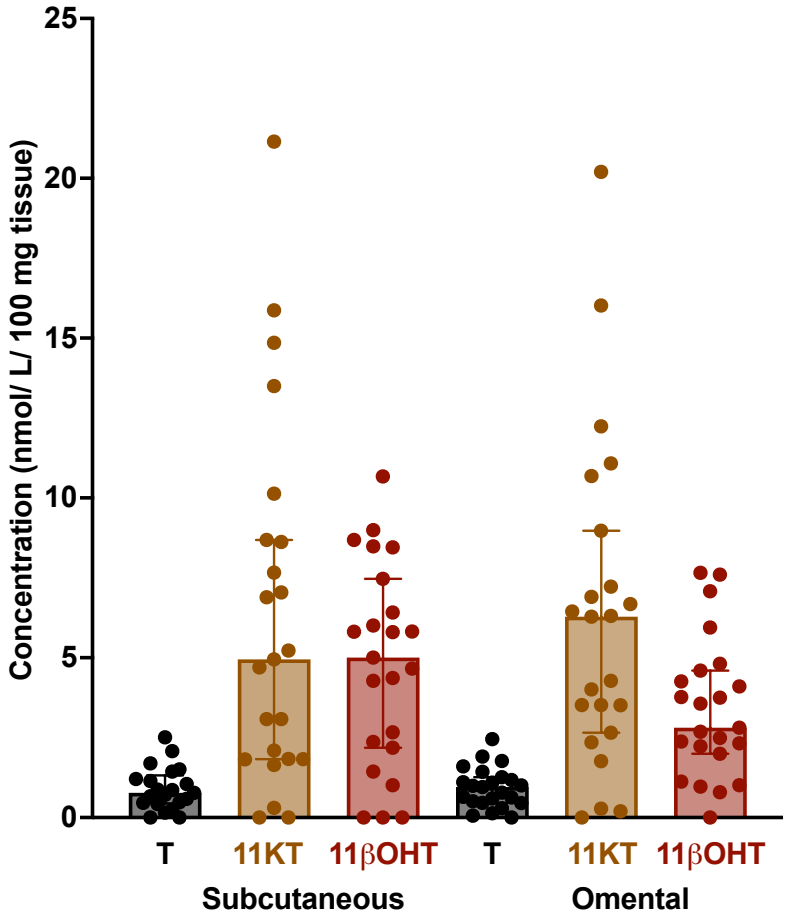

Figure 4.4 Ex vivo metabolism of classic precursor A4 to T (black) and 11-oxygenated precursor 11KA4 to 11KT (orange) and 11βOHT (red) by female subcutaneous and omental adipose tissue. Tissue was incubated with 100 nmol/L of either A4 or 11KA4 for 24 h. Cell culture medium samples were collected after 24 h and product formation (T, 11KT, or 11βOHT) was quantified using UHPLC-MS/MS and normalised to tissue mass. Data is representative of 23 biological replicates (n=23). The median and interquartile range for each product is indicated by the box and whiskers, respectively (performed GraphPad Prism version 9.5). Concentrations below the limit of quantification are shown as 0.

4.3.4. Classic and 11-oxygenated androgen levels in female serum

The relationship between BMI and circulating androgen levels in 25 women (23 of which provided tissue samples for *ex vivo* investigations) was also explored. Although A4, 11KA4 and 11βOHA4 appeared to be negatively associated with increasing BMI

and 11KT and 11βOHT appeared to be positively associated with increasing BMI, these trends were not statistically significant (**Figure 4.5**).

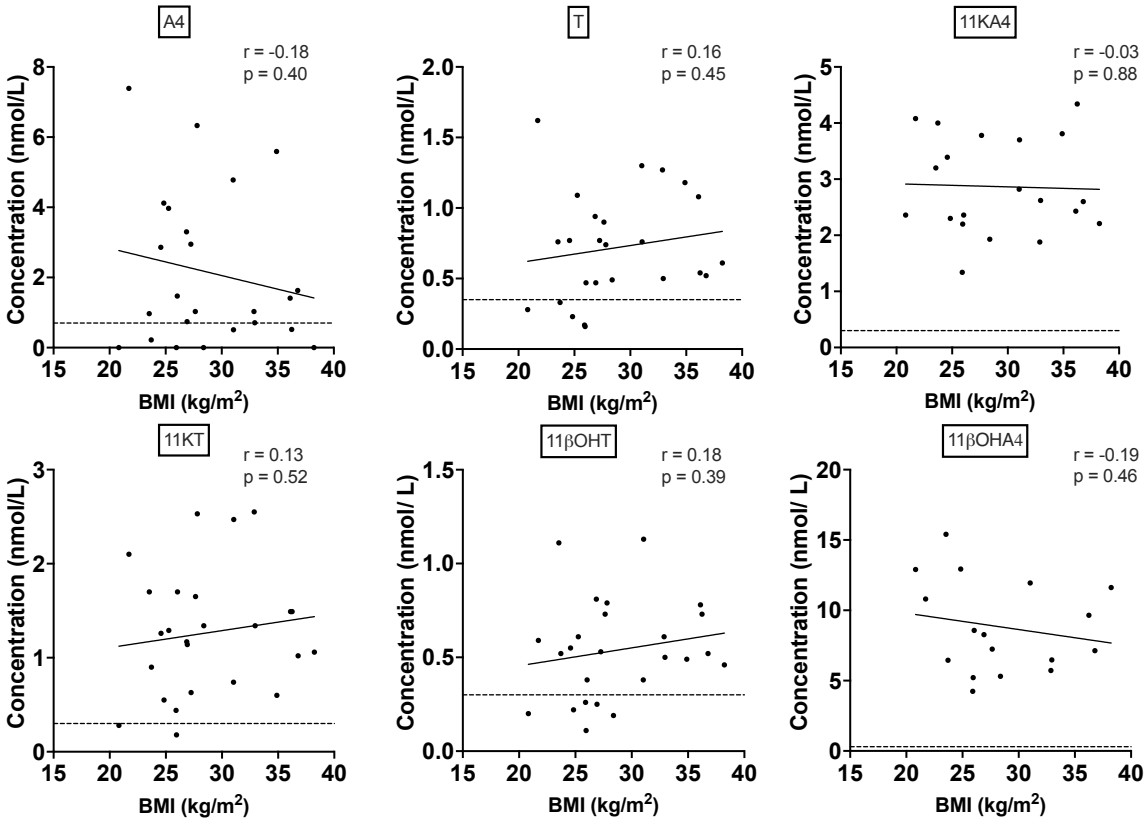

Figure 4.5 Serum concentrations of classic and 11-oxygenated androgens in relation to body mass index (BMI) in women (n = 25. Serum samples collected from 25 women undergoing elective gynaecological surgery were quantified by UHPLC-MS.MS. Steroids are shown as black boxes. Lower limits of quantification are indicated by dashed lines.**)**. Pearson correlation analysis was performed using GraphPad Prism version 9.5. Pearson correlation coefficient (r) and probability value (p) are shown in each graph panel.

4.3.5. Inhibition of AKR1C3 reduces active androgen generation in female adipose tissue

Adipose tissue has been identified as a major contributor to the circulating active androgen pool [37, 170]. Therefore, *ex vivo* adipose tissue exposure to an AKR1C3 inhibitor was conducted here, to explore the effect of AKR1C3 inhibition on active

androgen generation. BAY2 was used for *ex vivo* experiments, due to its suitable potency, non-steroidal structure and ongoing clinical program.

After a 24-hour incubation period, the concentration of T (generated via AKR1C3) detected in both subcutaneous and omental tissue was significantly reduced in the presence of 300 nmol/L of inhibitor (**Figure 4.6a**) on average by -22% and -32%, respectively. This difference was significant in both subcutaneous tissue (p=<0.0001) and omental tissue (p=0.0557). Exposure to AKR1C3 inhibitor, BAY2, had the greatest impact on generation of the active 11-oxygenated metabolite11KT, from precursor 11KA4 (**Figure 4.6b**). Significant decreases in 11KT concentration, in both subcutaneous and omental adipose tissue was observed (p=<0.0001 and p=0.0004, respectively). The average reduction in conversion of 11KA4 to 11KT was -80% and -81%, in subcutaneous and omental tissue, respectively. Inhibition of AKR1C3 also reduced observed generation of 11βOHT, a direct downstream product of 11KT, although this was not statistically significant for subcutaneous tissue but not omental (**Figure 4.6c**). The sum of 11KT and 11βOHT was also calculated. As expected, there was a reduction in the sum of these two 11-oxygenated metabolites when tissue was exposed to an AKR1C3 inhibitor (**Figure 4.6d**). The observed decrease in concentration of the sum of 11KT and 11βOHT was statistically significant in omental tissue (p=0.0286), yet interestingly this was not statistically significant (**Figure 4.6d**). Individual concentrations for T, 11KT and 11βOHT, for each participant, in the absence and presence of AKR1C3 inhibitor, are shown in **Figure 4.7**.

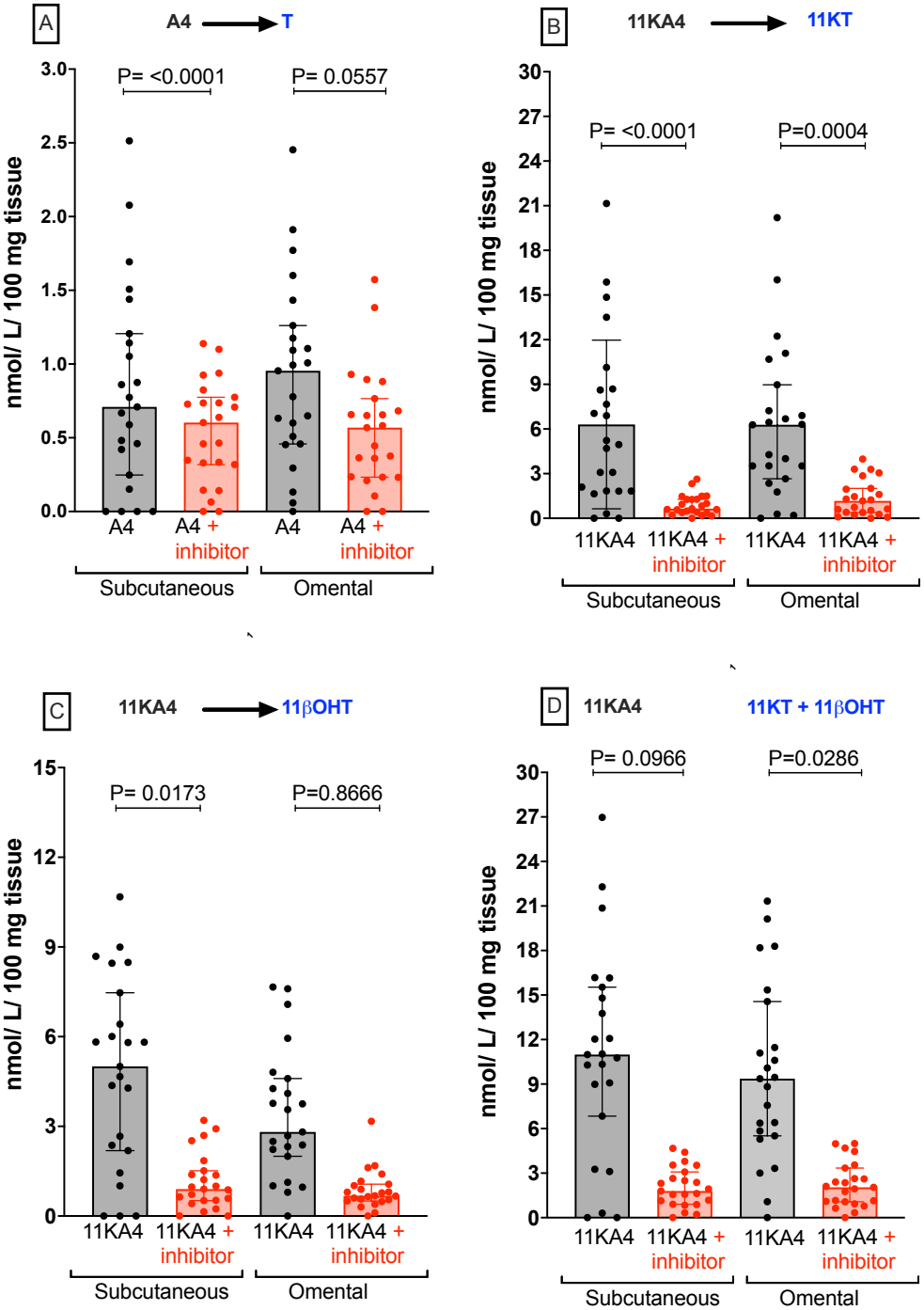

Figure 4.6 *Ex vivo* metabolism of classic androgen precursor A4 to products T (A) and 11 oxygenated precursor 11KA4 to products 11KT (B), 11βOHT (C) and 11KT + 11βOHT (D) in the absence and presence of 300 nmol/L AKR1C3 inhibitor, BAY2, by female subcutaneous and omental adipose tissue. Adipose tissue was incubated with 100 nmol/L of A4 or 11KA4, in the absence (black data points) and presence (red data points) of 300 nmol/L BAY2, for 24 h. Data is representative of 23 biological replicates. Graphs are shown as median ± interquartile range, indicated by the box and whiskers, respectively. Pearson correlation of p value was performed using GraphPad Prism version 9.5. Tissue was retrieved from women undergoing elective gynaecological surgery (n= 23; age range 36-60; BMI range; 20-38 kg/m^2). Cell culture incubation medium was collected after 24 hours and product formation quantified using UHPLC-MS/MS and normalised to tissue mass. Concentrations below the limit of quantification are shown as 0.

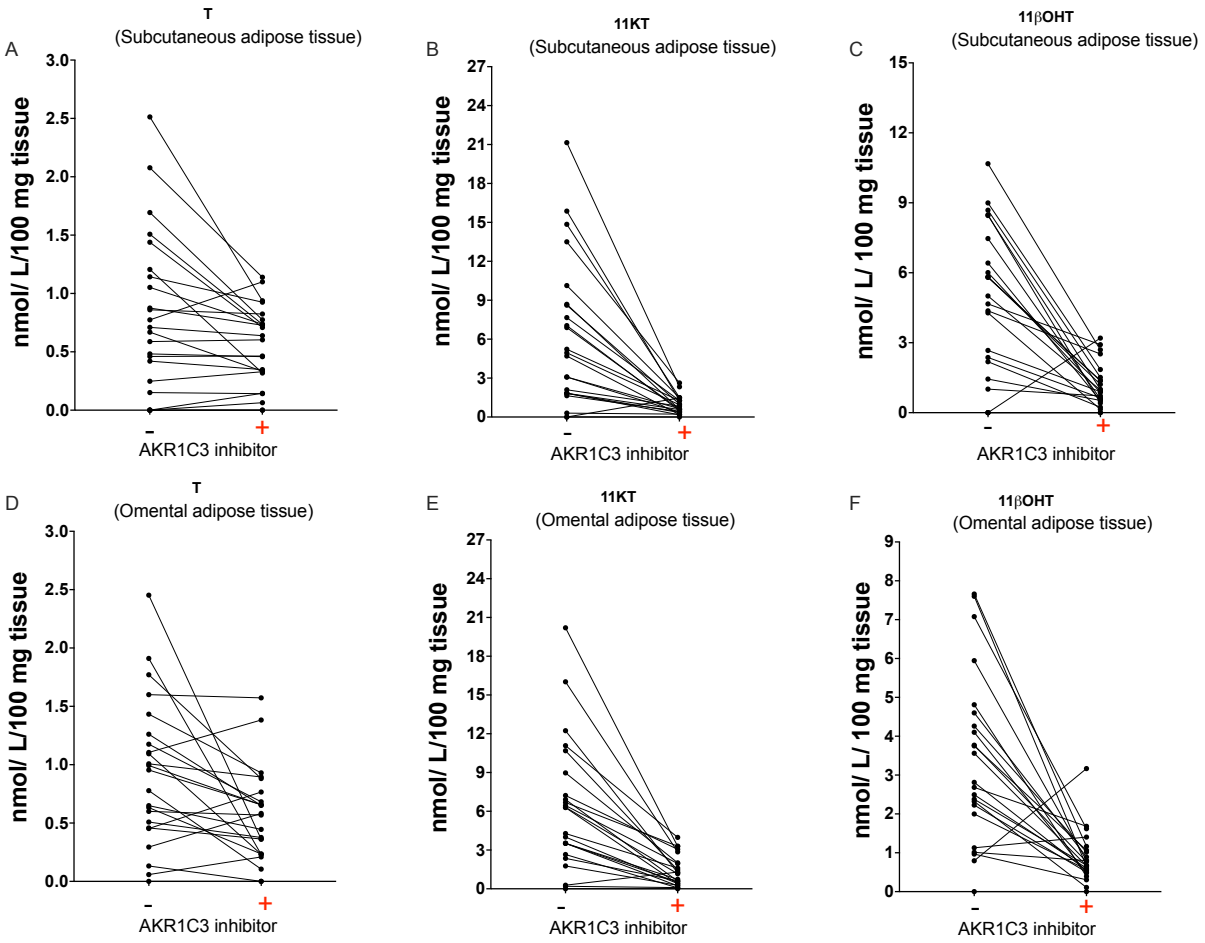

Figure 4.7 Individual values showing *ex vivo* metabolism of classic androgen precursor A4 to products T and 11-oxygenated precursor 11KA4 to products 11KT and 11βOHT by female subcutaneous (A, B and C) and omental (D, E and F) adipose tissue, respectively, in the absence and presence of 300 nmol/L AKR1C3 inhibitor, BAY2. Adipose tissue was incubated with 100 nmol/L of A4 or 11KA4, in the absence and presence of 300 nmol/L BAY2, for 24 h. Tissue was retrieved from women undergoing elective gynaecological surgery (n= 23; age range 36-60; BMI range; 20-38 kg/m^2). Cell culture incubation medium was collected after 24 hours and product formation quantified using UHPLC-MS/MS and normalised to tissue mass.

Changes in the concentration of substrate (A4 and 11KA4) and 11-oxygenated adrenal hydroxy precursor 11βOHA4 were also profiled (**Figure 4.8**). In response to treatment with an AKR1C3 inhibitor, mean changes in A4 in subcutaneous and omental tissue did not differ dramatically, although this was not statistically significant. A greater difference in mean concentration detected after 24 hours with or without inhibitor was

observed for 11KA4 and 11βOHA4, which was statistically significant in both tissue sub types investigated.

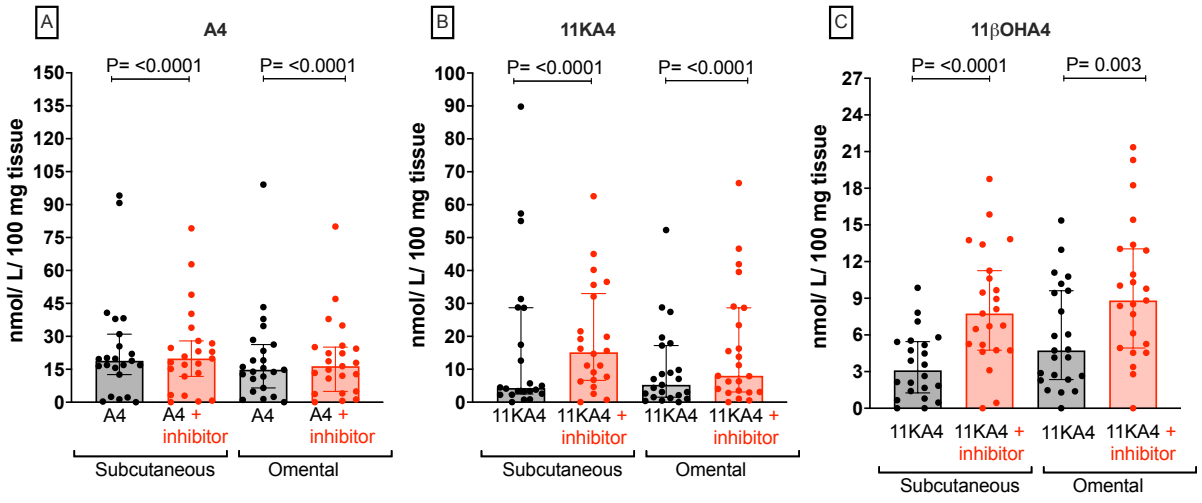

Figure 4.8 Detected concentration of androgen precursor A4 (A) and 11 oxygenated precursors 11KA4 (B) and 11βOHA4 (C) in the absence and presence of 300 nmol/L AKR1C3 inhibitor, BAY2, by female subcutaneous and omental adipose tissue during *ex vivo* tissue incubations. Adipose tissue was incubated with 100 nmol/L of A4 or 11KA4, in the absence (black data points) and presence (red data points) of 300 nmol/L BAY2, for 24 h. Data is representative of 23 biological replicates. Median ± interquartile range, indicated by the box and whiskers, respectively. Pearson correlation of p value analysis was conducted by GraphPad Prism version 9.5.Tissue was retrieved from women undergoing elective gynaecological surgery (n= 23; age range 36-60; BMI range; 20-38 kg/m^2). Cell culture incubation medium was collected after 24 hours, and product formation quantified using UHPLC-MS/MS and normalised to tissue mass. Concentrations below the limit of quantification are shown as 0.

Three of the twenty-three participants included in this study had a formal diagnosis of PCOS (indicated by the patient and/or surgeons notes). Since I hypothesize that AKR1C3 inhibition might be a promising treatment strategy to improve symptoms of androgen excess in women with PCOS, I performed separate analysis of the effect of BAY2 on androgen activation in adipose tissue from these three women. In all three cases, local generation of active androgen metabolites, was decreased in the presence of an AKR1C3 inhibitor (**Figure 4.9**). The reduction in generation of T in response to AKR1C3 inhibitor exposure, was marginal for both subcutaneous and omental tissue (mean ± SD: -27% ± 32% and -14% ± 10%, respectively). However, percent change

in 11-oxygenated metabolite generation in this cohort was substantial in subcutaneous tissue (mean ± SD: 11KT; -89% ± 6%, 11βOHT; -76%± 42%, sum of 11KT + 11βOHT; -83% ± 14%) and omental tissue (mean ± SD: 11KT; -87% ± 4%, 11βOHT; -84%± 3%, sum of 11KT + 11βOHT; -85% ± 2%).

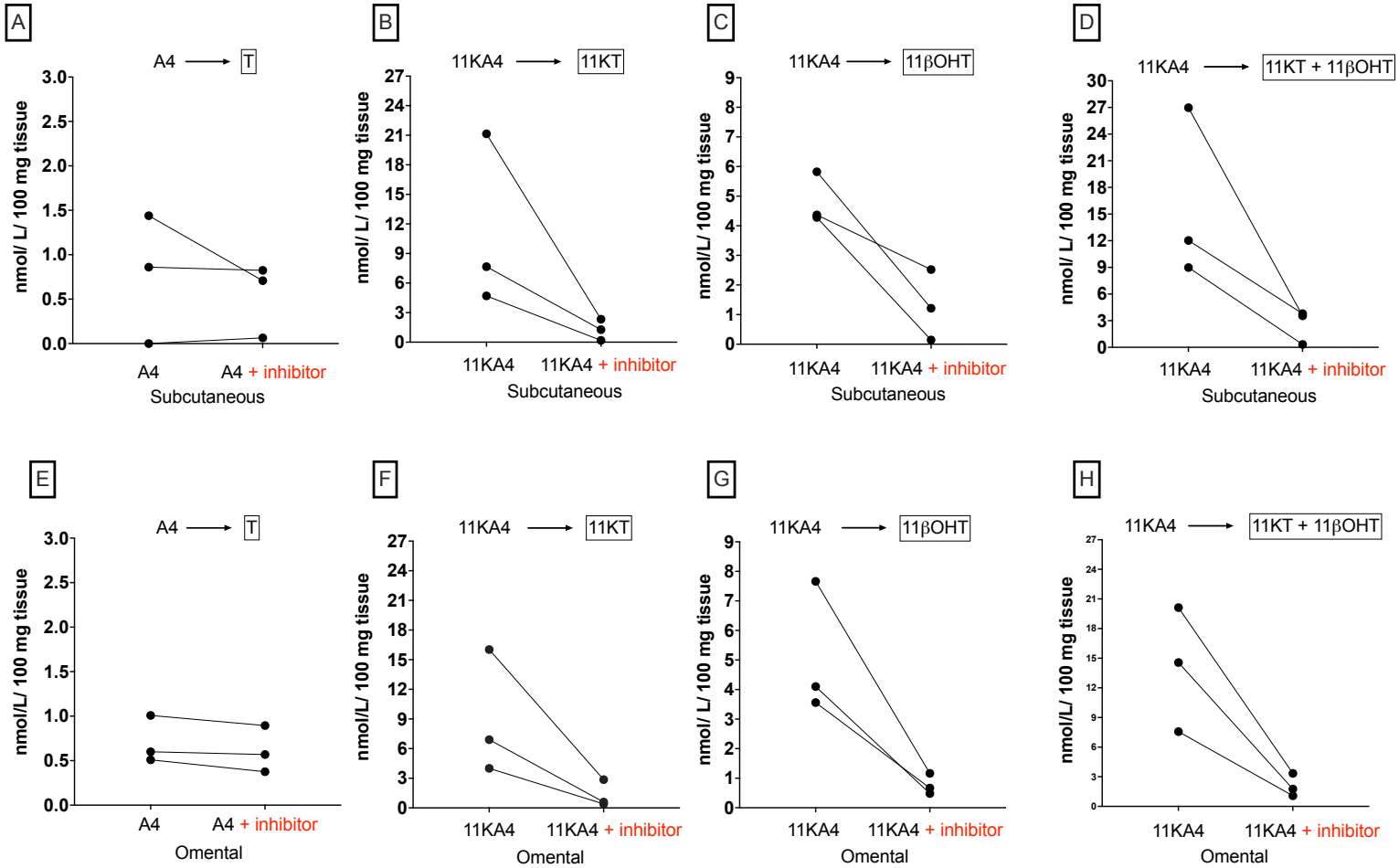

Figure 4.9 *Ex vivo* metabolism of classic and 11-oxygenated precursors A4 and 11KA4, in subcutaneous (A,B) and omental (E,F,G and H) adipose tissue, in the absence and presence of 300 nmol/L AKR1C3 inhibitor, BAY2, in women with PCOS (n=3). Tissue was incubated with 100 nmol/L of A4 or 11KA4, in the presence and absence of 300 nmol/L BAY2 for 24 h. Cell culture incubation medium samples were collected after 24 h and product formation (shown in black boxes) was quantified by UHPLC-MS/MS and normalised to tissue mass. Tissue was retrieved from three women with PCOS, undergoing elective gynaecological surgery (n= 3; age range 41-51; BMI range; 25-38 kg/m^2).

4.4. Discussion

4.4.1. AKR1C3 is a key regulator of androgen activation in female adipose tissue

The active contribution adipose tissue makes to the local pool of classic androgens, particularly in PCOS, is well known [36, 37, 170, 172]. This study aimed to further characterize local androgen activation in adipose tissue, including classic androgens and importantly 11-oxygenated androgens, considering their recently established bioactivity as active androgens and demonstrated importance in PCOS [29]. AKR1C3 is the key androgen activating enzyme present in adipose tissue and converts classic androgen precursor A4 to androgen receptor (AR) agonist T and 11-oxygenated precursor 11KA4 to AR agonist 11KT [37, 173, 174]. Considering the importance of AKR1C3 in the generation of active androgens, and therefore contribution to conditions of female hyperandrogenism such as PCOS, AKR1C3 has the potential to be a therapeutic target to reduce androgen levels. Previous work has established conversion of classic androgen substrates and metabolites in adipose tissue [170, 171] and *in-vitro* studies have shown that AKR1C3 has a higher catalytic activity for the activation of 11-oxygenated androgens than for classic androgens [175]. One such study was reported by Paulukinas *et al*. who profiled androgen conversion in differentiated Simpson-Golabi-Behmel Syndrome (SGBS) cells, they proposed to represent a model for PCOS adipocytes [169]. They showed superior AKR1C3 activity toward activation of 11-oxygenated androgen precursor 11KA4 to 11KT, over activation of classic precursor A4 to T, in cells treated with 10 nM of each precursor. SGBS preadipocyte cells originate from an infant with SGBS, a congenital overgrowth disease characterised by rapid weight gain and other distinctive facial features such

as large mouth and tongue, which predominantly affects men [176]. However, whilst the use of SGBS cells has its benefits (can be maintained up to 50 generations and capable of insulin induced AKR1C3 expression [169]) they do not reflect physiological gene expression, thus are not representative of PCOS or *in vivo* adipocytes, with relative overexpression of HSD11B1 in comparison to the physiologic situation. Comparison of SGBS cells and primary human white subcutaneous adipocytes derived from obese patients, showed distinct transcriptome differences in 3717 genes [177]. The experiments outlined in this thesis set out to study the action of AKR1C3 in adipose tissue and circumnavigate the limitations associated with cell line models, by use of human *ex vivo* subcutaneous and omental adipose tissue. I showed within subcutaneous and omental adipose tissue AKR1C3 preferentially activates the 11-oxygenated precursor 11KA4 to the active androgen 11KT, over activation of the classic precursor A4 to AR T. During *ex vivo* incubations, generation of 11KT was approximately 7-fold greater than generation of T in subcutaneous and omental adipose tissue, implicating 11KT as the predominant active androgen within adipose tissue. This finding is consistent with results published by Banard *et al.* who showed 11KA4 to be the preferred substrate compared to A4 for AKR1C3 cell lines with with overexpression of AKR1C3 and endogenous AKR1C3 expression, Furthermore, the findings I report are also consistent with Schiffer *et al*., who showed AKR1C3 preferentially activates 11KA4 over A4 in peripheral blood mononuclear cells (PBMCs) [178].

In this study, formation of 5α-reduced products 5α-DHT and 5α-dione in adipose tissue was not observed. This is consistent with the minimal expression of the two steroid 5α-

reductases SRD5A1/2 in subcutaneous and omental adipose (**Chapter1; Figure 1.4**). Due to the lack of 5α-reductase activity in adipose, 5α-DHT is most likely not a driver of androgen action in adipose tissue. Since 11KT is generated in higher amounts than T by AKR1C3, these investigations have established 11KT as an important AR agonist in adipose tissue.

Significant differences in AKR1C3 activity between subcutaneous and omental tissue were not observed for the conversion of A4 to T or 11KA4 to 11KT, which is consistent with the similar mRNA levels of AKR1C3 in subcutaneous and omental adipose tissue (**Chapter 1; Figure 1.4**). However, generation of 11βOHT, generated by HSD11B1 from 11KT (11KA4 → 11KT → 11βOHT), showed a trend to be higher in subcutaneous tissue than omental tissue, although this difference was not statistically significant. While expression analysis of subcutaneous and omental tissue has shown that HSD11B1 is abundantly expressed in both tissue subtypes, expression of HSD11B1 in subcutaneous tissue is slightly greater than expression in omental tissue (**Figure 4.10**). Therefore, the higher generation of 11βOHT observed for subcutaneous compared to omental tissue, is consistent with the expression of HSD11B1 in these tissues. AKR1C3 is an important enzyme in the context of androgen metabolism in adipose tissue. Interestingly, the work from this thesis has shown the impact of AKR1C3 in adipose tissue on activation of 11-oxygenated androgens was shown to be approximately 7-fold greater that classic androgens, further establishing 11-oxygenated androgens as key regulators of AR signalling in adipose. It has been established that classic androgens are key drivers of lipotoxic changes in lipid metabolism observed in women with PCOS, it can therefore be hypothesised that

11KT, which is equally as potent as T and generated in higher amounts, is also a driver of lipotoxicity [29, 36].

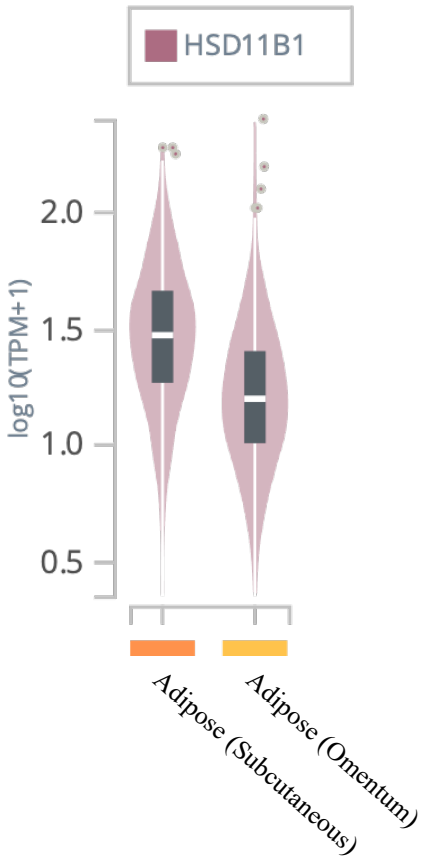

Figure 4.10 **GTEx expression for HSD11B1 in subcutaneous and omental adipose tissues.** Downloaded 28.06.23. Sample size; subcutaneous n=663, omentum n = 541**.** Combined male and female donors. Data Source: GTEx Analysis Release V8 (dbGaP Accession phs000424.v8.p2).

To further dissect the possible contribution of adipose tissue metabolism to circulating androgen levels, I also explored the relationship between BMI and serum concentrations of seven classic and 11-oxygenated androgen precursors and downstream metabolites (A4, T, 11KA4, 11KT, 11βOHA4 and 11βOHT). While T and 11βOHT had a positive association with BMI in the participants included (n=25), their precursors A4, 11KA4 and 11βOHA4 appeared to have a negative association. However, correlation analysis identified this was not statistically significant. Naturally,

due to the relatively small cohort number, there is limited ability to identify distinct correlations. I anticipate a larger cohort would show these trends to a level of significance. Taking into account factors such as precision of measurements and the magnitude of a clinically significant difference, power calculation analysis is used by researchers to determine the sample size required to answer a research question [179]. Although this analysis should ideally be performed prior to the experiment/ clinical trial to inform researchers of an appropriate sample size that would give the results acceptable power, power analysis can also be conducted upon completion of a study with null results [179]. It may be the case that the study was underpowered, potentially leading to a null hypothesis being incorrectly accepted [179]. The use of power calculation on the study I report here, may identify the current sample size of 25 subjects to be insufficient and confirm the need for additional data. Considering this, future studies would be guided by the use of power analysis during study design, to ensure a suitable number of participants are recruited and give results adequate power.

A recent cross-sectional study conducted by Schiffer *et al.* looked at the serum levels of androgens in a cohort of healthy women (n=165) [30], that was significantly larger than the cohort under investigation here. Using multiple linear regression analysis, and thus modelling the effect of BMI independently of age, they reported 11KT and 11βOHT increased with increasing BMI. Of note, my analysis did not control for the age of the participant, but the trend for 11KT and 11βOHT to increase with BMI in the cohort I describe is consistent with these findings. Additionally, it is important to note that the BMI range included in the study I report is of a smaller range (20-38 kg/m^2)

whereas the cross-sectional study included participants with BMIs ranging between 17-43 kg/m^2, which could contribute to the differences in the results between the two studies. Additional studies conducted with the aim of investigating the effect of BMI on androgen concentrations, also report T to increase with BMI, alongside A4 and 11KA4 to decrease with BMI [144]. Taken in conjunction with this previous literature, my results further serve to indicate adipose as a key determinant of active androgen concentrations in circulation, in particular 11-oxygenated androgens.

I also looked at the changes in BMI and androgen levels in a smaller cohort of women with PCOS (n=3). Interestingly, in the small subgroup of women with PCOS in the cohort all androgens profiled, except A4, trended to increase with increasing BMI – further suggesting that adipose is an important regulator of androgen concentration particularly in PCOS. However, due to the small number of women with PCOS included here, there is no conclusive evidence for this correlation, but further investigation on this may be of interest. Insulin receptor signalling has been described to increase adrenal 11-oxygenated androgen biosynthesis [180]. Thus, developing a better understanding how insulin resistance and obesity in PCOS dysregulate both adrenal androgen biosynthesis and peripheral androgen metabolism in adipose tissue can lead to the identification of improved biochemical markers of androgen excess.

4.4.2. Inhibition of AKR1C3 reduces levels of active 11-oxygenated androgen generation in female adipose tissue

As AKR1C3 is a central driver of androgen activation in adipose tissue [36, 37, 170, 172], it may serve as a suitable target for the treatment of female hyperandrogenism. As I was provided two selective AKR1C3 inhibitors by collaborators at BAYER

pharmaceuticals, I investigated their suitability for this study using HEK293 cells with overexpression of AKR1C3. I showed inhibition of this enzyme resulted in suppression of activity and generation of active classic androgen T (from precursor A4) and 11-oxygenated androgen 11KT (from precursor 11KA4). The efficiency of two AKR1C3 inhibitors, BAY1 and BAY2, were investigated. As both of these inhibitors showed similar potency (identified by IC_{50}) and efficiency (identified by maximum inhibition reached), BAY2 was progressed forward due to its non-steroidal structure was the preferred choice due to its reduced toxicity and *in vivo* hepatotoxicity, compared to BAY1 [181].

Treatment of subcutaneous and omental adipose tissue with BAY2 led to significant reduction in the generation of the classic androgen T and the active 11-oxygenated androgen 11KT, from their respective precursors. Moreover, AKR1C3 inhibition also resulted in lower levels of 11βOHT, a downstream metabolite of 11KT. AKR1C3 inhibition had a greater impact on the relative reduction of 11-oxygenated androgen 11KT generation than on the generation of T. As inhibition of AKR1C3 prevented conversion of 11KA4 to 11KT, increased formation of its hydroxy precursor 11βOHA4 via HSD11B1 was observed (**Figure 4.7**). The observed increase in 11βOHA4 generation was not discouraging to the aim of the study as this metabolite does not activate the AR [182]. Campana and colleagues transduced CV1 cells to express human androgen receptor and androgen-responsive gaussian luciferase genes, and reported a luciferase response to treatment with 300 nmol/L of 11KT, and 11βOHT but not 300 nmol/L of 11βOHA4 [182].

It was interesting to observe that AKR1C3 inhibition did not have a major effect on T detection, resulting in a reduction of only 22% ± 31% and 32% ± 44% (mean ±SD) in subcutaneous and omental tissue, respectively, yet reduction in detection of 11KT was substantial (81% ± 15% and 80% ± 13 %, respectively). The presence of the AKR1C3 inhibitor did not cause major differences in the mean concentration of A4 detected. Taken together, these results raise the question if enzymes other than AKR1C3 contribute to conversion of A4 to T. Considering the complex nature of androgen metabolism, adipose tissue composition and enzyme expression, it is plausible other enzymes are actively involved in generation of T. Complete inhibition of A4 to T was overserved in HEK293 cells overexpressing AKR1C3 in the absence of any other steroidogenic enzymes, suggesting that when AKR1C3 is the sole enzyme responsible for T generation inhibition by BAY2 is successful. Therefore, the lack of inhibition during *ex vivo* incubations does not reflect inhibitor insufficiency, but further points towards the potential for other enzymes to be involved in generation of T *in vivo*.

The cohort included in this study included 3 women who self-reported receiving a formal diagnosis of PCOS from a healthcare professional. In all three cases, the level of the active 11-oxygenated androgens, 11KT and 11βOHT, generated *ex vivo* by adipose tissue collected from these women with PCOS was substantially reduced in the presence of AKR1C3 inhibitor BAY2. Of note, in the entire cohort reported in this study, including the women with PCOS, treatment with BAY2 did not result in complete inhibition of AKR1C3 in regard to conversion of A4 to T. T is an important component of normal metabolic health and function in women [183, 184]. In PCOS, excess testosterone has a damaging influence on adipose, exerting its effects by causing

increased visceral adiposity and enhanced adipose size, contributing to insulin resistance, a key symptom of PCOS [89]. The contribution of T to the progression of PCOS symptoms, makes AKR1C3 inhibition a promising treatment approach. The physiological role 11-oxygenated androgens play in the normal metabolic function of healthy women has not yet been studied, however, since 11KT is also a potent, full agonist of AR, the receptor that mediates the adverse metabolic effects of classic androgens, it is likely that they also play an important role in female metabolic function. Importantly, 11-oxygenated androgens do not decline with age and 11-oxygenated precursor 11βOHA4 is the most abundant androgen after DHEAS [31, 185]. Thus, while classic androgen levels decline with age, 11-oxygenated androgens will contribute to the regulation of metabolism over the entire period of adult life.

A therapeutic intervention for the treatment of PCOS, which totally supresses androgen generation, would be undesirable due to the beneficial effects of androgens including the role of T in promotion of ovarian follicle growth and maintenance of pregnancy, immune regulation by DHEA and the role of classic androgens as precursors for the biosynthesis of oestrogens [186-189]. AKR1C3 inhibition, which only reduces the activation of androgens in peripheral tissues, like adipose, where they exert their adverse metabolic effects, is therefore an encouraging target as a potential therapeutic for PCOS. Furthermore, AKR1C3 inhibition specifically targets 11-oxygenated androgens due to the high catalytic efficiency of AKR1C3 for 11KT generation, which make the major contribution to the circulating androgen metabolome in PCOS [29]. Inhibition of AKR1C3 may not only serve to reduce active androgen generation, and thus lipid deposition in adipose tissue but may also directly regulate DNL via blockage

of AR stabilisation [190]. Using SGBS cells, R. Paulukinas and T. Penning showed knockdown of AR or insulin induced AKR1C3 in SGBS cells, downregulated fatty acid synthase (FASN), implicating AKR1C3 as an AR stabiliser in the absence of exogenous androgens [190]. The incorporation of bifunctional AKR1C3 inhibitors, which inhibit AKR1C3 and disrupt AR signalling, downregulated FASN, the key enzyme for DNL [190]. Of course, these experiments were conducted using SGBS cells which may not truly reflect physiological adipocytes, as described above, but these results further highlight the importance of AKR1C3 as potential therapeutic target in PCOS, where insulin resistance and obesity are key features.

4.4.3. Strengths and limitations

A key strength of this study is the inclusion of 11-oxygenated androgens. To date, 11-oxygenated androgen metabolism in adipose tissue has not been studied. Here I show for the first time, that subcutaneous and omental adipose tissue generated higher levels of 11KT than T from their respective precursors, in addition to the effect of AKR1C3 inhibition on 11-oxygenated androgen metabolism. In this study, I have shown the success of a selective AKR1C3 inhibitor, that is part of an ongoing clinical program at an industry collaborator (BAYER pharmaceuticals). This inhibitor will be available for future studies in women with PCOS. To the best of my knowledge, one previous study reported significant reduction of T generation, when a commercial AKR1C3 inhibitor was introduced to adipocytes [36]. However, this study looked at the effect of AKR1C3 inhibition on classic androgens only. The percentage of non-white women included in the study I present is an additional advantage. 56% of women self-reported their ethnicity as non-white, substantially surpassing the standard inclusion of

non-white participants in research studies (approximately 4.9% [191]). Importantly, previous research has shown that non-white women, particularly those of Southeast Asian or Hispanic decent, have the greatest prevalence and most symptomatically aggressive cases of PCOS [192-194].

Limitations of this study include the use of self-reported patient information and medical history. As participants were given a questionnaire by which they were asked to report their medical information, the accuracy of the reported values such as height and weight cannot be guaranteed. Furthermore, although only three patients reported PCOS, the actual number of women with PCOS may be larger due the level of women with PCOS that go undiagnosed [195]. Another limitation of this study includes the nature by which participants were recruited (undergoing elective gynaecological surgery). As a result, only a limited number of women of reproductive age were able to be included (age range: 36-74 years, mean age: 50 years). The preference would have been to recruit women of ages across a wider spectrum, but participant availability was an uncontrollable factor.

4.4.4. Conclusions

In conclusion, AKR1C3 plays a key role in generation of classic and 11-oxygenated active androgens in subcutaneous and omental female adipose tissue. Inhibition of this enzyme had a stronger impact on generation of 11-oxygenated androgens, significantly reducing the generation of 11-oxygenated active product 11KT, and a much lower effect on the generation of classic active metabolite T. Since 11-oxygenated androgens have been indicated as the predominant androgens in PCOS

and do not decline with age, meaning they are the significant androgens in post-menopausal women with PCOS, AKR1C3 is a promising therapeutic target for the treatment of female conditions of hyperandrogenism, with a particular focus on PCOS.

CHAPTER 5

ANDROGEN METABOLISM IN *EX VIVO* LIVER MODELS

5.1. Introduction

As introduced in **Chapter 1**, women diagnosed with PCOS are at an increased risk for developing MASLD, a collection of four progressive disease stages, classified by excessive fat accumulation in hepatocytes [105, 196]. Like PCOS, MASLD is a condition driven by hyperandrogenism [105]. Research has shown that women diagnosed with PCOS are four times more likely to develop MASLD than women who do not suffer from the condition [106]. MASLD is strongly associated with metabolic syndrome, and often concomitant with visceral obesity and insulin resistance, with insulin resistance being a major contributor to MASLD risk [124]. As insulin resistance, obesity and dyslipidaemia are central components of PCOS, it is thought that MASLD is the hepatic manifestation of PCOS [36, 107, 108]. Surprisingly, the early stages of MASLD are not often accompanied by severe or noticeable symptoms and can therefore go undiagnosed – increasing the chance of disease progression [109].

In recent years, there has been increasing evidence to suggest the relationship between PCOS and MASLD risk is driven by hyperandrogenism [105]. While the reason behind this has not been comprehensively investigated, it has been hypothesised that excess androgen generation in adipose tissue via AKR1C3 leads to lipid dysregulation which may cause an influx of fatty acids to the liver, which, in turn,

is incapable of coping with such large fat deposits [36, 135, 197]. Androgen generation in adipose tissue may be one of the main contributors to increased risk of MASLD in PCOS, but the potential contribution the liver may make to circulating androgen levels should not be ignored. The liver is a primary site of systemic metabolism and preparation of metabolites for excretion. It is also known to express the key enzymes involved in androgen metabolism, including AKR1C3 [9, 198] (**Figure 1.4 and Figure 4.1**). The liver therefore has the potential to contribute to generation of active classic and 11-oxygenated active androgens, thereby contributing to the regulation of both circulating and local androgen levels. Direct effects of local androgen action on liver lipid metabolism are understudied but represent a potential link between the androgen excess and MASLD development. Thus, identifying the key active androgens generated locally in the liver will inform the design of meaningful studies investigating the link between androgen signalling and lipid handling in the liver. Moreover, products of downstream androgen deactivation, such as 11βOHAn, have been proposed as potential biochemical markers for hyperandrogenism [24]. Thus, an understanding of liver contribution to the circulating androgen pool, even if by androgen deactivation, is of extreme importance. Despite this, androgen metabolism in the liver has not been studied and there is currently limited knowledge. It is therefore vital to ascertain a conclusive metabolic profile of classic and 11-oxygenated androgens in liver, as a metabolic target tissue. 11-oxygenated androgens, due to their relatively recent discovery, have not been studied using liver tissue but play a crucial role female hyperandrogenism and therefore MASLD onset in PCOS. Identifying the metabolic pathways of such androgens in the liver would therefore serve to reveal the contribution of liver tissue to the circulating androgen pool and provide understanding

as to possible influence of androgen metabolism in the liver on MASLD development, particularly in PCOS.

Currently, there are limited cells lines available that accurately model human liver physiology for the purpose of profiling androgen metabolism, and mouse models are not a suitable alternative as their steroid metabolising enzymes differ from humans. This chapter therefore describes the investigation of androgen metabolism in the liver using two human tissue *ex vivo* models; *ex vivo* liver tissue incubations in culture media and normothermic machine liver perfusion (NMLP) (**Chapter 1, Aim 3**). Due to the ease of use, low amounts of tissue required per incubation and cost efficiency, the *ex vivo* liver tissue model was used to investigate downstream metabolism of several classic and 11-oxygenated androgen precursors and downstream metabolites and develop a comprehensive picture of the liver androgen metabolome. Findings were subsequently supported by the use of NMLP. In clinic, NMLP is used as an alternative to static cold storage prior to organ transplantation but is now emerging as a tool to study liver physiology [137, 138, 142, 143]. We took advantage of this application and employed NMLP as a tool to investigate androgen metabolism, in conditions as close to human physiology as currently achievable.

5.2. Materials and methods

5.2.1. Source of research human livers

All donor livers were obtained from donor patients with intent for transplantation but were declined for transplantation by all UK liver transplant centres, according to the assessment of the retrieval or transplantation surgeon(s). Livers were retrieved with

the purpose transplantation but declined and offered for research, although still deemed to have 'normal' metabolic function. Explant livers were retrieved from patients with end stage liver disease. Donor/ explant liver demographics and characteristics are outlined in **Table 5.1** below. Due to the reduced availability of donor livers suitable for the purposes of this thesis, inclusion criteria consisted of male and female liver, of which male livers were most commonly available. Although this thesis explored the link between MASLD and PCOS, a syndrome affecting women only, this is pioneering work aiming to establish the technologies available and to identify key pathways for further investigations on liver androgen metabolism. Therefore, the use of male livers is suitable for the experimental requirements. The use of such livers for research by the University of Birmingham Centre for Liver Research (NIHR Liver BRU, Dr Simon Afford) was approved by the Local Research Ethics Committee (REC 13/LO/1926; Protocol RG-13-290; IRAS 141693).

Table 5.1 Donor/explant liver demographics and characteristics. Abbreviations: NMLP; normothermic machine liver perfusion, DBD; donation after brainstem death, DCD; donation after cardiac death, BMI; body mass index, n/a; not applicable, unk; unknown, ICH; intracerebral haemorrhage, Level of steatosis was indicated by the organ retrieval surgeon(s).

Experiment/ usage	**Androgen metabolism in *ex vivo* tissue incubations**				**Measurements of endogenous androgen levels in the perfusate during NMLP**								**Exogenous androgen precursor metabolism assay using NMLP**			**Exogenous testosterone metabolism using NMPL**	
Liver number	**Liver 1**	**Liver 2**	**Liver 3**	**Liver 4**	**Liver 5**	**Liver 6**	**Liver 7**	**Liver 8**	**Liver 9**	**Liver 10**	**Liver 11**	**Liver 12**	**Liver 13**	**Liver 14**	**Liver 15**	**Liver 18**	**Liver 19**
Donor/ Explant	Donor	Donor	Donor	Explant	Donor	Donor	Donor	Donor	Donor	Donor	Donor	Donor	Donor	Donor	Donor	Donor	Donor
Donor age (years)	46	68	60	36	60	43	78	31	75	44	45	60	67	64	48	47	42
Sex	Male	Male	Female	Female	Male	Male	Male	Male	Male	Female	Male	Male	Male	Male	Male	Male	Male
Race	White	White	White	White	unk	unk	unk	unk	unk	unk	unk	unk	White	Asian Indian	White	White	White
BMI (kg/m^2)	29	25	29	25	unk	unk	unk	unk	unk	unk	unk	unk	29	29	30	27	40
DBD/DCD	DCD	DCD	DBD	n/a	DCD	DBD	DBD	DCD	DBD	DBD	DBD	DBD	DBD	DCD	DBD	DCD	DBD
Cause of death	ICH	Cerebral vascular accident	unk	n/a	unk	unk	unk	unk	unk	unk	unk	unk	ICH	Cardiac arrest	ICH	ICH	Cerebral abscess
Reason for organ rejection	Long warm ischaemia time	Organ too large	Sub optimal anatomy	n/a	unk	unk	unk	unk	unk	unk	unk	unk	Moderate steatosis	Sub optimal Anatomy	Sub optimal appearance	Severe steatosis	Moderate steatosis

Steatosis	Minimal-moderate	Minimal-moderate	Minimal-moderate	severe	non	non	non	unk	unk	non	non	non	Moderate	Minimal	Moderate	Severe	Moderate

5.2.2. Androgen metabolism assay using *ex vivo* liver tissue model

Freshly retrieved human liver was preserved in University of Wisconsin fluid, on ice, for transportation to the laboratory, before being sliced and transferred to DMEM, at 4 °C. Approximately 300-400 mg of tissue was washed with PBS and cut into four smaller pieces. Diced tissue was then suspended in Williams E medium, supplemented with 100 units/mL penicillin, 100 µg/mL streptomyocin, 2 mM L-glutamate and containing 100 nmol/L of either DHEA, A4, T, 11OHA4, 11OHT, 11KA4 or 11KT (provided as 1 mg/mL stocks in MeOH). Additional cell-free incubations of all treatments and vehicle-treated cells (MeOH in medium) were prepared as controls. Treated tissue was incubated at 37 °C and rotated at 20 rpm for 48 hours. 1 mL of medium was collected at different timepoints over the 48-hour period. Medium samples were centrifuged for 10 minutes (4000 rpm, 4 °C), transferred to a sterile Costar 1.7 mL low binding snap cap minicentrifuge tubes and stored at -80 °C for solid phase extraction (**Chapter 2**). Androgens were quantified using the new UHPLC-MS/MS method described in **Chapter 3**.

Due to the reduced availability of donor livers suitable for the purposes of this thesis, inclusion criteria consisted of male and female liver donors. Exclusion criteria consisted of donors with severe steatosis, extended warm ischemia time or underlying medical conditions such as hepatitis B or HIV. As part of this study, an explant liver (n=1) was included during investigations in order to obtain preliminary insights into how severe liver malfunction might impact androgen metabolism. Inclusion criteria for explant livers consisted of explant livers retrieved from patients with end stage liver disease (from cirrhosis to HCC). Exclusion criteria also consisted of donors with extended warm

ischemia time or underlying autoimmune diseases such as hepatitis B/ HIV. Liver demographics and characteristics are outlined in **Table 5.1.**

5.2.3. Androgen metabolism in an *ex situ* normothermic machine liver perfusion model

5.2.3.1. Measurement of endogenous androgen levels in liver perfusate during normothermic machine liver perfusion

Androgen levels in the perfusate during NMLP were assessed by UHPLC-MS/MS without addition of exogenous androgens or precursors. Perfusate samples from eight independent perfusions from two previously published studies, were provided by collaborators in the Institute of immunology and immunotherapy (University of Birmingham, UK) [199, 200]. All livers included in both studies were donor livers. Each liver was perfused between 6 and 12 hours, with either packed red blood cells or hemopure [199, 200] (**Chapter 2; Table 2,3**). Perfusate samples were collected periodically for the duration of the perfusions and stored at -80 ºC. Samples were extracted by solid phase extraction (**Chapter 2**; **2.1.2**). Donor demographics are outlined in **Table 5.1.** Androgens in perfusate were quantified using the UHPLC-MS/MS described in **Chapter 3**.

5.2.3.2. Exogenous androgen precursor metabolism assay using Normothermic machine liver perfusion

The procedure was conducted as outlined in (**Chapter 2; 2.5.2**). Briefly, livers were connected to a Liver Assist device and primed with the hemopure based perfusate described in **Chapter 2; Table 2.3**. Livers were then cannulated and connected to the device. To confirm liver viability prior to exogenous androgen intervention, the liver was perfused in the absence of exogenous androgens. Viability criteria (lactate clearance < 2mmol/L in 2 hours, evidence of bile production, in combination with two or more of the following: homogenous perfusion, vascular flow >150 mL/min for hepatic artery and > 500mL/min for portal vein) was reached between two – three hours, after which, 200 nmol/L of [$^{13}C_3$]-A4 or [$^{13}C_3$]-11KA4 was added the machine reservoir or hepatic artery cannula. Due to the nature of the perfusion device (multiple tubing and constant re circulation of perfusate), it was difficult to confirm the final concentration added to the device. Therefore, addition of 200 nmol/L of substrate was calculated based on the concentration if diluted into the total volume of the perfusate (2 L). Perfusate samples, taken from the hepatic artery oxygenator, were collected every 30 minutes for 4 hours and then every 2 hours until the end of the perfusion. Samples were immediately snap frozen in liquid nitrogen and stored at -80 ºC, for solid phase extraction. Liver biopsies were taken before the start of the perfusion (T0), before the start of androgen treatment (T2 or T3) and periodically throughout until the end of the perfusion. 8 mm punch biopsies were collected from left and right lobes, and immediately snap frozen in liquid nitrogen and stored at -80 ºC for future analysis. Androgens in perfusate were quantified using a new UHPLC-MS/MS method designed specifically for application to this assay (**Chapter 3**).

5.2.3.3. Exogenous testosterone metabolism assay by normothermic machine liver perfusion

In collaboration with the institute of immunology and immunotherapy (University of Birmingham), we were able to assess the metabolism of excess amounts of testosterone incorporated into the NMLP perfusion fluid during 'liver defatting' perfusions. The purpose of these perfusions was to assess the power of NMLP as a tool to recondition fatty livers by incorporation of a 'defatting' drug cocktail. The drug cocktail (unpublished) was revised from previous literature and contains a final concentration of 40 μmol/L (40,000 nmol/L) of testosterone. The addition of T to the drug cocktail used to recondition steatotic livers is standard procedure and was not an additional experiment variable for the purpose of this thesis. By analysis of androgens present in perfusate samples during these perfusions, I was therefore able to gain an indication of testosterone metabolism within severely fatty livers. Perfusions were conducted according to a previously published protocol [142]. Briefly, a Liver Assist device was prepped with packed red blood cells and additional constituents (**Chapter 2**, **Table 2.3**). Once livers were added to the device, they were immediately given a bolus injection the drug cocktail and monitored by blood-gas analysis over time. Total perfusion time was up to 72 hours. Due to the extended perfusion time and closed circuit NMLP device system, a continuous veno-venous haemofiltration dialysis machine was connected to the device to correct electrolyte balances and acidosis. Perfusate samples were taken periodically throughout the duration of 72-hour perfusions, snap frozen in liquid nitrogen and stored at -80 ºC. To assess testosterone metabolism, samples underwent one freeze/thaw cycles and were extracted by solid

phase extraction (as described in detail in **Chapter 2; 2.1.2**). Donor demographics are outlined in **Table 5.1**.

Androgens were quantified using a new UHPLC-MS/MS method designed specifically for application to NMLP (**Chapter 3**). Due to the high concentration of testosterone added and as packed red blood cells were using during these perfusions, calibrators were prepared in 0.1 % BSA in PBS (to match the matrix of the samples), in the concentrations outlined in **Table 5.2** below**.**

Table 5.2 Calibrant concentrations for androgen quantification during liver defatting NMLP assay (5mL per calibrant). Stock 2 is made up in 50% (vol/vol) UHPLC methanol and UHPLC water, containing all analytes at 1000 ng/mL.

Calibrant number	Added volume of serum steroid stock 2 (µL)	Added volume of dilutant matrix (µL)	Final concentration ng/mL (nmol/L)
C0	0	5000	0
C1	2.5	4997.5	0.5 (1.7)
C2	5	4995	1 (3.47)
C3	25	4975	5 (17.36)
C4	50	4950	10 (34.7)
C5	125	4875	25 (86)
C6	250	4750	50 (175)
C7	500	4500	100 (347)
C8	1250	3750	250 (868)
C9	2500	2500	500 (1736.1)

5.3. Results

5.3.1. Expression of genes encoding steroid-metabolising enzymes in liver tissue

Investigations using qPCR on 10 donor livers and one liver explant sample (n=11) showed HSD11B1 to have the highest levels in liver tissue amongst the targets assessed, yet HSD11B2 mRNA expression was not detected (**Figure 5.1**). Detection of the reductive, deactivating hydroxysteroid dehydrogenase AKR1D1 was also consistently detected in all tissue samples. The reductive, activating hydroxysteroid dehydrogenase, AKR1C3, was expressed in all tissue samples (n=11).

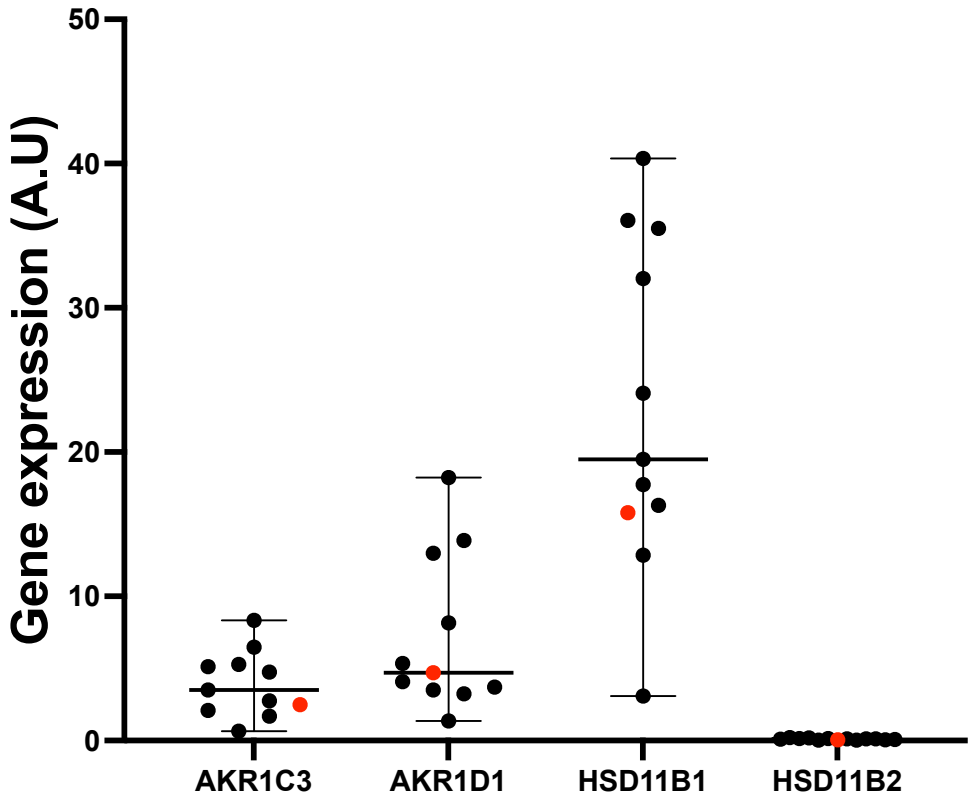

Figure 5.1 Expression of genes encoding androgen-metabolizing enzymes in liver tissue from ten healthy donors (black) and one explant (red) sample assessed by qPCR (donor livers; n=10, age range 29-67 years, BMI range 25-30 kg/m^2, explant liver; n=1, age 36 years, BMI 25 kg/m^2). Data

points indicating gene expression in explant liver are highlighted in red. Gene expression was assessed by semi-quantitative PCR, normalized to 18S and GAPDH and arbitrary units (A.U.) were calculated as $1000*E^{-\Delta Ct}$.

5.3.2. Androgen metabolism favours androgen deactivation during *ex vivo* liver tissue assays

Ex vivo incubations of liver tissue were performed with classic (DHEA, A4 and T) and 11-oxygenated (11KA4, 11KT, 11βOHT and 11βOHA4) androgen precursors and active androgens to provide comprehensive insight into the pathways of androgen metabolism in the liver. Androgen metabolites were measured in the incubation medium from time-dependent experiments with liver tissue from three different donors and quantified using UHPLC-MS/MS. Donor demographics and characteristics can be found in **Table 5.1.** The final timepoint for experiments was increased 48 hours. Initial incubations (n= 3) also revealed minimal 3β-hydroxysteroid dehydrogenase activity indicating that DHEA is not a relevant substrate for metabolism in liver (data not shown). DHEA was thus excluded from further experiments.

Incubations with A4 and T yielded predominantly inactive 5β-reduced product Et and 5α-reduced product An, both of which increased in concentration over the 48-hour time period (**Figure 5.2 and Figure 5.3**). T was not detected in quantifiable concentrations in any of the incubations with A4, indicating minimal AKR1C3 activity in liver tissue. Incubations with T revealed minimal conversion to A4, which was detected in quantifiable levels only at the first time point (1h) indicating rapid downstream metabolism. Conversion of T to DHT, the most potent androgen, was not detected in

any incubations, further indicating the liver is a site of androgen deactivation not activation.

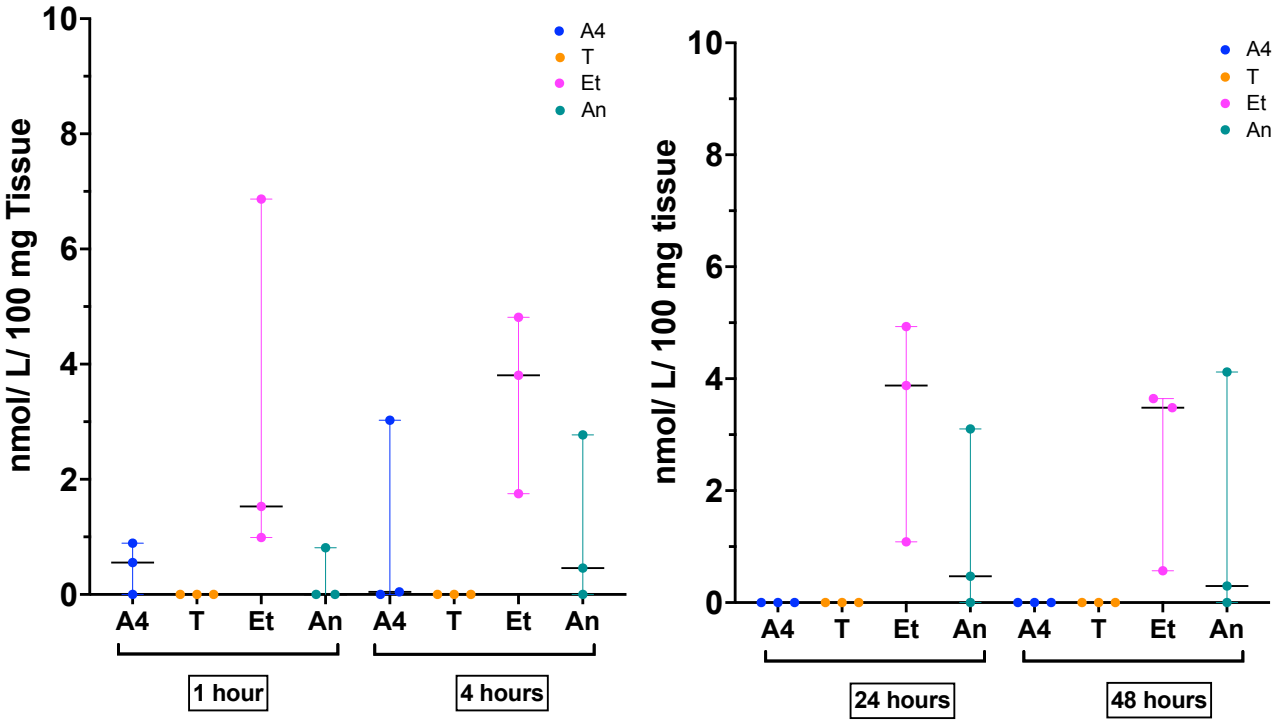

Figure 5.2. *Ex vivo* metabolism of androstenedione (A4) by tissue from donor livers (n = 3; age range 46-68 years; BMI range 25-29 kg/m^2). Liver tissue was incubated with 100 nmol/L substrate for 48 hours. The substrate is shown in a black box. Data is representative of three biological replicates. Each biological replicate is representative of the mean of two technical replicates. Product formation was quantified by UHPLC-MS/MS and normalized to tissue mass. Median and range are indicated. Product concentrations below the limit of quantification are shown as 0.

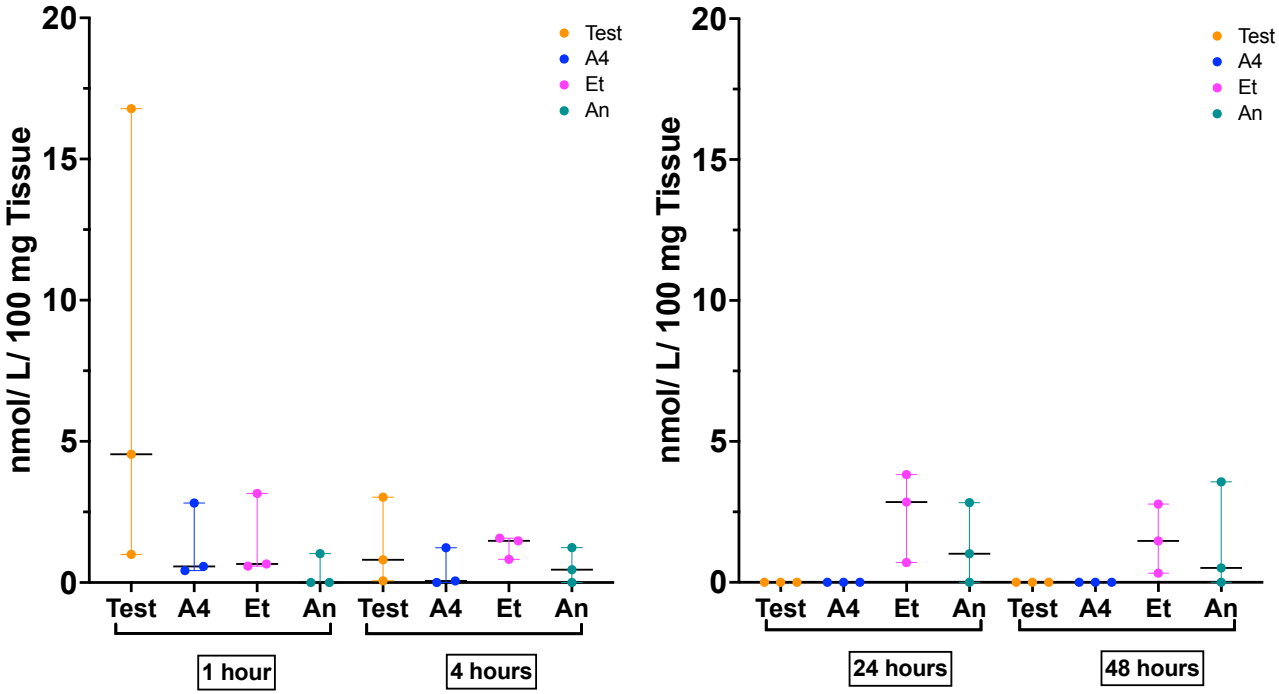

Figure 5.3 ***Ex vivo* metabolism of testosterone (T) by donor livers** (n = 3; age range 46-68 years; BMI range 25-29 kg/m^2). Liver tissue was incubated with 100 nmol/L substrate for 48 hours. The substrate is shown in a black box. Data is representative of three biological replicates. Each biological replicate is representative of the mean of two technical replicates. Medium samples were collected after 48 hours and product formation was quantified by UHPLC-MS/MS and normalized to tissue mass. Median and range are indicated. Product concentrations below the limit of quantification are shown as 0.

Incubations with 11KA4 and 11KT identified 11βOHEt and 11βOHAn as the dominant products, increasing in concentration in 2/3 donors over the 48-hour time course period, highlighting HSD11B1 activity in liver tissue (**Figure 5.4 and Figure 5.5**). While 11KEt, was detected in 2/3 donors at 1 hour and a major metabolite detected in 1/3 donor at 24 and 48 hours in incubations with 11KA4 (**Figure 5.4**), it was not detected in incubations with 11KT (**Figure 5.5**). 11KAn was not in incubations with 11KA4 or 11KT, presumably due to rapid conversion to its hydroxy product. Generation of 11βOHA4 from 11KA4 was quantifiable in 3/3 donors, at 1 and 4 hours only, after which it was completed depleted. Conversely, 11βOHA4 was undetectable in incubations with 11KT. Incubations with 11KT yielded 11βOHT in 3/3 donors at 1 hour and 4 hours, but which was later consumed by 48 hours. In line with the observed absence of A4 conversion to T, activation of androgen precursor 11KA4 to active metabolite 11KT was also not observed in incubations, and incubations with 11KT showed very minimal interconversion between 11KA4 and 11KT, in comparison to generation of further downstream metabolites.

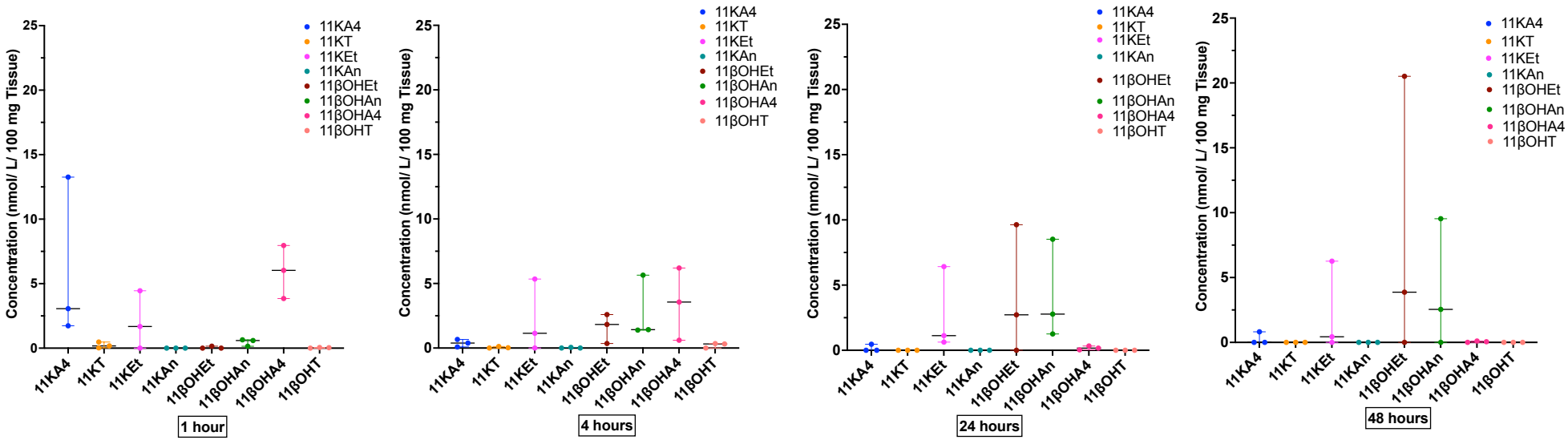

Figure 5.4 *Ex vivo* metabolism of 11-ketoandrostenedione (11KA4) by donor livers (n = 3; age range 46-68 years; BMI range 25-29 kg/m^2). Liver tissue was incubated with 100 nmol/L substrate for 48 hours. The substrate is shown in a black box. Data is representative of three biological replicates. Each biological replicate is representative of the mean of two technical replicates. Medium samples were collected after 48 hours and product formation was quantified by UHPLC-MS/MS and normalized to tissue mass. Median and range are indicated. Product concentrations below the limit of quantification are shown as 0.

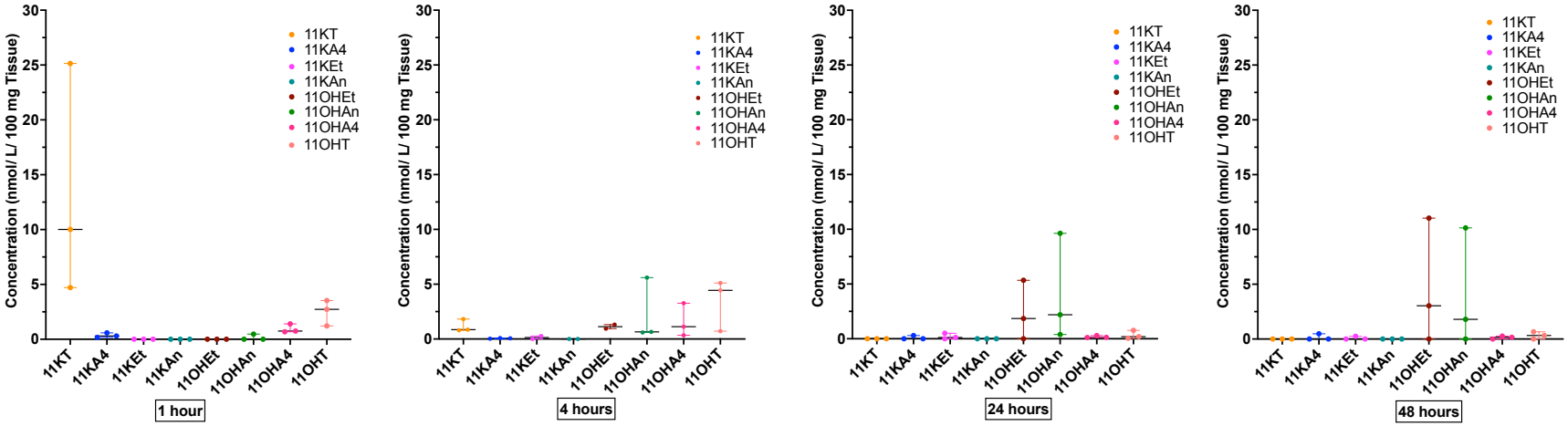

Figure 5.5 *Ex vivo* metabolism of 11-ketotestosterone (11KT) by donor livers (n = 3; age range 46-68 years; BMI range 25-29 kg/m^2). Liver tissue was incubated with 100 nmol/L substrate for 48 hours. The substrate is shown in a black box. Data is representative of three biological replicates. Each biological replicate is representative of the mean of two technical replicates. Medium samples were collected after 48 hours and product formation was quantified by UHPLC-MS/MS and normalized to tissue mass. Median and range are indicated. Product concentrations below the limit of quantification are shown as 0.

Incubations with 11βOHA4 showed complete consumption of substrate after 48 hours (**Figure 5.6**). The quantitatively predominant metabolite detected was 11βOHAn (2/3 donors), followed by 11βOHEt. (1/3 donors). 11KEt and 11KAn were not detected, indicating conversion of 11βOHA4 to 11βOHEt and 11βOHAn, may be generated by 5β reduction via 11βOH-5β-dione, and 5α reduction via 11OH-5α-dione, respectively (**Chapter 1, Figure 1.4**). Conversion to 11KA4 was detected in 3/3 donors after 1 hour only. In incubations with 11βOHT, quantifiable generation of 11KA4, 11KT and 11βOHA4 was observed for 1/3 donors, 2/3 donors and 3/3 donors, respectively, was detected after 1 hour and 4 hours, but subsequently depleted by 24 hours (**Figure 5.7**). The residual metabolites detected after 24 hours were 11βOHEt and 11βOHAn.

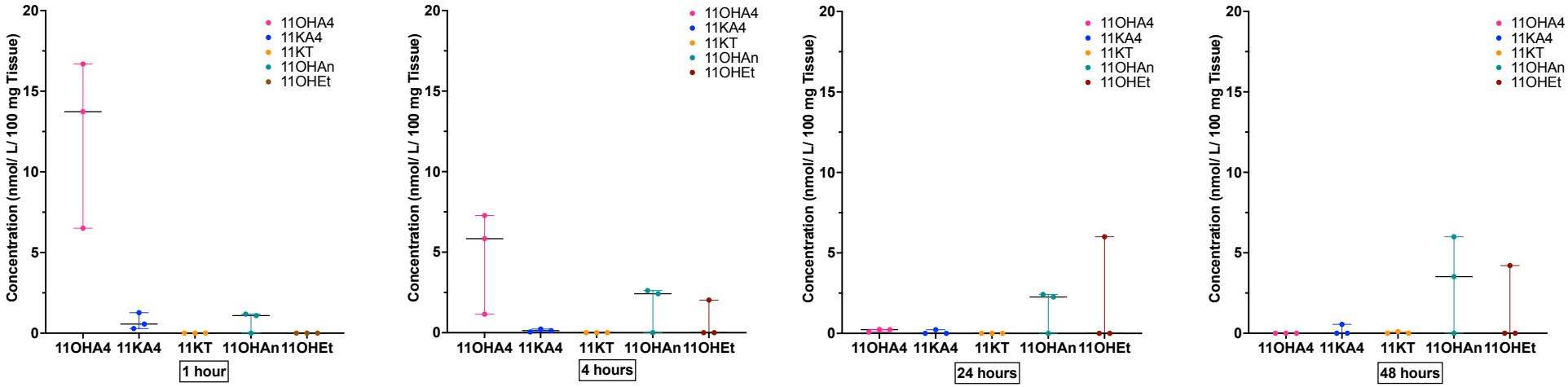

Figure 5.6 *Ex vivo* metabolism of 11βhydroxyandrostenedione (11βOHA4) by tissue from donor livers (n = 3; age range 46-68 years; BMI range 25-29 kg/m^2). Liver tissue was incubated with 100 nmol/L substrate for 48 hours. The substrate is shown in a black box. Data is representative of three biological replicates. Each biological replicate is representative of the mean of two technical replicates. Medium samples were collected after 48 hours and product formation was quantified by UHPLC-MS/MS and normalized to tissue mass. Median and range are indicated. Product concentrations below the limit of quantification are shown as 0.

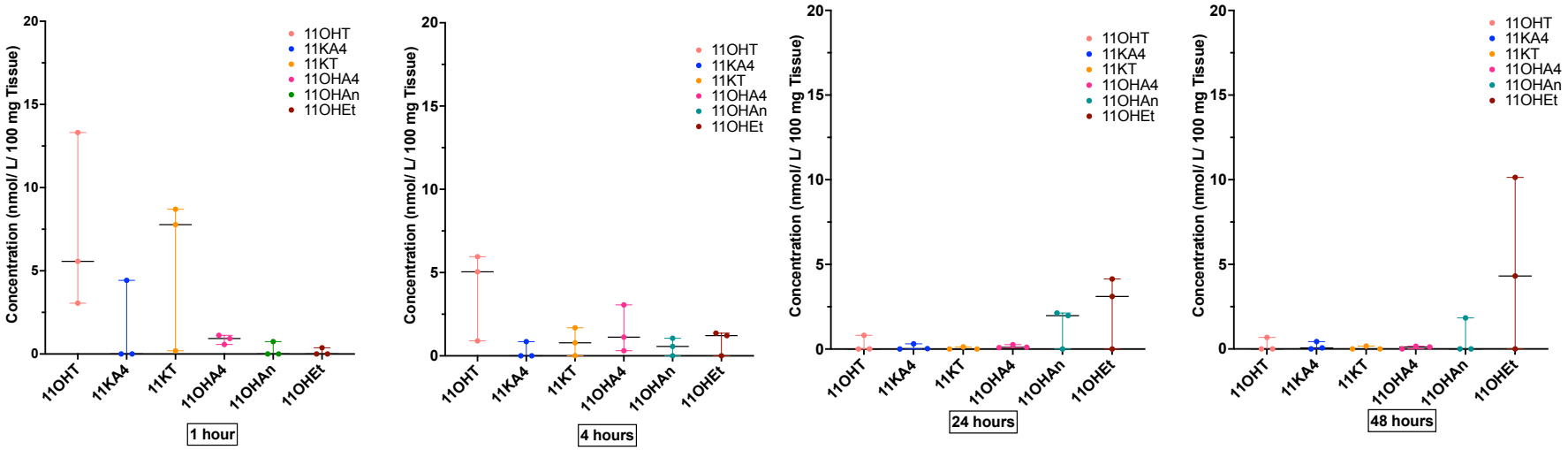

Figure 5.7 *Ex vivo* metabolism of 11βhydroxytestosterone (11βOHT) by tissue from donor livers (n = 3; age range 46-68 years; BMI range 25-29 kg/m^2). Liver tissue was incubated with 100 nmol/L substrate for 48 hours. The substrate is shown in a black box. Data is representative of three biological replicates. Each biological replicate is representative of the mean of two technical replicates. Medium samples were collected after 48 hours and product formation was quantified by UHPLC-MS/MS and normalized to tissue mass. Median and range are indicated. Product concentrations below the limit of quantification are shown as 0.

5.3.3. Androgen metabolism in liver explants is divergent to androgen metabolism in donor liver tissue

In contrast to donor tissue, explant liver tissue is retrieved from patients who have end stage liver disease, causing reduced function of the liver. Androgen metabolism in a liver retrieved from a patient with end stage liver disease, undergoing liver transplantation, was profiled. Consumption of substrates by tissue from explant liver occurred at a much slower rate than tissue from donor livers, and in some cases metabolic pathways were opposing (**Figure 5.8**). Treatment with A4 revealed that testosterone was produced, although in minimal amounts, throughout the 48-hour time period and peaked at 24 hours. Et was not a major product and detected after 4 hours only. Whilst the data indicated that A4 was being consumed at a steady rate over the 48-hour period, the amount of testosterone and Et detected did not account for total A4 consumption, suggesting A4 may have been metabolised to a compound not included in the UHPLC-MS/MS assay. In contrast to healthy tissue, explant incubations with testosterone showed that testosterone was preferentially converted to precursor A4 via HSD17B2/4 rather than deactivated to Et via AKR1D1. A4 generation accounted for the majority of products of testosterone conversion, before it began to decline at 4 hours. At this time point, Et detection coincided with A4 decline, suggesting that the Et detected could be a metabolite generated from A4. 5α-reduced metabolite An, was not detected in incubations with A4 or T. Treatment with 11KA4 showed minimal 11KT production, increasing at 24 hours. The predominant metabolite detected in these incubations was 11βOHA4 and to a lesser extent 11βOHT (**Figure 5.8**). The predominant metabolite detected in incubations with 11KT was 11βOHA4, although interconversion to 11KA4 and 11βOHT was also detected. In explant tissue, there

11βOHA4 was the chief metabolite present all 11-oxygenated substrate incubations. Interestingly, there was also reduced consumption of 11βOHA4 when it was added as a substrate, further evidencing a shift in equilibrium toward 11βOHA4 generation and maintenance. 11βOHT was a recurring metabolite in incubations with explant tissue yet was only produced in small amounts for donor livers, which also indicates higher HSD11B1 activity in explant tissue. However, the low sample number (n=1), does not allow for final conclusions to be made.

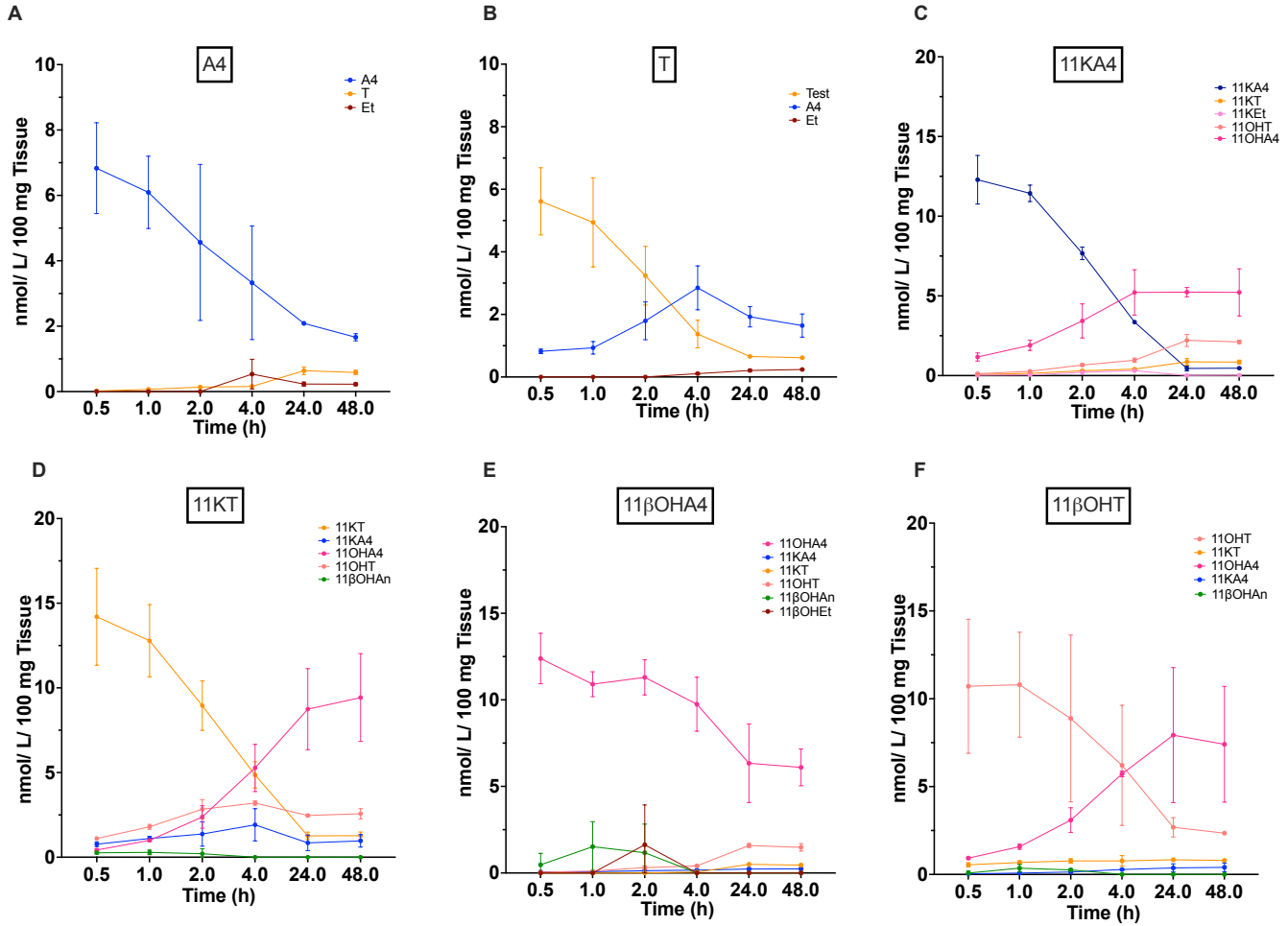

Figure 5.8 *Ex vivo* metabolism of classic (A and B) and 11 oxygenated (C,D,E and F) androgens by tissue from an unhealthy, explant liver, retrieved from a patient with non-cirrhotic portal hypertension (n = 1; age 36 years; BMI range 29 kg/m^2; female). Liver tissue was incubated with 100 nmol/L substrate for 48 hours. The substrate is shown in a black box. Data is representative of one biological replicate. Each biological replicate is representative of the mean of two technical replicates. Medium samples were collected after 48 hours and product formation was quantified by UHPLC-MS/MS and normalized to tissue mass. Median and range are indicated. Product concentrations below the limit of quantification are shown as 0.

5.3.4. Androgen metabolism favours androgen deactivation during normothermic machine liver perfusion (NMLP)

5.3.4.1. Endogenous androgen levels in liver perfusate during NMLP

Donor livers may contain residual androgens that can undergo metabolism during the course of the perfusion. Thus, when performing metabolism assays adding exogenous androgens of interest to the NMLP set up, the androgens already present in the liver might interfere with the interpretation of the results. It was therefore important to identify which, and in what quantity, androgens are present in perfusate of the liver after connection to the NMLP machine. Therefore, I analysed perfusate samples collected over time during eight perfusions. Donor demographics and characteristics of livers included can be found in **Table 5.1**. UHPLC-MS/MS analysis of the perfusate samples revealed that An, Et and 11βOHAn were detected in 7/8 liver perfusions, with an increase in their concentrations over the period of sample collection (**Figure 5.9**). DHEA and 11KEt were detected in 6/8 perfusions, showing an increase in concentration over the sample period. T (4/8), 11βOHEt (2/8) and 11KAn (1/8) were detected in only a subset of liver perfusions with levels around the limit of quantification (**Figure 5.9**).

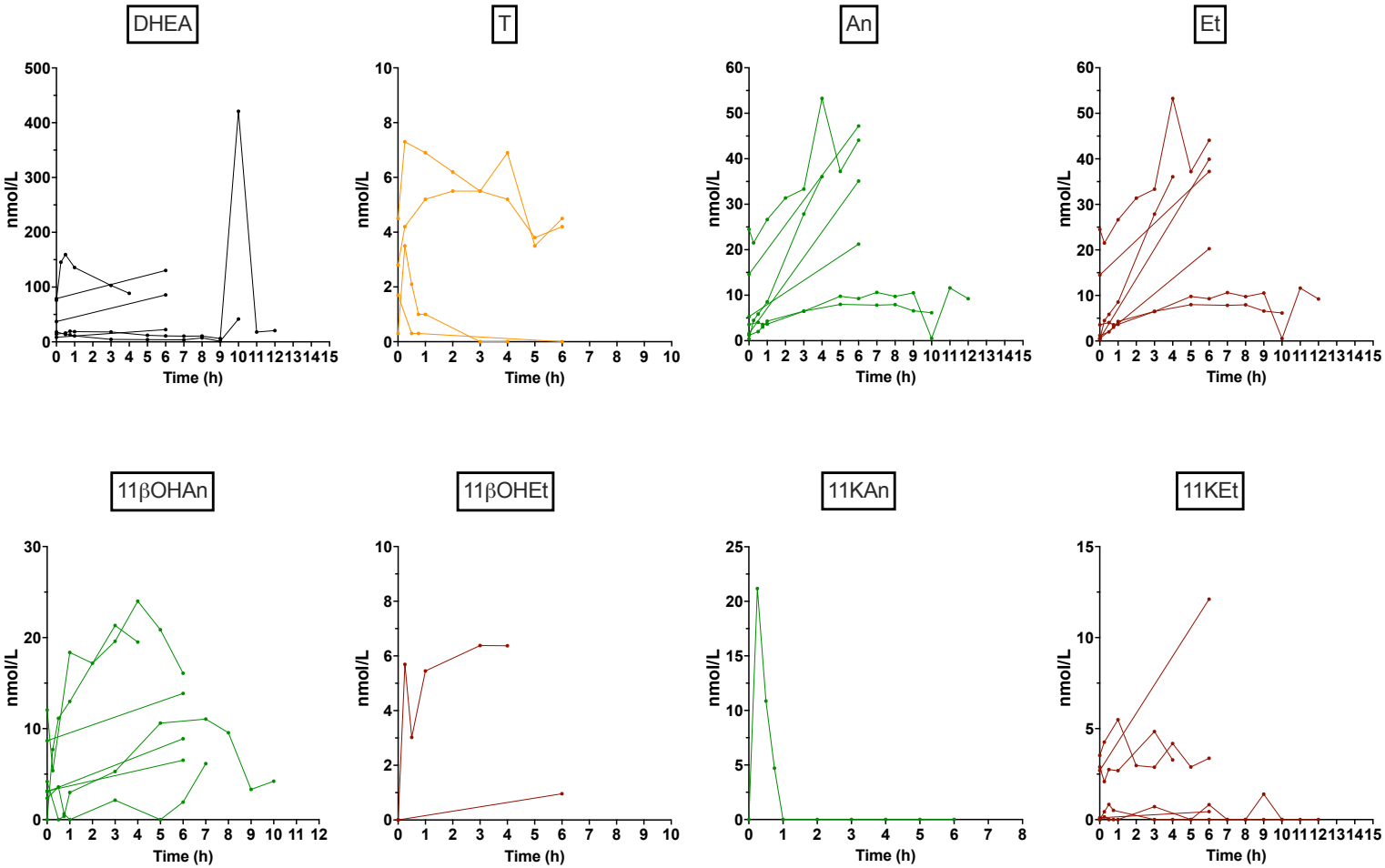

Figure 5.9 Concentration of endogenous classic (A, B, C and D) and 11-oxygenated (E,F,G and H) androgen metabolites detected over time in perfusate collected from 8 independent liver perfusions, in the absence of androgen treatment Perfusions were conducted using donor livers (n= 8; 7 male and 1 female, age range 31-78). Data is representative of eight biological replicates only. Each line represents an individual perfusion. Profiled metabolites are shown in a black box. Quantification was performed using UHPLC-MS/MS.

5.3.4.2. Classic and 11-oxygenated androgen precursors are converted to final excretive metabolites during NMLP

Due to the significant residual levels of androgens and androgen metabolites present in circulation during NMLP, [$^{13}C_3$]-labelled androgen precursors ([$^{13}C_3$]-A4 and [$^{13}C_3$]-11KA4) were used for androgen precursor metabolism assays (**Figure 5.10**). The use of labelled substrates allowed for the selective measurement of the metabolites generated from precursors added to the NMLP circuit, in the absence of interference from androgens already present.

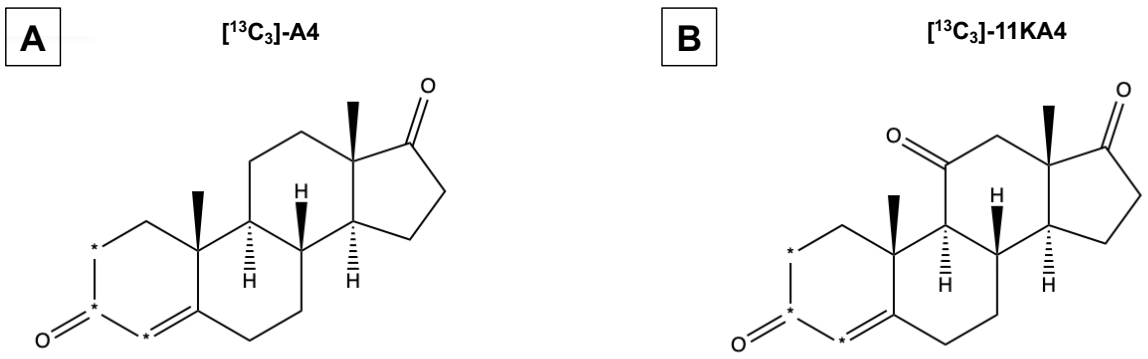

Figure 5.10: Chemical structures of 4-androstene-3,17-dione-2,3,4-[$^{13}C_3$] ([$^{13}C_3$]-A4) (A) and 4-androstene-11,3,17-trione-2,3,4-[$^{13}C_3$] ([$^{13}C_3$]-11KA4) (B). The position of ^{13}C atoms is indicated by asterisks.

To investigate androgen metabolism in a physiological representative model, classic and 11-oxygenated androgen precursors, [$^{13}C_3$]-A4 or [$^{13}C_3$]-11KA4, were added to the liver during NMLP, via addition of steroid diluted in perfusate, to the perfusate reservoir or direct injection into the arterial cannula. As the liver perfusion device is a closed

circuit, meaning all perfusate is recirculated through the liver during the entirety of the perfusion, the addition of steroid precursors in this manner would result in systemic circulation directly into the liver blood vessels, and subsequently liver cells. Classic androgen precursor [$^{13}C_3$]-A4 was added to two independent perfusions (n=2, age range 64-67 years; BMI 29 kg/m^2). All analytes included in the UHPLC-MS/MS assay developed for the quantification [^{13}C]-labelled products during NMLP (**Chapter 3)** were profiled during perfusate analysis. However, I only report those that were detected. Analysis of perfusate samples revealed that androgen metabolism in the liver by NMLP, mirrored androgen metabolism observed during *ex vivo* liver tissue incubations (**5.3.2**). When [$^{13}C_3$]-A4 was added into the perfusion circuit, it was immediately converted (within 30 minutes) to its final 5β-reduced metabolite [$^{13}C_3$]-Et via AKR1D1 and 5α-reduced metabolite [$^{13}C_3$]-An (**Figure 5.11A**). Et an An are the major urine metabolites of classic androgens. [$^{13}C_3$]-An was the major metabolite formed. The formation of these metabolites appeared to follow a similar pattern, whereby the concentration of each metabolite reached their maximum after 1 hour post precursor addition, and then remained relatively constant until the end of the perfusion. The observed plateau is a result of the perfusion device by nature being a closed circuit, where perfusate is recirculated throughout the liver continuously. Minimal levels of the active androgen [$^{13}C_3$]- 5α-DHT and its inactive metabolite [$^{13}C_3$]- 3αadiol, which is converted to An, were detected post [$^{13}C_3$]-A4 addition in one replicate only. Their levels appeared to increase over the first hour after [$^{13}C_3$]-A4 addition followed by consumption overtime (**Figure 5.11B**). [$^{13}C_3$]-T was not detected, further indicating the liver as a major site for androgen deactivation.

The addition of [$^{13}C_3$]-11KA4 to the NMLP circuit (n=1, age 48 years; BMI 30 kg/m^2) further maintained the notion of androgen deactivation by liver tissue. In this case, the predominant metabolite detected was [$^{13}C_3$]-11βOHAn (**Figure 5.12**). Lower levels of [$^{13}C_3$]-11βOHA4, [$^{13}C_3$]-11KEt and [$^{13}C_3$]-11βOHEt were also detected. [$^{13}C_3$]-11βOHA4 spiked 30 minutes after addition of [$^{13}C_3$]-11KA4, but was subsequently consumed, while concentrations of [$^{13}C_3$]-11βOHEt and [$^{13}C_3$]-11KEt remained relatively constant 30 minutes post of [$^{13}C_3$]-11KA4 addition. The active metabolite [$^{13}C_3$]-11KT was not detected.

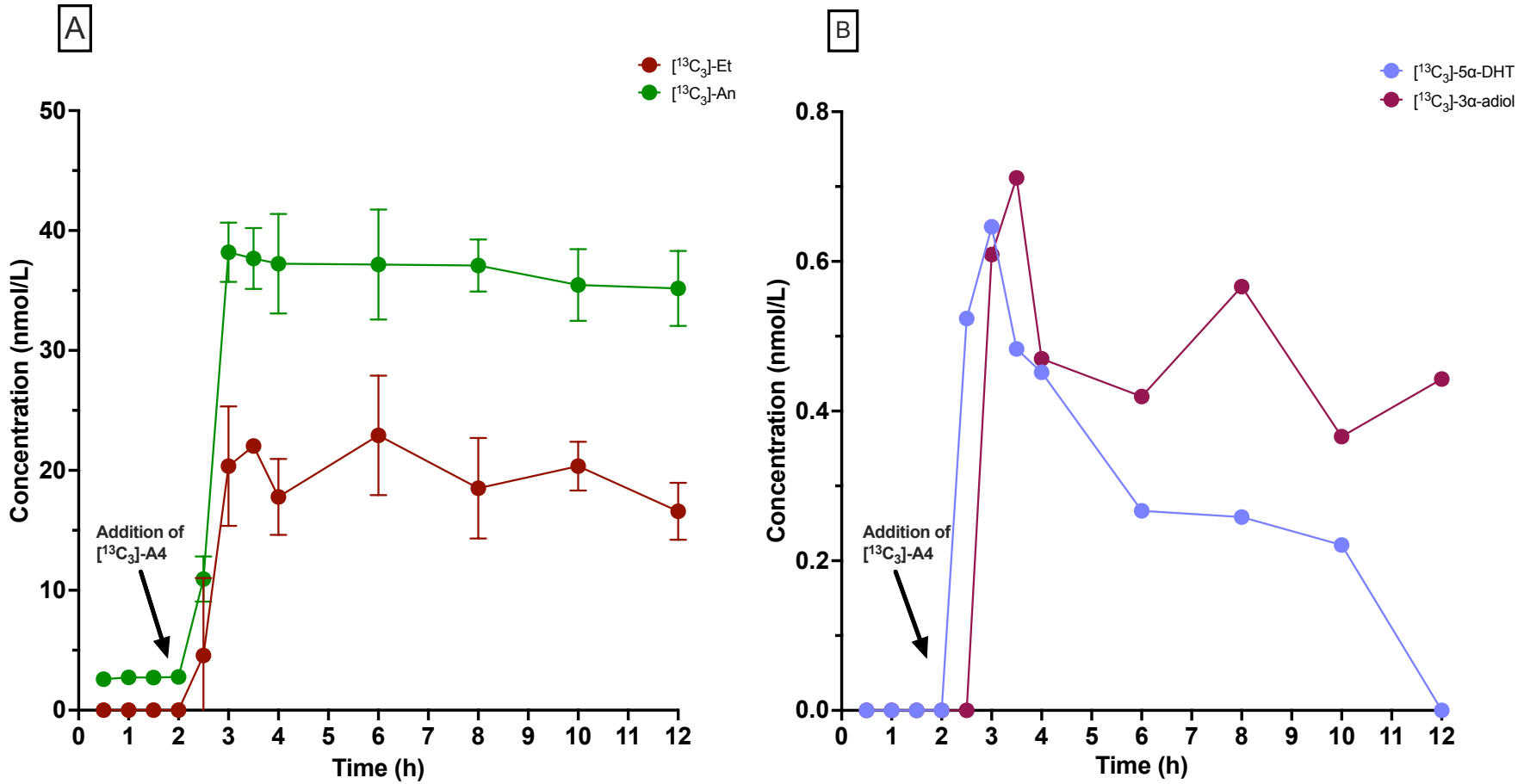

Figure 5.11 Metabolism of [$^{13}C_3$]-A4 during NMLP (n = 2; age range 64-67 years; BMI both 29 kg/m^2). **(A)** Formation of end stage inactive metabolites [$^{13}C_3$]-Et and [$^{13}C_3$]-An **(B)** Formation of intermediate metabolites [$^{13}C_3$]- 5α-DHT and [$^{13}C_3$]- 3α-adiol (detected in one liver perfusion only). LLOQs; [$^{13}C_3$]-Et = 3.5 nmol/L (indicated by dashed brown line), [$^{13}C_3$]-An = 8.6 nmol/L (indicated by dashed green line), [$^{13}C_3$]- 5α-DHT = 3.5 nmol/L and [$^{13}C_3$]- 3α-adiol = 25.7 nmol/L. 200 nmol/L of [$^{13}C_3$]-A4 was added to the NMLP circuit (via perfusate reservoir), after confirmation of liver viability, at T2. Total perfusion time was 12 hours. Product formation was quantified by UHPLC-MS/MS. Data is representative of two biological replicates only. Mean and standard deviation are indicated (performed using GraphPad Prism version 9.5).

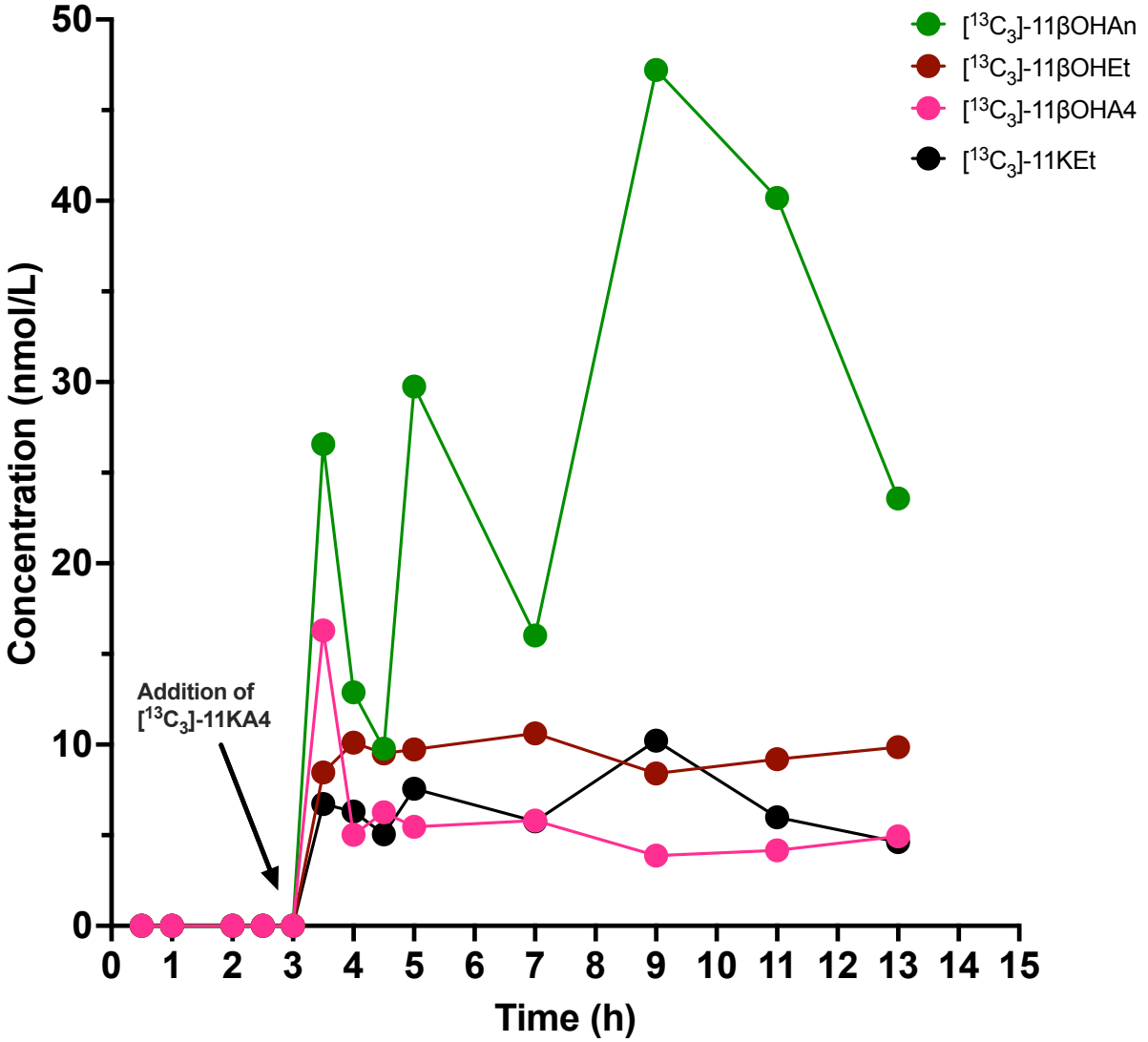

Figure 5.12 Metabolism of [$^{13}C_3$]-11KA4 during NMLP (n = 1; age; 68 years; BMI 30 kg/m^2). Formation of end stage inactive metabolites [$^{13}C_3$]-11KEt, [$^{13}C_3$]-11βOHAn and [$^{13}C_3$]-11βOHEt, and conversion to the immediate precursor of [$^{13}C_3$]-11KA4, [$^{13}C_3$]- 11βOHA4. LLOQs; [$^{13}C_3$]-11KEt = 8.2 nmol/L (indicated by black dashed line), [$^{13}C_3$]-11βOHAn = 3.5 nmol/L (indicated by green dashed line), [$^{13}C_3$]- 11βOHEt = 1.6 nmol/L (indicated by brown dashed line) and [$^{13}C_3$]- 11βOHA4= 1.7 nmol/L (indicated by pink dashed line). 200 nmol/L of [$^{13}C_3$]-11KA4 was added to the NMLP circuit via arterial cannula, after confirmation of liver viability, at T3. Total perfusion time was 13 hours. Product formation was quantified by UHPLC-MS/MS. Data is representative of one biological replicate only.

5.3.4.3. Testosterone metabolism in the normothermic machine liver perfusion model

An application of NMLP, which is rapidly gaining traction, is its use as a tool to recondition fatty livers [142, 201]. The nature of the NMLP system, which is designed to replicate *in vivo* conditions, enables the infusion of pharmacological agents into the liver. Fatty Livers can therefore be added to the NMLP device and treated with a drug cocktail aimed to reduce the level of steatosis. I was provided with perfusate samples from such perfusions (collaborators at the Institute of immunology and immunotherapy, University of Birmingham), who incorporate bolus injection of a solution containing 40 µmol/L of T into their liver perfusion circuit as part of a liver drug cocktail designed to reverse liver steatosis overtime. It is important to note, the addition of T to the drug cocktail is standard procedure was not an additional experiment variable for the purpose of this thesis. Samples were extracted by UHPLC-MS/MS and the metabolism of T was profiled over time. As the concentration of testosterone added (and therefore subsequent metabolites formed) was in great excess compared to the anticipated endogenous residual androgens levels (**Figure 5.9**), T metabolism could be effectively monitored, as endogenous androgens would not be expected to interfere with accurate quantification of exogenous testosterone metabolism. Therefore, this could be done in the absence of ^{13}C isotopic labels. Analysis of perfusate samples identified complete consumption of testosterone after 36 hours, although the initial decrease in testosterone concentration was rapid. An average of only 200 nmol/L of T was detected after just 30 minutes – a significant reduction compared to the 40 µmol/L of testosterone added to the liver at the start of the liver perfusions as a bolus treatment (**Figure 5.13**). As expected, based on the *ex vivo* and NMLP investigations outlined

above, a large proportion of testosterone was converted to inactive downstream metabolites Et and An. Interestingly, the most potent androgen, 5α-DHT, was the major metabolite detected in the first couple of hours. The concentration of each metabolite detected reached a peak between five and twenty hours, before starting to deplete. It is important to note that 5α-DHT peaked before An, reflecting the order of conversion of 5α-DHT to An. Interconversion to A4 via HSD17β2 was not detected.

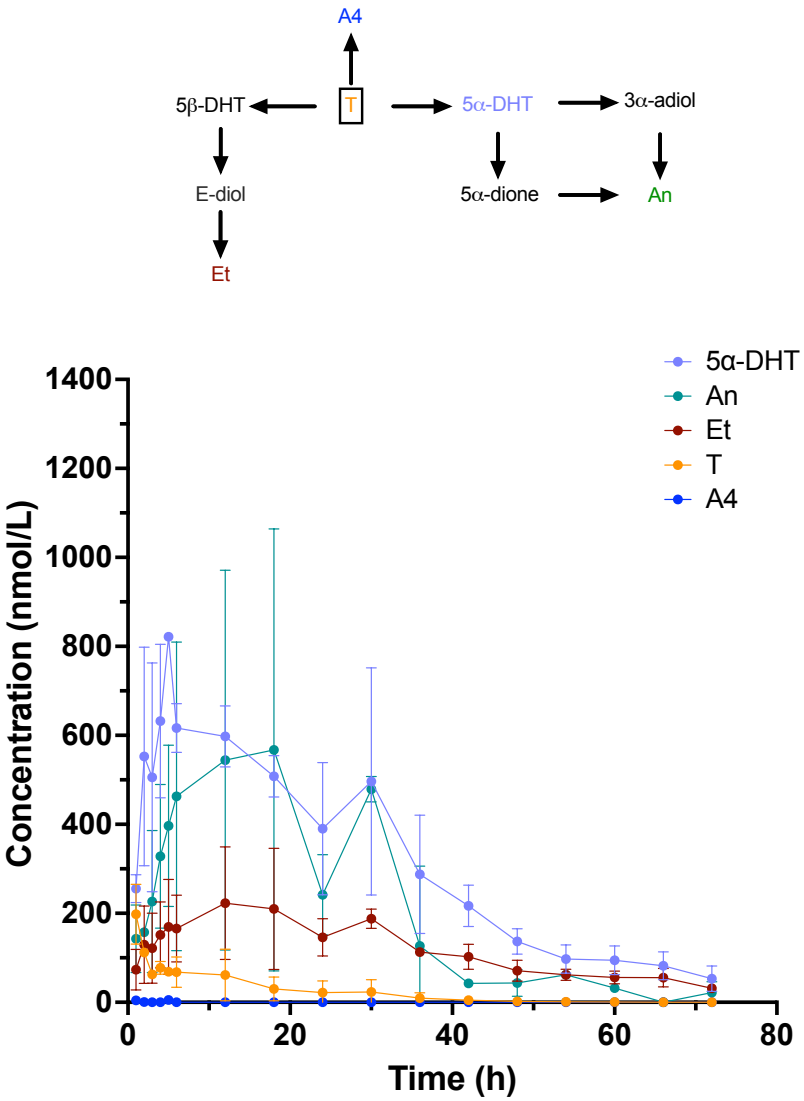

Figure 5.13 Metabolism of 40 µmol/L testosterone during reconditioning of fatty livers by NMLP (n = 2; age range 42-47 years; BMI range 27-40 kg/m^2). NMLP was used as a tool to 'defat' severely steatotic livers. Livers were provided with a bolus injection of a drug cocktail, containing 40 µmol/L testosterone, immediately after being connected to the NMLP device and perfused for 72 hours. Product

formation was quantified by UHPLC-MS/MS. Mean and standard deviation are indicated. Data is representative of three biological replicates only. Mean and standard deviation are indicated (performed using GraphPad Prism version 9.5).

5.4. Discussion

5.4.1. Androgens are primarily converted to inactive metabolites in human liver

Excess androgen levels in women with PCOS are associated with an increased risk of MASLD [105]. The liver is a key organ controlling steroid metabolism and excretions, yet the local pathways of androgen metabolism in the liver are understudied. Despite the unequivocal links between androgen excess and risk for MASLD, investigation into the full metabolic pathways of classic and 11-oxygenated androgens in the liver has not been previously described. This chapter provides insight on androgen metabolism in liver.

In human tissue, androgen precursors A4 and the 11-oxygenated precursor, 11KA4, can follow three possible metabolic pathways; 1) activation to active androgens T/11KT via AKR1C3, which can be further metabolised the most potent androgens 5α-DHT/ 11K-5α-DHT via SRD5A1/SRD5A2 2) conversion to 3β-hydroxy inactive end stage excretive metabolites Et/11KEt via AKR1D1 3) conversion to 5α-hydroxy inactive end stage excretive metabolites An/11KAn via AKR1C2. Specific to 11-oxygenated androgens only, all 11-keto metabolites can be converted to their hydroxy products via HDS11B1 (**Chapter 1, Figure 1.3**) [9, 20, 28]. T, 11KT, 5α-DHT and 11K-5α-DHT activate the AR, while Et, 11KEt, An and 11KAn are final excretive metabolites and are not AR agonists [202].

5.4.1.1. Classic androgen metabolism in the liver

The investigations conducted and detailed within this chapter revealed that classic androgen precursor A4 was predominantly converted to inactive end stage metabolites in donor liver tissue. During *ex vivo* incubations with A4 and T, the overwhelming majority was converted to the inactive urine metabolites Et and An. AKR1C3 did not appear to play a role in liver androgen metabolism, given incubations with A4 did not lead to quantifiable amounts of T. Interestingly, the generation of 5α-reduced product An and 5β-reduced product Et, was predominant over the generation of T. This result indicates that despite comparable levels of SRD5A1/2, AKR1D1 and AKR1C3 in liver tissue the presence of AKR1D1 and SRD5A1/1 leads to the removal of AKR1C3 substrates. AKR1D1 and SRD5A1 are therefore key enzymes in the regulation of androgen activation in liver tissue. These results, which indicate a preference of androgen deactivation rather than activation in liver tissue, are in in accordance with Granata *et al*. who investigated androgen metabolism in minced healthy liver samples and found generation of active androgens, from incubations with A4 and T, was limited. Generation of inactive products formed by the 5β-reductase pathway accounted for the majority of products detected [203]. The most important classic androgen pathways occurring in healthy donor liver tissue, as identified by these investigations, are outlined in **Figure 5.14** below.

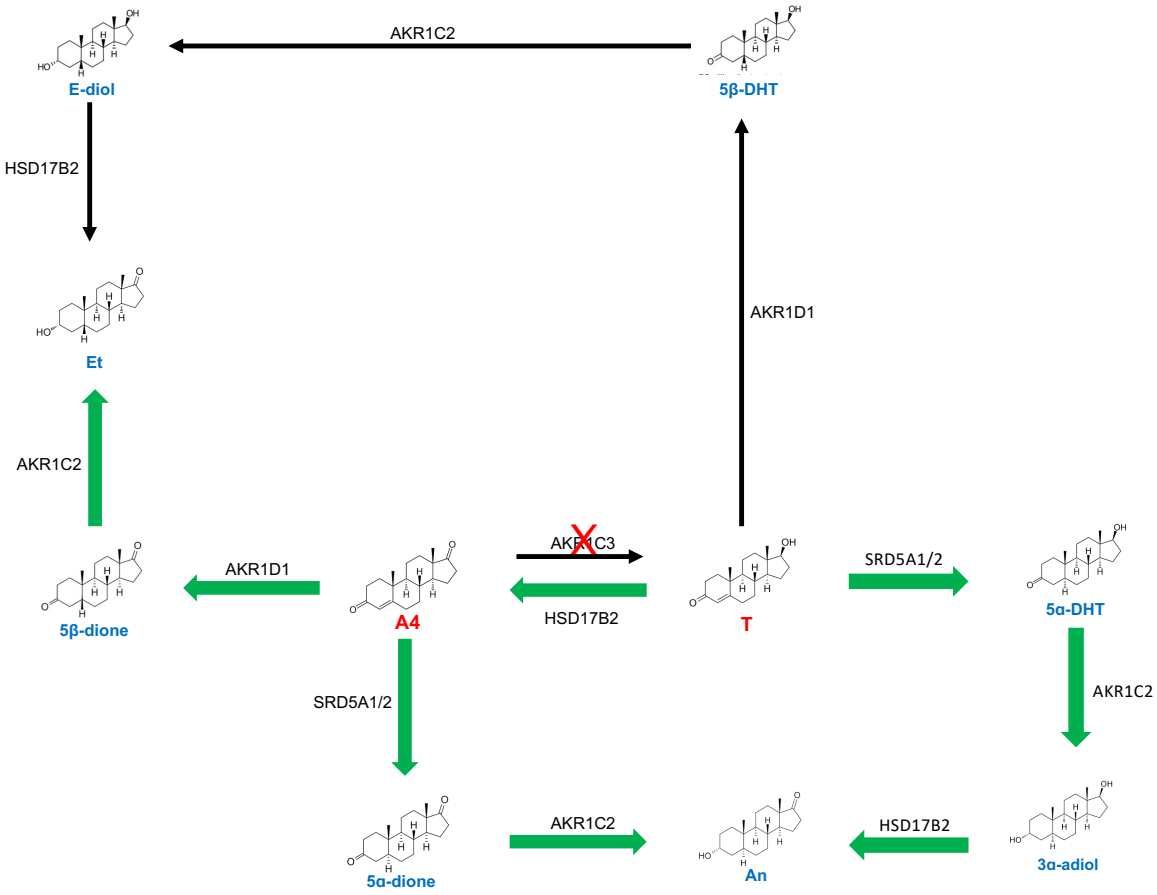

Figure 5.14 Schematic representation of the metabolic pathways of classic androgen precursor androstenedione (A4) and active metabolite testosterone (T) in the liver. The major pathways that occur are shown as green arrows. A4 is converted to inactive Et and An via AKR1D1 and SRD5A1/2, respectively. Conversion of A4 to T does not occur, although the reverse reaction (T to A4) does, facilitating formation of Et and An via A4. T may also be converted directly to Et via AKR1D1.

In tandem with *ex vivo* liver tissue incubations, NMLP was utilised as a physiological model, to further gain an accurate picture of androgen metabolism in human liver. As initial *ex vivo* incubations using donor tissue revealed minimal 3β-hydroxysteroid dehydrogenase activity toward precursor DHEA, it was removed as a relevant precursor substrate for metabolism in liver (data not shown). NMLP procedures were therefore conducted using classic precursor A4 and the equivalent 11-oxygenated precursor, 11KA4. Prior to androgen metabolism investigations, endogenous residual

androgens were shown to be detected in perfusate, in the absence of exogenous androgen intervention (**Figure 5.10**). Importantly, as Et was shown to be a major metabolite of A4 and 11OHEt/11OHAn were shown to be major metabolites of 11KA4 during *ex vivo* incubations, pre-existing circulating levels of these metabolites would interfere with accurate quantification of A4/11KA4 conversion. To ensure that the results would not be compromised, ^{13}C-labelled precursors ([$^{13}C_3$]-A4 and [$^{13}C_3$]-11KA4) were used.

Generation of [$^{13}C_3$]-An and [$^{13}C_3$]-Et were predominant metabolites during perfusions incorporating [$^{13}C_3$]-A4, further reflected the liver as a site of androgen clearance. The observed plateau was of course due to these metabolites being end stage and therefore not substrates for conversion. Since the NMLP is a closed system where perfusate is recirculated, once the generation of these metabolites had reached their maximum they were recirculated at the same concentration throughout the system until the end of the perfusion. 5α reduced active metabolite [$^{13}C_3$]- 5α-DHT and minor amounts of [$^{13}C_3$]- 3α-adiol were detected and found decline overtime in one replicate only, presumably due to downstream conversion to [$^{13}C_3$]-An formation. While [$^{13}C_3$]-5α-DHT and [$^{13}C_3$]- 3α-adiol were not detected during *ex vivo* incubations, I would account their detection during NMLP to the different assay models. A whole liver was used during NMLP compared to only 200 – 300 mg of tissue used during *ex vivo* investigations. It highly likely that the greater tissue mass during the NMLP procedure (and greater substrate concentration added) resulted in a greater number of liver cells involved in the metabolism of A4, which contributed to [$^{13}C_3$]- 5α-DHT and [$^{13}C_3$]- 3α-adiol detection. The fact that such a small level of these metabolites was detected (<1 nmol/L), in comparison to the [$^{13}C_3$]-Et and [$^{13}C_3$]-An detected, confirms that these

intermediate metabolites do not make a substantial contribution to the local liver androgen pool. Rapid consumption of these metabolites over time strengthens the argument that the liver is a site of androgen deactivation. Despite active androgen [$^{13}C_3$]- 5α-DHT being present, it was promptly depleted, presumably contributing to [$^{13}C_3$]-An levels. It should be noted, however, that due to the potency of 5α-DHT, only a small amount is required to have a local effect. It is also important to note that T was not detected in these incubations, which further confirmed rapid conversions and insignificant levels of active metabolites. Additionally, An was detected in *ex vivo* incubations with T, meaning 5α-DHT and/or 3α-adiol may have been present, as direct intermediates to An formation, but converted so rapidly they could not be detected. The detection of [$^{13}C_3$]- 5α-DHT and [$^{13}C_3$]- 3α-adiol during one replicate of NMLP is therefore still in alignment with the results of the *ex vivo* investigations.

Time course incubations with explant liver tissue (tissue retrieved from a patient with end stage liver disease) revealed that the metabolism of A4 differed to that in donor tissue. While qPCR analysis of liver tissue used during this study (Figure 5.1) did not highlight differences in the expression of steroidogenic enzymes between explant and donor tissue, formation of Et and thus activity of AKR1D1 appeared to be minimal in explant tissue. In such cases of disparity detected between qPCR expression and detected enzyme activity, it is important to note that qPCR provides an indication of transcript abundance not enzyme activity. Interestingly, I did not detect An in any incubations. Although the explant tissue used during the investigation was retrieved from a patient with non-cirrhotic portal hypertension (NCPH), causes of NCPH include MASH (severe MASLD) and manifestations of NCPH and MASLD are so similar, patients are often mis-diagnosed with cirrhosis (early onset MASLD) prior to liver

transplantation [204, 205]. Using liver biopsies, Nikolaos Nikolaou et al. showed that mRNA levels of AKR1D1, the enzyme responsible for androgen deactivation to Et/11KEt production, decreases across the spectrum of MASLD [206]. The results outlined in this chapter provide insights on how a decrease in in AKR1D1 expression may manifest itself, in the context of androgen metabolism, during end stage liver disease. Since androgen clearance by deactivation can be dysregulated in tissue with liver disease [207], the differential steroidogenic metabolism of A4 and T observed in this explant tissue may be a result of this. Considering the sample size number (n=1), it is difficult to draw absolute conclusions from the outcome of experiments involving explant liver tissue. However, these experiments certainly highlight the differences in androgen metabolism in healthy human liver tissue compared to livers with end stage liver disease and provide insights on areas within the context of liver androgen metabolism that may of interest to study further down the line.

Samples from perfusions where NMLP was used as a tool to recondition severely steatotic livers, allowed for the profiling of T metabolism during NMLP, without the need for isotopic labelling were also analysed. In this study, a drug cocktail, which contained high levels of T, was infused into the liver at the start of the perfusion and T was shown to be predominantly converted to the most potent classic androgen 5a-DHT, followed by An, and Et. This inclination to active androgen production suggests, during liver disease only, the liver may play a proactive role in active androgen generation. This preliminary work with explants/steatotic livers indicates that their androgen metabolism might be altered which could impact local androgen action and systemic androgen levels. The differential effects of androgens between men and women are well known,

and while reduced testosterone levels in men are associated with MASLD, the opposite is true for women [131, 208, 209]. Therefore, further investigations on androgen metabolism across the stages of MASLD, in the context of contributions to female androgen excess may be of interest in the future. Investigations on the metabolism of 11-oxygenated androgens during liver disease, using NMLP, would also provide valuable insights.

5.4.1.2. 11-oxygenated androgen metabolism in the liver

Despite abundant expression of AKR1C3 in liver tissue, 11KT was not detected in incubations with 11KA4. 5α-reduced product 11βOHAn and the 5β-reduced product 11βOHEt were the major metabolites, confirming that that although SRD5A1/2, AKR1D1 and AKR1C3 are expressed in liver tissue, the presence of AKR1D1 and SRD5A1/1 leads to the removal of AKR1C3 11-oxygenated substrates, as well as classic substrates. Previous studies have shown that AKR1C3 preferentially activates 11KA4 to 11KT, over A4 to T, during *in vitro* analysis using LNCaP cells and *ex vivo* peripheral blood mononuclear cells (PBMCs) [175, 178]. However, as neither T nor 11KT were detected in incubations with their respective precursors A4 and 11KA4, the data from this study shows, for the first time, that the preference for 11KA4 activation by AKR1C3 is not observed in liver tissue. It may be possible that both T and 11KT were formed and immediately metabolised to further downstream metabolites, obstructing detection by the UHPLC-MS/MS assay. It may also be of interest to investigate expression of HSD17B2, the enzyme responsible for the reverse reaction of AKR1C3. HSD17B2 activity may have impacted interpretation of the results.

The metabolic profile of 11-oxygenated androgens within the liver has not previously been reported. I have shown, for the first time, the metabolism of 11-oxygenated androgens in the liver shows a preference for formation of inactive downstream metabolites. Incubations with 11-oxygenated precursor 11KA4, led to the formation of inactive end stage metabolite 11KEt and incubations with the immediate precursor of 11KA4, 11βOHA4 and downstream metabolite 11βOHT further confirmed the liver as a site of androgen deactivation for 11-oxygenated androgens, as quantifiable conversion to 11KT was not detected. Additionally, incubations with 11KT showed rapid conversion to inactive urinary products 11βOHAn and 11βOHEt. In all 11-oxygenated incubations, 11βOHA4 was a major product, generated and later completely consumed. Bearing in mind the amount of 11βOHAn detected, yet insufficient levels of 11KT, I would postulate that 11βOHA4 is the main contributor to observed 11βOHAn levels within these incubations. Findings from ex vivo incubations were supported by NMLP investigations and again, the liver behaved as a site of active androgen clearance, producing no [$^{13}C_3$]-11KT but consistent levels of [$^{13}C_3$]-11βOHAn, [$^{13}C_3$]-11βOHEt and [$^{13}C_3$]-11βOHA4. As [$^{13}C_3$]-11βOHA4 was detected to the lowest degree, and its decline in concentration corresponded to the increased levels of [$^{13}C_3$]-11βOHAn, this further confirmed 5α-reduction of [$^{13}C_3$]-11βOHA4 via SRD5A1/2 to be the major contributor to [$^{13}C_3$]-11βOHAn levels. Considering the results from these investigations, the primary metabolic pathways of 11-oxygenated androgens within the liver, are outlined in **Figure 5.15** below. As seen during *ex vivo* liver tissue incubations, treatments with 11KA4 during NMLP produced inactive urinary metabolites [$^{13}C_3$]-11βOHAn and [$^{13}C_3$]-11βOHEt in the majority, but [$^{13}C_3$]-11βOHA4

(the immediate precursor of [$^{13}C_3$]-11KA4) and [$^{13}C_3$]-11KEt, were also present in quantifiable amounts.

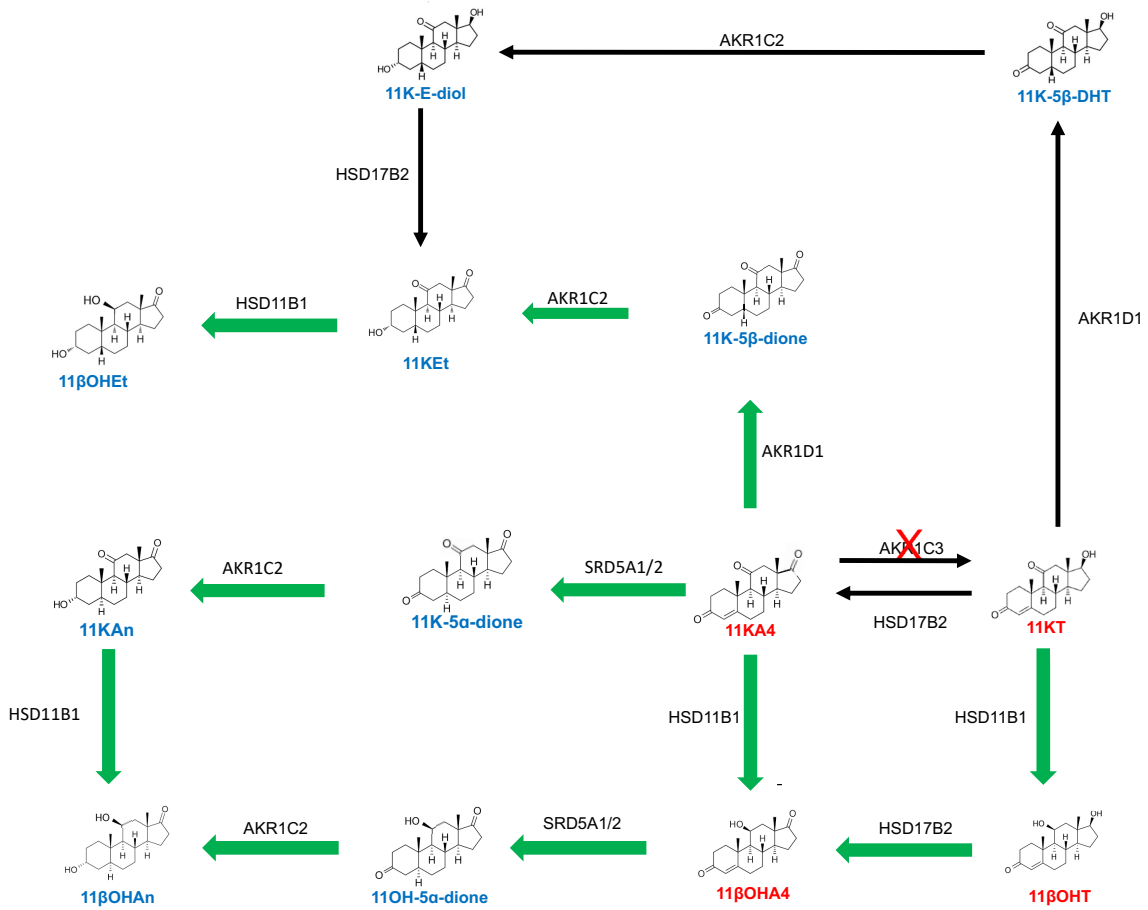

Figure 5.15 Schematic representation of the metabolic pathways of 11-oxygenated androgen precursors 11-ketoandrostenedione (11KA4), 11βhydroxyandrostenedione (11βOHA4) and metabolites 11-ketotestosterone (11KT) and 11βhydroxytestosterone (11βOHT) in the liver. Substrates investigated in this thesis are shown in red. The major pathways that occur are shown as green arrows. 11KA4 is converted to inactive metabolite 11KEt via AKR1D1, which if further converted to 11βOHEt. 11KA4 is also converted to its immediate precursor 11βOHA4 via HDS11B1, leading 11βOHAn. Interconversion of 11βOHA4 to 11KA4 was not a major pathway observed but can lead to generation of 11βOHEt. Conversion of 11KA4 to 11KT was not observed. 11KT and 11βOHT are both readily converted to 11βOHA4 via HSD11B1 and HSD17B2, respectively, leading to final excretive products 11βOHEt and 11βOHAn.

5.4.1.3. HSD11B1 is a major regulator of 11-oxygenated androgen levels in the liver

For 11-oxygenated androgens, HSD11B1 can be considered the central androgen metabolism regulator in liver tissue by a) clearance of 11KA4 to 11βOHAn and 11βOHEt b) by inactivating 11KT to 11βOHT. Additionally, AKR1D1 5β-reduction to 11KEt was detected during incubations with 11KA4, 11βOHAn and 11βOHEt were found to be the predominant metabolites formed in incubations containing 11-oxygenated androgens and were detected consistently in all incubations, particularly for 11KA4 and 11KT. This result is not surprising, as HSD11B1, which responsible for conversion of 11-ketonated androgens to their 11-hydroxylated is highly expressed in the liver [210, 211]. This was confirmed during qPCR analysis of eleven liver tissue samples (**Figure 5.1**), which showed abundant expression of HSD11B1.

Previous literature concerning the involvement of HSD11B1 in liver health is conflicting. Ahmed *et al* reported HSD11B1 expression in 16 individuals with histologically proven MASLD, was reduced in the early stages of steatosis, yet activity was increased in MASH [212]. In contrast, Lutz *et al* reported 12-week *in vivo* HSD11B1 inhibition in 327 participants led to significant reduction in liver fat [213]. Studies on single nucleotide polymorphisms of HSD11B1 have also implicated increased expression in metabolic syndrome and steatosis disease progression [214-216]. HSD11B1 is a major enzyme in the regeneration of the key glucocorticoid, cortisol, from inactive cortisone, [217]. The association between elevated cortisol levels and liver failure are well documented [218-220]. The influence of HSD11B1 on liver health is therefore multi-faceted and not only governed by androgen metabolism. It is clear that the relationship between HSD11B1, liver failure requires more extensive study, and the results outlined in this thesis spotlight the importance of HSD11B1 in liver androgen metabolism.

5.4.1.4. Key differences between classic and 11-oxygenated androgen metabolism in the liver

My results show that both classic and 11-oxygenated androgens undergo a process of conversion to inactive urinary metabolites in the liver. It appears that metabolism of classic androgens A4 and T is regulated by SRD5A1/2 (leading to formation of An) and AKR1D1 (leading to formation of Et), yet metabolism of 11-oxygenated androgens is regulated by HSD11B1. The abundant expression of HSD11B1 in the liver and thus potential for 11-ketonated androgens to be converted to their 11-hydroxy products via HSD11B1, constitutes the major difference between liver metabolism of the two androgen classes investigated.

While 11KEt is formed in the same manner as Et (via AKR1D1), subsequent hydroxylation of 11KEt by HSD11B1 leads to 11βOHEt. It is important to note, that a key difference between classic and 11-oxygenated androgen metabolism in the liver is the formation of 11βOHAn from 11KA4. I have shown that the 11-oxygenated androgen precursor 11KA4 is first converted to 11βOHA4, which is subsequently converted to 11βOHAn via SRD5A1/2. The generation of 11βOHAn may be a result of SRD5A1/2 activity toward 11KA4, as shown in **Figure 1.15** above, yet 11KAn was not detected during this assay. The presented results indicate adrenal 11-hydroxy precursor 11βOHA4 to be a large contributor 11βOHAn formation, further highlighting its importance in 11-oxygenated androgen metabolism. 11βOHA4 is clearly more than just a intermediate metabolite between classic and 11 oxygenated androgen precursors A4 and 11KA4, but rather crucial to understanding clearance of 11-oxygenated androgens in the liver. The clinical importance of 11βOHA4 in 11-

oxygenated androgen metabolism has been previously emphasised, and it has been proposed as a promising biomarker of androgen excess [15]. My work has further supported 11βOHA4 as an important mediator of liver androgen metabolism and therefore potential biomarker of androgen excess.

5.4.2. NMLP as a new tool to study androgen metabolism

NMLP has been used as a tool to introduce and monitor the effects of adding exogenous substances to a liver during NMLP [143, 221]. Bral *et al* profiled the metabolism of transaminases (potential biomarker to directly assess graft viability) during NMLP of porcine livers. A highly concentrated transaminase solution was infused into the device circuit via injection into liver cannula and profiled liver function (lactate clearance and oxygen consumption), as well as transaminase clearance by biochemical analysis of perfusate samples taken over a 48-hour period [143]. However, to date, no such research has been conducted on human livers, exploring androgen metabolism. We have shown for the first time, that NMLP can be used as a successful tool for androgen metabolic profiling. Two different methods for the addition of steroids to the liver perfusion system, to achieve optimal liver exposure, were trialled: addition of steroid to perfusate reservoir and direct infusion of steroid into the arterial cannula. As the perfusate circuit comprises of a circulatory system where perfusate is constantly being recirculated in and out of the liver, the volume of diluted steroid to be added to the circuit was calculated based to the desired final concentration in the total volume of perfusate (2 L), assuming even dispersion throughout the system. It is therefore difficult to determine the starting concentration, how long it takes for full circulation of the substrate to be achieved and absolute liver

exposure. However, the results from the NMLP investigations described in this chapter provide evidence that the methods used during these investigations lead to adequate steroid uptake into the liver. Steroid uptake was confirmed by the detection of relevant metabolites in all perfusions, which parallel the findings during *ex vivo* investigations with liver tissue. Uptake occurred within just 30 minutes of steroid substrate ([$^{13}C_3$]-A4 and [$^{13}C_3$]-11KA4) addition, identified by the absence of substrate detection in perfusate samples at this time point and all subsequent timepoints. Considering this, our experimental design can be deemed a successful and reliable method leading to suitable liver exposure, allowing for informative liver androgen metabolism analysis. This experimental method could therefore be used in the future to explore the role of other steroids classes, such as oestrogens, glucocorticoids and mineralocorticoids, on liver health and metabolism.

There may be concern that *ex vivo* incubations cannot truly represent liver physiology as viability cannot be confirmed. These limitations do not apply for NMLP, as the liver is supplied with oxygen and nutrients throughout the perfusion. Additionally, liver viability can be assessed in real time by blood-gas analysis (pH, pCO_2, pO_2, HCO_3, blood flows) [222, 223]. The conclusions drawn from *ex vivo* experiments and NMLP experiments are concordant. Taken together, these results provide further confidence that the pathways of androgen metabolism in the human liver have been successfully, and most importantly, accurately illustrated.

5.4.3. Limitations

Although this thesis has a focus on female androgen metabolism in the liver, in the context of PCOS, unfortunately due to reduced availability of female research donor

livers, profiling androgen metabolism in livers from only female donors was not possible. However, these pilot investigations aimed at developing a general understanding of androgen metabolism in healthy liver tissue. Although it has been well established that the responses to androgen metabolism in men and women differ [224], differences in steroidal metabolic pathways have not been highlighted. In addition, the results from these tissue incubations are from two males and one female donor, and they all follow the same pattern of androgen deactivation. Therefore, whilst it would be ideal to conduct these studies using liver from female donors only, we are able to gain valuable insights into androgen metabolism from the available cohort. Additionally, androgen metabolism in such *ex vivo* models, particularly the metabolism of 11-oxygnated androgens, has not been investigated before. The results described here are the first to comprehensively discern androgen metabolism in the human liver.

One drawback of *ex vivo* tissue culture is the inability to confirm viability and integrity of the tissue over extended periods of time [225]. However, *ex vivo* liver slices have been successfully used for decades to assess liver metabolism, such as caffeine metabolism and endogenous metabolism of cholesterol [226]. Therefore, for the purposes of this thesis, and due to the relatively short incubation time used, it is plausible to accept that liver viability is not a major concern and would therefore did not negatively impact experimental outcomes.

Unfortunately, due to reduced availability of donor research livers, the lack of diversity in the donor cohort during NMLP investigations (**Table 5.1**) is an unavoidable limitation of this study. All the livers included were retrieved from middle aged males. Ideally, androgen metabolism in female donors would have been beneficial to build a

comprehensive picture of androgen metabolism, especially in the context of female androgen metabolism. The [$^{13}C_3$]-A4 NMLP cohort did, however, include a liver provided by a South Asian male, which added an additional dimension of influences of ethnicity on liver androgen metabolism. There were no significant differences in the observed metabolism of [$^{13}C_3$]-A4 between ethnicities.

There were minimal, but noticeable, losses in steroid recovery, particularly in the case of explant liver incubations with A4. These differences may be attributed to steroid recovery as identified during UHPLC-MS/MS method development (**Chapter 3**) or could be a result of conversion to steroids such as oestrogens or oestrogen precursors not included in the UHPLC-MS/MS assay. Aromatase activity on A4 and T to oestrogens is well reported. Of note, Gordon *et al.* have shown increased aromatase activity in liver disease such cirrhosis, and Granata *et al*. reported prominent aromatase activity when treating *in vitro* liver cell line HepG2 with A4 [203, 227]. It was not possible to include oestrogens into the assay, maintain the specificity and sensitivity of the assay and keep the time efficient manner achieved for the assay used for this thesis (**Chapter 3**). If the identification of oestrogens was important the samples could be run on method designed for oestrogen quantification. This project focussed on androgens only and the results achieved, a comprehensive picture of androgen metabolism in the liver has been illustrated. The quantification of oestrogens was therefore beyond the scope of this project.

Limitations of quantification of steroids during NMLP experiments have been described in **Chapter 3**, consisting of matrix effects due to the use of blood substitute hemopure which affected steroid recovery. Additionally, the method did not include all potential

metabolites. However, these pioneering experiments using NMLP as a tool to introduce steroids aimed to identify steroid metabolism patterns, not exact numbers. The investigation was therefore qualitative and consequently, the inability to account for all of the substrate added to the system was not paramount.

5.4.4. Conclusions

In conclusion, I have successfully profiled androgen metabolism in two liver models: ex vivo incubation and NMLP. Using *ex vivo* liver incubations, I show both classic and 11-oxgenated precursors and metabolites preferably undergo conversion to inactive end stage A ring reduced androgen metabolites. In the case of 11-oxygenated androgens, HSD11B1 has been identified as a major regulator of active androgen. The validity of these results was confirmed using NMLP. NMLP has been confirmed as a highly suitable tool for *ex situ* whole organ assessment of steroid metabolism and the results described here provide proof-of-principle of the use of this technique to investigate androgen metabolism in the human liver. This technique has the potential to be utilised to dissect the role of androgens in the development of conditions such as MASLD.

CHAPTER 6

CONCLUSIONS AND FUTURE DIRECTIONS

6.1. Conclusions

PCOS is a metabolic disorder affecting approximately 10-20 % of women and underpinned by androgen excess. PCOS is associated with increased risk of obesity and MASLD both driven by androgen excess. Adipose and liver are both metabolically functioning tissues, expressing the AR and the key androgen activating enzyme AKR1C3. Thus, local androgen generation in adipose and liver has the potential to control local levels of active androgens and to contribute to the circulating androgen pool, causing and/or worsening obesity and MASLD in PCOS. This thesis described local androgen metabolism in these target tissues and explored the potential for AKR1C3 inhibition as a potential therapeutic to control androgen excess. I aimed to answer the following three research questions:

1) Is it feasible to develop an accurate and efficient ultra-high performance liquid chromatography tandem mass spectrometry (UHPLC-MS/MS) method for multi-androgen profiling?

Presented here is a developed and optimised UHPLC-MS/MS method, specifically designed for multi-androgen profiling during *ex vivo* liver tissue and NMLP investigations (**research aim 3**). The method successfully separated and quantified nineteen classic and 11-oxygenated androgens, previously quantified using two or more assays, with an overall run time of just 5 minutes. This assay was applied to different matrices used during liver androgen metabolism studies by performing

extensive method validation. The method accuracy, intra and inter assay precision, matrix effects, upper and lower limits of quantification, analyte recovery and carry over following published guidelines [155]. The method met clinical standard criteria when applied to medium used to culture cell lines and tissue but was judged to be semi quantitative when applied to perfusate used for NMLP (hemopure), due to significant matrix effects. Although the method was deemed semi-quantitative when applied to hemopure, however it was sufficient to explore androgen metabolism in hemopure samples. Due to the nature of NMLP investigations use Carbon 13 labelled substrates was required. [$^{13}C_3$]-labelled classic and 11-oxygenated androgens were generated *in vitro* and used to modify the UHPLC-MS/MS method retention times and mass transitions for accurate quantification of sixteen [$^{13}C_3$]-labelled classic and 11-oxygenated androgens, not previously reported. The modified method was successfully applied to the analysis of NMLP samples.

2) <u>What is the activity of AKR1C3 in female adipose tissue, and what is the impact of AKR1C3 inhibition on classic and 11-oxygenated androgen levels?</u>

Primary human female subcutaneous and omental *ex vivo* adipose tissue were used to show that adipose tissue, *ex vivo*, generates active classic and 11-oxygenated androgens (T and 11KT) from their respective inactive precursors (A4 and 11KA4). Thus, I have presented a pragmatic investigation on the activity of AKR1C3 in subcutaneous and omental female adipose tissue. AKR1C3 converted inactive classic precursor A4 to its active metabolite T and 11-oxygenated androgen precursor 11KA4 to its active metabolite 11KT, which was further converted to active 11βOHT via HSD11B1. AKR1C3 preferentially activated 11KA4 in subcutaneous and omental

adipose tissue, identified by approximately 7-fold higher conversion of 11KA4 compared to A4. 11βOHT generated from 11KT via HSD11B1 was lower in omental tissue, corresponding to previously reported reduced expression of HSD11B1 in omental tissue. Inhibition of AKR1C3 was a suitable approach to reduce the local generation of active androgens in adipose tissue. Interestingly, the effect of AKR1C3 inhibition was stronger for reduction of active 11-oxygenated androgens and AKR1C3 inhibition did not fully supress T generation, potentially indicating the involvement of other steroidogenic enzymes in testosterone generation in adipose.

3) <u>What is the metabolic profile of classic and 11-oxygenated androgens in the liver?</u>

To understand why women with PCOS have an increased risk for MASLD development and how this is exacerbated by androgen excess, we must first understand how androgens are metabolised in the liver and whether this metabolism can contribute to the local pool of active androgens. Therefore, two liver models were employed (primary human liver *ex vivo* incubations and NMLP) to dissect androgen metabolism in the liver. The overwhelming majority of classic androgens served as substrates for conversion to inactive downstream 5β-reduced metabolite Et, via AKR1D1, and inactive downstream 5a-reduced metabolite An, via SRD5A1/2. Thus, these results demonstrate for the first time that classic androgens are converted to inactive downstream metabolites in the liver. All 11-oxygenated androgens were predominantly converted to 11b-hydroxy metabolites 11βOHA4, 11βOHEt and 11βOHAn. These results propose that HSD11B1 is a key regulator of 11-oxygenated androgen action in the liver. Conversion of classic or 11-oxygenated precursors A4

and 11KA4 to their respective 17b-hydroxy active androgens, T and 11KT, was not observed. Preliminary work on livers retrieved from a patient with non-cirrhotic portal hypertension (end stage liver disease) and a severely steatotic liver during NMLP highlighted alterations in androgen metabolism. The presence of 5a-reduced downstream metabolites indicates that DHT, the most potent human androgen, could be formed locally in the liver, but that it is rapidly inactivated. The NMLP investigations outlined herein have provided proof-of-principle that established NMLP as a successful tool for androgen metabolism analysis by the introduction of androgen substrates into the circulatory device system.

6.2. Future directions

The results have provided a strong foundation on which future work can be built. The next steps are outlined below.

1) Development of an ultraperformance convergence chromatography tandem mass spectrometry (UPC^2-MS/MS) method for multi-androgen profiling

The multi-androgen UHPLC-MS/MS method herein developed can be used as an accurate tool for androgen profiling without further development. However, this method can be used as framework to develop an additional multi-androgen profiling method using ultraperformance convergence chromatography tandem mass spectrometry (UPC^2-MS/MS), an alternative technique to UHPLC-MS/MS. The structural similarity of C_{19} androgenic steroids means it can be difficult to separate them chromatographically. This was characterised in the problematic separation of four pairs of analytes (11βOHA4 and 11K-5α-dione; 11βOHT and 11K-5α-DHT; 11βOHAn and

11KAn; 11βOHEt and 11KEt). During UPC^2-MS/MS chromatography, supercritical CO_2 is used as the mobile phase, which provides the same dissolving capacity as liquid CO_2 but with greater diffusivity and viscosity, resulting in superior chromatographic separation and resolution [228, 229]. The use of UPC^2-MS/MS for steroid separation has been previously reported by Toit *et al*., who were able to separate 11βOHT and 11KDHT [230]. However, this UPC^2-MS/MS did not include the full panel of androgens included in the assay described in this thesis (Et, 11OHEt and 11βOH5α-dione). Keeping the chromatographic parameters reported by Toit and team in mind, development of a UPC^2-MS/MS method designed to separate these classic and 11-oxygenated androgens may be possible. In addition, due to the properties chromatographic separation by UPC^2 has the potential to separate α/β isomers, as demonstrated by Toit et al who reported separation of 3α/β-hydroxy isomers of etiocholanolone. Therefore, it may be possible to develop a method capable of separating more 5α/β pairs, such as 5α-DHT and 5β-DHT. The panel of androgens included could therefore be expanded for an even more comprehensive approach to multi-androgen profiling and used as a valuable clinical tool to diagnose hyperandrogenism.

2) Effect of androgen metabolism on the global metabolomic profile in *ex vivo* adipose tissue

The results in this thesis have demonstrated that the steroid metabolome in adipose tissue favours generation of 11-oxygenated androgens, it would therefore be insightful to explore key transcriptome changes, if any, in gene expression of steroidogenic enzymes in response to treatment with classic and 11-oxygenated androgens and

AKR1C3 inhibitor. O'Reilly and team have shown increased generation of classic androgen testosterone leads to an increase in AKR1C3 expression via increased insulin resistance consequent to androgen-mediated increases in *de novo* lipogenesis, suppression of lipolysis and eventually free fatty acid release from the adipocyte once storage capacity is exhausted [36]. Future endeavours would therefore involve RNA sequencing on collected adipose tissue pre and post treatment. By incorporating RNA sequencing into future investigations, we would be able to further profile the changes in RNA expression in response to androgen exposure of both classic and 11-oxygenated androgens within *ex vivo* adipose tissue. A deeper understanding of the mechanisms by which androgen metabolism and RNA expression are linked may provide further insights on the impact of androgen activation in adipose tissue on conditions of female hyperandrogenism, like PCOS.

To further piece the puzzle of androgen impact on global adipose metabolic health, changes in the overall metabolic response to treatment with classic androgens compared to 11-oxygenatted androgens, using non-targeted metabolomics, would also be investigated. During *ex vivo* analysis of androgen metabolism in adipose tissue, additional media samples were collected for the purpose of non-targeted metabolomics. These samples will be used to determine the differential impact of classic verses 11-oxygenated androgens on the global metabolic response in adipose tissue, in particular lipid metabolism. Using non-targeted metabolomic, O'Reilly *et al* showed enhanced lipogenesis in a PCOS cohort compared to controls, identified by changes in 119 metabolites, with significant increase in serum concentrations of Glycerophospholipids (GPLs) and lysoglycerophospholipids (LGPLs) [36].

Perturbations to the global metabolic profile in response to classic Vs 11-oxygenated androgen exposure during *ex vivo* adipose investigations may therefore demonstrate such changes and identify potential biomarkers for androgen excess and may have the potential to identify biomarkers specific to excess of each androgen class. As 11-oxygenated androgens are preferentially activated in adipose tissue, exposure to these androgens may cause differential changes (and observed metabolites) to lipid metabolism and *de novo* lipogenesis within adipose tissue. Therefore, depending on the sample used, non-targeted metabolomics has the potential to provide a non-invasive method to identify androgen excess in patients with PCOS and categorize the type of androgen excess (i.e., classic or 11-oxygenated). Additionally, as AKR1C3 is the key androgen activating enzyme expressed in adipose tissue, differences in the metabolome in response to AKR1C3 inhibitor treatment could be explored in the hopes of further identifying the effect of AKR1C3 inhibition on adipose metabolic health. The aim would be to confirm if treatment with an AKR1C3 inhibitor, and therefore reduction in androgen activation, reverses changes in metabolome, compared to adipose exposed to androgens in the absence of an AKR1C3 inhibitor.

3) Characterise effects of androgen metabolism on insulin resistance and glucose uptake in liver tissue using NMLP

This data shows that the liver is a site of androgen inactivation. Thus, the next steps would involve the assessment of excess circulating androgens on liver health. Using the established NMLP model described here, an investigation into the direct effect of androgen excess on parameters such as insulin resistance and uptake/conversion of insulin and glucose could be completed. Continuous perfusion with a concentrated androgen solution would be incorporated to replicate the milieu of androgen excess

and histological assessment of liver biopsies taken pre during and post treatment to identify changes in fat composition of hepatocytes. Changes in androgen metabolism and liver health would be compared to non-insulin/glucose treated livers. These investigations will also be supported by further characterisation of liver androgen metabolism by continued use of *ex vivo* liver tissue incubations.

4) Further characterise alterations in androgen metabolism induced by liver steatosis using NMLP

This thesis presented differential metabolism between healthy donor livers and livers retrieved from patients with liver disease. Further investigations using livers deemed severely steatotic and metabolism of classic and 11-oxygenated androgens investigated. This would provide further understanding on androgen impact on liver health and how androgen metabolism changes across the stages of MASLD. As livers can be perfused up to seven days using NMLP, it would be interesting to take advantage of the scope of NMLP and look at androgen metabolism of severely steatotic livers pre and post steatosis reconditioning. In this case, steatotic livers would be connected to the NMLP device, treated with androgen precursors, before being given a drug cocktail to reverse steatosis, and once steatosis had been successfully reversed, livers would be treated again with the same androgen precursor. These experiments would provide the platform to determine if changes in liver metabolism as a result of liver disease are reversible, and/or if the severity of liver disease is reversed.

Final concluding remarks

In conclusion, inactive classic and inactive 11-oxygenated androgen precursors A4 and 11KA4 are converted to their active products T and 11KT in *ex vivo* adipose tissue, mediated by androgen activating enzyme AKR1C3. AKR1C3 preferentially activates 11-oxygenated androgens over classic androgens in adipose tissue. AKR1C3 inhibition successfully reduced local generation of androgens in female adipose tissue and could therefore serve as a potential therapeutic intervention to improve the adverse, androgen-driven metabolic phenotype of women with PCOS. UHPLC-MS/MS analysis allowed for comprehensive delineation of the androgen metabolic pathways in liver tissue and NMLP was successfully established as an *ex situ* tool which can be used to profile androgen metabolism in whole liver. The liver is a site of androgen deactivation and therefore does not actively contribute to the local androgen pool in PCOS and MASLD, both of which are negatively impacted by androgen excess. The results from this thesis can be used as a solid starting framework to inform future investigations, as those described above, aiming to fully understand the mechanisms by which androgen excess leads to MASLD in PCOS.

REFERENCES

1. Cole, T.J., K.L. Short, and S.B. Hooper, *The science of steroids.* Semin Fetal Neonatal Med, 2019. **24**(3): p. 170-175.
2. Miller, W.L. and R.J. Auchus, *The molecular biology, biochemistry, and physiology of human steroidogenesis and its disorders.* Endocr Rev, 2011. **32**(1): p. 81-151.
3. Dutt, M., C.J. Wehrle, and I. Jialal, *Physiology, Adrenal Gland*, in *StatPearls*. 2023: Treasure Island (FL).
4. K. Bloch, D.R., *On the utilization of acetic acid for cholesterol formation.* J. Biol. Chem, 1942. **145**: p. 625-636.
5. H.H.N. Little, K.B., *Studies on the utilization of acetic acid for the biological synthesis of cholesterol.* J. Biol. Chem, 1950. **183**: p. 33-46.
6. Rittenberg, D. and K. Bloch, *The utilization of acetic acid for the synthesis of fatty acids.* J Biol Chem, 1945. **160**: p. 417-24.
7. Gwynne, J.T. and J.F. Strauss, 3rd, *The role of lipoproteins in steroidogenesis and cholesterol metabolism in steroidogenic glands.* Endocr Rev, 1982. **3**(3): p. 299-329.
8. John S. Davis, H.A.L., *Chapter 15 - Molecular Regulation of Progesterone Production in the Corpus Luteum*. The Ovary (Third Edition), ed. E.Y.A. Peter C.K. Leung. 2019: Academic Press. 16.
9. Schiffer, L., et al., *Human steroid biosynthesis, metabolism and excretion are differentially reflected by serum and urine steroid metabolomes: A comprehensive review.* J Steroid Biochem Mol Biol, 2019. **194**: p. 105439.
10. Kraemer, F.B., *Adrenal cholesterol utilization.* Mol Cell Endocrinol, 2007. **265-266**: p. 42-5.
11. Holst, J.P., et al., *Steroid hormones: relevance and measurement in the clinical laboratory.* Clin Lab Med, 2004. **24**(1): p. 105-18.
12. Megha, R., et al., *Anatomy, Abdomen and Pelvis: Adrenal Glands (Suprarenal Glands)*, in *StatPearls*. 2023: Treasure Island (FL).
13. Thau, L., J. Gandhi, and S. Sharma, *Physiology, Cortisol*, in *StatPearls*. 2023: Treasure Island (FL).
14. Nakamura, Y., et al., *3betaHSD and CYB5A double positive adrenocortical cells during adrenal development/aging.* Endocr Res, 2015. **40**(1): p. 8-13.
15. Turcu, A.F. and R.J. Auchus, *Clinical significance of 11-oxygenated androgens.* Curr Opin Endocrinol Diabetes Obes, 2017. **24**(3): p. 252-259.
16. Storbec, K.-H., *A commentary on the origins of 11-ketotestosterone.* European society of endocrinology, 2022. **187**(6).
17. David L. Keefe, K.P.W., *Chapter 2 - Reproductive Physiology*. General Gynecology, ed. E.R.S. Andrew I. Sokol. 2007. 20.
18. Ghizzoni, L., G. Mastorakos, and A. Vottero, *Adrenal hyperandrogenism in children.* J Clin Endocrinol Metab, 1999. **84**(12): p. 4431-5.
19. Richards, J.S. and S.A. Pangas, *The ovary: basic biology and clinical implications.* J Clin Invest, 2010. **120**(4): p. 963-72.

20. Schiffer, L., W. Arlt, and K.H. Storbeck, *Intracrine androgen biosynthesis, metabolism and action revisited.* Mol Cell Endocrinol, 2018. **465**: p. 4-26.
21. Orlowski, M. and M.S. Sarao, *Physiology, Follicle Stimulating Hormone*, in *StatPearls*. 2023: Treasure Island (FL).
22. Ehrmann, R.L.R.a.D.A., *The Pathogenesis of Polycystic Ovary Syndrome (PCOS): The Hypothesis of PCOS as Functional Ovarian Hyperandrogenism Revisited.* Endocr Rev., 2016. **37**(5): p. 467–520.
23. Antoniou-Tsigkos A, Z.E., Ghizzoni L, et al, *Adrenal Androgens*. Endotext [Internet], ed. A.B. Feingold KR, Blackman MR, et al. Updated 2019 Jan 5, South Dartmouth (MA): MDText.com, Inc., South Dartmouth (MA).
24. Barnard, L., et al., *The A-ring reduction of 11-ketotestosterone is efficiently catalysed by AKR1D1 and SRD5A2 but not SRD5A1.* J Steroid Biochem Mol Biol, 2020. **202**: p. 105724.
25. Storbeck, K.H. and M.W. O'Reilly, *The clinical and biochemical significance of 11-oxygenated androgens in human health and disease.* Eur J Endocrinol, 2023. **188**(4): p. R98-R109.
26. Barnard, L., T. du Toit, and A.C. Swart, *Back where it belongs: 11beta-hydroxyandrostenedione compels the re-assessment of C11-oxy androgens in steroidogenesis.* Mol Cell Endocrinol, 2021. **525**: p. 111189.
27. Elzette Pretorius, D.J.A., Maré Vlok, Meghan S. Perkins, Jonathan Quanson and Karl-Heinz Storbeck, *11-Ketotestosterone and 11-Ketodihydrotestosterone in Castration Resistant Prostate Cancer: Potent Androgens Which Can No Longer Be Ignored.* PLoS One, 2016. **11**(7): p. e0159867.
28. Swart, A.C. and K.H. Storbeck, *11beta-Hydroxyandrostenedione: Downstream metabolism by 11betaHSD, 17betaHSD and SRD5A produces novel substrates in familiar pathways.* Mol Cell Endocrinol, 2015. **408**: p. 114-23.
29. O'Reilly, M.W., et al., *11-Oxygenated C19 Steroids Are the Predominant Androgens in Polycystic Ovary Syndrome.* J Clin Endocrinol Metab, 2017. **102**(3): p. 840-848.
30. Schiffer, L., et al., *Classic and 11-oxygenated androgens in serum and saliva across adulthood: a cross-sectional study analyzing the impact of age, body mass index, and diurnal and menstrual cycle variation.* Eur J Endocrinol, 2023. **188**(1).
31. Aya T Nanba, J.R., Jianwei Ren, Richard J Auchus, William E Rainey, Adina F Turcu, *11-Oxygenated C19 Steroids Do Not Decline With Age in Women.* J Clin Endocrinol Metab, 2019. **104**(7): p. 2615–2622.
32. Davey, R.A. and M. Grossmann, *Androgen Receptor Structure, Function and Biology: From Bench to Bedside.* Clin Biochem Rev, 2016. **37**(1): p. 3-15.
33. Dehm, S.M. and D.J. Tindall, *Androgen receptor structural and functional elements: role and regulation in prostate cancer.* Mol Endocrinol, 2007. **21**(12): p. 2855-63.
34. Bennett, N.C., et al., *Molecular cell biology of androgen receptor signalling.* Int J Biochem Cell Biol, 2010. **42**(6): p. 813-27.
35. Jin, H.J., J. Kim, and J. Yu, *Androgen receptor genomic regulation.* Transl Androl Urol, 2013. **2**(3): p. 157-177.
36. O'Reilly, M.W., et al., *AKR1C3-Mediated Adipose Androgen Generation Drives Lipotoxicity in Women With Polycystic Ovary Syndrome.* J Clin Endocrinol Metab, 2017. **102**(9): p. 3327-3339.

37. O'Reilly, M.W., P.J. House, and J.W. Tomlinson, *Understanding androgen action in adipose tissue.* J Steroid Biochem Mol Biol, 2014. **143**: p. 277-84.
38. Fouad Mansour, M., M. Pelletier, and A. Tchernof, *Characterization of 5alpha-reductase activity and isoenzymes in human abdominal adipose tissues.* J Steroid Biochem Mol Biol, 2016. **161**: p. 45-53.
39. Amai, K., et al., *Quantitative analysis of mRNA expression levels of aldo-keto reductase and short-chain dehydrogenase/reductase isoforms in human livers.* Drug Metab Pharmacokinet, 2020. **35**(6): p. 539-547.
40. JAMES F. DUNN, B.C.N., DAVID RODBARD, *Transport of Steroid Hormones: Binding of 21 Endogenous Steroids to Both Testosterone-Binding Globulin and Corticosteroid-Binding Globulin in Human Plasma.* The Journal of Clinical Endocrinology & Metabolism, 1981. **53**(1): p. 58-68.
41. Mendel, C.M., *The free hormone hypothesis: a physiologically based mathematical model.* Endocr Rev, 1989. **10**(3): p. 232-74.
42. Hayley R. Price, C.J., Désirée R. Seib, Chunqi Ma, Dickson Lai, Kiran K. Soma and Abby C. Collier, *Measurement of Steroids in the Placenta, Maternal Serum, and Fetal Serum in Humans, Rats, and Mice: A Technical Note.* Separations, 2023. **10**(4).
43. Olivier Salamin, R.N., Cheng Xu, Julien Boccard, Serge Rudaz, Nelly Pitteloud, Martial Saugy, Tiia Kuuranne, *Steroid profiling by UHPLC-MS/MS in dried blood spots collected from healthy women with and without testosterone gel administration.* Journal of Pharmaceutical and Biomedical Analysis, 2011. **204**.
44. Mittal, R.D., *Tandem mass spectroscopy in diagnosis and clinical research.* Indian J Clin Biochem, 2015. **30**(2): p. 121-3.
45. Delitala, A.P., et al., *Polycystic ovary syndrome, adipose tissue and metabolic syndrome.* Arch Gynecol Obstet, 2017. **296**(3): p. 405-419.
46. Neven, A.C.H., et al., *A Summary on Polycystic Ovary Syndrome: Diagnostic Criteria, Prevalence, Clinical Manifestations, and Management According to the Latest International Guidelines.* Semin Reprod Med, 2018. **36**(1): p. 5-12.
47. Subramani Parasuraman, A., Subramani Balamurugan, Selvadurai Muralidharan, Kalaimani Jayaraj Kumar and Venugopal Vijayan, *An Overview of Liquid Chromatography-Mass Spectroscopy Instrumentation.* Pharmaceutical Methods, 2014. **5**(2).
48. Beauchemin, N.W.S., *Sample Introduction Systems in ICPMS and ICPOES*. Chapter 4: Liquid chromatography. 2020: Elsevier.
49. Canene-Adams, K., *Reverse-phase HPLC analysis and purification of small molecules.* Methods Enzymol, 2013. **533**: p. 291-301.
50. Huhtaniemi, A.E.T.a.B.G.K.a.I.T., *Mass spectrometry and immunoassay: how to measure steroid hormones today and tomorrow.* European journal of endocrinology, 2015. **173 2**: p. D1-12.
51. Pitt, J.J., *Principles and applications of liquid chromatography-mass spectrometry in clinical biochemistry.* Clin Biochem Rev, 2009. **30**(1): p. 19-34.
52. CS Ho, C.L., MHM Chan, RCK Cheung, LK Law, LCW Lit, KF Ng, MWM Suen, and HL Tai, *Electrospray Ionisation Mass Spectrometry: Principles and Clinical Application.* Clin Biochem Rev, 2003 **24**(1): p. 3–12.

53. F.A.Mellon, *MASS SPECTROMETRY. Principles amd Instrumentation*. Encyclopedia of Food Sciences and Nutrition, ed. B. Caballero. 2003: Academic Press. 10.
54. Fu, Y., et al., *Evaluation, identification and impact assessment of abnormal internal standard response variability in regulated LC-MS bioanalysis.* Bioanalysis, 2020. **12**(8): p. 545-559.
55. Schiffer, L., et al., *Multi-steroid profiling by UHPLC-MS/MS with post-column infusion of ammonium fluoride.* J Chromatogr B Analyt Technol Biomed Life Sci, 2022. **1209**: p. 123413.
56. Sadeghi, H.M., et al., *Polycystic Ovary Syndrome: A Comprehensive Review of Pathogenesis, Management, and Drug Repurposing.* Int J Mol Sci, 2022. **23**(2).
57. Uche Anadu Ndefo, A.E., and Monica Robinson Green, *Polycystic Ovary Syndrome.* P T., 2013. **38**(6): p. 336-355.
58. Rodriguez Paris, V. and M.J. Bertoldo, *The Mechanism of Androgen Actions in PCOS Etiology.* Med Sci (Basel), 2019. **7**(9).
59. Rasquin Leon, L.I., C. Anastasopoulou, and J.V. Mayrin, *Polycystic Ovarian Disease*, in *StatPearls*. 2023: Treasure Island (FL).
60. Wolf WM, W.R., Kinkade ON, Olfert MD, *Geographical Prevalence of Polycystic Ovary Syndrome as Determined by Region and Race/Ethnicity.* Int J Environ Res Public Health., 2018. **15**(11).
61. Samer El Hayek , L.B., Layal H Hamdar , Fadi G Mirza, Georges Daoud *Poly Cystic Ovarian Syndrome: An Updated Overview.* Front Physiol, 2016. **7**(124).
62. Ricardo Azziz , K.S.W., Rosario Reyna, Timothy J Key, Eric S Knochenhauer, Bulent O Yildiz, *The prevalence and features of the polycystic ovary syndrome in an unselected population.* J Clin Endocrinol Metab, 2004. **89**(6).
63. Zhu, T. and M.O. Goodarzi, *Causes and Consequences of Polycystic Ovary Syndrome: Insights From Mendelian Randomization.* J Clin Endocrinol Metab, 2022. **107**(3): p. e899-e911.
64. Legro, R.S., *Evaluation and Treatment of Polycystic Ovary Syndrome*, in *Endotext*, K.R. Feingold, et al., Editors. 2000: South Dartmouth (MA).
65. Collee, J., et al., *Polycystic ovarian syndrome and infertility: overview and insights of the putative treatments.* Gynecol Endocrinol, 2021. **37**(10): p. 869-874.
66. Barthelmess, E.K. and R.K. Naz, *Polycystic ovary syndrome: current status and future perspective.* Front Biosci (Elite Ed), 2014. **6**(1): p. 104-19.
67. (MD), B., *Antiandrogens*. Clinical and Research Information on Drug-Induced Liver Injury 2014: National Institute of Diabetes and Digestive and Kidney Diseases.
68. Azziz, R., D.A. Dumesic, and M.O. Goodarzi, *Polycystic ovary syndrome: an ancient disorder?* Fertil Steril, 2011. **95**(5): p. 1544-8.
69. Stein I.F., L.M.L., *Amenorrhea associated with bilateral polycystic ovaries.* Am J Obstet Gynecol., 1935. **29**: p. 181-191.
70. Adashi, E.Y., et al., *The polycystic ovary syndrome: the first 150 years of study.* F S Rep, 2023. **4**(1): p. 2-18.
71. Dunaif, S.C.a.A., *Diagnosis of Polycystic Ovary Syndrome: Which Criteria to Use When?* Endocrinol Metab Clin North Am, 2021. **50**(1): p. 11-23.
72. Lujan, M.E., D.R. Chizen, and R.A. Pierson, *Diagnostic criteria for polycystic ovary syndrome: pitfalls and controversies.* J Obstet Gynaecol Can, 2008. **30**(8): p. 671-679.

73. Rotterdam, E.A.-S.P.c.w.g., *Revised 2003 consensus on diagnostic criteria and long-term health risks related to polycystic ovary syndrome (PCOS).* Hum Reprod, 2004. **19**(1): p. 41-7.
74. Ricardo Azziz, E.C., Didier Dewailly, Evanthia Diamanti-Kandarakis, Hector F Escobar-Morreale, Walter Futterweit, Onno E Janssen, Richard S Legro, Robert J Norman, Ann E Taylor, Selma F Witchel, *Positions statement: criteria for defining polycystic ovary syndrome as a predominantly hyperandrogenic syndrome: an Androgen Excess Society guideline.* J Clin Endocrinol Metab, 2006. **91**(11): p. 4237-4245.
75. Azziz, R., et al., *The Androgen Excess and PCOS Society criteria for the polycystic ovary syndrome: the complete task force report.* Fertil Steril, 2009. **91**(2): p. 456-88.
76. Yildiz, S.M.a.B.O., *Polycystic ovary syndrome phenotypes and prevalence: Differential impact of diagnostic criteria and clinical versus unselected population.* Current Opinion in Endocrine and Metabolic Research, 2020. **12**: p. 66-71.
77. O'Reilly, M.W., et al., *Hyperandrogenemia predicts metabolic phenotype in polycystic ovary syndrome: the utility of serum androstenedione.* J Clin Endocrinol Metab, 2014. **99**(3): p. 1027-36.
78. Barth, J.H., E. Yasmin, and A.H. Balen, *The diagnosis of polycystic ovary syndrome: the criteria are insufficiently robust for clinical research.* Clin Endocrinol (Oxf), 2007. **67**(6): p. 811-5.
79. De Leo, V., et al., *Genetic, hormonal and metabolic aspects of PCOS: an update.* Reprod Biol Endocrinol, 2016. **14**(1): p. 38.
80. Singh, S., et al., *Polycystic Ovary Syndrome: Etiology, Current Management, and Future Therapeutics.* J Clin Med, 2023. **12**(4).
81. Raju, G.A., et al., *Luteinizing hormone and follicle stimulating hormone synergy: A review of role in controlled ovarian hyper-stimulation.* J Hum Reprod Sci, 2013. **6**(4): p. 227-34.
82. Magoffin, D.A., *Ovarian theca cell.* Int J Biochem Cell Biol, 2005. **37**(7): p. 1344-9.
83. Pellatt, L., S. Rice, and H.D. Mason, *Anti-Mullerian hormone and polycystic ovary syndrome: a mountain too high?* Reproduction, 2010. **139**(5): p. 825-33.
84. Lebbe, M., et al., *The Steroid Metabolome in the Isolated Ovarian Follicle and Its Response to Androgen Exposure and Antagonism.* Endocrinology, 2017. **158**(5): p. 1474-1485.
85. Nigel K. Stepto, S.C., Anju E. Joham, Samantha K. Hutchison, Cheryce L. Harrison, Rebecca F. Goldstein, Helena J. Teede, *Women with polycystic ovary syndrome have intrinsic insulin resistance on euglycaemic–hyperinsulaemic clamp.* Human Reproduction, 2013. **28**(3): p. 777-784.
86. Amisi, C.A., *Markers of insulin resistance in Polycystic ovary syndrome women: An update.* World J Diabetes, 2022. **13**(3): p. 129-149.
87. Baptiste, C.G., et al., *Insulin and hyperandrogenism in women with polycystic ovary syndrome.* J Steroid Biochem Mol Biol, 2010. **122**(1-3): p. 42-52.
88. Xu, W., J. Morford, and F. Mauvais-Jarvis, *Emerging role of testosterone in pancreatic beta-cell function and insulin secretion.* J Endocrinol, 2019.
89. Sanchez-Garrido, M.A. and M. Tena-Sempere, *Metabolic dysfunction in polycystic ovary syndrome: Pathogenic role of androgen excess and potential therapeutic strategies.* Mol Metab, 2020. **35**: p. 100937.

90. P.M. Spritzer, B.R.S., T.M. Fighera, L.B. Marchesan, S.B. Lecke f, *Intrinsic abnormalities of adipose tissue and adipose tissue dysfunction in PCOS*. Intrinsic abnormalities of adipose tissue
and adipose tissue dysfunction in PCOS. 2022: Challenging Issues in the Modern Era of Individualized Medicine. 73-76.
91. Garg, D. and R. Tal, *Inositol Treatment and ART Outcomes in Women with PCOS.* Int J Endocrinol, 2016. **2016**: p. 1979654.
92. Dadachanji, R., N. Shaikh, and S. Mukherjee, *Genetic Variants Associated with Hyperandrogenemia in PCOS Pathophysiology.* Genet Res Int, 2018. **2018**: p. 7624932.
93. Prapas, N., et al., *Genetics of polycystic ovary syndrome.* Hippokratia, 2009. **13**(4): p. 216-23.
94. Livadas, S. and E. Diamanti-Kandarakis, *Polycystic ovary syndrome: definitions, phenotypes and diagnostic approach.* Front Horm Res, 2013. **40**: p. 1-21.
95. Lizneva, D., et al., *Criteria, prevalence, and phenotypes of polycystic ovary syndrome.* Fertil Steril, 2016. **106**(1): p. 6-15.
96. Garima Sachdeva, S.G., Vanita Suri, Naresh Sachdeva and Seema Chopra, *Comparison of the Different PCOS Phenotypes Based on Clinical Metabolic, and Hormonal Profile, and their Response to Clomiphene.* Indian J Endocrinol Metab., 2019. **23**(3): p. 326-331.
97. Gluszak, O., et al., *Phenotype and metabolic disorders in polycystic ovary syndrome.* ISRN Endocrinol, 2012. **2012**: p. 569862.
98. Rahman, M.S., et al., *Role of Insulin in Health and Disease: An Update.* Int J Mol Sci, 2021. **22**(12).
99. Petersen, M.C. and G.I. Shulman, *Mechanisms of Insulin Action and Insulin Resistance.* Physiol Rev, 2018. **98**(4): p. 2133-2223.
100. author, L.M.S., *The insulin receptor substrate (IRS) proteins.* Cell cycle, 2011. **10**(11): p. 1750-1756.
101. Gastaldelli, A., M. Gaggini, and R.A. DeFronzo, *Role of Adipose Tissue Insulin Resistance in the Natural History of Type 2 Diabetes: Results From the San Antonio Metabolism Study.* Diabetes, 2017. **66**(4): p. 815-822.
102. Andrew M. Freeman, N.P., *Insulin Resistance.* StatPearls Publishing, 2022.
103. Villa, J. and R.E. Pratley, *Adipose tissue dysfunction in polycystic ovary syndrome.* Curr Diab Rep, 2011. **11**(3): p. 179-84.
104. Han Zhao, J.Z., Xiangyi Cheng, Xiaozhao Nie, and Bing He, *Insulin resistance in polycystic ovary syndrome across various tissues: an updated review of pathogenesis, evaluation, and treatment.* J Ovarian Res, 2023. **16**(9).
105. Kumarendran, B., et al., *Polycystic ovary syndrome, androgen excess, and the risk of nonalcoholic fatty liver disease in women: A longitudinal study based on a United Kingdom primary care database.* PLoS Med, 2018. **15**(3): p. e1002542.
106. Asfari, M.M., et al., *Association of non-alcoholic fatty liver disease and polycystic ovarian syndrome.* BMJ Open Gastroenterol, 2020. **7**(1).
107. Spiers, J., et al., *What's new in non-alcoholic fatty liver disease?* Frontline Gastroenterol, 2022. **13**(e1): p. e102-e108.
108. Nd, A.M., *Non-Alcoholic Fatty Liver Disease, an Overview.* Integr Med (Encinitas), 2019. **18**(2): p. 42-49.

109. Hashimoto, E., M. Taniai, and K. Tokushige, *Characteristics and diagnosis of NAFLD/NASH.* J Gastroenterol Hepatol, 2013. **28 Suppl 4**: p. 64-70.
110. Emir Muzurović, D.P.M., Christos Mantzoros e f, *Non-alcoholic fatty liver disease, insulin resistance, metabolic syndrome and their association with vascular risk.* metabolism clinical and experimental, 2021.
111. Singh, S.P., et al., *Nonalcoholic Fatty Liver Disease (NAFLD) Name Change: Requiem or Reveille?* J Clin Transl Hepatol, 2021. **9**(6): p. 931-938.
112. Nassir, F., et al., *Pathogenesis and Prevention of Hepatic Steatosis.* Gastroenterol Hepatol (N Y), 2015. **11**(3): p. 167-75.
113. Fernando, D.H., et al., *Development and Progression of Non-Alcoholic Fatty Liver Disease: The Role of Advanced Glycation End Products.* Int J Mol Sci, 2019. **20**(20).
114. in Wang, W.H., Ping-Ju Tsai, Pei-Hsuan Chen, Manxiang Ye, Jiao Guo and Zhengquan Su, *Mutual interaction between endoplasmic reticulum and mitochondria in nonalcoholic fatty liver disease.* Lipids in Health and Disease 2020. **19**(72).
115. Dyson, J.K., Q.M. Anstee, and S. McPherson, *Non-alcoholic fatty liver disease: a practical approach to diagnosis and staging.* Frontline Gastroenterol, 2014. **5**(3): p. 211-218.
116. Sharma, B. and S. John, *Nonalcoholic Steatohepatitis (NASH)*, in *StatPearls*. 2023: Treasure Island (FL).
117. Hassen, G., et al., *Nonalcoholic Fatty Liver Disease: An Emerging Modern-Day Risk Factor for Cardiovascular Disease.* Cureus, 2022. **14**(5): p. e25495.
118. Kwabena O, A.-A., Hrishikesh Samant, *Hepatocellular Carcinoma.* StatPearls Publishing,, 2023.
119. Lisa M. Glass, C.M.H., Michael Fuchs and Grace L. Su, *Comorbidities and Nonalcoholic Fatty Liver Disease: The Chicken, the Egg, or Both?* Fed Pract., 2019. **36**(2): p. 64-71.
120. Paternostro, R. and M. Trauner, *Current treatment of non-alcoholic fatty liver disease.* J Intern Med, 2022. **292**(2): p. 190-204.
121. Kudaravalli P, J.S., *Nonalcoholic Fatty Liver.* StatPearls Publishing, 2022.
122. Pouwels, S., et al., *Non-alcoholic fatty liver disease (NAFLD): a review of pathophysiology, clinical management and effects of weight loss.* BMC Endocr Disord, 2022. **22**(1): p. 63.
123. Pierantonelli, I. and G. Svegliati-Baroni, *Nonalcoholic Fatty Liver Disease: Basic Pathogenetic Mechanisms in the Progression From NAFLD to NASH.* Transplantation, 2019. **103**(1): p. e1-e13.
124. Zarghamravanbakhsh, P., M. Frenkel, and L. Poretsky, *Metabolic causes and consequences of nonalcoholic fatty liver disease (NAFLD).* Metabol Open, 2021. **12**: p. 100149.
125. Giorgio, V., et al., *Pediatric non alcoholic fatty liver disease: old and new concepts on development, progression, metabolic insight and potential treatment targets.* BMC Pediatr, 2013. **13**: p. 40.
126. Kaplan, A. and R. Rosenblatt, *Symptom Management in Patients with Cirrhosis: a Practical Guide.* Curr Treat Options Gastroenterol, 2022. **20**(2): p. 144-159.
127. Christopher F. Rose, P.A., Jasmohan S. Bajaj, Radha Krishan Dhiman, Sara Montagnese, Simon D. Taylor-Robinson, Hendrik Vilstrup, Rajiv Jalan, *Hepatic encephalopathy:*

Novel insights into classification, pathophysiology and therapy. Journal of Hepatology, 2020. **73**: p. 1526–1547.
128. Yamasandhi, M.D.a.P.G., *Nonalcoholic Fatty Liver Disease and Type 2 Diabetes Mellitus.* Indian J Endocrinol Metab., 2018. **22**(3): p. 421-428.
129. Utzschneider, K.M. and S.E. Kahn, *Review: The role of insulin resistance in nonalcoholic fatty liver disease.* J Clin Endocrinol Metab, 2006. **91**(12): p. 4753-61.
130. Friedman, S.L., et al., *Mechanisms of NAFLD development and therapeutic strategies.* Nat Med, 2018. **24**(7): p. 908-922.
131. Cui, P., et al., *Long-term androgen excess induces insulin resistance and non-alcoholic fatty liver disease in PCOS-like rats.* J Steroid Biochem Mol Biol, 2021. **208**: p. 105829.
132. Petta, S., et al., *Insulin resistance and hyperandrogenism drive steatosis and fibrosis risk in young females with PCOS.* PLoS One, 2017. **12**(11): p. e0186136.
133. Song, M.J. and J.Y. Choi, *Androgen dysfunction in non-alcoholic fatty liver disease: Role of sex hormone binding globulin.* Front Endocrinol (Lausanne), 2022. **13**: p. 1053709.
134. Stanley Andrisse, M.F., Zhiqiang Wang, Olubusayo Awe, Lexiang Yu, Haiying Zhang, Sheng Bi, Hongbing Wang, Linhao Li, Serene Joseph, Nicola Heller, Franck Mauvais-Jarvis, Guang William Wong, James Segars, Andrew Wolfe, Sara Divall, Rexford Ahima, and Sheng Wu, *Androgen-induced insulin resistance is ameliorated by deletion of hepatic androgen receptor in females.* FASEB J, 2021. **35**(10): p. e21921.
135. Alves-Bezerra, M. and D.E. Cohen, *Triglyceride Metabolism in the Liver.* Compr Physiol, 2017. **8**(1): p. 1-8.
136. Kitade, H., et al., *Nonalcoholic Fatty Liver Disease and Insulin Resistance: New Insights and Potential New Treatments.* Nutrients, 2017. **9**(4).
137. Fungai Dengu, S.H.A., Georg Ebeling and David Nasralla, *Normothermic Machine Perfusion (NMP) of the Liver as a Platform for Therapeutic Interventions during Ex-Vivo Liver Preservation: A Review.* J Clin Med, 2020. **9**(4): p. 1046.
138. Chuanyan Shen, H.C., Tingting Zong, Hongli Zhu, *The role of normothermic machine perfusion (NMP) in the preservation of ex-vivo liver before transplantation: A review.* Front. Bioeng. Biotechnol., 2023. **11**.
139. Srikanth P Reddy, J.B., and PJ Friend, *Normothermic perfusion – a mini-review.* Transplantation. , 2009. **87**(5): p. 631–632.
140. Bianca Lascaris, A.M.T., Ton Lisman, Maarten W. N. Nijsten, Robert J. Porte, and Vincent E. de Meijer, *Long-term normothermic machine preservation of human livers: what is needed to succeed?* American Journal of Physiology-Gastrointestinal and Liver Physiology, 2022. **322**(2): p. 183-200.
141. George Clarke, H.M., Angus Hann, M. Thamara P. R. Perera, Simon C. Afford, and Darius F. Mirza, *How Machine Perfusion Ameliorates Hepatic Ischaemia Reperfusion Injury.* Int J Mol Sci, 2021. **22**(14).
142. Boteon, Y.L., et al., *Manipulation of Lipid Metabolism During Normothermic Machine Perfusion: Effect of Defatting Therapies on Donor Liver Functional Recovery.* Liver Transpl, 2019. **25**(7): p. 1007-1022.
143. Bral, M., et al., *Clearance of transaminases during normothermic ex situ liver perfusion.* PLoS One, 2019. **14**(4): p. e0215619.
144. Davio, A., et al., *Sex Differences in 11-Oxygenated Androgen Patterns Across Adulthood.* J Clin Endocrinol Metab, 2020. **105**(8): p. e2921-9.

145. Marina A Skiba, R.J.B., Rakibul M Islam, David J Handelsman, Reena Desai, Susan R Davis, *Androgens During the Reproductive Years: What Is Normal for Women?* The Journal of Clinical Endocrinology & Metabolism, 2019. **104**(11): p. 5382–5392.
146. Mergental, H., et al., *Development of Clinical Criteria for Functional Assessment to Predict Primary Nonfunction of High-Risk Livers Using Normothermic Machine Perfusion.* Liver Transpl, 2018. **24**(10): p. 1453-1469.
147. Arnaldi, G. and M. Martino, *Androgens in Cushing's Syndrome.* Front Horm Res, 2019. **53**: p. 77-91.
148. Koal, T., et al., *Standardized LC-MS/MS based steroid hormone profile-analysis.* J Steroid Biochem Mol Biol, 2012. **129**(3-5): p. 129-38.
149. Fanelli, F., et al., *Androgen profiling by liquid chromatography-tandem mass spectrometry (LC-MS/MS) in healthy normal-weight ovulatory and anovulatory late adolescent and young women.* J Clin Endocrinol Metab, 2013. **98**(7): p. 3058-67.
150. Raad A. Haddad, D.G.a.A.L.B., *Interpretation of common endocrine laboratory tests: technical pitfalls, their mechanisms and practical considerations.* Clinical Diabetes and Endocrinology, 2019. **5**(12).
151. Keevil, B.G., *LC-MS/MS analysis of steroids in the clinical laboratory.* Clin Biochem, 2016. **49**(13-14): p. 989-97.
152. Livingston, M., et al., *An audit of the measurement and reporting of male testosterone levels in UK clinical biochemistry laboratories.* Int J Clin Pract, 2020. **74**(11): p. e13607.
153. Casals, G. and F.A. Hanzu, *Cortisol Measurements in Cushing's Syndrome: Immunoassay or Mass Spectrometry?* Ann Lab Med, 2020. **40**(4): p. 285-296.
154. Bancos, I., et al., *Urine steroid metabolomics for the differential diagnosis of adrenal incidentalomas in the EURINE-ACT study: a prospective test validation study.* Lancet Diabetes Endocrinol, 2020. **8**(9): p. 773-781.
155. Honour, J.W., *Development and validation of a quantitative assay based on tandem mass spectrometry.* Ann Clin Biochem, 2011. **48**(Pt 2): p. 97-111.
156. Iannone, M., et al., *Development and validation of a liquid chromatography-tandem mass spectrometry method for the simultaneous analysis of androgens, estrogens, glucocorticoids and progestagens in human serum.* Biomed Chromatogr, 2022. **36**(5): p. e5344.
157. Turcu, A.F., et al., *Adrenal-derived 11-oxygenated 19-carbon steroids are the dominant androgens in classic 21-hydroxylase deficiency.* Eur J Endocrinol, 2016. **174**(5): p. 601-9.
158. Zeidler, R., et al., *Inclusion of 11-Oxygenated Androgens in a Clinical Routine LC-MS/MS Setup for Steroid Hormone Profiling.* Int J Mol Sci, 2022. **24**(1).
159. Ke, Y., et al., *A sensitive, simple and robust LC-MS/MS method for the simultaneous quantification of seven androgen- and estrogen-related steroids in postmenopausal serum.* J Steroid Biochem Mol Biol, 2014. **144 Pt B**: p. 523-34.
160. Methlie, P., et al., *Multisteroid LC-MS/MS assay for glucocorticoids and androgens, and its application in Addison's disease.* Endocr Connect, 2013. **2**(3): p. 125-136.
161. Panuwet, P., et al., *Biological Matrix Effects in Quantitative Tandem Mass Spectrometry-Based Analytical Methods: Advancing Biomonitoring.* Crit Rev Anal Chem, 2016. **46**(2): p. 93-105.

162. Zhou, W., S. Yang, and P.G. Wang, *Matrix effects and application of matrix effect factor.* Bioanalysis, 2017. **9**(23): p. 1839-1844.
163. Trufelli, H., et al., *An overview of matrix effects in liquid chromatography-mass spectrometry.* Mass Spectrom Rev, 2011. **30**(3): p. 491-509.
164. Singh, S., C.C. Kerndt, and D. Davis, *Ringer's Lactate*, in *StatPearls*. 2022: Treasure Island (FL).
165. Thomas Berg, D.H.S., *13C labelled internal standards—A solution to minimize ion suppression effects in liquid chromatography–tandem mass spectrometry analyses of drugs in biological samples?* Journal of Chromatography A, 2011. **52**(1218): p. 9366-9374.
166. Coelho, M., T. Oliveira, and R. Fernandes, *Biochemistry of adipose tissue: an endocrine organ.* Arch Med Sci, 2013. **9**(2): p. 191-200.
167. Cadagan, D., R. Khan, and S. Amer, *Female adipocyte androgen synthesis and the effects of insulin.* Mol Genet Metab Rep, 2014. **1**: p. 254-263.
168. Yildiz, B.O., et al., *Ovarian and adipose tissue dysfunction in polycystic ovary syndrome: report of the 4th special scientific meeting of the Androgen Excess and PCOS Society.* Fertil Steril, 2010. **94**(2): p. 690-3.
169. Paulukinas, R.D., C.A. Mesaros, and T.M. Penning, *Conversion of Classical and 11-Oxygenated Androgens by Insulin-Induced AKR1C3 in a Model of Human PCOS Adipocytes.* Endocrinology, 2022. **163**(7).
170. Quinkler, M., et al., *Androgen generation in adipose tissue in women with simple obesity--a site-specific role for 17beta-hydroxysteroid dehydrogenase type 5.* J Endocrinol, 2004. **183**(2): p. 331-42.
171. Blouin, K., et al., *Pathways of adipose tissue androgen metabolism in women: depot differences and modulation by adipogenesis.* Am J Physiol Endocrinol Metab, 2009. **296**(2): p. E244-55.
172. Saad A Amer, N.G.A., Avril Warren, Rebecca Tarbox and Raheela Khan, *Excess androgen production in subcutaneous adipose tissue of women with polycystic ovarian syndrome is not related to insulin or LH.* Journal of Endocrinology, 2019. **241**: p. 99–109.
173. Penning, T.M., *AKR1C3 (type 5 17beta-hydroxysteroid dehydrogenase/prostaglandin F synthase): Roles in malignancy and endocrine disorders.* Mol Cell Endocrinol, 2019. **489**: p. 82-91.
174. Schiffer L, S.A., Ludwig C, O'Reilly M, Westgate C, Singhal R, Taylor A, Dunn W, Arlt W, Storbeck KH. , *MON-203 Local Activation of 11-Oxygenated Androgens by AKR1C3 Is the Predominant Source of Androgens in Human Female Adipose Tissue.* J Endocr Soc., 2019. **3**.
175. Barnard, M., et al., *11-Oxygenated androgen precursors are the preferred substrates for aldo-keto reductase 1C3 (AKR1C3): Implications for castration resistant prostate cancer.* J Steroid Biochem Mol Biol, 2018. **183**: p. 192-201.
176. Center, G.a.R.D.I. *Simpson-Golabi-Behmel syndrome*. 2023 February 2023 [cited 2023; Available from: https://rarediseases.info.nih.gov/diseases/7649/simpson-golabi-behmel-syndrome.
177. Chia Rou Yeo, M.A., Shawn Hoon, Asim Shabbir, Manu Kunaal Shrivastava, Shiqi Huang, Chin Meng Khoo, Vanna Chhay, M. Shabeer Yassin1, E. Shyong Tai, Antonio Vidal-Puig

& Sue-Anne Toh, *SGBS cells as a model of human adipocyte browning: A comprehensive comparative study with primary human white subcutaneous adipocytes.* Scientific Reports, 2017. **4**(4031).

178. Schiffer, L., et al., *Peripheral blood mononuclear cells preferentially activate 11-oxygenated androgens.* Eur J Endocrinol, 2021. **184**(3): p. 353-363.
179. Jones, S.R., S. Carley, and M. Harrison, *An introduction to power and sample size estimation.* Emerg Med J, 2003. **20**(5): p. 453-8.
180. Walzer, D., et al., *Excess 11-Oxygenated Androgens in Women With Severe Insulin Resistance Are Mediated by Adrenal Insulin Receptor Signaling.* J Clin Endocrinol Metab, 2022. **107**(9): p. 2626-2635.
181. Hilpert, J., et al., *Hepatotoxicity of AKR1C3 Inhibitor BAY1128688: Findings from an Early Terminated Phase IIa Trial for the Treatment of Endometriosis.* Drugs R D, 2023.
182. Campana, C., et al., *Development of a novel cell based androgen screening model.* J Steroid Biochem Mol Biol, 2016. **156**: p. 17-22.
183. Davis, S.R. and S. Wahlin-Jacobsen, *Testosterone in women--the clinical significance.* Lancet Diabetes Endocrinol, 2015. **3**(12): p. 980-92.
184. Smith, T. and P. Batur, *Prescribing testosterone and DHEA: The role of androgens in women.* Cleve Clin J Med, 2021. **88**(1): p. 35-43.
185. Turcu, A.F., et al., *11-Oxygenated androgens in health and disease.* Nat Rev Endocrinol, 2020. **16**(5): p. 284-296.
186. C L Enriori, J.R.-M., *Peripheral aromatization as a risk factor for breast and endometrial cancer in postmenopausal women: a review.* Gynecol Oncol, 1984. **17**(1): p. 1-21.
187. Cao, J., et al., *Effect of dehydroepiandrosterone on the immune function of mice in vivo and in vitro.* Mol Immunol, 2019. **112**: p. 283-290.
188. Khorram, O., L. Vu, and S.S. Yen, *Activation of immune function by dehydroepiandrosterone (DHEA) in age-advanced men.* J Gerontol A Biol Sci Med Sci, 1997. **52**(1): p. M1-7.
189. Hammes, S.R. and E.R. Levin, *Impact of estrogens in males and androgens in females.* J Clin Invest, 2019. **129**(5): p. 1818-1826.
190. Paulukinas, R.D. and T.M. Penning, *Insulin-Induced AKR1C3 Induces Fatty Acid Synthase in a Model of Human PCOS Adipocytes.* Endocrinology, 2023. **164**(5).
191. Ma, M.A., et al., *Minority Representation in Clinical Trials in the United States: Trends Over the Past 25 Years.* Mayo Clin Proc, 2021. **96**(1): p. 264-266.
192. Rodin, D.A., et al., *Polycystic ovaries and associated metabolic abnormalities in Indian subcontinent Asian women.* Clin Endocrinol (Oxf), 1998. **49**(1): p. 91-9.
193. Mehta, J., V. Kamdar, and D. Dumesic, *Phenotypic expression of polycystic ovary syndrome in South Asian women.* Obstet Gynecol Surv, 2013. **68**(3): p. 228-34.
194. Lawrence Engmann, M., Susan Jin, MPH, Fangbai Sun, MPH, Richard S Legro, MD, Alex J. Polotsky, MD, Karl R Hansen, MD, Christos Coutifaris, MD, Michael P Diamond, MD, Esther Eisenberg, MD, MPH, Heping Zhang, PhD, Nanette Santoro, MD, *Racial and Ethnic Differences in the Polycystic Ovary Syndrome (PCOS) Metabolic Phenotype.* Am J Obstet Gynecol., 2017. **5**(216): p. 493.e1–493.e13.
195. Patel, V.H., *Polycystic Ovarian Syndrome: An Autobiographical Case Report of an Often Overlooked Disorder.* Cureus. , 2022. **14**(1): p. e21171.

196. Shahbaz, M., et al., *A Systematic Review of the Risk of Non-alcoholic Fatty Liver Disease in Women With Polycystic Ovary Syndrome.* Cureus, 2022. **14**(10): p. e29928.
197. Duwaerts, C.C. and J.J. Maher, *Macronutrients and the Adipose-Liver Axis in Obesity and Fatty Liver.* Cell Mol Gastroenterol Hepatol, 2019. **7**(4): p. 749-761.
198. Nakamura, Y., et al., *Type 5 17beta-hydroxysteroid dehydrogenase (AKR1C3) contributes to testosterone production in the adrenal reticularis.* J Clin Endocrinol Metab, 2009. **94**(6): p. 2192-8.
199. Attard, J.A., et al., *Ex situ Normothermic Split Liver Machine Perfusion: Protocol for Robust Comparative Controls in Liver Function Assessment Suitable for Evaluation of Novel Therapeutic Interventions in the Pre-clinical Setting.* Front Surg, 2021. **8**: p. 627332.
200. Laing, R.W., et al., *Viability testing and transplantation of marginal livers (VITTAL) using normothermic machine perfusion: study protocol for an open-label, non-randomised, prospective, single-arm trial.* BMJ Open, 2017. **7**(11): p. e017733.
201. Goumard, C., et al., *Ex-Vivo Pharmacological Defatting of the Liver: A Review.* J Clin Med, 2021. **10**(6).
202. Therina du Toita, L.M.B., Jonathan L. Quansona, Riaan Ehlersa, Antonio M. Serafinb, Amanda C. Swarta, *Profiling adrenal 11b-hydroxyandrostenedione metabolites in prostate cancer cells, tissue and plasma: UPC2-MS/MS quantification of 11b-hydroxytestosterone, 11keto-testosterone and 11keto-dihydrotestosterone.* Journal of Steroid Biochemistry & Molecular Biology 2017. **166**: p. 54-67.
203. Granata, O.M., et al., *Androgen metabolism and biotransformation in nontumoral and malignant human liver tissues and cells.* J Steroid Biochem Mol Biol, 2009. **113**(3-5): p. 290-5.
204. Gioia, S., et al., *Causes and Management of Non-cirrhotic Portal Hypertension.* Curr Gastroenterol Rep, 2020. **22**(12): p. 56.
205. Taneja, S., Y. Chawla, and R.K. Dhiman, *Noncirrhotic portal fibrosis: a rare cause of end-stage liver disease requiring liver transplantation.* Hepatol Int, 2013. **7**(2): p. 313-5.
206. Nikolaos Nikolaou , L.L.G., Lea Marchand, Sara Althari, Niall J. Dempster, Charlotte J. Green, Martijn van de Bunt, Catriona McNeil, Anastasia Arvaniti, Beverly A. Hughes, Bruno Sgromo, Richard S. Gillies, Hanns-Ulrich Marschall, Trevor M. Penning, John Ryan, Wiebke Arlt, Leanne Hodson, Jeremy W. Tomlinson, *AKR1D1 is a novel regulator of metabolic phenotype in human hepatocytes and is dysregulated in non-alcoholic fatty liver disease.* Metabolism Clinical and Experimental, 2019. **99**: p. 67-80.
207. Giannini, E.G., R. Testa, and V. Savarino, *Liver enzyme alteration: a guide for clinicians.* CMAJ, 2005. **172**(3): p. 367-79.
208. Seidu, T., et al., *DHT causes liver steatosis via transcriptional regulation of SCAP in normal weight female mice.* J Endocrinol, 2021. **250**(2): p. 49-65.
209. Angelo Di Vincenzo, L.R., Carlo Giovanni Doroldi, Roberto Vettor, Marco Rossato, *Sex hormones abnormalities in non-alcoholic fatty liver disease: pathophysiological and clinical implications.* Explor Med., 2021. **2**: p. 311-323.
210. Seckl, J.R. and B.R. Walker, *Minireview: 11beta-hydroxysteroid dehydrogenase type 1-a tissue-specific amplifier of glucocorticoid action.* Endocrinology, 2001. **142**(4): p. 1371-6.

211. Zou, X., et al., *11Beta-hydroxysteroid dehydrogenase-1 deficiency or inhibition enhances hepatic myofibroblast activation in murine liver fibrosis.* Hepatology, 2018. **67**(6): p. 2167-2181.
212. Ahmed, A., et al., *A switch in hepatic cortisol metabolism across the spectrum of non alcoholic fatty liver disease.* PLoS One, 2012. **7**(2): p. e29531.
213. Lutz, S.Z., et al., *Genetic Variation in the 11beta-hydroxysteroid-dehydrogenase 1 Gene Determines NAFLD and Visceral Obesity.* J Clin Endocrinol Metab, 2016. **101**(12): p. 4743-4751.
214. Alessandra Gambineri , F.T., Alessandra Munarini, Roland H Stimson, Roberto Mioni, Uberto Pagotto, Karen E Chapman, Ruth Andrew, Vilma Mantovani, Renato Pasquali, Brian R Walker, *A combination of polymorphisms in HSD11B1 associates with in vivo 11{beta}-HSD1 activity and metabolic syndrome in women with and without polycystic ovary syndrome.* Eur J Endocrinol, 2011. **165**(2): p. 283-292.
215. Janice M Paterson , N.M.M., Catherine Fievet, Christopher J Kenyon, Megan C Holmes, Bart Staels, Jonathan R Seckl, John J Mullins, *Metabolic syndrome without obesity: Hepatic overexpression of 11beta-hydroxysteroid dehydrogenase type 1 in transgenic mice.* Proc Natl Acad Sci U S A, 2004. **18**(101): p. 7088-7093.
216. Moon, S.S., et al., *Association of 11beta-hydroxysteroid dehydrogenase type 1 gene polymorphisms with serum alanine aminotransferase activity.* Diabetes Res Clin Pract, 2013. **99**(3): p. 343-50.
217. Tomlinson, J.W., et al., *11beta-hydroxysteroid dehydrogenase type 1: a tissue-specific regulator of glucocorticoid response.* Endocr Rev, 2004. **25**(5): p. 831-66.
218. Acevedo, J., et al., *Relative adrenal insufficiency in decompensated cirrhosis: Relationship to short-term risk of severe sepsis, hepatorenal syndrome, and death.* Hepatology, 2013. **58**(5): p. 1757-65.
219. Jie, F.R., et al., *[Clinical significance of peripheral cortisol level in patients with hepatitis B virus-related acute-on-chronic liver failure].* Zhonghua Gan Zang Bing Za Zhi, 2017. **25**(5): p. 383-385.
220. Marik, P.E., *Adrenal-exhaustion syndrome in patients with liver disease.* Intensive Care Med, 2006. **32**(2): p. 275-280.
221. Beal, E.W., et al., *A Small Animal Model of Ex Vivo Normothermic Liver Perfusion.* J Vis Exp, 2018(136).
222. Mergental, H., et al., *Transplantation of discarded livers following viability testing with normothermic machine perfusion.* Nat Commun, 2020. **11**(1): p. 2939.
223. Boteon, Y.L., et al., *Combined Hypothermic and Normothermic Machine Perfusion Improves Functional Recovery of Extended Criteria Donor Livers.* Liver Transpl, 2018. **24**(12): p. 1699-1715.
224. Meital Charni-Natan1†, R.A.-G., 2†, Etty Osher3 and Varda Rotter1*, *Liver and Steroid Hormones—Can a Touch of p53 Make a Difference.* Front. Endocrinol, 2019. **10**(374).
225. van de Merbel, A.F., et al., *An ex vivo Tissue Culture Model for the Assessment of Individualized Drug Responses in Prostate and Bladder Cancer.* Front Oncol, 2018. **8**: p. 400.
226. Parrish AR, G.A., Brendel K. , *Precision-cut tissue slices: applications in pharmacology and toxicology.* Life Sci., 1995. **57**: p. 1887–1901.

227. Gordon, G.G., et al., *Conversion of androgens to estrogens in cirrhosis of the liver.* J Clin Endocrinol Metab, 1975. **40**(6): p. 1018-26.
228. Storbeck, K.H., et al., *The utility of ultra-high performance supercritical fluid chromatography-tandem mass spectrometry (UHPSFC-MS/MS) for clinically relevant steroid analysis.* J Chromatogr B Analyt Technol Biomed Life Sci, 2018. **1085**: p. 36-41.
229. Yongshun Feng, D.M., *Comparison of supercritical CO2, liquid CO2, and solvent extraction of chemicals from a commercial slow pyrolysis liquid of beech wood.* Biomass and Bioenergy, 2016. **85**: p. 346-354.
230. Therina du Toit, M.A.S., Amanda C. Swart, *A high-throughput UPC2-MS/MS method for the separation and quantification of C19 and C21 steroids and their C11-oxy steroid metabolites in the classical, alternative, backdoor and 11OHA4 steroid pathways.* Journal of Chromatography B, 2018. **1080**: p. 71-81.